



SECRETARÍA
DE SALUD



Federación Nacional de Colegios de la Química Clínica A.C.
Universidad Juárez del Estado de Durango
Secretaría de Salud de Durango
Facultad de Ciencias Químicas de la UJED
Colegio de Profesionales de la Química de Durango A.C.

Otorgan la presente

CONSTANCIA

a

Dr. C. Estela Ruiz Baca

Por su asistencia al

**“XVI Congreso Nacional de Química Clínica y
Medicina de Laboratorio, EXPOLAB Durango 2016”**

Centro Cultural y de Convenciones Bicentenario del 5 al 8 de Mayo de 2016

Valor curricular de 22 horas.

MC. Martha Elia Muñoz Martínez
Directora
Facultad de Ciencias Químicas de la UJED

MC. Rosa Emma Saucedo Herrera
Presidenta
Colegio de Profesionales de la Química de Durango A.C.

M.A. Alfonso Salinas García
Presidente
Federación Nacional de Colegios
de la Química Clínica A. C.

Durango, Dgo. 8 de mayo del 2016



THE GRASS FOUNDATION

P.O. Box 241458, Los Angeles, CA 90024 • tel 310 266-0300

June 7th, 2016

To Whom it May Concern:

This is to confirm that Angelica Lopez will be attending the Grass Foundation 65th Reunion at the Marine Biology Laboratory in Woods Hole, MA from July 22 to July 24, 2016.

She will be presenting a poster at this meeting entitled:

"Defective trafficking on CNG channels"

Yours Sincerely

Felix Schweizer Ph.D.
President Grass Foundation

CURRENT TRUSTEES OF THE GRASS FOUNDATION

F.E. SCHWEIZER, Ph.D., President
B. GRAFSTEIN, Ph.D., Vice-President
R.F. LARKIN, CPA, Treasurer
M.B. MCFARLANE, Ph.D., J.D., Clerk
V.F. CHIN, , CFA
M. J. COLEMAN, Ph.D.
H.J. GRASS, M.D.

G.L. HOLMES, M.D.
R.R. HOY, Ph.D.
G.M. LANGFORD, Ph.D.
J.W. LICHTMAN, M.D., Ph.D.
A.R. SEGAL, Esq.
J.C. WEEKS, Ph.D.
S.J. ZOTTOLI, Ph.D.

FOUNDING TRUSTEES

A.M. GRASS
E.R. GRASS, LL.D, SC.D.
A. FORBES, M.D.
F.A. GIBBS, M.D.
W. LENNOX, M.D.
R.S. MORISON, M.D.
A. ROSENBLUETH, M.D.
R.A. ZOTTOLI, LL.B.

Defective trafficking in mutant CNG channels
Martínez-Delgado G, Perales-García M, Ruiz-Baca E, Saucedo-Mendiola ML, López-Rodríguez A.

Plasma membrane proteins mediate interaction between cells and the external environment; this makes them excellent therapeutic targets for developing new drugs modulating cell function. Ion channels are membrane proteins that allow ion flow in a regulated manner into or out of the cell by activating signaling cascades in response to different stimuli. Mutations in these proteins are related to some associated diseases called "channelopathies". A simple nucleotide change could induce the inappropriate folding of mutant proteins, leading to premature degradation or intracellular retention. Sometimes the mutant protein is potentially functional but its function is impaired because it cannot reach plasma membrane. In the best scenario the population of mutant proteins reaching the final destination is diminished thereby affecting their function. Cyclic nucleotide dependent ion channels (CNG channels) involved in signal transduction for vision and smell, are related to various channelopathies and represent a good example of membrane proteins that induce cellular localization defects when the protein is mutated. As a first approach towards understanding the mechanisms related to defects in traffic of various mutant CNG channel associated pathologies, we determined the intracellular localization of five CNG channel mutants expressed in HEK-293, analyzing the co-localization using fluorescent intracellular markers by confocal microscopy.



UJED

UNIVERSIDAD JUÁREZ
DEL ESTADO DE DURANGO



FORO
INTERINSTITUCIONAL
DE EDUCACIÓN SUPERIOR

“La educación superior de Durango,
una visión de futuro”

La Universidad Juárez del Estado de Durango otorga la presente

Constancia

A: ESTELA RUIZ BACA

Por su asistencia en los trabajos realizados durante el **“Foro Interinstitucional de Educación Superior”** denominado **“La educación superior de Durango, una visión de futuro”**, celebrado los días 26 y 27 de octubre de 2017.



M. I. Oscar Erasmo Najar García
Rector

PFCE

Este evento ha sido financiado con recursos del Programa de Fortalecimiento de la Calidad Educativa 2017 (PFCE/SEP), este programa es público, ajeno a cualquier partido político. Queda prohibido su uso para fines distintos a los establecidos en el programa.



UNIVERSIDAD JUAREZ DEL ESTADO DE DURANGO
FACULTAD DE CIENCIAS QUIMICAS



CONSTANCIA

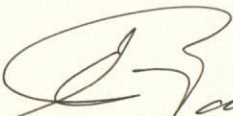
ESTHELA RUIZ BACA

Por su asistencia a la:



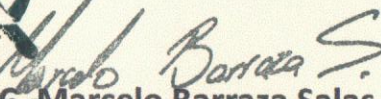
1^{ra} JORNADA ACADÉMICO - CIENTÍFICA

En el marco del XXXIII Aniversario de la Facultad de Ciencias Químicas
del 25 al 29 de Septiembre de 2017.


D.C. Eda Guadalupe Ramírez Valles

Directora




D.C. Marcelo Barraza Salas
Secretario Académico



El **Gobierno del Estado de Durango** a través de la
Secretaría de Salud otorga la presente

Constancia

A:

Estela Ruiz Baca

Por su asistencia a la I Jornada Nacional de Investigación en Salud Durango 2017
Los días 30, 31 de Agosto y 1 de septiembre de 2017
Duración 16 horas con valor curricular

José Rosas Aispuro Torres

Gobernador del Estado de Durango

Dr. César Humberto Franco Mariscal

Secretario de Salud y Dir. Gral. de los Servicios de Salud

Victoria de Durango, Dgo. a Agosto de 2017

Objetivo: Contribuir a la difusión de los resultados de la investigación en el área de salud, así como promover el fortalecimiento del desarrollo de la investigación científica nacional.

Dirección de Enseñanza, Capacitación, Calidad e Investigación en Salud		
	HORAS	CREDITOS
TEORIA	16	2
PRACTICA	0	0
TOTAL	16	2
Folio: 3599		
		
Coordinación Estatal de Capacitación		

	DESCRIPCIÓN	HORAS
1	Diagnóstico molecular: Biología molecular aplicada en la práctica clínica.	1
2	Gestión de recursos de financiamiento para la investigación	1
3	Tomando mejores decisiones clínicas basadas en evidencia científica	1
4	Consentimiento informado en la práctica clínica y la investigación	1
5	Investigación y Desarrollo de Medicamento*	1
6	Alcances de la Inmunogenética en México y su aplicación en Trasplantes de Células Progenitoras Hematopoyéticas: Registro Mexicano de Donadores Altruistas de Médula Ósea"	1
7	Exposición de trabajos de investigación en las modalidades de Poster Científico y Ponencias orales del XV Concurso de investigación.	10
	Horas crédito	16

Emerging Concepts in Ion Channel Biophysics

Mexico City, Mexico | October 10–13, 2017



nanjion

THORLABS

JGP



Biophysical Journal



44-POS Board 44**Virtual Rescuing of CNG_{F547L} Mutant Channel by Cyclic Nucleotide Analogues**

Liliana I. Lozano-M., Estela Ruiz-Baca, Leticia Saucedo-Mendiola, **Angelica Lopez-Rodriguez** |
Fac. C. Químicas UJED, Durango, Durango, México.

Cyclic nucleotide-gated (CNG) channels are critical to the phototransduction cascade that underlie in vertebrate vision. These channels open and close in response to light-induced changes in the intracellular cyclic GMP concentration. Approximately, 75% of the mutations related to achromatopsia, a retinal disorder with impaired color vision, are in the genes encoding CNG channels. The F547L mutation is located at the cyclic nucleotide binding domain (CNBD) in the CNGA3 subunit. This mutant channel reaches the plasma membrane, but it is not functional at 37°C. Interestingly, its function is rescued at 27°C or by co-expressing CNGB3 subunits; nevertheless, apparent affinity to cGMP is increased, suggesting that correct folding of the protein can be induced leading to the functional rescue of the channel.

We have modelled the human CNGA3 channel and the CNGA3_{F547L} mutant using as template the crystal structure of the *C. elegans* CNG channel. The model of the mutant suggests a constriction of the structure due to formation of new hydrogen bonds. By docking, we also tested the affinity of natural CNG channel ligands such as cGMP and cAMP along with twelve cyclic nucleotide analogues. Supporting the increased apparent affinity for ligand, previously reported, CNGA3_{F547L} mutation induces the reduction in size and volume of CNBD, increasing the score affinity for most of the ligands tested, except two molecules that we consider good candidates to rescue the mutant channel function as they keep the same score affinity in the wild type and mutant channel.

OTORGA LA PRESENTE
CONSTANCIA A:

Estela Ruiz Baca

Por su asistencia y destacada participación en los Foros de Discusión,
Análisis y Conformación de Redes Temáticas en el

**ENCUENTRO ESTATAL DE CIENCIA,
TECNOLOGÍA E INNOVACIÓN 2018**

Dentro del Programa de Fortalecimiento Institucional de este Consejo,
así como, para la elaboración del
"Plan Estratégico de CTI 2017-2022 del Estado de Durango".

Durango, Dgo., Mayo 23 de 2018



DRA. JULIANA MORALES CASTRO

Directora General del Consejo de Ciencia y Tecnología del Estado de Durango



PARA TODOS
Dgo

PARA TODOS
Dgo

CONSEJO
DE CIENCIA
Y TECNOLOGÍA



SECRETARÍA
DE SALUD



COMISIÓN ESTATAL DE
BIOÉTICA
DURANGO



LA SECRETARÍA DE SALUD Y LOS SERVICIOS DE SALUD DE DURANGO A TRAVÉS
DE LA DIRECCIÓN DE ENSEÑANZA, CAPACITACIÓN, CALIDAD E INVESTIGACIÓN EN SALUD

Otorgan la presente

CONSTANCIA

A:

Estela Ruiz Baca

Por su asistencia al **1er. Congreso Estatal de Bioética “Fortalecimiento del Vínculo entre la Bioética y la Sociedad”** y la **XII Reunión Regional de Comisiones Estatales de Bioética**.

Realizado los días 23 y 24 de agosto de 2018 en el Auditorio del Hospital General 450.

Duración 10 horas



**1ER CONGRESO ESTATAL
DE BIOÉTICA**
FORO REGIONAL DE LA BIOÉTICA Y LA SOCIEDAD

Dr. Sergio González Romero

Secretario de Salud y Director General
de los Servicios de Salud de Durango



Victoria de Durango, Dgo. Agosto de 2018



II Jornada Nacional de Investigación en Salud

DURANGO 2018
EMPODERAMIENTO A TRAVÉS DE LA CIENCIA

El Gobierno del Estado de Durango a través de
la Secretaría de Salud

Otorga la presente

CONSTANCIA

ESTELA RUIZ BACA

a:

Por su **asistencia** a la
II Jornada Nacional de Investigación en Salud Durango 2018
los días 18, 19 y 20 de octubre del 2018, en el
Centro Cultural y de Convenciones Bicentenario, Durango, Dgo.
Duración 16 horas con valor curricular

Dr. José Rosas Aispuro Torres
GOBERNADOR DEL ESTADO DE DURANGO

Dr. Sergio González Romero
SECRETARIO DE SALUD Y DIR. GRAL. DE
LOS SERVICIOS DE SALUD

		Dirección de Enseñanza, Capacitación, Calidad e Investigación en Salud	Objetivo Difundir los resultados de la investigación generada en el área de salud, con el fin de promover la interacción e intercambio de conocimientos entre los investigadores participantes, que coadyuve a mejorar la calidad de la misma.
		Horas	
Teoría		16	
Práctica		0	
Total		16	
Créditos		2	Temas <ul style="list-style-type: none"> • Ansiedad Social y Suicidio. • Abordaje de la Diabetes en México. • Internet de las Cosas Médicas. • Epidemiología de la Diabetes y Pie Diabético. • Enfermedades Respiratorias, Oportunidad de Investigación. • Aplicación y Análisis de la Microscopía Confocal en la búsqueda de un Biomarcador Especifico para la Enfermedad de Alzheimer. • Recorrido por Carteles Científicos en Investigación en Salud Publica, Ciencias Sociales y Humanidades, en Clínica Básica, Casos Clínicos y Fotografía Científica.
Folio: 4065  Coordinación Estatal de Capacitación			

Download PDF | Share | Export

Search ScienceDirect | Advanced

Biophysical Journal

Volume 116, Issue 3, Supplement 1, 15 February 2019, Pages 339a-339a



Recommended articles
No articles found
Citing articles (0)

Effect of Hsp70 Chaperone on CNG Ion Channels Related to Channelopathies

Katrina Jabra, Angelica Lopez-Rodriguez, Ivan Meneses-Morales

Show more

https://doi.org/10.1016/j.bpj.2018.11.3894

Get rights and content

Previous article in issue | Next article in issue

Diseases caused by defects in folding or trafficking of cell-surface ion channels demonstrate how genetic mutations lead to problems with physiological consequences, for example, many mutations in the genes encoding cyclic nucleotide-gated (CNG) channels reflect the impaired trafficking or dysfunctionality as a spectrum of inherited retinal disorders. The effect of physical variables such as temperature had been previously analyzed, mimicking *in vitro* the principles encountered during *in vivo* folding, where protein folding and unfolding, provides thermotolerance to the cell through the heat shock proteins (Hsp) assistance, favoring the structural recovery and the function of abnormal proteins. As an alternative to rescue improper targeted membrane protein in this work, using the HEK-293 cells we overexpressed the Hsp70 isoform along with wild type CNG channel or two inheritable mutants previously reported as misfolded proteins. Comparing the effect of the proteins co-expression on cells incubated at different temperatures, monitoring the cell morphology, and channel location through fluorescence microscopy while functionality was tested by the patch clamp inside out technique.

View Abstract

and thermodynamics of folding are routinely modulated by changing solvent conditions, but such changes are not protein specific. Here we demonstrate a general principle by which specific kinetic modulation can be achieved for any protein whose folding route is known. Our strategy is to design a pre-stabilized folding nucleus of a protein. We show that the β 1- β 2 part (residues 1 to 17) of ubiquitin, which is the segment known to fold first (into a β -hairpin shape)^[1], can make folding faster when introduced as a separate conformationally constrained peptide at excess concentrations. A weaker but still significant effect is observed when this ‘decoy nucleus’ peptide is not conformationally constrained, or is in an unfolding buffer to start with. Interestingly, the thermodynamic stability of the protein remains unchanged, as the unfolding rate also becomes faster. We simulate the system for both a weakly constrained and a strongly constrained decoy nucleus, and observe that the decoy interacts strongly with the protein only when it is conformationally constrained. Together, our results suggest that the folding of almost any protein which possesses a well-defined folding nucleus can be modulated, by introducing a nucleus-mimicking molecule with a stabilized structure. It also implies that *in vivo*, fragments of proteins which are naturally present as degradation by-products can in principle affect the folding of the full length proteins.

^[1] Atomic-level description of ubiquitin folding. Piana et al., *PNAS*, **2013**, *110* (15), 5915-5920

1671-Pos

Interplay between Native State Topology and Sequence in Two-State Protein Folding

Stefan Wallin, Daniel Trotter.

Physics and Physical Oceanography, Memorial University, St John's, NL, Canada.

Why is the folding into some native state topologies, including all- α folds, more sensitive to sequence variations than other, more nonlocal protein folds? To explore this question, we design and study three 35-54 amino acid sequences within a coarse-grained and sequence-based model for protein folding, and show that they fold spontaneously at low temperatures into stable 3α , $4\beta + \alpha$ and β -barrel native folds, respectively. Their thermodynamic behavior exhibit features in line with experimental data, including appropriate rank order in folding cooperativity and temperature-driven Hammond shifts of transition states. Using a novel generalized ensemble Monte Carlo algorithm (A. Aina and S. Wallin, *Journal of Chemical Physics* **147** 095102, (2017)) we then determine the thermodynamics of all possible single-point mutations and random sets of 5-12% of all double-point mutations of each of the three proteins (>300 mutants/protein). We find that the proteins respond to sequence variations in a topology-dependent manner. In particular, the free energy landscape of the β -barrel protein is more robust to mutational effects than the 3α and $4\beta + \alpha$ proteins, especially the region corresponding to the transition state. Moreover, we show that the presence of structural heterogeneity during folding, as indicated by a local ‘‘flatness’’ in free energy surfaces, is linked to a heterogeneity in folding behavior among sequence variants. In other words, proteins with diverse folding pathways might be more sensitive to variations in sequence than proteins with restricted pathways.

1672-Pos

Structural Characterization of a Ubiquitin Folding Intermediate by Pressure-Jump NMR

Joseph M. Courtney, Cyril Charlier, Ad Bax.

Lab of Chemical Physics, National Institutes of Health, Bethesda, MD, USA.

Small proteins rapidly fold on the timescale of milliseconds or less. Proteins with a substantial difference between the volumes of the folded and unfolded states experience large shifts in thermodynamic equilibrium upon variation of hydrostatic pressure, enabling experimental control over folding and unfolding. Using hardware that performs rapid and repeatable pressure switching within an NMR sample cell, we study the folding process of a pressure-sensitized mutant of ubiquitin in the absence of denaturants. This approach makes it possible to record 2D and 3D NMR spectra of the folding protein at atmospheric pressure, and to monitor chemical shift changes with sub-millisecond resolution, providing residue-specific information on the folding process. ¹H, ¹⁵N, and ¹³C chemical shifts measured immediately after dropping the pressure from 2.5 kbar (favoring unfolding) to 1 bar provide direct evidence for parallel folding pathways, with approximately one-half of the protein molecules folding through an on-pathway kinetic intermediate, whereas the other half fold in a single step. Combining time-resolved measurements of NMR observables, we develop a structural model for the folding intermediate, providing new insight into folding dynamics and kinetic traps present even in small, single-domain proteins.

1673-Pos

Interfaces of the Topoisomerase V (HhH)₂ Domains have Surprising Contributions to Thermodynamic Stability

Mark Petersen¹, Rebecca Fang¹, Ananya Majumdar², Doug Barrick¹.

¹Biophysics, Johns Hopkins Univ, Baltimore, MD, USA, ²Biomolecular NMR, Johns Hopkins Univ, Baltimore, MD, USA.

Thermodynamic stability is an important consideration when designing proteins for use as drugs or biochemical tools. Highly stable proteins may have longer shelf lives, higher tolerance to temperature extremes and denaturants, and better processivity during catalysis. Topoisomerase V (TopoV) from the extremophile *Methanopyrus kandleri* has gained attention for its helix-hairpin-helix ((HhH)₂) domains. These domains play a role in non-specific DNA binding, and as such they are found in proteins such as ligases and polymerases. TopoV has twelve (HhH)₂ domains, significantly more than any known mesophilic protein. In various crystal structures, these domains extend from the globular topoisomerase domain in an arc, suggesting that there are stabilizing interfacial interactions between adjacent domains. These domains have DNA repair activity, but they are also important for TopoV's processivity and incredible tolerance at extremophile conditions. Indeed, fusion proteins with TopoV (HhH)₂ domains attached to common laboratory polymerases have increased processivity and longer lifetimes in the high temperature conditions characteristic of PCR.

To understand how these (HhH)₂ domains are thermodynamically coupled, we have expressed constructs containing either one or two (HhH)₂ domains from TopoV. These constructs have NMR spectra that are characteristic of folded proteins, and their high-helical content makes them particularly amenable to thermodynamic studies by CD. We separate the contributions to folding free energy using a simplified 1D-Ising model. We have applied this approach to characterize the energetics of most of the (HhH)₂ domains in the array. Surprisingly, TopoV has a mixture of stabilizing and destabilizing interfaces, which may be important for how the domains wrap around DNA. Using parameters from our dimer data, we can construct the partition function for the entire array of domains at the 1D Ising level to determine local stabilities and populations of partly folded states.

1674-Pos

Unravelling the Role of S100A9 in the Development of Neurodegenerative Disease

Philip T.F. Williamson¹, Jack Horrocks¹, Luckshi Maheswaran¹, Maria Concistre², Ludmilla Morozova-Roche³.

¹Biological Sciences, University of Southampton, Southampton, United Kingdom, ²Chemistry, University of Southampton, Southampton, United Kingdom, ³Department of Medical Biochemistry and Biophysics, University of Umeå, Umeå, Sweden.

S100A9 is a pro-inflammatory calcium binding protein released by neutrophils in response to neuroinflammatory events. These events can be triggered by a range of conditions including traumatic brain injury and bacterial infection but are also observed in a range of neurodegenerative conditions including Alzheimer's Disease and Parkinson's Disease. S100A9 is intrinsically amyloidogenic self-aggregating to form organised fibrils both *in vitro* and *in vivo*. These S100A9 fibrils congregate with amyloid- β to seed and accelerate the growth of amyloid- β fibrils, as observed in *in vitro* studies. S100A9 possesses two Ca²⁺ binding sites which when vacant increase its propensity to aggregate into an ordered fibrillar state. Inversely, increasing calcium concentration inhibits S100A9 fibril formation as verified by Thioflavin-T assay. Our solution-state NMR studies indicate that in the absence of calcium the protein is largely unfolded adopts a number of interconverting states which become more structured upon calcium binding. Interestingly complementary synchrotron radiation circular dichroism measurements suggest a high alpha-helical content irrespective of calcium levels, suggesting that these interconverting species are rich in short-lived helical states. To determine the structural transition that occur upon fibril formation, solid-state NMR investigations have been utilised. These studies demonstrate that S100A9 fibrils formed *in vitro* have a single well-ordered structure with mobile regions limited to 15-25 residues in size. Analysis of the chemical shifts indicate the protein exists as a single polymorph with a rigid protein core that is predominantly β -strand in structure. Employing paramagnetic relaxation assisted data collection (PAC) progress is being made towards a complete assignment permitting a detailed analysis of the conformation of S100A9 within amyloid fibres.

1675-Pos

Effect of Hsp70 Chaperone on CNG Ion Channels Related to Channelopathies

Karina Juárez, Angelica Lopez-Rodriguez, Ivan Meneses-Morales.

Universidad Juárez del Estado de Durango, Durango, Mexico.

Diseases caused by defects in folding or trafficking of cell-surface ion channels demonstrate how genetic mutations lead to problems with physiological

consequences, for example, many mutations in the genes encoding cyclic nucleotide gated (CNG) channels reflect the impaired trafficking or dysfunctionality as a spectrum of inherited retinal disorders. The effect of physical variables such as temperature had been previously analyzed, mimicking *in vitro* the principles encountered during *in vivo* folding; where protein folding and unfolding, provides thermotolerance to the cell through the heat shock proteins (Hsp) assistance, favoring the structural recovery and the function of abnormal proteins. As an alternative to rescue improper targeted membrane protein in this work, using the HEK-293 cells we overexpressed the Hsp70 isoform along with wild type CNG channel or two inheritable mutants previously reported as misfolded proteins. Comparing the effect of the proteins co-expression on cells incubated at different temperatures, monitoring the cell morphology, and channel location through fluorescence microscopy while functionality was tested by the patch clamp inside out technique.

1676-Pos

Innovation of a Novel Pulse-Chase in Cell Footprinting Method for the Study of Protein Folding Phenomena

Danté T. Johnson¹, Benjamin Punshon-Smith², Anne Gershenson³, Lisa M. Jones¹.

¹Pharmaceutical Sciences, University of Maryland Baltimore, Baltimore, MD, USA, ²University of Maryland Baltimore County, Baltimore, MD, USA, ³University of Massachusetts Amherst, Amherst, MA, USA.

Protein structure determines function for globular proteins, and the understanding of protein folding pathways aids in the understanding of their function. Traditionally, protein folding has been observed *in vitro* using full length protein sequences, but folding in the cell is quite different from folding studies in an isolated environment due to macromolecular crowding and specific interactions with the ribosome, chaperones and modifying enzymes. To overcome these limitations, we have begun development of a new method for protein folding studies. This method, Pulse Chase In-Cell Fast Photochemical Oxidation of Proteins (pcIC-FPOP), couples pulse-chase technology with mass spectrometry-based in cell footprinting which will allow for detailed characterization of short lived protein folding intermediates. FPOP coupled with mass spectrometry has become an invaluable tool used in structural proteomics to study surface accessibility in proteins. In our lab, FPOP has already been extended to protein labeling in live cells, allowing the study of protein conformations in the complex cell environment, and providing insight into ligand induced structural changes or conformational changes accompanying protein complex formation within the cellular context. pcIC FPOP will allow proteins synthesized during the pulse to be studied from birth to death. The novel pcIC-FPOP method required the design of a new platform for in-cell footprinting that includes a stage-top cell incubator and nanopositioning system automated to meet the high speed demands required to study protein folding intermediates. We are optimizing the new platform to demonstrate its efficacy for pcIC-FPOP. Preliminary benchmark data, will show the ability of this new method to provide comparable results to the already published method of in cell oxidative labeling, IC-FPOP. We believe this method will become powerful tool in probing protein folding and misfolding in the native cellular environment.

1677-Pos

Monitoring Protein Folding On and Off the Ribosome using X-Ray Footprinting Mass Spectrometry

Shawn M. Costello¹, Natalie R. Dall², Avi J. Samelson³, Sayan Gupta⁴, Corie Y. Ralston⁴, Susan Marqusee².

¹Biophysics, UC Berkeley, Berkeley, CA, USA, ²Molecular and Cell Biology, UC Berkeley, Berkeley, CA, USA, ³Institute for Neurodegenerative Diseases, UC San Francisco, San Francisco, CA, USA, ⁴Molecular Biophysics and Integrated Bioimaging, Lawrence Berkeley National Laboratory, Berkeley, CA, USA.

All proteins are synthesized by the ribosome, and the relatively slow nature of this process allows for nascent proteins to sample conformational space before the entire protein length has been synthesized. This conformational search differs significantly from re-folding: (i) translation is vectorial (ii) the folding environment near the ribosome is highly charged and sterically restricted. To understand how the co-translational folding differs from re-folding *in vitro*, we must develop techniques to quantitatively measure biophysical properties, namely the relative energies, energetic barriers, and structures of conformations populated during both re-folding and co-translational folding. We have determined and compared the stabilities and folding rates of several proteins both in solution and as ribosome stalled nascent chains (RNCs) using pulse proteolysis and optical tweezers. Additionally, using hydrogen exchange mass spectrometry (HX/MS) and cysteine accessibility assays, we have shown that the folding intermediate populated by the protein HaloTag during *in vitro* re-folding is different from the intermediate formed during co-translational

folding. We have now begun to develop x-ray footprinting mass spectrometry (XF/MS), a technique that reports on the solvent accessibility of individual amino acids in a protein, as a tool for determining detailed structural and thermodynamic properties of folded and intermediate states on the ribosome. We have shown that XF/MS provides local structural information consistent with other techniques and can be used to probe both global and regional stabilities of proteins in complex environments.

1678-Pos

Cochaperones Enable Hsp70 to Use ATP Energy for Non-Equilibrium Stabilization of Native Proteins

Huafeng Xu.

Unaffiliated, Forest Hills, NY, USA.

The heat shock protein 70 (Hsp70) chaperones, vital to the proper folding of proteins inside cells, consume ATP and require cochaperones in assisting protein folding. It is unclear whether Hsp70 can utilize the free energy from ATP hydrolysis to fold a protein into a native state that is thermodynamically unstable in the chaperone-free equilibrium. Here I present a model of Hsp70-mediated protein folding, which predicts that Hsp70, as a result of differential stimulation of ATP hydrolysis by its Hsp40 cochaperone, dissociates faster from a substrate in fold-competent conformations than from one in misfolding-prone conformations, thus elevating the native concentration above and suppressing the misfolded concentration below their respective equilibrium values. In contrast to the prevailing notion that Hsp70 is an unfoldase/holdase that pulls proteins out of their misfolded states, my model suggests that Hsp70 actively folds proteins into the native state. My model quantitatively reproduces experimental refolding kinetics, predicts how modulations of the Hsp70/Hsp40 chaperone system affect protein folding, and suggests new approaches to regulating cellular protein quality. The key prediction of my model, that Hsp70 can use ATP energy for non-equilibrium stabilization of native proteins, is in agreement with recent experimental results. I propose additional new experiments to further test my model.

Posters: Protein Dynamics and Allostery I

1679-Pos

Description of Structural Changes by Motion Tree

Ryotaro Koike¹, Kei Moritsugu², Motonori Ota¹.

¹Nagoya Univ, Nagoya, Japan, ²Yokohama City Univ, Yokohama, Japan.

Proteins are flexible molecules and change their structures. Some protein-functions are involved in structural changes due to external stimuli such as ligand binding. The multiple structures of the identical protein under different conditions, e.g. ligand-bound and -unbound forms, are invaluable resources to perceive the structural changes between two forms. The comparison of structures under different conditions enables the description of structural change; which parts of the protein move as rigid bodies and how large the motions are. The rigid bodies and their motions are the key to understanding their functions.

We developed a tool to compare distinct structures of identical proteins and describe the structural changes. The two structures are denoted by distance matrices. By taking the difference between the corresponding elements of the matrices, the distance difference matrix is derived. A hierarchical clustering procedure is applied to the matrix and a tree diagram named "Motion Tree" is obtained. Motion Tree identifies rigid parts of the protein at any magnitudes of motions, and presents them in a hierarchical manner.

We have applied the method to a number of proteins in the PDB. The extensive analysis on protein structural changes revealed certain of relationships between motions and functions. We also applied the method to the huge number of structures in the trajectories of molecular dynamics simulations, and detected intrinsic dynamics of proteins in simulations.

1680-Pos

Simulating the Folding Trajectories of Lattice Proteins within an Oscillatory Environment

Xuanye Zhu, Qizhang Jia, Kateri H. DuBay.

Chemistry, University of Virginia, Charlottesville, VA, USA.

Proteins fold into specific three-dimensional structures to fulfill different cellular functions. Such folding process within a static environment has been extensively studied, but the folding process *in vivo* requires additional insights. Our research aims to investigate protein folding that occurs concurrently with oscillations in the interactions between its constituent amino acids, implemented in our Monte Carlo simulations as temperature oscillations. The folding of a small, 3D lattice protein model is simulated and the resulting trajectories are analyzed to understand how the folding pathways of our model protein differ when oscillations are present in the folding environment.

Iracilda Zeppone Carlos *Editor*

Sporotrichosis

New Developments and
Future Prospects

 Springer

Chapter 3

Components and Virulence Factors of the *Sporothrix schenckii* Species Complex

Estela Ruiz-Baca, Carlos A. Alba-Fierro, Armando Pérez-Torres,
and Conchita Toriello

Abstract Sporotrichosis is a fungal infection caused by the *Sporothrix schenckii* species complex, which includes species of clinical relevance such as *S. brasiliensis*, *S. schenckii sensu stricto*, *S. globosa*, *S. mexicana*, and *S. luriei*. When *S. schenckii* was discovered as a species complex with several entities, the similarities and differences among these pathogenic species began to be studied with respect to their virulence, susceptibility to antifungal agents, protein production, and immunogenicity, among other characteristics. Still, little is known about the factors that contribute to the virulence of this species complex and about the mechanisms involved in the establishment and development of sporotrichosis. This chapter reviews the virulence factors and main components described for the *S. schenckii* complex, which include fungal dimorphism, thermotolerance, melanin production, secretion of proteases, and cell surface components.

Keywords *Sporothrix schenckii* complex • Virulence factors • Cell wall • Antigens

3.1 Introduction

Sporotrichosis is a subcutaneous mycosis that until this past century was attributed to only one species, *Sporothrix schenckii*. The frequency of this infection has increased in recent years, mainly in immunocompromised patients (López-Romero et al. 2011). Also in current years, the phylogeny and taxonomic status of this

E. Ruiz-Baca (✉) • C.A. Alba-Fierro
Departamento de Biología Celular y Molecular, Facultad de Ciencias Químicas, Universidad Juárez del Estado de Durango, Av. Veterinaria s/n, Durango, Dgo., México C.P. 34120, México
e-mail: erb750@hotmail.com; eruiz@ujed.mx

A. Pérez-Torres
Departamento de Biología Celular y Tisular, Facultad de Medicina, Universidad Nacional Autónoma de México, México D.F. 04510, México
e-mail: armandop@unam.mx

C. Toriello
Departamento de Microbiología y Parasitología, Facultad de Medicina, Universidad Nacional Autónoma de México, México D.F. 04510, México

fungus have been widely studied through molecular biology methods, and it has been demonstrated that this fungus is indeed a complex of cryptic species (Marimon et al. 2006). Different *Sporothrix* species are now considered to be human pathogens: *S. brasiliensis*, *S. globosa*, *S. mexicana*, *S. luriei*, *S. pallida*, and *S. schenckii sensu stricto* (Marimon et al. 2007, 2008; de Meyer et al. 2008). All these species share the same ecological niche and very similar phenotypic traits, and they all are dimorphic fungi; that is, they exhibit a mycelial morphotype in nature and a parasitic yeast morphotype in the host. All the information regarding its biological characteristics has been studied for one species, *S. schenckii*, and it has only been in this recent century that other species have been identified and that work to clarify specific characteristics has just begun.

The “damage-response framework” of microbial pathogenesis of Casadevall and Pirofski (1999, 2001, 2003) refers to the interaction among microbes, host, and environment. The damage to the host may be given by either the microbial factors (or virulence factors) or the host response. To date, information regarding the microbial pathogenesis in the establishment and development of sporotrichosis and specific virulence factors of *Sporothrix* spp. is still scarce. Current data on the *Sporothrix* species complex virulence in animal models has shown *S. brasiliensis* to be the most virulent species, followed by *S. schenckii s. str.*, *S. globosa*, and *S. mexicana* (Arillaga-Moncrieff et al. 2009).

In this chapter, microbial factors (virulence factors), such as dimorphism, thermotolerance, melanin production, proteases, and cell wall (CW) biochemical components are discussed, mainly in connection with *S. schenckii*, although all available information concerning other relevant clinical species is also included. In Chaps. 4 and 7, these and other virulence factors of *S. schenckii* are discussed again, highlighting their role in the environment and during the infectious process.

3.2 Dimorphism

Dimorphism is the ability of some fungal agents to exhibit a phenotypic duality coupled with a cellular differentiation process, which in turn may be related to pathogenicity and virulence mechanisms. In sporotrichosis, as well as in other subcutaneous and systemic mycoses, fungi exhibit an infectious mycelial morphotype distributed in their specific ecological niche that switches to a parasitic yeast morphotype when introduced in their host. The mycelial and yeast morphotypes can also be easily obtained at 25 °C and 35–37 °C, respectively, with appropriate culture media in laboratory conditions. Conidia of the mycelial morphotype vary according to each species (Marimon et al. 2007), but, in general, mycelia show hyaline, septate, thin hyphae, with sympodially borne conidia, singly or in groups, whereas sessile conidia, in some cases, with time of incubation, develop thick walls and a dark brown pigment, generally along the sides of hyphae (Fig. 3.1a, b).

Mycelial morphotype colonies, initially described as white and glabrous, in time become wrinkled and membranous with black areas (Fig. 3.2a, b). Yeast

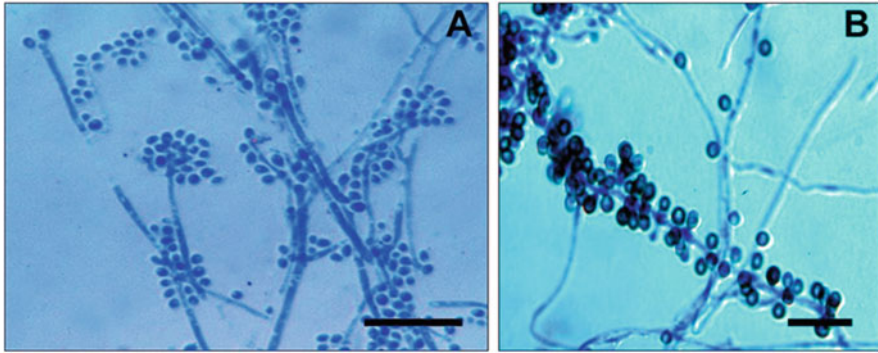


Fig. 3.1 *Sporothrix schenckii* EH-143 mycelial morphotype. (a) Hyaline, septate, thin hyphae with sympodially borne conidia. (b) Thick-walled, dark brown sessile conidia along the sides of hyphae. Bars = 10 µm

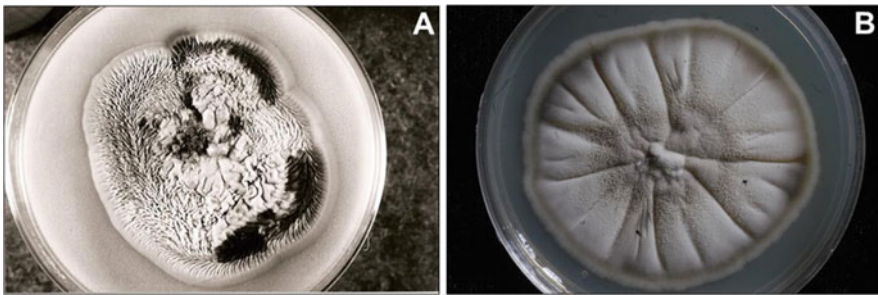


Fig. 3.2 Mycelial morphotype colonies. (a) *Sporothrix schenckii* EH-143 and (b) *Sporothrix globosa* EH-230, at 28 °C on potato dextrose agar medium for 15 days

morphotype cells are fusiform and ovoid with single, double, or multiple budding; although scarcely observed in human biological samples (asteroid bodies), they are generally described and easily observed as “cigar bodies” in experimental host tissues (Fig. 3.3).

The dimorphic transition of *S. schenckii* was first described by Howard in 1961; since then, environmental changes such as moisture, pH, temperature, nutrients, oxygen availability, G proteins, and calcium uptake, among others, have been mentioned as factors with an effect on this transition. In response to these changes, the fungus modifies its physiology and morphology to be able to cope with new physiological conditions and to evade the immune response of the host (Szanişzlo 1985). This dimorphism, both in its ecological niches and within different hosts (Casadevall et al. 2003), is not essential for its life cycle, but it is relevant for its pathogenicity (Nemecek et al. 2006; Gauthier and Klein 2008).

Dimorphism in *S. schenckii* has rarely been studied when compared with other human pathogenic dimorphic fungi; however, since 1983, studies by Rodríguez del Valle et al. (1983) have demonstrated that this fungus dimorphic switch is controlled not only by temperature but also by the pH of the culture medium, relevant

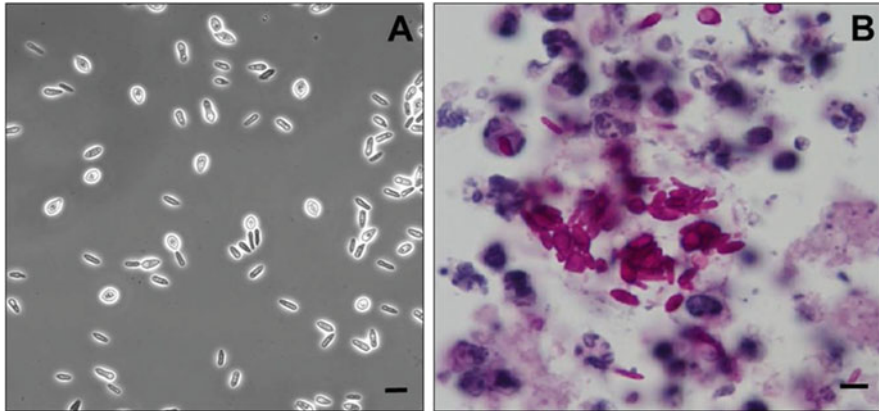


Fig. 3.3 *Sporothrix schenckii* EH-143 yeast morphotype. (a) Yeast budding cells at 37 °C on YPG (yeast extract-peptone-glucose) medium. (b) Single yeast cells (cigar bodies) within macrophages and neutrophils but abundant PAS-positive yeast cells are observed inside a foam cell in *S. schenckii* EH-143-infected mice at 8 weeks of infection. Bars = 10 μ m

in the development of a particular morphotype. Mycelial morphotype without yeast cells was obtained at 25 °C and low pH (4.0–5.0); neutral to alkaline pH favored the yeast morphotype. Aeration of cultures favored the yeast morphotype in a pH range from 6.0 to 8.0 at 25 °C. Since these investigations concerning the *S. schenckii* dimorphic switch were conducted, other works have been carried out with reference to calcium uptake (Serrano and Rodríguez del Valle 1990; Rivera-Rodríguez and Rodríguez del Valle 1992), and a calcium/calmodulin-dependent protein kinase (CaMK), encoded by the calcium/calmodulin kinase I (*sscmk1*) gene, has been described (Valle-Avilés et al. 2007). Using CaMK inhibitors, these authors demonstrated that the transition from yeast cells to hyphae was inhibited, thereby suggesting a calcium/calmodulin pathway in the regulation of *S. schenckii* dimorphism. The same phenomenon was demonstrated by RNA interference (RNAi) technology, with RNAi transformants being unable to grow as yeast cells at 35 °C (Rodríguez-Caban et al. 2011).

Protein kinase C (PKC) is an important signal transduction enzyme and a family of proteins made up of different isoforms described in different fungi. Studies concerning the response to PKC effector molecules during the induction of the yeast-to-mycelium transition indicated the presence and involvement of this enzyme in *S. schenckii* dimorphism (Colon-Colón and Rodríguez del Valle 1993). In later studies, two PKC-like genes were identified in *S. schenckii* and, using reverse transcription-polymerase chain reaction (RT-PCR), the *pkcSs-2* gene was found to be expressed at all intervals tested during the yeast-to-mycelium transition in this fungus (Aquino-Piñero & Rodríguez del Valle 2002).

In other dimorphic human fungal pathogens as *Blastomyces dermatitidis* and *Histoplasma capsulatum*, a long-sought regulator that controls the switch from the mycelial morphotype to a pathogenic yeast morphotype was found by Nemecek

et al. (2006). This control corresponded to DRK1, a hybrid dimorphism-regulating histidine kinase that regulates dimorphism and virulence for both of the above-mentioned fungi. DRK1 is required for the transition from the mycelial to the pathogenic yeast morphotype, the expression of virulence genes, and pathogenicity in vivo. Recently, Hou et al. (2013), by means of molecular cloning, characterization, and differential expression, obtained the partial complementary DNA (cDNA) sequence of DRK1 of *S. schenckii*, designated *SsDRK1*. Quantitative real-time RT-PCR revealed that *SsDRK1* was more highly expressed in the yeast stage than in the mycelial stage, indicating that it may be involved in the dimorphic transition of *S. schenckii*.

Other research projects are in process concerning additional proteins (Valentin-Berrios et al. 2009; González-Velazquez et al. 2012; Zhang et al. 2012, 2013) and lipids (Kitajima 2000) in the dimorphic transition of *S. schenckii*. Information regarding the dimorphic switch of *Sporothrix* spp., which is now essential to help us understand the mechanism of pathogenesis of this enigmatic *S. schenckii* species complex, is only starting to flow.

3.3 Thermotolerance

Not all isolates of *S. schenckii* from the environment have the ability to adapt to the temperature of the host's body. In 1979, Kwon-Chung showed that cutaneous strains of clinical origin are able to grow in vitro at 35 °C but not at 37 °C. Previous studies with young male mice inoculated intraperitoneally and intracardially showed that the lesions were more pronounced when mice were kept at lower room temperatures, thereby suggesting a connection between thermotolerance and virulence (Mackinnon and Conti-Díaz 1962; Hogan et al. 1996). De Albornoz et al. (1986) found that different isolates, in fixed cutaneous or disseminated form, can grow either at 27 °C or at 35 °C. In some recent work, isolates from Colombia with low thermotolerance showed a higher incidence of fixed cutaneous sporotrichosis; in contrast, isolates from Mexico with a higher thermotolerance showed a higher incidence of lymphocutaneous sporotrichosis (Mesa-Arango et al. 2002). Clinically, local thermotherapy has an excellent therapeutic effect and has been found to increase the rate of death of neutrophils in short-term assays (Hogan et al. 1996). The factor or genes responsible for thermotolerance are still unknown, as are the differences exhibited by the diverse clinically relevant species of *Sporothrix*.

3.4 Melanin Production

Melanin is considered a large group of polymers with diverse molecular structures typically with a black or dark brown color, formed by the oxidative polymerization of phenolic or indolic compounds. In fungi, melanin is synthesized in the cytoplasm and deposited in the CW or excreted as an extracellular polymer (Eisenman and Casadevall 2012). These pigments are not essential for fungal growth and development (Hogan et al. 1996). There are two types of melanin among fungi. The most frequent ones are 1,8-dihydroxynaphthalene melanin (DHN-melanin) as in *Aspergillus fumigatus* (Latsé 2001) and melanin via dihydroxyphenylalanine (DOPA) by which tyrosinases or laccases hydroxylate DOPA to dopaquinone (Langfelder et al. 2003) as in *Cryptococcus neoformans* (Polacheck and Kwon-Chung 1988). Other fungi produce still another type of soluble melanoid pigment from L-tyrosine called pyomelanin (Almeida-Paes et al. 2012). Observations suggest that melanin contributes to the virulence of fungal agents by protecting them from the host defense response, oxidizing agents, and hydrolytic enzymes, and reducing phagocytosis or the induction of cell death (Jacobson 2000). The *S. schenckii* species complex is able to synthesize melanin, which is evident in the varied colony pigmentation shown by different strains (Fig. 3.2). Generally, a fungal colony isolated from the patient initially shows a creamish color; the pigmentation then increases during the incubation time until, finally, some colonies turn black after 3 or 4 weeks (Rippon 1988). The presence of melanin has been associated with the virulence of this fungus (Rippon 1988; Hogan et al. 1996; Almeida-Paes et al. 2009; Madrid et al. 2010). *S. schenckii* has the ability to produce melanin in a very wide pH range, which is considered a survival advantage (Almeida-Paes et al. 2009). Melanin production varies in different strains of the fungus, and it has been reported that the strains with more melanin cause a faster infection than those that produce less pigment (Almeida-Paes et al. 2009; Madrid et al. 2010). These findings suggest that the melanized conidia CW prevents *S. schenckii* from being killed, enhances protection from ultraviolet (UV) solar irradiation, and, during infection, it affects host defense mechanisms by reducing phagocytosis and scavenging reactive oxygen and nitrogen species. Furthermore, melanized conidia from a *S. schenckii* wild type were more resistant than conidia from two melanin-deficient mutants to oxidant killing in vitro and to phagocytosis by human monocytes and murine macrophages (Romero-Martinez et al. 2000).

There is now evidence that *S. schenckii* isolates have the capacity to produce DHN- and DOPA-melanin (Romero-Martinez et al. 2000; Almeida-Paes et al. 2009, 2012), with this last pigment accumulating on the fungal CW of conidia, yeast cells, and hyphae (Almeida-Paes et al. 2009). Furthermore, recent research showed that not only *S. schenckii* but also *S. brasiliensis* and *S. globosa* were able to produce pyomelanin in the presence of tyrosine, thereby suggesting that this pigment could be involved in virulence (Almeida-Paes et al. 2012).

It appears that future research on microbial factors will have to allow for the clarification of so many unanswered questions regarding *Sporothrix* virulence.

3.5 Proteases

It has been postulated that certain extracellular enzymes, such as acid phosphatase, play an important role in the interaction of the yeast forms of *S. schenckii* with macrophages and other host cells (Garrison and Arnold 1983; Hogan et al. 1996). The activity of acid phosphatase is produced by conidia, mycelia, and the yeast forms of *S. schenckii*; greater amounts of activity are associated with the yeast extracts (Arnold et al. 1986; Hogan et al. 1996). Other studies have reported two different extracellular proteinases when *S. schenckii* is grown in media containing albumin and collagen as a nitrogen source (Tsuboi et al. 1987). Proteinase I is a 36.5 kDa serine protease that is inhibited by chymostatin, with an optimum pH of 6.0. Proteinase II is a 39 kDa aspartyl proteinase with an optimum pH of 3.5. The ability of *S. schenckii* to invade cutaneous tissues is associated with proteinases. Experimental mouse infections appear to confirm this, since the inoculation of inhibitors of these enzymes largely suppresses the formation of nodules and promotes spontaneous healing (Hogan et al. 1996). Recent studies by Sandoval-Bernal et al. (2010) suggest that the damage to the epithelial monolayer caused by the interaction of *S. schenckii* yeasts may be mediated by the action of proteases such as serine and aspartyl proteases, acid phosphatase, collagenase, and gelatinase, all of which have been thought to have a key role in the pathogenicity of the *S. schenckii* complex (Lima and Lopes Bezerra 1997). The presence of proteases can vary depending on the virulence of the species of the *S. schenckii* complex. Fernandes et al. (2013) found that highly virulent strains from isolates of *S. schenckii* show a number of secreted enzymes, such as proteinases, caseinases, gelatinases, DNase, and ureases, which have not been observed in the hypervirulent species of *S. brasiliensis*.

3.6 Cell Surface Components

The virulence of the *S. schenckii* complex has also been attributed to the presence of certain cell components involved in the interactions with the host, such as adhesins present on the cell surface, which increase adhesion to epithelial cells and extracellular matrix (Lima et al. 1999; Teixeira-Castelo et al. 2009; Ruiz-Baca et al. 2009), or to the ability to revert ergosterol peroxide to ergosterol, which has been proposed as an evasion mechanism of the fungal response (Sgarbi et al. 1997).

The CW of *S. schenckii* consists of alkali-soluble and alkali-insoluble glucans found in the same proportion in the two morphological phases of the fungus (Previato et al. 1979; López-Romero et al. 2011). The cell surface polysaccharides appear to influence macrophage function. In vitro studies have shown that yeast phagocytosis by peritoneal macrophages is inhibited by purified galactomannans and rhamnmannans from the cell surface of *S. schenckii* (Oda et al. 1983). One of its main components is a peptidorhamnmannan (Fig. 3.4), which was isolated from

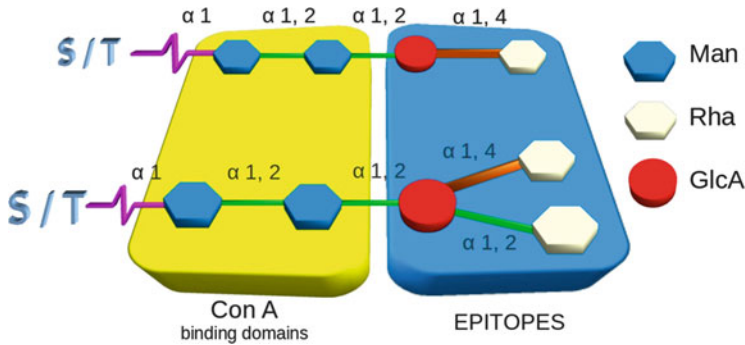


Fig. 3.4 General structure of the main antigenic epitopes and Con-A binding sites, described on the peptidorhamnomannan, both morphotypes (yeast and mycelium) of *S. schenckii* (Modified: Lopes-Alves et al. 1992)

the CW of *S. schenckii* yeast morphotype, a compound of polysaccharides such as D-mannose (50 %), L-rhamnose (33 %), galactose (1 %), and a peptide fraction of about 16 % (Lloyd and Bitoon 1971; Travassos et al. 1977; Lopes-Bezerra 2011; López-Romero et al. 2011).

The peptidorhamnomannans reacted with the carbohydrate-binding protein concanavalin A (ConA); this reactivity was associated with the presence of *O*-glycosidically linked chains. The peptidorhamnomannans are also recognized by antisera from patients with sporotrichosis, and it is thus capable of stimulating the immune mechanisms of these patients (Lloyd and Bitoon 1971; Travassos et al. 1977). The major immunogens of peptidorhamnomannans are associated with its carbohydrate residues, which are linked by *N*-glycosidic and *O*-glycosidic bonds present in both fungal morphotypes (Lopes-Alves et al. 1992, 1994; Lopes-Bezerra 2011). Fernandes et al. (1999) suggest that the *S. schenckii* conidia virulence may be determined by the CW sugar composition, with a molar ratio of rhamnose:mannose of 1.7:1.0 in cells grown for 4 days, and a ratio of 1.0:1.7 in conidia grown for 12 days.

Another component of the CW of *S. schenckii*, but of a lipid nature, seems to play an important role in the development of fungal mycosis, since it was able to inhibit it in *in vitro* phagocytosis assays (Carlos et al. 2003). The polysaccharide peptide, or peptidorhamnomannan, and the lipid antigen have been extensively studied: the kind of response they induce (Carlos et al. 1999, 2003; Maia et al. 2006; Verdan et al. 2012; Alegranci et al. 2013), the receptors involved in their recognition (Sassá et al. 2009, 2012; Negrini et al. 2013, 2014), and the corresponding signaling pathways that are activated (Gonçalves et al. 2015). However, which molecules are responsible for each of these effects is still not well known because they are handled as extracts not as a pure antigen.

One of the main antigens detected in the CW of both morphologies of *S. schenckii* is an adhesin-like glycoprotein with an apparent molecular weight of 70 kDa (gp70) (Fig. 3.5) that mediates the interaction of the fungus with

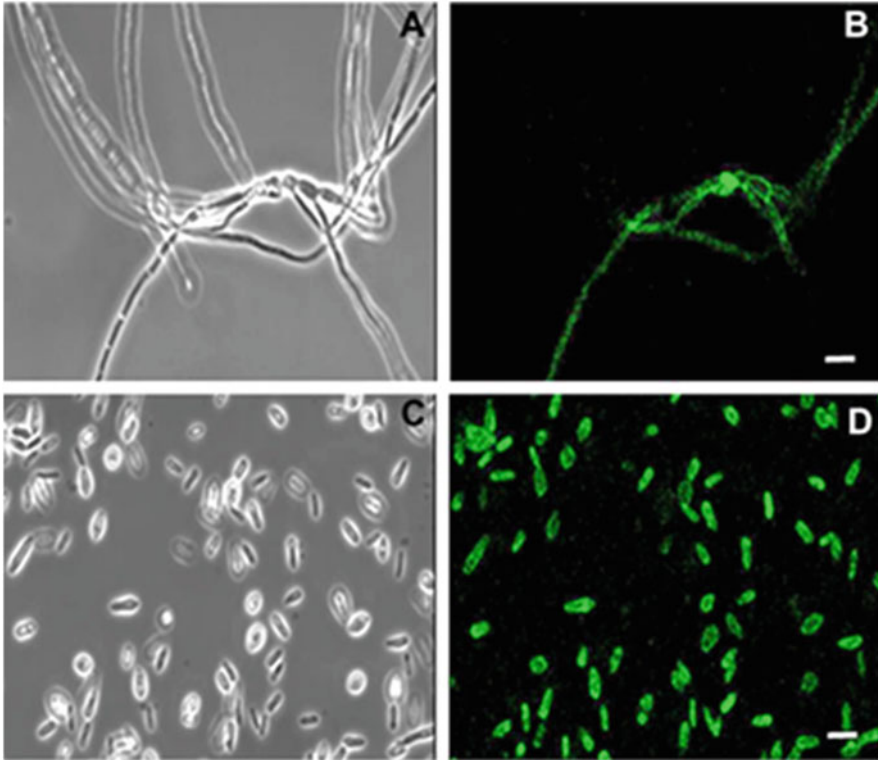


Fig. 3.5 Immunolocalization of gp70 in *S. schenckii* ATCC 58251 by confocal microscopy. Mycelium (a, b) and yeast cells (c, d). Bars = 10 μ m

extracellular matrix proteins and the host tissue (Ruiz-Baca et al. 2009; Teixeira-Castelo et al. 2009). Passive immunized mice with monoclonal antibodies against gp70 showed a *S. schenckii* infection that was less severe, but inflammatory response seems to be promoted, according to the cytokine profile expressed (Nascimento et al. 2008). gp70 is distributed in different subcellular compartments and is not restricted to the CW of *S. schenckii* and *S. brasiliensis* yeast-like cells, according to transmission electron microscopy studies. Furthermore, gp70 was detected in the extracellular space, suggesting that it could also be secreted (Castro et al. 2013), and has been associated with the virulence of *S. schenckii* complex species that kill infected mice (Fernandes et al. 2013). However, in more recent studies, an inverse relationship was found between the expression of this antigen and the virulence of clinical isolates of *S. brasiliensis* (Castro et al. 2013). gp70 was characterized by mass spectrometry, and the peptide sequences identified in the genome of *S. schenckii* and *S. brasiliensis* corresponded to a 3-carboxymuconate cyclase, an enzyme involved in the degradation of benzoate (Castro et al. 2013). Studies of the CW of *S. schenckii* s. str., *S. brasiliensis*, and *S. globosa* using two-dimensional polyacrylamide gels (2D PAGE) and Western blot (Fig. 3.6)

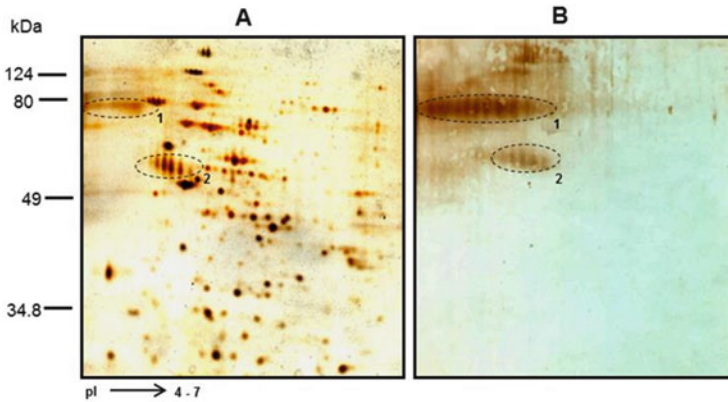


Fig. 3.6 2D-gel electrophoresis and immunoblotting analysis of CW proteins from *S. schenckii*. Proteins extracted from the CW of the yeast morphotype of *S. schenckii* ATCC 58251 were analyzed by 2D PAGE in gels that were stained by silver (a) or immunoblotted (b). Proteins marked with broken lines as 1 and 2 correspond to antigens gp70 (pIs 4.0–5.0) and gp60 (pIs 4.5–5.5), respectively (Ruiz-Baca et al. 2011)

identified two immunoreactive antigens of glycoprotein nature (Fig. 3.7) with apparent molecular weights of 70 (gp70) and 60 (gp60) kDa (Ruiz-Baca et al. 2011; Ruiz-Baca et al. 2014). However, characterization of peptide sequences by mass spectrometry indicated that gp70 and gp60 antigens corresponded to a 3-carboxymuconate cyclase.

A recent study evaluates the protein secretion of *S. brasiliensis*, *S. globosa*, and *S. schenckii s. str.* to define a virulence profile and connects it with the humoral immune response induced by these species (Fernandes et al. 2013). A great deal of heterogeneity of virulence among the different isolates of *S. schenckii s. str.* species was observed, and no correlation was found between virulence profile of isolates with thermotolerance or geographical origin. The most virulent strain induced mortality in a short time of infection, with a high fungal load mainly in lungs and spleen, colonizing the evaluated organs. This contrasted with a non-virulent strain, because no fungus was recovered from any organ, and infected mice survived to the end of the experiment. Interestingly, the most virulent isolate (*S. schenckii s. str.*) expressed less virulence factors as proteinase, caseinase, gelatinase, urease, and DNase activities, showing that the mechanism of pathogenesis is much more complex, involving these virulence factors and other molecules for evasion of the immune system (Fernandes et al. 2013). All of the isolates, including *S. brasiliensis* and *S. globosa*, secreted 60- and 46-kDa molecules, and probably represent important components that are common to all of the studied species. All isolates that had the 60-kDa molecule recognized by antisera from infected mice could kill them. On the other hand, sera from mice infected with non-virulent isolates did not recognize the 60-kDa molecule, which could be the immunodominant molecule in the *S. schenckii* complex. Using an immunoproteomic approach, Rodrigues et al. (2015) characterized proteins of potential significance in pathogenesis and

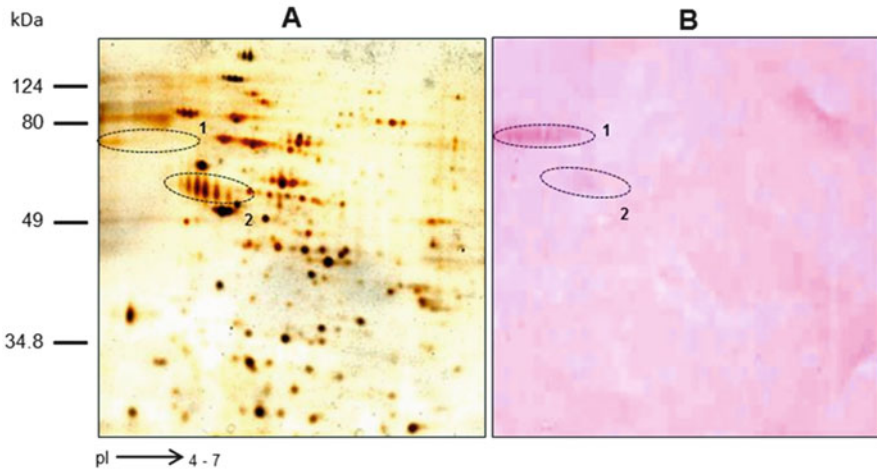


Fig. 3.7 Glycoprotein staining of 2D-PAGE of *S. schenckii* ATCC 58251 CW protein. Proteins extracted with hot SDS from yeast-like cells were analyzed by 2D-PAGE in gels that were stained by silver (a) or transfer to nitrocellulose membranes (b), they were stained with periodic acid-Schiff (PAS) reagent. Stained glycoproteins are indicated by spot numbers: 1, 70 kDa (pI 4.0–5.0); 2, 60 kDa (pI 4.5–5.5) (Ruiz-Baca et al. 2011)

invasion that trigger the humoral response during human sporotrichosis. The data showed gp70 to be a cross-immunogenic protein shared among pathogenic *Sporothrix* spp. (*S. brasiliensis*, *S. schenckii*, and *S. globosa*) but absent in the ancestral environmental (non-virulent) *S. mexicana*, supporting the hypothesis that gp70 plays key roles in pathogenicity. Also, identified by MALDI-TOF (MS/MS), the major antigen of human sporotrichosis (gp60–70) is 3-carboxymuconate cyclase. According to Rodrigues et al. (2015), a convergent humoral response highlights 3-carboxymuconate cyclase as an important target for serological diagnosis and for vaccine development among phylogenetically related agents of sporotrichosis. The MS/MS data showed that the 60 kDa molecule reported as a virulence factor in the *S. schenckii* complex by Fernandes et al. (2013) is a variant of gp70, as both gp60 and gp70 were identified with the same peptide sequences. gp70/gp60 is a highly polymorphic protein, experimentally ranging from 55 to 73 kDa and 4.33 to 4.85 pI. These physicochemical variations seem to be the result of post-translational modifications that include isoforms and/or glycoforms. Furthermore, the protein regarded as 60 kDa is a complex of iso-glycoforms oscillating between 60 and 70 kDa. Other immunoreactive proteins in human sporotrichosis, related to signal transduction, pathogenicity, or metabolic/energetic processes, such as F-type H⁺-transporting ATPase subunit beta, saccharopepsin, signal peptidase protein, guanine nucleotide-binding protein (G protein), and catalase/oxidase, have been identified. In addition, a common hypothetical protein was identified in *S. brasiliensis*, *S. schenckii*, and *S. globosa*, and an exclusive hypothetical protein in *S. mexicana*.

More studies should be conducted to characterize virulence profiles and virulence factors, correlating the pigmentation of conidia (Romero-Martinez et al. 2000), thermotolerance (Dixon et al. 1991), routes of infection (Tachibana et al. 1998), origin (Kong et al. 2006; Brito et al. 2007), culture conditions and CW (Fernandes et al. 1999), and secreted components (Fernandes et al. 2013), to the immunogenicity among the *S. schenckii* complex for a better understanding of sporotrichosis pathogenesis.

3.7 Conclusions and Future Perspectives

Although some advances have been made in the identification of components and factors of virulence in the *S. schenckii* complex, much work remains to be done. Some of the biggest problems we face when dealing with this dimorphic fungus are its genetic complexity and the lack of an adequate transformation system to characterize virulence factors. The recent release of the genome of *S. schenckii* and of *S. brasiliensis* will promote molecular studies and comparative genomics, as well as transcriptomic and proteomic analyses, of the components and virulence factors involved in the pathogenesis of the *S. schenckii* species complex. This will contribute to the discovery and characterization of new molecules with therapeutic target potential, and of vaccines against this mycosis of global importance.

Acknowledgments This work was partially supported by grant CB-2011 No. 167737 from the Consejo Nacional de Ciencia y Tecnología (CONACyT, México) to ERB. CAAF thanks the scholarship No. 201509 granted by the Consejo Nacional de Ciencia y Tecnología (CONACyT), México. The authors wish to thank Amelia Pérez Mejía for her documental assistance and Omar Posada Villarreal for editing Fig. 3.4.

References

- Alegranci P, Abreu-Ribeiro LC, Souza-Ferreira L et al (2013) The predominance of alternatively activated macrophages following challenge with cell wall peptide-polisaccharide after prior infection with *Sporothrix schenckii*. *Mycopathologia* 176:57–65
- Almeida-Paes R, Frases S, Fialho MPC et al (2009) Growth conditions influence melanization of Brazilian clinical *Sporothrix schenckii* isolates. *Microbes Infect* 11:554–562
- Almeida-Paes R, Frases S, Araújo Gde S et al (2012) Biosynthesis and functions of a melanoid pigment produced by species of the *Sporothrix* complex in the presence of L-tyrosine. *Appl Environ Microbiol* 78:8623–8630
- Aquino-Piñero E, Rodríguez del Valle N (2002) Characterization of a protein kinase C gene in *Sporothrix schenckii* and its expression during the yeast-to-mycelium transition. *Med Mycol* 40:185–199
- Arillaga-Moncrieff CJ, Mayayo E et al (2009) Different virulence levels of the species of *Sporothrix* in a murine model. *Clin Microbiol Infect* 15:651–655
- Arnold WN, Mann LC, Sakai KH et al (1986) Acid phosphatases of *Sporothrix schenckii*. *J Gen Microbiol* 132:3421–3432

- Brito MM, Conceição-Silva F, Morgado FN et al (2007) Comparison of virulence of different *Sporothrix schenckii* clinical isolates using experimental murine model. *Med Mycol* 45: 721–729
- Carlos IZ, Sgarbi GBD, Placeres CP (1999) Host organism defense by a peptide-polysaccharide extracted from the fungus *Sporothrix schenckii*. *Mycopathologia* 144:9–14
- Carlos IZ, Sgarbi DBG, Santos GC et al (2003) *Sporothrix schenckii* inhibits macrophage phagocytosis: Involvement of nitric oxide and tumour necrosis factor- α . *Scand J Immunol* 57:214–220
- Casadevall A, Pirofski LA (1999) Host-pathogen interactions: Redefining the basic concepts of virulence and pathogenicity. *Infect Immun* 67:3703–3713
- Casadevall A, Pirofski LA (2001) Host-pathogen interactions: the attributes of virulence. *J Infect Dis* 184:337–344
- Casadevall A, Pirofski LA (2003) The damage-response framework of microbial pathogenesis. *Nat Rev Microbiol* 1:17–24
- Casadevall A, Steenbergen JN, Nosanchuk JD (2003) Ready made virulence and dual use virulence factors in pathogenic environmental fungi the *Cryptococcus neoformans* paradigm. *Curr Opin Microbiol* 6:332–337
- Castro RA, Kubitschenk-Barreira PH, Teixeira PA et al (2013) Differences in cell morphometry, cell wall topography and gp70 expression correlate with the virulence of *Sporothrix brasiliensis* clinical isolates. *PLoS One* 8, e75656
- Colón-Colón W, Rodríguez del Valle N (1993) Studies on phase transitions in *Sporothrix schenckii*: possible involvement of protein kinase C. In: Vanden Bossche H, Odds FC, Kerridge D (eds) *Dimorphic fungi in biology and medicina*. Plenum, New York, pp 225–246
- de Albornoz MB, Mendoza M, de Torres ED (1986) Growth temperatures of isolates of *Sporothrix schenckii* from disseminated and fixed cutaneous lesions of sporotrichosis. *Mycopathologia* 95: 81–83
- de Meyer EM, de Beer W, Summerbell RC et al (2008) Taxonomy and phylogeny of new wood- and soil-inhabiting *Sporothrix* species in the *Ophiostoma stenoceras-Sporothrix schenckii* complex. *Mycologia* 100:647–661
- Dixon DM, Salkin IF, Duncan RA et al (1991) Isolation and characterization of *Sporothrix schenckii* from clinical and environmental sources associated with the largest U.S. epidemic of sporotrichosis. *J Clin Microbiol* 29:1106–1113
- Eisenman HC, Casadevall A (2012) Synthesis and assembly of fungal melanin. *Appl Microbiol Biotechnol* 93:931–940
- Fernandes GS, Oliveira-dos Santos P, Rodrigues AM et al (2013) Characterization of virulence profile, protein secretion and immunogenicity of different *Sporothrix schenckii sensu stricto* isolates compared with *S. globosa* and *S. brasiliensis*. *Virulence* 4:241–249
- Fernandes KS, Mathews HL, Lopes Bezerra LM (1999) Differences in virulence of *Sporothrix schenckii* conidia related to culture conditions and cell-wall components. *J Med Microbiol* 48: 195–203
- Garrison RG, Arnold WN (1983) Cytochemical localization of acid phosphatases in the dimorphic fungus *Sporothrix schenckii*. *Curr Microbiol* 9:253–258
- Gauthier G, Klein BS (2008) Insights into fungal morphogenesis and immune evasion: fungal conidia, when situated in mammalian lungs, may switch from mold to pathogenic yeasts or spore-forming spherules. *Microbe Wash DC* 3:416–423
- Gonçalves AC, Maia DCG, Ferreira LS et al (2015) Involvement of major components from *Sporothrix schenckii* cell wall in the caspase-1 activation, nitric oxide and cytokines production during experimental sporotrichosis. *Mycopathologia* 179:21–30
- González-Velázquez W, Gonzalez-Mendes R, Rodriguez del Valle N (2012) Characterization and ligand identification of a membrane progesterone receptor in fungi: existence of a novel PAQR in *Sporothrix schenckii*. *BMC Microbiol* 12:194
- Hogan LH, Bruce SK, Levitz SM (1996) Virulence factors of medically important fungi. *Clin Microbiol Rev* 9:469–488

- Hou B, Zhang Z, Zheng F et al (2013) Molecular cloning, characterization and differential expression of DRK1 in *Sporothrix schenckii*. *Int J Mol Med* 31:99–104
- Howard DH (1961) Dimorphism of *Sporotrichum schenckii*. *J Bacteriol* 81:464–469
- Jacobson ES (2000) Pathogenic roles for fungal melanins. *Clin Microbiol Rev* 13:708–717
- Kitajima Y (2000) Structural and biochemical characteristics of pathogenic fungus: cell walls, lipids and dimorphism, and action modes of antifungal agents. *Nippon Ishinkin Gakkai Zasshi* 41:211–217
- Kong X, Xiao T, Lin J et al (2006) Relationships among genotypes, virulence and clinical forms of *Sporothrix schenckii* infection. *Clin Microbiol Infect* 12:1077–1081
- Kwon-Chung KJ (1979) Comparison of isolates of *Sporothrix schenckii* obtained from fixed cutaneous lesions with isolates from other types of lesions. *J Infect Dis* 139:424–431
- Langfelder K, Streibel M, Jahn B et al (2003) Biosynthesis of fungal melanins and their importance for human pathogenic fungi. *Fungal Genet Biol* 38:143–158
- Latgé JP (2001) The pathobiology of *Aspergillus fumigatus*. *Trends Microbiol* 9:382–389
- Lima OC, Lopes Bezerra LM (1997) Identification of Concanavalin A-binding antigen of the cell surface of *Sporothrix schenckii*. *J Med Vet Mycol* 35:167–172
- Lima OC, Figueiredo CC, Pereira BA et al (1999) Adhesion of the human pathogen *Sporothrix schenckii* to several extracellular matrix proteins. *Braz J Med Biol Res* 32:651–657
- Lloyd KO, Bitoon MA (1971) Isolation and purification of a peptidorhamnomannan from the yeast form of *Sporothrix schenckii* structural and immunochemical studies. *J Immunol* 107:663–671
- Lopes-Alves LM, Mendoca-Previano L, Fournet B et al (1992) O-glycosidically linked oligosaccharides from peptidorhamnomannans of *Sporothrix schenckii*. *Glycoconj J* 9:75–81
- Lopes-Alves L, Travassos LR, Previano JO et al (1994) Novel antigenic determinants from peptidorhamnomannans of *Sporothrix schenckii*. *Glycobiology* 4:281–288
- Lopes-Bezerra LM (2011) *Sporothrix schenckii* cell wall peptidorhamnomannans. *Front Microbiol* 2:243
- López-Romero E, Reyes-Montes MR, Pérez A et al (2011) *Sporothrix schenckii* complex and sporotrichosis, an emerging health problem. *Future Microbiol* 6:85–102
- Mackinnon JE, Conti-Díaz IA (1962) The effect of temperature on sporotrichosis. *Sabouraudia* 2:56–59
- Madrid IM, Xavier MO, Mattei AS et al (2010) Role of melanin in the pathogenesis of cutaneous sporotrichosis. *Microbes Infect* 12:162–165
- Maia DC, Sassá MF, Polesi MC (2006) Influence of Th1/Th2 cytokines and nitric oxide in murine systemic infection induced by *Sporothrix schenckii*. *Mycopathologia* 161:11–19
- Marimon R, Gene J, Cano J et al (2006) Molecular phylogeny of *Sporothrix schenckii*. *J Clin Microbiol* 44:3251–3256
- Marimon R, Cano J, Gene J et al (2007) *Sporothrix brasiliensis*, *Sporothrix globosa* and *Sporothrix mexicana*, three new *Sporothrix* species of clinical interest. *J Clin Microbiol* 45:3198–3206
- Marimon R, Gene J, Cano J et al (2008) *Sporothrix luriei*: a rare fungus from clinical origin. *Med Mycol* 46:621–625
- Mesa-Arango AC, Reyes-Montes MR, Perez-Mejia A et al (2002) Phenotyping and genotyping of *Sporothrix schenckii* isolates according to geographic origin and clinical form of sporotrichosis. *J Clin Microbiol* 40:3004–3011
- Nascimento RC, Espíndola NM, Castro RA et al (2008) Passive immunization with monoclonal antibody against 70-kDa putative adhesin of *Sporothrix schenckii* induces protection in murine sporotrichosis. *Eur J Immunol* 38:3080–3089
- Negrini TC, Ferreira LS, Alegranci P et al (2013) Role of TLR-2 and fungal surface antigens on innate immune response against *Sporothrix schenckii*. *Immunol Invest* 42:36–48
- Negrini TC, Ferreira LS, Arthur RA et al (2014) Influence of TLR-2 in the immune response in the infection induced by fungus *Sporothrix schenckii*. *Immunol Invest* 43:370–390
- Nemecek JC, Wüthrich M, Klein BS (2006) Global control of dimorphism and virulence in fungi. *Science* 312:583–588

- Oda LM, Kubelka CF, Alviano CS et al (1983) Ingestion of yeast forms of *Sporothrix schenckii* by mouse peritoneal macrophages. *Infect Immun* 39:497–504
- Polacheck I, Kwon-Chung KJ (1988) Melanogenesis in *Cryptococcus neoformans*. *J Gen Microbiol* 134:1037–1041
- Previato JO, Gorin PAJ, Haskins RH et al (1979) Soluble and insoluble glucans from different types of the human pathogen *Sporothrix schenckii*. *Exp Mycol* 3:92–105
- Rippon JW (1988) Sporotrichosis. In: Rippon JW (ed) *Medical mycology*. The W. B. Saunders Company, Philadelphia, PA, pp 325–352
- Rivera-Rodríguez N, Rodríguez del Valle N (1992) Effects of calcium ions on the germination of *Sporothrix schenckii* conidia. *J Med Vet Mycol* 30:185–195
- Rodrigues AM, Kubitschek-Barreira PH, Fernandes GF et al (2015) Immunoproteomic analysis reveals a convergent humoral response signature in the *Sporothrix schenckii* complex. *J Proteomics* 115:8–22
- Rodríguez-Caban J, González-Velázquez W, Pérez-Sánchez L et al (2011) Calcium/calmodulin kinase 1 and its relation to thermotolerance and hsp90 in *Sporothrix schenckii*: an RNAi and yeast two-hybrid study. *BMC Microbiol* 11:162
- Rodríguez-Del Valle N, Rosario M, Torres-Blasini G (1983) Effects of pH, temperature, aeration and carbon source on the development of the mycelial or yeast forms of *Sporothrix schenckii* from conidia. *Mycopathologia* 82:83–88
- Romero-Martínez R, Wheeler M, Guerrero-Plata A et al (2000) Biosynthesis and functions of melanin in *Sporothrix schenckii*. *Infect Immun* 68:3696–3703
- Ruiz-Baca E, Toriello C, Perez-Torres A et al (2009) Isolation and some properties of a glycoprotein of 70 kDa(gp70) from the cell wall of *Sporothrix schenckii* involved in fungal adherence to dermal extracellular matrix. *Med Mycol* 47:185–196
- Ruiz-Baca E, Mora-Montes HM, López-Romero E et al (2011) 2D-immunoblotting analysis of *Sporothrix schenckii* cell wall. *Mem Inst Oswaldo Cruz* 106:248–250
- Ruiz-Baca E, Hernández-Mendoza G, Cuéllar-Cruz M et al (2014) Detection of two immunoreactive antigens of the cell wall of *Sporothrix brasiliensis* and *S. globosa*. *Diagn Microbiol Infect Dis* 79:328–330
- Sandoval-Bernal G, Barbosa-Sabanero G, Shibayama M et al (2010) Cell wall glycoproteins participate in the adhesion of *Sporothrix schenckii* to epithelial cells. *Mycopathologia* 171: 251–259
- Sassá MF, Sauri AET, Souza LF et al (2009) Response of macrophage toll-like receptor 4 to a *Sporothrix schenckii* lipid extract during experimental sporotrichosis. *Immunology* 128:301–309
- Sassá MF, Souza LF, de Abreu-Ribeiro LC et al (2012) Immune response against *Sporothrix schenckii* in TLR-4-deficient mice. *Mycopathologia* 174:21–30
- Serrano S, Rodríguez del Valle N (1990) Calcium uptake and efflux during the yeast to mycelium transition in *Sporothrix schenckii*. *Mycopathologia* 112:1–9
- Sgarbi GDB, Ribeiro-Da Silva AJ, Carlos IZ et al (1997) Isolation of ergosterol peroxide and its reversion to ergosterol in the pathogenic fungus *Sporothrix schenckii*. *Mycopathologia* 139: 9–14
- Szanzlo P (1985) *Fungal dimorphism with emphasis on fungi pathogenic for humans*. Plenum Press, New York, pp 3–67
- Tachibana T, Matsuyama T, Mitsuyama M (1998) Characteristic infectivity of *Sporothrix schenckii* to mice depending on routes of infection and inherent fungal pathogenicity. *Med Mycol* 36: 21–27
- Teixeira-Castelo PA, Alves de Castro R, Nascimento-Cícera R et al (2009) Cell Surface expression of adhesins for fibronectin correlates with virulence in *Sporothrix schenckii*. *Microbiology* 155:3730–3738
- Travassos LR, de Souza W, Mendoza-Previato L et al (1977) Location and biochemical nature of surface components reacting with concanavalin A in different cell types of *Sporothrix schenckii*. *Exp Mycol* 1:293–305

- Tsuboi R, Sanada T, Takamori K et al (1987) Isolation and properties of extracellular proteinases from *Sporothrix schenckii*. *J Bacteriol* 169:4104–4109
- Valentin-Berrios S, González-Velázquez W, Pérez-Sánchez L et al (2009) Cytosolic phospholipase A2: a member of the signalling pathway of a new G protein α subunit in *Sporothrix schenckii*. *BMC Microbiol* 9:100
- Valle-Avilés L, Valentin-Berrios S, González-Méndez RR et al (2007) Functional, genetic and bioinformatic characterization of a calcium/calmodulin kinase gene in *Sporothrix schenckii*. *BMC Microbiol* 7:107
- Verdan FF, Faleiros JC, Ferreira LS (2012) Dendritic cells are able to differentially recognize *Sporothrix schenckii* antigens and promote Th1/Th17 response *in vitro*. *Immunobiology* 217: 788–794
- Zhang Z, Hou B, Xin Y et al (2012) Protein profiling of the dimorphic pathogenic fungus, *Sporothrix schenckii*. *Mycopathologia* 173:1–11
- Zhang Z, Hou B, Zheng F et al (2013) Molecular cloning, characterization and differential expression of a *Sporothrix schenckii* STE20-like protein kinase SsSte20. *Int J Mol Med* 31: 1343–1348

Iracilda Zeppone Carlos *Editor*

Sporotrichosis

New Developments and
Future Prospects

 Springer

Chapter 8

Diagnosis of Sporotrichosis: Current Status and Perspectives

Rosely M. Zancope-Oliveira, Rodrigo Almeida-Paes, Estela Ruiz-Baca, and Conchita Toriello

Abstract Definitive diagnosis of sporotrichosis is based on fungal detection in culture. Microscopic methods for the detection of *Sporothrix* yeast cells in clinical samples have low sensitivity. Although culture methods have high sensitivity, they also have some limitations, such as the time required to conclude the diagnosis, usually from 10 to 15 days, and the difficulty of obtaining an adequate clinical specimen for the test in cases of extracutaneous sporotrichosis. Serological methods are useful tools for a presumptive diagnosis of this infection. The most-used antigenic *Sporothrix* molecules are the peptide-rhamnomannan and secreted exoantigens. The enzyme-linked immunosorbant assay (ELISA) technique using the peptide-rhamnomannan has high efficiency, and it is useful in the serological follow-up of infection. Exoantigens were first used in immunoprecipitation and agglutination tests, but they have been used more recently in immunoenzymatic tests, with high sensitivity and specificity for both human and feline disease. A glycoprotein of 70 kDa was purified from *Sporothrix* exoantigens, presenting high immunogenicity, which allows its use in the development of more sensitive and specific methods for sporotrichosis serodiagnosis. Molecular methods of diagnosis can lower the time for diagnosis conclusion, but described methodologies in this field are scarce. In conclusion, the diagnosis of sporotrichosis is a challenging field, and the development of new serological and molecular diagnostic methods is mandatory.

R.M. Zancope-Oliveira (✉)

Fundação Oswaldo Cruz, Instituto de Pesquisa Clínica Evandro Chagas, Rio de Janeiro, RJ, Brazil

e-mail: rosely.zancope@ini.fiocruz.br; rzancope@gmail.com

R. Almeida-Paes

Laboratório de Micologia, Instituto Nacional de Infectologia Evandro Chagas, Fundação Oswaldo Cruz, Rio de Janeiro, Brazil

E. Ruiz-Baca

Departamento de Biología Celular y Molecular, Facultad de Ciencias Químicas, Universidad Juárez del Estado de Durango, Durango, Dgo, Mexico

C. Toriello

Departamento de Microbiología y Parasitología, Facultad de Medicina, Universidad Nacional Autónoma de México, México D.F. 04510, Mexico

Keywords Exoantigens • Peptide-rhamnomannan • Serodiagnosis • Sporotrichin • Molecular methods

8.1 Introduction

Mycoses can be challenging to diagnose, and accurate interpretation of laboratory data is important to ensure appropriate treatment. Although the clinical manifestations of sporotrichosis are well described, the diagnosis of this mycosis cannot be based on clinical information alone because the symptoms of sporotrichosis overlap with those of other diseases.

Sporotrichosis is classically diagnosed by correlating clinical, epidemiological, and laboratory data (Zancope-Oliveira et al. 2011). Typical laboratory analyses include microscopic examination using 10 % potassium hydroxide or 4 % sodium hydroxide to detect parasitic cigar-shaped, budding, yeast-like cells. These fungal cells are small (2–6 μm in diameter), rare, and difficult to detect during direct examination of specimens obtained from human patients (Kwon-Chung and Bennett 1992) or from domestic animals, such as dogs (Schubach et al. 2006). On the other hand, when this test is performed on skin biopsies collected from cats infected with *Sporothrix schenckii*, yeast cells are easily observed because cats have a high fungal burden on their lesions (Schubach et al. 2004). Microscopic methods for yeast detection in clinical samples are of low sensitivity (Barros et al. 2011), and asteroid body observation varies among different works (Quintella et al. 2011). However, definitive diagnosis of sporotrichosis is based on fungal detection in culture (Zhang et al. 2011). Cultivation of clinical specimens in mycological media such as Sabouraud dextrose agar or mycobiotic agar yields white filamentous colonies that become brown to black after a few days. Subculturing these colonies in brain–heart infusion at 35–37 °C results in white to creamy yeast-like colonies (Barros et al. 2011). *S. schenckii* identification is based on the macro- and micro-morphologies of the mycelial (Fig. 8.1) and yeast forms (Zancope-Oliveira et al. 2011). However, these characteristics do not differentiate the newly described species of the *Sporothrix* complex. To physiologically differentiate the species within this complex, other tests such as carbohydrate assimilation (especially sucrose and raffinose), growth rates at 30 and 37 °C, as well as production of dematiaceous sessile conidia are necessary (Marimon et al. 2007, 2008). However, discrepancies between physiological and molecular methods of identification have been described (Oliveira et al. 2011). Moreover, although positive cultures provide the strongest evidence for sporotrichosis, there are some significant limitations. In particular, in some manifestations of the disease, such as *S. schenckii*-induced arthritis, the collection of material for culture is difficult (Morris-Jones 2002). In addition, sporotrichosis may be mistaken for other infections, such as tuberculosis, leishmaniasis, paracoccidioidomycosis, gummatous syphilis, and chromoblastomycosis (Rippon 1988; Sharma et al. 2005).

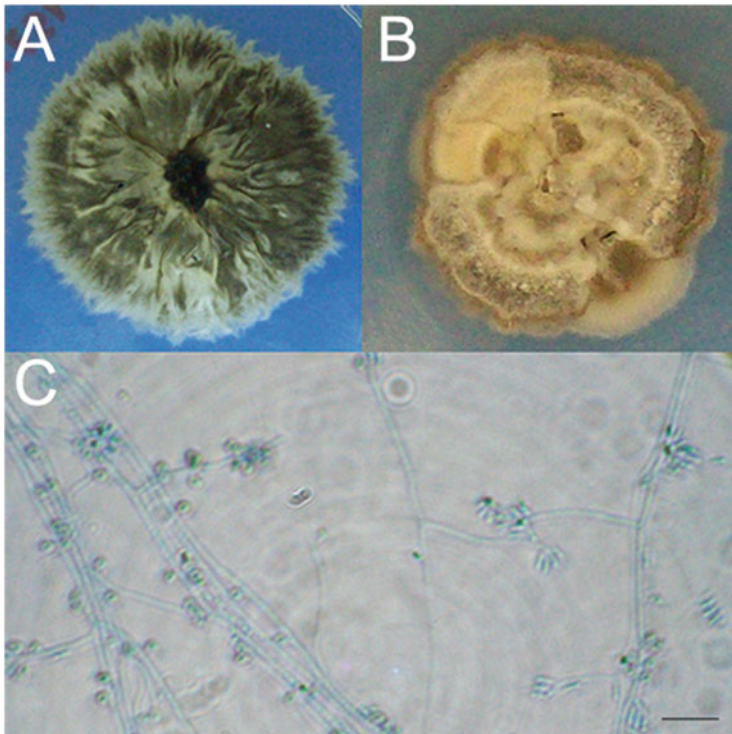


Fig. 8.1 Morphologic characteristics of the mycelial form of the *Sporothrix* complex. (a) *Sporothrix schenckii* sensu stricto colony on potato dextrose agar, incubated at 30 °C for 21 days. (b) Colony of a *S. brasiliensis* strain, showing a similar morphology to the *S. schenckii* strain. (c) Slide culture of the *S. schenckii* strain, showing hyaline conidia on sympodial conidiophores and dematiaceous conidia on denticles arising from the hyphae. Bar 10 μ m

Non-culture methods have been developed to improve the rate and speed of diagnosis. Additional diagnostic tools are currently available for diagnosis of sporotrichosis to supplement culture and microscopic examination. These laboratory tests have a rapid turnaround time and reasonable specificity and sensitivity. For instance, serological techniques involving antibody detection have been developed using different methodologies. Molecular methods to detect *Sporothrix* species complex DNA in clinical specimens, including tissue fragments, are also being studied in several laboratories to facilitate rapid diagnosis of infection (Ruiz-Baca et al. 2013; Oliveira et al. 2014). The results from the described tests can provide a presumptive diagnosis of sporotrichosis and require clinical correlation for the correct evaluation and determination of the final diagnosis.

Serological techniques are usually simpler than culture and very useful in the diagnosis and follow-up of patients with sporotrichosis. The following serologic tests have been applied in the diagnosis of Diagnostic methods: agar gel immunodiffusion (ID), slide (SLA), tube (TA) and latex agglutination (LA), complement

fixation reaction (CF), immunofluorescence (IF) (Blumer et al. 1973), immunoelectrophoresis (IEP) (Albornoz et al 1984), and immunoenzyme assays in several formats, such as ELISAs, and immunoblots. These techniques have advanced considerably in recent decades because of the development of innovative detection schemes in the identification of relevant *Sporothrix* spp. antigens. However, the literature concerning the serodiagnosis of sporotrichosis is neither extensive nor diverse.

A range of antigenic preparations, derived both from whole yeast cells and from culture filtrate in their crude and/or purified states, have been applied in serological tests, which has resulted in high cross-reactivity, one of the most persistent problems found in the serodiagnosis of sporotrichosis. Moreover, these antigenic preparations are highly variable, making it very difficult to standardize diagnostic techniques in different laboratories.

The next sections focus on the main antigens and serologic methods applied for the presumptive diagnosis of sporotrichosis, as well as the application of some antigenic preparations in skin tests and molecular diagnosis.

8.2 Antigen Detection

The antigenic composition of the members of the *Sporothrix* complex is poorly understood. The most studied molecules with immunological reactivity of these fungi are the peptide-rhamnomannan, the exoantigens, and the newly described gp-70.

The *Sporothrix* peptide-rhamnomannan is a fraction of the fungal cell wall that presents an affinity to concanavalin A(Con-A) and that reacts with antibodies present in sera from patients with sporotrichosis (Lloyd and Bitoon 1971). Through a western blot analysis, this Con-A binding fraction of the *Sporothrix* cell wall was characterized as a mixture of three antigenic fractions of 84, 70, and 58 kDa. Moreover, through a β -elimination procedure, it was verified that the 70-kDa molecule is a deglycosylated form of the 84-kDa antigen (Lopes-Bezerra and Lima 1997). This antigen is stable, and its immunological reactivity does not significantly change if different *Sporothrix* strains are used in the extract preparation (Bernardes-Engemann et al. 2009). The potential application of this antigen to the serodiagnosis of sporotrichosis was initially suggested by the observation that cross-reactions with paracoccidioidomycosis, cryptococcosis, aspergillosis, candidiasis, and histoplasmosis were absent in the Con-A binding fraction of the cell wall peptide-rhamnomannan (Loureiro Y Penha and Lopes-Bezerra 2000). Later, an ELISA to detect immunoglobulin (Ig)-G in serum from patients with several clinical forms of sporotrichosis was described using this specific antigenic fraction, with a sensitivity of 90 % and specificity of 80 % (Bernardes-Engemann et al. 2005). The Con-A binding fraction of the *Sporothrix* cell wall peptide-rhamnomannan can also be used to detect antibodies in the synovial fluid (Costa

et al. 2008) and to monitor therapeutic response to antifungal treatment (Orofino-Costa et al. 2009).

The exoantigens from *Sporothrix* spp. were first applied in several immunological assays, such as IEP, LA, and double ID (Karlin and Nielsen 1970; Blumer et al. 1973; Casserone et al. 1983; Albornoz et al. 1984). However, there were no standard procedures for the production of the antigenic extracts used. In fact, changes in sugar composition of the exoantigens occur during *Sporothrix* growth, indicating a need for standardization (Takata and Ishizaki 1983). Differences in exoantigen composition and immunological reactivity were also related to the morphological state of the fungus (Albornoz et al. 1984), to the culture medium employed (Mendoza et al. 2002; Fernandes et al. 2009), and to the geographical origin of strains (Fernandes et al. 2009). Differences in exoantigen composition among the species of the *Sporothrix* complex are poorly studied, but it does not appear to significantly impact the antigenic composition of secreted molecules. A recent study showed heterogeneous protein profiles of exoantigens obtained from the mycelial form of *S. brasiliensis*, *S. globosa*, and *S. schenckii sensu stricto* in Sabouraud dextrose medium. The proteins of 60 and 46 kDa were observed in all extracts, regardless of species. Moreover, it was not possible to characterize specific secreted molecules for these species (Fernandes et al. 2013). Similar observations were obtained with the secreted antigens from the yeast form of *S. brasiliensis* and *S. schenckii s. str.* A molecule of 85 kDa was detected in both species, and no significant differences in antigenic composition or immunological reactivity were observed among the species (Almeida-Paes et al. 2012).

In a study of the yeast-phase *Sporothrix* exoantigens, it was verified that a 70-kDa antigenic fraction was always reactive against serum antibodies present in experimentally infected mice after 14 days of infection (Nascimento and Almeida 2005). Further studies against this antigen showed that a monoclonal antibody with affinity to this protein was able to enhance phagocytosis by macrophages. Moreover, this monoclonal antibody reduced the fungal burden and inhibited the *Sporothrix* interaction with the extracellular matrix (Nascimento et al. 2008). The role of this antigen as an adhesin was elucidated in subsequent studies (Ruiz-Baca et al. 2009; Teixeira et al. 2009). It is interesting to note that an immunological reactivity against the *Sporothrix* gp-70 was consistently observed in these studies, which encourages its use in the serodiagnosis of sporotrichosis. Furthermore, this antigen is produced by the three major species of the *Sporothrix* complex (*S. brasiliensis*, *S. globosa*, and *S. schenckii*), thus allowing the sporotrichosis diagnosis regardless of the infective species (Ruiz-Baca et al. 2014).

In general, serological tests as an aid for diagnosis do not use purified or recombinant antigens, because described immune reactive proteins are scarce, especially for the newly described *Sporothrix* species such as *S. brasiliensis*. An immunoblot assay allied with computer-based analysis was used to identify putative antigenic molecules in cell-free extracts of both morphological phases of this fungus, and to delineate antigenic polymorphism among seven *S. brasiliensis* isolates and one *S. schenckii* Brazilian strain. The mycelial and yeast phase of the fungus originated 14 and 23 reactive bands, respectively, which varied in intensity.

An 85-kDa antigen, verified in the yeast phase of the fungus, was observed in all strains used, and the immunodominant protein was identified. However, this protein cross-reacted with sera samples from patients infected with other pathogens (Almeida-Paes et al. 2012). It was also demonstrated that the use of different strains or even the morphological form of *Sporothrix* isolates could have an effect on the antigenic reactivity of a *Sporothrix* extract. Therefore, an adequate standardization of antigens must be produced before their general use in the serodiagnosis of sporotrichosis.

8.3 Antibody Detection

8.3.1 Immunoprecipitation and Agglutination Techniques

Immunoprecipitation and agglutination methodologies were first used in the diagnosis of sporotrichosis in the period 1970–1980 (Albornoz et al. 1984; Blumer et al. 1973; Casserone et al. 1983; Karlin and Nielsen 1970). The first TA and CF tests for sporotrichosis were reported in 1910 (Widal et al. 1910), and a diagnostic precipitin test that employed a polysaccharide antigen was subsequently described by González-Ochoa and Figueroa (1947). The ID test for sporotrichosis usually does not cross-react with sera from patients with chromoblastomycosis or leishmaniasis, infectious diseases with similar clinical manifestations (Albornoz et al. 1984). IEP has also been used, and in all positive cases, an anodic arc, called an S arc, is observed (Albornoz et al. 1984). Both methodologies that use an antigenic complex from fungal culture filtrate are highly sensitive. TA and LA both have high sensitivity and specificity and have been used for sporotrichosis serodiagnosis since the 1970s (Blumer et al. 1973; Casserone et al. 1983; Karlin and Nielsen 1970). However, these tests lack sensitivity in cases of cutaneous sporotrichosis (Albornoz et al. 1984; Rippon 1988) and do not enable the determination of the immunoglobulin isotype involved. The lack of standardization of reagents and methodologies applied in these techniques means they are not routinely used in the diagnosis of sporotrichosis in clinical laboratories.

8.3.2 Immunoenzymatic Assays

The serodiagnosis of this mycosis has increasingly used immunoassays. The first immunoblot assay used for diagnosis of sporotrichosis dates back to 1989, when exoantigen preparations from the *S. schenckii* yeast form showed 100 % sensitivity and 95 % specificity for the detection of antibodies (Scott and Muchmore 1989). Later, another immunoassay (ELISA) was developed, using the Con-A binding peptide-rhamnomannan from the *S. schenckii* yeast cell wall, and antibodies were

detected in 35 serum samples from patients with culture-proven sporotrichosis, resulting in 100 % sensitivity. However, the specificity was lower than previous tests because there was cross-reactivity with sera from patients with cutaneous leishmaniasis (Penha and Lopes-Bezerra 2000). The same group reported on an ELISA test using the same antigenic preparation against sera from 92 patients with different clinical forms of sporotrichosis in Rio de Janeiro and reported 90 % sensitivity, 80 % specificity, and a global efficiency of 86 % (Bernardes-Engemann et al. 2005). Other studies showed that the use of different strains during the preparation of the antigen might result in different sensitivity and specificity, despite the purification of the antigen involved in this methodology. This difference is due to the *O*-glycan residues linked to the molecules (Bernardes-Engemann et al. 2009).

An ELISA to detect IgG antibodies reactive to the mycelial-phase *Sporothrix* exoantigens produced after 21 days of growth in Sabouraud dextrose medium at 28 °C showed 97 % sensitivity and 89 % specificity when performed on 90 sera from patients with different clinical forms of sporotrichosis, 72 sera from patients with other infectious diseases, and 76 healthy controls. The major antigenic components present in this preparation were proteins of 90, 70, 63, 51, and 42 kDa (Almeida-Paes et al. 2007a). This assay was further improved to detect IgG, IgM, and IgA antibodies, which improves the global efficiency for diagnosis and therapeutic follow-up of sporotrichosis (Almeida-Paes et al. 2007b). Mendoza et al. (2002) previously described this exoantigen, and the lack of cross-reactivity of this preparation with sera from patients with other mycoses was remarkable. The same antigen was used previously in ID and IEP techniques without cross-reactivity with sera from patients with leishmaniasis or chromoblastomycosis (Albornoz et al. 1984).

When the ELISAs probed with different antigenic preparations are compared, the crude exoantigens (Almeida-Paes et al. 2007a) gave slightly higher sensitivity and specificity than those using the con-A binding fraction of the *S. schenckii* yeast cell wall (Bernardes-Engemann et al. 2005). A similar observation was found when using this con-A binding fraction and crude exoantigens for the serodiagnosis of feline sporotrichosis. The use of crude exoantigens showed slightly better results than the purified peptide-rhamnomannan in terms of sensitivity (96 and 90 %) and specificity (98 and 96 %, respectively), suggesting that the *Sporothrix* secreted proteins are highly immunogenic and specific (Fernandes et al. 2011).

More recently, an immunoblot assay using cell-free exoantigens of the yeast form of *S. brasiliensis* was described to detect IgG antibodies in serum samples from human patients. In this assay, a sensitivity of 100 % was achieved, but a low specificity (50 %) was observed. However, if the authors verified a positive serum sample only if at least two immunological bands appeared in the immunoblots, the specificity increased to 80 % with 93 % sensitivity (Almeida-Paes et al. 2012).

8.3.3 *Sporotrichin Skin Test*

The skin test (ST), with mycelial extracts or yeast cells called sporotrichin, has been widely used throughout the world, especially for epidemiological studies of sporotrichosis. It has also been applied as support for diagnosis in Latin America (Lopes-Bezerra et al. 2006; Barros et al. 2011; Bonifaz and Vázquez-González 2013) and in atypical forms of the disease, such as the case of a recent bulbar conjunctival sporotrichosis (Kashima et al. 2010). However, sporotrichin is not available commercially in many countries (Dominguez-Soto and Hojyo-Tomoka 1983; Bonifaz and Vázquez-González 2013), but it is accessible in many institutions dedicated to biomedical research. Reports are contradictory concerning its usefulness as a diagnostic tool due to false-positive results without signs or symptoms of the disease, but this condition suggests a previous immunosensitizing contact (exposure) with *S. schenckii*. Other reports mention almost 100 % positive sporotrichin ST in lymphocutaneous and fixed cutaneous forms of sporotrichosis (Barros et al. 2011; Bonifaz and Vázquez-González 2010).

The use of sporotrichin ST in epidemiological surveys has been extensively developed from the first surveys in Mexico (González-Ochoa and Ricoy 1970), Guatemala (Mayorga et al. 1978), and Brazil (Rocha-Posada 1968), among others. This practical test has been used until the present (Bonifaz et al. 2013), demonstrating the usefulness of these antigens to identify endemic regions of sporotrichosis worldwide, an option to gain insight in disease emergence scenarios such as the recent cat zoonosis in Brazil (Barros et al. 2004; Oliveira et al. 2011; Freitas et al. 2010; Silva et al. 2012).

Concerning the term sporotrichin, there are reports of different type of antigens. Culture filtrate extracts from the mycelial (28 °C) or yeast (37 °C) forms, commonly called metabolic antigens, were first described by González-Ochoa and Figueroa (1947) and consisted of glycopeptide antigens. Another described and used antigen is a 1:1000, 1:2000, or 1:4000 dilution of heat-killed yeast cells. In addition, their biological properties depend on culture conditions (Takata and Ishizaki 1983; Arenas and Toriello 1986). A commonly used antigen for epidemiological surveys is a culture filtrate of the mycelial form standardized to 10 µg protein/0.1 ml of intradermal ST (Toriello et al. 1991; Bonifaz et al. 2013). The ST may be applied on the back or forearm and readings made at 24 and 48 h. A reaction of 8 mm of induration after 24 and 48 h constitutes a positive test.

The lack of standardization in the above-mentioned antigens would account for the difference in reactivity with sporotrichin ST, such as a 6.25 % positivity with a 1:4000 dilution of a yeast antigen in the southern state of Oaxaca, Mexico with *S. schenckii* isolates recovered from soil (Sánchez-Aleman et al. 2004). This is in contrast with the 14 % positivity observed with a mycelial metabolic antigen at 10 µg protein/0.1 ml in an endemic region of sporotrichosis in Puebla, Mexico, without any fungal isolation (Mendez-Tovar et al. 2003).

Additional epidemiological studies of sporotrichosis and the *S. schenckii* complex are necessary because changes in the interplay of pathogens, hosts, and

environment lead to the formation of novel disease patterns as observed for sporotrichosis.

8.4 Molecular Diagnosis

Molecular methods have been developed based on polymerase chain reaction (PCR) techniques that show good sensitivity, specificity, and speed for early diagnosis of *S. schenckii* (Berbee and Taylor 1992; Kano et al. 2001, 2003; Hu et al. 2003; Xu et al. 2010; Mendoza et al. 2012; Liu et al. 2013; Ruiz-Baca et al. 2013; Oliveira et al. 2014). Sandhu et al. (1995) proposed the pioneering DNA-based methodologies used for the diagnosis of fungal infections, and developed 21 specific nucleic acid probes targeting the large subunit of the ribosomal RNA (*rRNA*) gene from several fungi, including *S. schenckii*. Among the major genes described for the diagnosis of sporotrichosis are the chitin-synthase gene 1 (*CHS1*), 18S rDNA, and mitochondrial DNA (mtDNA) (Berbee and Taylor 1992; Kano et al. 2001, 2003; Hu et al. 2003; Xu et al. 2010). The trials with nested PCR using the 18S rDNA gene and mtDNA as targets showed high sensitivity and specificity, indicating that these tests can provide a rapid diagnosis with sufficient accuracy to be used clinically in patients with sporotrichosis (Hu et al. 2003; Xu et al. 2010; Oliveira et al. 2014). A drawback of these methods is that they are not commercially available and require specialized equipment; therefore, they are not carried out in most clinical laboratories.

8.5 Conclusions and Perspectives

Sporotrichosis is classically diagnosed by correlation among clinical, epidemiological, and laboratory data. The conventional method for definitive diagnosis of sporotrichosis is based on etiological agent isolation in culture and its identification. A disadvantage of the culture methods, is that they are difficult to apply in disseminated and/or systemic sporotrichosis; therefore, detection of an antibody response in patients could provide a faster method for diagnosis. Sporotrichin ST remains an option for epidemiological studies to gain insight in disease emergence scenarios such as the recent cat zoonosis in Brazil. To date, serological techniques (like ELISA, Western blot, immunodiffusion, etc.) are used for sporotrichosis diagnosis and involve antibody detection against soluble antigens and different molecules of the *S. schenckii* cell wall, such as peptide-rhamnomannans, exoantigens, and the newly described molecule gp70. The sensitivity and specificity of these methods differ depending on the antigenic fraction used. Fluorescent antibodies and immunohistochemical techniques are alternative methods that also provide a rapid diagnosis of sporotrichosis in tissue samples. The diagnosis of *S. schenckii* by PCR in clinical samples has also shown a high degree of sensitivity

and specificity. These tests can provide a rapid diagnosis with sufficient precision to be used clinically for patients with sporotrichosis, with PCR studies for the disseminated cases of the disease.

The different methods described in this review are not available in many clinical laboratories, which compromises the ability to diagnose and provide individual treatment for sporotrichosis. The search for new protein biomarkers for the development of an easy, sensitive, and specific methodology could help lower the treatment costs and offer alternatives to current tests for the diagnosis of sporotrichoid infections that can be confused by infections caused by other pathogens. To date, efforts continue to improve or develop new diagnostic tests that are more sensitive and specific for this mycosis. However, these tests require validation prior to general application in routine diagnosis. The development and application of new biomarker molecules for the diagnosis of sporotrichosis remains to be done either with exoantigens or cell wall antigens. The recent release of the *S. schenckii* genome, and the use of certain tools such as genomics, proteomics, immunoproteomics, metabolomics, interactomics, etc., would enable major advances in the search and identification of new biomarker antigens for sporotrichosis, which are expected to be introduced to the clinical laboratory in the short or medium term.

References

- Albornoz MB, Villanueva E et al (1984) Application of immunoprecipitation techniques to the diagnosis of cutaneous and extracutaneous forms of sporotrichosis. *Mycopathologia* 85:177–183
- Almeida-Paes R, Pimenta MA, Pizzini CV et al (2007a) Use of mycelial-phase *Sporothrix schenckii* exoantigens in an Enzyme-linked Immunosorbent Assay for diagnosis of sporotrichosis by antibody detection. *Clin Vac Immunol* 14:244–249
- Almeida-Paes R, Pimenta MA, Monteiro PC et al (2007b) Immunoglobulins G, M, and A against *Sporothrix schenckii* exoantigens in patients with sporotrichosis before and during treatment with itraconazole. *Clin Vac Immunol* 14:1149–1157
- Almeida-Paes R, Bailão AM, Pizzini CV et al (2012) Cell-free antigens of *Sporothrix brasiliensis*: antigenic diversity and application in an immunoblot assay. *Mycoses* 55:467–475
- Arenas G, Toriello C (1986) Actividad inmunológica de antígenos miceliales y levaduriformes de diferentes fases de crecimiento de *Sporothrix schenckii*. *Rev Mex Mic* 2:131–144
- Barros MB, Schubach AO, Valle AC et al (2004) Cat-transmitted sporotrichosis epidemic in Rio de Janeiro, Brazil: description of a series of cases. *Clin Infect Dis* 38:529–535
- Barros MBL, Almeida-Paes R, Schubach AO (2011) *Sporothrix schenckii* and sporotrichosis. *Clin Microbiol Rev* 24:633–654
- Berbee ML, Taylor JW (1992) 18S ribosomal RNA gene sequence characters place the human pathogen *Sporothrix schenckii* in the genus *Ophiostoma*. *Exp Mycol* 16:87–91
- Bernardes-Engemann AR, Costa RC, Miguens BR et al (2005) Development of an enzyme-linked immunosorbent assay for the serodiagnosis of several clinical forms of sporotrichosis. *Med Mycol* 43:487–493
- Bernardes-Engemann AR, Loureiro y Penha CV, Benvenuto F et al (2009) A comparative serological study of the SsCBF antigenic fraction isolated from three *Sporothrix schenckii* strains. *Med Mycol* 47:874–878

- Blumer SO, Kaufman L, Kaplan W et al (1973) Comparative evaluation of five serological methods for the diagnosis of sporotrichosis. *Appl Microbiol* 26:4–8
- Bonifaz A, Vázquez-González D (2010) Diagnostic methods: an update. *G Ital Dermatol Venereol* 145:659–673
- Bonifaz A, Vázquez-González D (2013) Diagnosis and treatment of lymphocutaneous Diagnostic methods: what are the options? *Curr Fungal Infect Rep* 7:252–259
- Bonifaz A, Araiza J, Perez-Mejía A et al (2013) Prueba intradérmica con esporotricina en una comunidad de la Sierra Norte de Puebla. *Dermatol Rev Mex* 57:428–432
- Casseroni S, Conti-Diaz IA, Zanetta E et al (1983) Serologia de la esporotricosis cutánea. *Sabouraudia* 21:317–321
- Costa RO, de Mesquita KC, Damasco PS et al (2008) Infectious arthritis as the single manifestation of Diagnostic methods: serology from serum and synovial fluid samples as an aid to diagnosis. *Rev Iberoam Micol* 25:54–56
- Dominguez-Soto L, Hojyo-Tomoka MT (1983) The intradermal sporotrichin test and the diagnosis of sporotrichosis. *Int J Dermatol* 22:520
- Fernandes GF, Amaral CC, Sasaki A et al (2009) Heterogeneity of proteins expressed by *Sporothrix schenckii* isolates. *Med Mycol* 47:855–861
- Fernandes GF, Lopes-Bezerra LM, Bernardes-Engemann AR et al (2011) Serodiagnosis of sporotrichosis infection in cats by enzyme-linked immunosorbent assay using a specific antigen, SsCBF, and crude exoantigens. *Vet Microbiol* 147:445–449
- Fernandes GF, Santos PO, Rodrigues AM et al (2013) Characterization of virulence profile, protein secretion and immunogenicity of different *Sporothrix schenckii sensu stricto* isolates compared with *S. globosa* and *S. brasiliensis* species. *Virulence* 4:241–249
- Freitas DFS, Valle ACF, Almeida-Paes R et al (2010) Zoonotic sporotrichosis in Rio de Janeiro, Brazil: a protracted epidemic yet to be curbed. *Clin Infect Dis* 50:453
- González-Ochoa A, Figueroa ES (1947) Polisacáridos del *Sporotrichum schenckii*. Datos inmunológicos: intradermoreacción en el diagnóstico de la esporotrichosis. *Rev Inst Salubr Enferm Trop* 8:143–153
- González-Ochoa A, Ricoy E (1970) Valoración comparativa de los antígenos polisacáridos y celular de *Sporothrix schenckii*. *Rev Invest Salud Publica* 30:303–315
- Hu S, Chung WH, Hung SI et al (2003) Detection of *Sporothrix schenckii* in clinical samples by a nested PCR assay. *J Clin Microbiol* 41:1414–1418
- Kano R, Nakamura Y, Watanabe S et al (2001) Identification of *Sporothrix schenckii* based on sequences of the chitin synthase 1 gene. *Mycoses* 44:261–265
- Kano R, Matsuoka A, Kashima M et al (2003) Detection of *Sporothrix schenckii* chitin synthase 1 (CHS1) gene in biopsy specimens from human patients with sporotrichosis. *J Dermatol Sci* 33:73–74
- Karlin JV, Nielsen HS (1970) Serologic aspects of sporotrichosis. *J Infect Dis* 121:316–327
- Kashima T, Honma R, Kishi S et al (2010) Bulbar conjunctival sporotrichosis presenting as a salmon-pink tumor. *Cornea* 29:573–576
- Kwon-Chung KJ, Bennett JE (eds) (1992) *Medical mycology*. Lea & Febiger, London
- Liu X, Zhang Z, Hou B et al (2013) Rapid identification of *Sporothrix schenckii* in biopsy tissue by PCR. *J Eur Acad Dermatol Venereol* 27:1491–1497
- Lloyd KO, Bitoon MA (1971) Isolation and purification of a peptido-rhamnomannan from the yeast form of *Sporothrix schenckii*. Structural and immunochemical studies. *J Immunol* 107:663–671
- Lopes-Bezerra LM, Lima OC (1997) Identification of a concavalin A-binding antigen of the cell surface of *Sporothrix schenckii*. *J Med Vet Mycol* 35:167–172
- Lopes-Bezerra LM, Schubach A, Costa RO (2006) *Sporothrix schenckii* and sporotrichosis. *Ann Acad Bras Ciencias* 78:293–308
- Marimon R, Cano J, Gené J et al (2007) *Sporothrix brasiliensis*, *S. globosa*, and *S. mexicana*, three new *Sporothrix* species of clinical interest. *J Clin Microbiol* 45:198–3206

- Marimon R, Gené J, Cano J et al (2008) *Sporothrix luriei*: rare fungus from clinical origin. *Med Mycol* 46:621–625
- Mayorga R, Cáceres A, Toriello C et al (1978) Etude d'une zone d'endemie sporotrichosique au Guatemala. *Sabouraudia* 16:185–198
- Mendez-Tovar LJ, Lemini-López A, Hernández-Hernández F et al (2003) Frecuencia de micosis en tres comunidades de la sierra norte de Puebla. *Gac Med Mex* 139:1–6
- Mendoza M, Diaz AM, Hung MB et al (2002) Production of culture filtrates of *Sporothrix schenckii* in diverse culture media. *Med Mycol* 40:447–454
- Mendoza M, Brito A, Schaper DA et al (2012) Evaluación de la técnica PCR anidada para el diagnóstico de la esporotricosis experimental. *Rev Iberoam Micol* 29:120–125
- Morris-Jones R (2002) Sporotrichosis. *Clin Exp Dermatol* 27:427–431
- Nascimento RC, Almeida SR (2005) Humoral immune response against soluble and fractionate antigens in experimental sporotrichosis. *FEMS Immunol Med Microbiol* 43:241–247
- Nascimento RC, Espíndola NM, Castro RA et al (2008) Passive immunization with monoclonal antibody against a 70-Kda putative adhesin of *Sporothrix schenckii* induces protection in murine sporotrichosis. *Eur J Immunol* 38:3080–3089
- Oliveira MME, Almeida-Paes R, Muniz MM et al (2011) Phenotypic and molecular identification of *Sporothrix* isolates from an epidemic area of sporotrichosis in Brazil. *Mycopathologia* 172:257–267
- Oliveira MME, Almeida-Paes R, Gutierrez-Galhardo MC et al (2014) Molecular identification of the *Sporothrix schenckii* complex. *Rev Iberoam Micol* 31:2–6
- Orofino-Costa R, Bóia MN, Magalhães GAP et al (2009) Arthritis as a hypersensitivity reaction in a case of sporotrichosis transmitted by a cat: clinical and serological follow up of 13 months. *Mycoses* 53:81–83
- Penha CV, Lopes-Bezerra LM (2000) Concanavalin A-binding cell wall antigens of *Sporothrix schenckii*: a serological study. *Med Mycol* 38:1–7
- Quintella LP, Passos SRL, Valle ACF et al (2011) Histopathology of cutaneous sporotrichosis in Rio de Janeiro: a series of 119 consecutive cases. *J Cutan Pathol* 38:25–32
- Rippon JW (1988) Sporotrichosis. *Medical mycology: the pathogenic fungi and pathogenic actinomycetes*. WB Saunders, Philadelphia
- Rocha-Posada H (1968) Pruebas cutáneas con esporotricina. *Mycopathologia* 36:42–54
- Ruiz-Baca E, Toriello C, Pérez-Torres A et al (2009) Isolation and some properties of a glycoprotein of 70 kDa (Gp70) from the cell wall of *Sporothrix schenckii* involved in fungal adherence to dermal extracellular matrix. *Med Mycol* 47:185–196
- Ruiz-Baca E, Cuéllar-Cruz M, López-Romero E, Reyes Montes MR, Toriello C (2013) Fungal cell wall antigens for the diagnosis of invasive fungal infections. *Fungal cell wall*. Nova Science Publishers, Inc., New York, pp 207–208
- Ruiz-Baca E, Hernández-Mendoza G, Cuéllar-Cruz M et al (2014) Detection of 2 immunoreactive antigens in the cell wall of *Sporothrix brasiliensis* and *Sporothrix globosa*. *Diagn Microbiol Infect Dis* 79:328–330
- Sánchez-Aleman MA, Araiza J, Bonifaz A (2004) Aislamiento y caracterización de cepas silvestres de *Sporothrix schenckii* e investigación de reactores a la esporotricina. *Gac Med Mex* 140:507–513
- Sandhu GS, Kline BC, Stockman L et al (1995) Molecular probes for diagnosis of fungal infections. *J Clin Microbiol* 33:2913–2919
- Schubach TMP, Schubach AO, Okamoto T et al (2004) Evaluation of an epidemic of sporotrichosis in cats: 347 cases (1998-2001). *J Am Vet Med Assoc* 224:1623–1629
- Schubach TMP, Schubach AO, Okamoto T et al (2006) Canine sporotrichosis in Rio de Janeiro, Brazil: clinical presentation, laboratory diagnosis and therapeutic response in 44 cases (1998-2003). *Med Mycol* 44:87–92
- Scott EN, Muchmore HG (1989) Immunoblot analysis of antibody responses to *Sporothrix schenckii*. *J Clin Microbiol* 27:300–304

- Sharma S, Choudhary R, Juneja M et al (2005) Cutaneous tuberculosis mimicking sporotrichosis. *Indian J Pediatr* 72:86
- Silva MB, Costa MM, Torres CC et al (2012) Urban Diagnostic methods: a neglected epidemic in Rio de Janeiro, Brazil. *Cad Saude Publica* 28:1867–1880
- Takata M, Ishizaki H (1983) Correlations among culture times, sugar composition and biological activities of *Sporothrix schenckii* antigens. *Mycopathologia* 84:31–39
- Teixeira PAC, Castro RA, Nascimento RC et al (2009) Cell spots surface expression of adhesins for fibronectin correlates with virulence of *Sporothrix schenckii*. *Microbiology* 155:3730–3738
- Toriello C, ArjonaRosado L, Taylor ML (1991) Efficiency of crude and purified fungal antigens in serodiagnosis to discriminate mycotic from other respiratory diseases. *Mycoses* 34:133–140
- Widal F, Abrami P, Joltrain E et al (1910) Sero diagnostic mycosique. Applications audiagnostic de la sporotrichose et de l'ctinomycose. Les coagglutination set cofixations mycosiques. *Ann Inst Pasteur* 24:1–33
- Xu TH, Lin JP, Gao XH et al (2010) Identification of *Sporothrix schenckii* of various mtDNA types by nested PCR assay. *Med Mycol* 48:161–165
- Zancope-Oliveira RM, Almeida-Paes R, Oliveira MME et al (2011) New diagnostic applications in sporotrichosis. In: Khopkar U (ed) *Skin biopsy perspectives*, 1st edn. InTech, Croatia
- Zhang Z, Liu X, Lv X et al (2011) Variation in genotype and higher virulence of a strain of *Sporothrix schenckii* causing disseminated cutaneous sporotrichosis. *Mycopathologia* 172:439–446

Molecular Components of the *Sporothrix schenckii* Complex that Induce Immune Response

Carlos A. Alba-Fierro¹ · Armando Pérez-Torres² · Conchita Toriello³ · Yolanda Romo-Lozano⁴ · Everardo López-Romero⁵ · Estela Ruiz-Baca¹

Received: 7 January 2016 / Accepted: 12 March 2016
© Springer Science+Business Media New York 2016

Abstract Sporotrichosis is a fungal disease caused by the *Sporothrix schenckii* complex that includes species such as *S. brasiliensis*, *S. schenckii* sensu stricto, *S. globosa*, *S. luriei*, *S. mexicana*, and *S. pallida*, which exhibit different potentially antigenic molecular components. The immune response of susceptible hosts to control infection and disease caused by these fungi has been little studied. Besides, the fungus–host interaction induces the activation of different types of immune response. This mini-review analyzes and discusses existing reports on the identification and functional characterization of molecules from species of the *S. schenckii* complex with clinical relevance, and the mechanisms that mediate the type and magnitude of the immune response in experimental models in vivo and in vitro. This knowledge is expected to contribute to the development of protective and therapeutic strategies against sporotrichosis and other mycoses.

Introduction

Sporothrix schenckii, which was for over a century the only *Sporothrix* species described as pathogenic to humans, currently defines a complex of species known as the *Ophiostoma stenoceras*–*Sporothrix schenckii* complex [20], due to the ecological association of these species which belong to the *Ophiostomatales* and share the same ecological niche. To date, 30 *Sporothrix* taxa have been described [94], but few species of *Sporothrix schenckii* complex such as *S. brasiliensis*, *S. schenckii* sensu stricto (*s.st.*), *S. globosa*, *S. luriei* [23, 42, 44, 45], *S. mexicana* [49, 63], and *S. pallida* [17, 43] are clinically relevant. Besides these, there are other *Sporothrix* species, some pathogenic to insects such as *S. insectorum* [21], and other saprophytic such as *S. stylites* and *S. lignivora*, which grow on wood and bark. On their part, *S. humicola*, *S. inflata*, and *S. pallida* grow on soil and decaying organic matter [22]. Other recognized environmental species include *S. variocibatus* [64], *S. brunneoviolacea*, and *S. dimorphospora* [38]. The differences in biological behavior of both pathogenic and saprophytic species suggest an extreme genetic diversity in the *Sporothrix* genus not yet fully disclosed.

S. schenckii, which is found all over the world, infects humans via penetration of plant material through skin traumas, inhalation of conidia, or zoonosis by cats. *S. globosa* has been reported in several countries with a very low frequency [39]; it is prevalent in Asia [94], although its low genetic diversity might suggest an association with another source of environmental infection [62]. *S. brasiliensis* is described as a highly virulent species [8, 26] in epidemic outbreaks for both humans and cats, and it is predominant in Southern Brazil [26, 63]. Another pathogenic species, *S. luriei*, has been so far isolated in only four

✉ Estela Ruiz-Baca
erb750@hotmail.com; eruiz@ujed.mx

¹ Facultad de Ciencias Químicas, Universidad Juárez del Estado de Durango, Av. Veterinaria S/N, 34120 Durango, Dgo., Mexico
² Departamento de Biología Celular y Tisular, Facultad de Medicina, Universidad Nacional Autónoma de México, 04510 Mexico, D.F., Mexico
³ Departamento de Microbiología y Parasitología, Facultad de Medicina, Universidad Nacional Autónoma de México, 04510 Mexico, D.F., Mexico
⁴ Departamento de Microbiología, Centro de Ciencias Básicas, Universidad Autónoma de Aguascalientes, Av. Universidad # 940, 20131 Aguascalientes, Ags., Mexico
⁵ Departamento de Biología, División de Ciencias Naturales y Exactas, Campus Guanajuato, Universidad de Guanajuato, Noria Alta S/N, C.P. 36050 Guanajuato, Gto., Mexico

cases in South Africa, Italy, Spain, and India [1, 48, 56] and from one case of canine sporotrichosis [54]. It was only recently positioned in the species rank based on its phenotypic characteristics and multilocus sequence analysis [44]. *S. mexicana* has been to date isolated from one clinical case of sporotrichosis in Portugal [49], three cases in Brazil [63], and from plant and soil material in Mexico [44, 63]. Finally, we should mention *S. pallida*, reported as causing fungal keratitis in a corneal ulcer [43] and from a human case of onychomycosis [17]. *S. pallida* is isolated from the environment and is currently a synonym for *S. albicans* [22].

Presently, there are sophisticated molecular methods to study species differentiation, including those based on mass spectrometry protocols [55]; however, a current problem regarding the various human pathogenic species is that they were characterized initially by molecular methods, particularly by sequence analysis, as recent as 2006 [45]. As a result, prior to this date most reports considered *S. schenckii* as almost the unique etiological agent of sporotrichosis. In a recent review by Zhang et al. [92], both medical and veterinarian cases of sporotrichosis caused by *S. globosa* and *S. brasiliensis* are described. However, until recently the presence of other species in collections of clinical cases of *S. schenckii* began to be demonstrated using molecular characterization. For instance, Rodrigues et al. [63] re-identified six strains originally classified as *S. schenckii*, three of them as *S. mexicana* and the other as *S. globosa*.

Only when it was recognized that the *S. schenckii* complex contained several species, researchers started to compare these clinically relevant pathogenic species concerning their susceptibility to antifungal agents, virulence, protein production, and immunogenicity, among other parameters. When 92 isolates of *Sporothrix* species, including *S. brasiliensis*, *S. schenckii*, *S. globosa*, *S. mexicana*, and *S. pallida* were tested for their in vitro susceptibility to 12 antifungal agents, significant differences were observed among them, with *S. brasiliensis* and *S. mexicana* showing the best and worst responses, respectively [43]. Additional studies have shown that *S. brasiliensis* was the most virulent, the strains of *S. schenckii* showed different levels of virulence while *S. globosa* was the least virulent. The species also caused diverse histopathological lesions in mice [7, 8, 26, 27]. Among the humoral response patterns of mice infected with *S. schenckii*, *S. brasiliensis*, and *S. globosa*, recognition of molecules of 60 and 110 kDa was observed in several isolates of virulent strains of *S. schenckii* and *S. brasiliensis*, suggesting the involvement of these molecules in virulence [26].

The characteristics of the *S. schenckii* complex have begun to be understood, but not the process of sporotrichosis, mainly in view of the differences in virulence

among human pathogenic species. In this regard, Texeira et al. [87] compared the genomics of *S. brasiliensis* and *S. schenckii*, the most virulent species of the *Sporothrix* complex, and concluded that in silico analysis is not sufficient to identify the molecules responsible of the differences in virulence observed among the species. A detailed analysis of these differences, the identification of molecules involved in virulence, and how they trigger the immunological mechanisms, should certainly lead to a better understanding of the pathogenesis of sporotrichosis. On this scenario, the following review deals with some of the immune response-inducing components in these extremely variable fungi.

Immune Response-Inducing Molecular Components

The study of infection development by *S. schenckii* suggests that the cellular immune defense plays an important role [24, 77, 81, 82, 85]. Patients on immunosuppressive therapy or HIV-positive, with decreased number of CD4+T cells, develop disseminated forms of the infection [25, 31, 84]. Freitas et al. [31], described the association between low CD4+T cells levels and disseminated clinical forms of sporotrichosis. In this report, patients with low count of CD4+T cells suffered disseminated osteoarticular, meningoencephalitis, and mucosal forms. However, disseminated forms can also be observed in HIV-positive patients with normal CD4+ cells count [79, 83]. Freitas et al. [30] have also shown disseminated sporotrichosis in HIV-negative patients with normal CD4+T cells count. Noteworthy, a change in *S. brasiliensis* virulence was observed, since different samples from a patient with disseminated sporotrichosis taken over a period of 5 years revealed different virulence levels. Studies in mice experimentally infected with *S. schenckii* yeast cells have demonstrated the presence of a delayed hypersensitivity response (DTH) [15]. However, other studies have highlighted the involvement of macrophages in the control of infection by *S. schenckii* [85]. Thus, it is not possible to rule out, in the context of innate and adaptive immunity, the participation of other defense mechanisms in the integrated response of the host. In this regard, *S. schenckii* yeast cells activate the alternative complement pathway in vitro independently of antibody [75]. Macrophages can be activated by soluble and lipidic antigens of the fungal cell surface via toll-like receptors (TLRs) and play a leading role in the infection progress [53, 73], together with humoral immunity mediated by specific antibodies to components of *S. schenckii* [50, 51]. However, the host immune response mechanisms that control infection are unknown. While it appears that *S. schenckii* has various

potentially antigenic molecular components, it is clear that hosts also differ both quantitatively and qualitatively in the type of immune response expressed upon interaction with the fungus. Therefore, it is worth pursuing further the identification and characterization of antigenic molecules in clinically relevant species of the *S. schenckii* complex, and to define the type of stimulation and immune response they trigger in experimental models *in vitro* and *in vivo*. This approach may help to generate strategies and alternatives to prevent, diagnose, and treat this mycosis.

Innate Immunity

The role of innate immunity in fighting infections begins with the recognition of pathogen-associated molecular patterns (PAMPs) present on the surface of fungal cells through pattern recognition receptors (PRRs) expressed in the host cells. These receptors include TLRs, C-type lectin receptors (CLRs), proteins of the galectin family, and nucleotide-binding oligomerization domain (NOD)-like receptors (NLRs) [65]. By expressing these receptors and recognizing PAMPs, macrophages play a central role in the innate response by eliminating pathogens through phagocytosis, by modulating the inflammatory response and presenting pathogen antigens [57]. In phagocytosis assays, macrophages are capable of internalize opsonized and unopsonized conidia and yeast of *S. schenckii*, with the participation of the mannose receptor during conidia recognition for further Th1 response development, and the participation of the complement receptor during yeast recognition [34]. The mannose receptor is mainly related to Th1 and Th17 response development in other fungi [65]. Interestingly, although conidia were recognized by the mannose receptor, the induced inflammatory response was weak, which might favor the dimorphic transition of conidia to yeast cell of *S. schenckii* within macrophages. However, this phenomenon is not reproduced in other conditions or with other cells, where the conidia induce greater secretion of pro-inflammatory mediators compared to yeasts [67, 68, 73]. Nevertheless, it has been shown that there are differences associated to species-specific virulence factors, and to the host immunological state [14, 18, 26, 89, 90, 93]. This may be related to the differential expression of surface molecules in conidia and yeast that are recognized by different PRRs. These observations justify the need to investigate the molecular differences between these morphotypes of *S. schenckii* to explain variations in the associated inflammatory process.

S. schenckii has molecules that function in the evasion or modulation of the host immune responses. For instance, the organism can reverse ergosterol peroxide to ergosterol, a molecule with potential detoxification effects on reactive oxygen species (ROS) during phagocytosis [33, 35, 78].

Additionally, ergosterol peroxide is capable of inducing a cytotoxic effect by a mechanism not yet well-described for *S. schenckii* [59]. In this sense, a constitutive lipid component in *S. schenckii* exerts an ambiguous effect on macrophages, as it induces synthesis of reactive nitrogen species (RNS) such as nitric oxide (NO), but completely inhibiting phagocytosis of yeast-like cells *in vitro* [12]. Furthermore, Gonçalves et al. [32] found that peritoneal exudate cells from mice infected with *S. schenckii* yeast-like cells cultured in the presence of the lipid extract from fungus, increase IL-18 and IL-1 β production through caspase-1 activation, suggesting a participation of the inflammasome and the cytosolic oligomerization domain (NOD)-like receptors. Noteworthy, within the fourth and sixth week post-infection, the cytokine levels decreased and NO production increased, correlating with a worsening of the disease [41].

Regarding the role of TLR-2 in the recognition of a lipid antigen of *S. schenckii*, Negrini et al. [53] demonstrated that macrophages from TLR-2-deficient mice, expressed lower levels of pro-inflammatory cytokines such as TNF- α and IL-1 β compared to controls when incubated with yeast morphotype. Furthermore, incubation of spleen cells from mice not expressing TLR-2 with the lipid antigen did not produce characteristic cytokines of the Th1 response such as IFN- γ [52]. Similar results were obtained when the interaction of the lipid antigen with TLR-4 was examined. Macrophages from TLR-4-deficient mice were unable to produce high levels of cytokines such as IL-1 β , IL-12, and TNF- α , with a concomitantly reduced expression of NF- κ B, in contrast with the wild-mice group [73]. A further study showed that a lipid extract induces macrophages from TLR-4-deficient mice to produce a larger amount of TGF- β , reducing the inflammatory response in these mice [72].

The cell wall (CW) is the main source of PAMPs in fungi. The three main components of the CW of medically important fungi are β -glucans, chitin, and mannans [65]. A peptido-rhamnomannan is a glycoprotein fraction consisting of 33.5 % rhamnose, 57 % mannose, and 14.2 % galactose that was isolated from the CW of the yeast morphotype of *S. schenckii* [37]. Exoantigens obtained from the CW of this morphotype are efficient inhibitors of the production of IL-1 β , IL-6 [72], TNF- α , IL-12, and IL-10 [53]. More recently, the exoantigen containing the peptido-rhamnomannan has been proposed as a modulator of the immune response as it is capable of inducing pro- and anti-inflammatory responses in *in vitro* assays [40]. The inflammatory immune response generated by *S. schenckii* has also been studied in other characteristic cells of the innate response such as mast cells [67, 68] and keratinocytes [36]. Mast cells challenged with both conidia and yeast cells of *S. schenckii* produce TNF- α and IL-6.

Furthermore, the extracellular signal-regulated kinase (ERK) signaling pathway was activated when the mast cells were challenged with yeast cells [67, 68]. Similarly, keratinocytes treated with both conidia and yeast, overexpress mRNA's of TLR2 and TLR4, and upregulated the levels of IL-6 and IL-8 through the NF- κ B signaling pathway [36].

Cellular Adaptive Immunity

Dendritic cells (DCs) play a key role in the balance between pro- and anti-inflammatory responses that increase or decrease cell immunity [76]. The activation of Th1 cells seems to be determined in part by the response of DCs to specific fungal antigens and to the cutaneous or visceral origin of the *S. schenckii* strain. Treating DCs with *S. schenckii* conidia or yeast cells of cutaneous origin preferentially induced IFN- γ production by T cells, with ERK pathway activation in DCs, suggesting a Th1 response, while the presentation of antigens of visceral strains increased the production of IL-4, a cytokine of humoral immunity [89]. However, according to murine models of infection, Arillaga et al. [8] demonstrated that virulence levels could be explained by different species, where *S. brasiliensis* followed by *S. schenckii* were the most virulent strains within the *S. schenckii* complex. In this regard, Almeida-Paes et al. [3] found that the most virulent strains of *S. brasiliensis* obtained from severe clinical forms of sporotrichosis, showed a higher number of virulence factors, concluding that species and virulence level may determine the clinical form of the disease. Nowadays, it is well known that strains with different virulence levels exist within the same species [4, 5]. This characteristic may be determined by different environmental factors such UV exposure, the presence of metals, chemical contaminants, or the interaction with other microorganisms. All together, these factors can cause the expression of survival mechanisms in some species, resulting in virulence factors when they interact with a susceptible host [86].

An exoantigen of *S. schenckii* is capable of increasing macrophages and DCs pro-inflammatory cytokine levels [41, 91]. Accordingly, co-incubation of T cells with exoantigen-activated DCs elicits a Th1/Th17 cytokine pattern (IFN- γ /Th17, IL-23, and TGF- β , respectively). In contrast, DCs stimulated with *S. schenckii* yeasts activated Th1 response only [91]. In mice with systemic infection, the Th17 response is required for optimal fungal clearance, since IL-23 depletion leads to an increase in fungal burden [28]. The effect of the exoantigen on murine splenic macrophages is interesting as it is capable of stimulating the production of IFN- γ and RNS such as NO. Moreover, during the first weeks of systemic infection with *S. schenckii* yeast cells, peritoneal macrophages of Swiss

mice costimulated with the exoantigen increased the secretion of IFN- γ and IL-12. During the last weeks, IL-4 was the predominant cytokine, suggesting the development of Th1 and Th2 responses in early and late stages of the infection, respectively [41], with a classical and alternative response of macrophage activation.

The exoantigen is not the only component in *S. schenckii* able to induce a mixed pattern of Th1/Th2 responses. A peptide-polysaccharide extracted from the CW of yeast cells of *S. schenckii* is capable of activating macrophages through the classical pathway (M1), with secretion of IL-12 and a Th1 response, as well as through the alternative pathway (M2), with high levels of IL-10 associated with a Th2 response [2]. Known stimuli for M1 polarization include pathogen components such as lipopolysaccharide and muramyl dipeptide, recognized by TLRs [47]. Thus, M1 activation mediated by peptide-polysaccharide and its receptors is suitable [52, 53]. However, the role of this antigen in M2 polarization is not easy to explain. A feasible explanation is that macrophage subsets are not stable; rather, they can interact with other immune cells or receive different stimuli such as IL-13 or IL-4 that trigger different activation pathways [46] and result in mixed phenotypes during the last weeks of infection. The peptide-polysaccharide of *S. schenckii* can induce immediate- and DTH immune reactions in guinea pigs and it appears that the peptide fraction is responsible for the DTH and the polysaccharide fraction for the immediate-type reaction [80]. Another effect of this antigen is to stimulate the proliferation of T lymphocytes by direct mitogenic activity [13]. Further, the subcutaneous application of a soluble antigen obtained by sonication of *S. schenckii* yeast cells induces the DTH response in mice [15]. To date, most of the known antigens from *S. schenckii* that stimulate cellular immunity have not been characterized, and therefore a detailed analysis of each of the components of these antigens is required to elucidate the specific immune response they are involved in.

Humoral Adaptive Immunity

Cellular and humoral immune responses are linked to the generated cytokine profile. The strongest activation signals to drive T cell differentiation into the Th2 lineage are triggered by IL-4 and IL-13, with a concomitant decrease in the Th1 response. A feature of the Th2 response is the secretion of antibodies. There seems to be a different serum profile of specific antibodies to *S. schenckii* antigens in sporotrichosis, depending on the clinical form of the disease. This was suggested by the observation that 15–20 antigens in the range of 22 to 70 kDa present in a soluble peptide extract of the fungus were recognized by sera from patients with extracutaneous sporotrichosis, while sera

from patients with cutaneous sporotrichosis recognized only 8–10 antigens [74]. Nevertheless, it seems that the clinical form of sporotrichosis is not the unique determinant for specificity or intensity of antibodies against *S. schenckii* antigens, despite evidences as sera from patients with extracutaneous sporotrichosis that recognized the highest number of fungal antigens, or strains isolated from other visceral form of the disease as inducers of a preferential Th2 response [89], or even the report of Bernardes-Engemann et al. [11] where patients with severe clinical forms of sporotrichosis presented higher titers of antibodies. Considering that before 2006 the *S. schenckii* species were not differentiated by molecular methods, the species-specific immune response must not be discarded. In this sense, several forms of sporotrichosis are able to induce the same response, as observed by Almeida-Paes et al. [4] where *S. brasiliensis* strains isolated from different clinical forms showed the same antigenic pattern. Noteworthy, when they compared the antibody response induced by a *S. brasiliensis* strain isolated from a patient with a lymphocutaneous form with the response induced by *S. schenckii* isolated of the same clinical form, the profile was different, suggesting that the different species of the complex are responsible from the specificity of the response. In addition, they demonstrated that the geography is unrelated with the response, since species from different geographical areas showed the same recognition pattern. Using serological probes such as the ELISA test, Almeida-Paes et al. [5] evaluated the potential of an antigen from the mycelial morphotype of *S. schenckii*, observing no differences in the antigen recognition by sera from patients with different clinical forms. However, it should be considered that the groups with different clinical forms were not homogeneous in terms of size thus affecting the statistical analysis. In a recent work, a *S. schenckii* Concanavalin A-Binding Fraction (SsCBF) was validated as a tool in serodiagnosis and it was detected in 100 % of the most severe clinical forms of sporotrichosis. However, as in the Almeida's report [5], they do not specify the species involved in every clinical form, difficulting the association of the antibodies titer with the species.

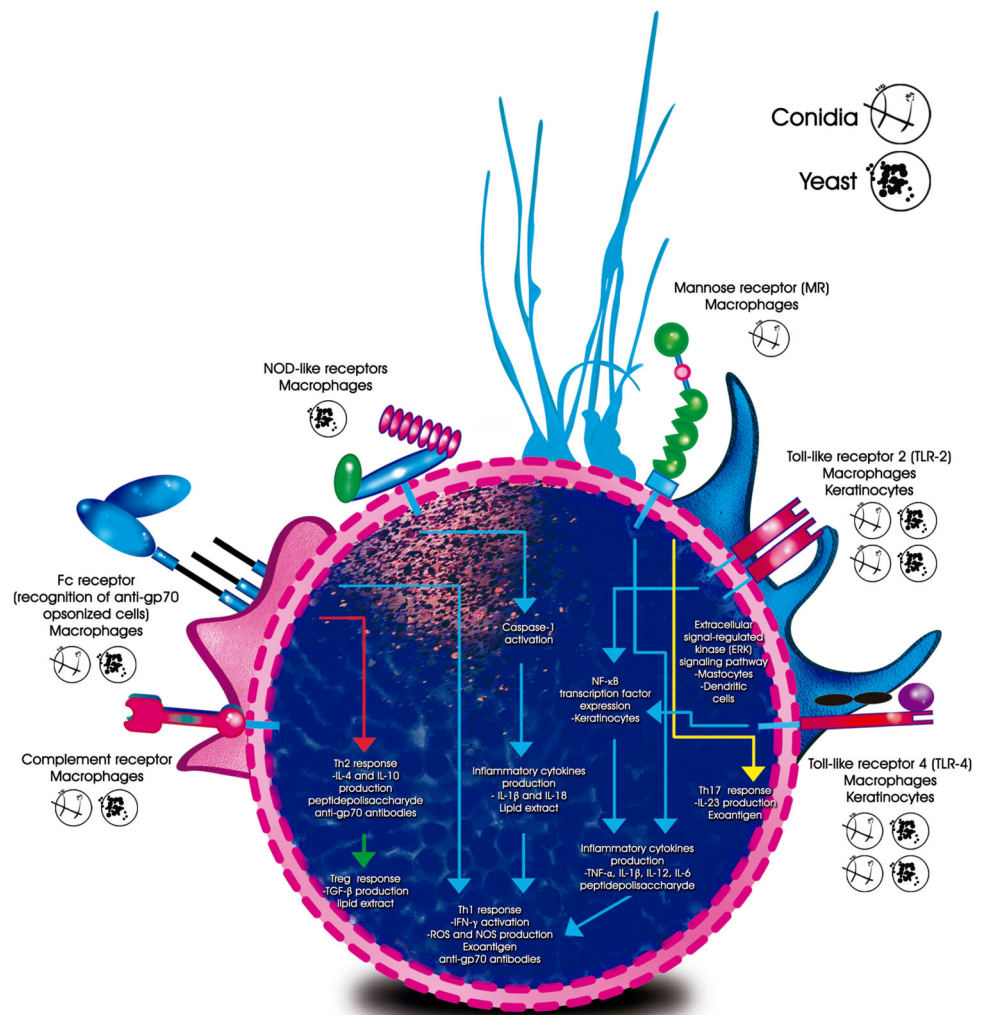
There are important aspects to consider with respect to the methodology used to study the humoral response during sporotrichosis, namely, the morphological phase of strains or the *Sporothrix* species used. For instance, it was seen that the *S. schenckii* yeast form produced an antigenic extract more reactive than the mycelial form on different strains. Besides, different *Sporothrix* species may present similar antigenic profiles, regardless of their geographic origin [4]. It has also been proposed that variations in antibody titers during sporotrichosis could be due to previous contact with *S. schenckii* in a region where this mycosis is endemic, or that the analysis was done before

the humoral response was performed [6]. In this sense, it is required to carry out a study that considers the same number of sera from different clinical forms, the species involved in every form, and the antibody response induced by each species in order to correlate with the clinical form. Moreover, in order to minimize variations, the antigens or extracts used during the assay must be standardized, considering the fungal morphotype, the growth conditions as well as the species and the strain since different strains of the same species may give rise to differences during the serological tests [10].

Humoral immune responses can be exploited not only with therapeutic purposes, but also as diagnostic proofs. In this regard, two antigens of 50 and 63 kDa from *S. schenckii* mycelial morphotype have shown to be potentially useful in serodiagnosis tests as they show high sensitivity and specificity and a feasible application in all clinical forms of sporotrichosis [5]. In the same line, a 85-kDa protein present in both morphotypes of *S. brasiliensis* and *S. schenckii* has been shown to be immunodominant, since it is detected in all sera from patients with different clinical forms of sporotrichosis. However, this antigen presented cross reactivity with other mycoses. Unlike the 85-kDa protein, other antigens of 131 and 120 kDa did not show cross reactivity but exhibited low sensitivity [4]. Recently, SsCBF from a *S. schenckii* yeast extract has shown significant potential in serodiagnosis, according to ELISA results using 177 serum samples from patients with different clinical forms of sporotrichosis and 92 sera from patients with other fungal and non-fungal diseases. This test resulted in 89 and 81 % of sensitivity and specificity, respectively [9]. Further characterization of the antigenic components from SsCBF will be very important.

Prior to the report by Rodrigues et al. [61], two immunodominant glycoprotein antigens of *S. schenckii*, named as gp70 and gp60, were described [69–71]. Recently, these molecules have proved useful for sporotrichosis diagnosis with 100 % specificity by ELISA using sera from cats with sporotrichosis, healthy cats, and cats with other diseases [60]. gp60 was thought to be mainly in the CW of the yeast morphotype of three different species of the *Sporothrix* complex, namely, *S. schenckii s.st.*, *S. brasiliensis*, and *S. globosa* and showed to be immunodominant since it was recognized by sera from mice infected with *S. schenckii* complex strains [26]. However, Rodrigues et al. [61] showed that gp70 suffers post-translational modifications, probably glycosylation and amino acid substitution, since at least six proteins ranging from 60 to 70 kDa shared the same peptide after they were analyzed by mass spectrometry (MS), thus concluding that gp60 and gp70 were the same antigen. Despite the observation that gp60 and gp70 share the same

Fig. 1 Signaling pathways involved during recognition of different antigens expressed in yeast cells and conidia of *S. schenckii* by phagocytes and their relationship with the immune responses triggered by the fungus



peptide, the glycosylation pattern may significantly influence the type of initial response triggered after its recognition by the immune response cell receptors. Thus, the analysis of the carbohydrate moiety will be a necessary future approach to explore and understand the influence of glycosylation on these antigens. gp70 is in the CW of both fungal morphotypes, it has an isoelectric point of 4.1, and 5.7 % of its weight is contributed by oligosaccharides joined by *N*-glycosidic bonds, without evidence of *O*-glycosidic-bound sugars. This glycoconjugate has been proposed as a fungal adhesin with affinity for extracellular matrix proteins [70, 88] and possibly associated with *S. schenckii* virulence, since the most virulent strains of the fungus exhibit a greater binding capacity [88]. However, Castro et al. [16] and Rodrigues et al. [61] have identified a soluble protein of 70 kDa by MS that is associated with benzoate metabolism and is highly expressed in low virulent strains of *S. brasiliensis*, showing an inverse relationship between expression and virulence. Whether this

glycoprotein represents a soluble isoform of the CW-located gp70 remains to be demonstrated.

Sera from mice infected with *S. schenckii* presented specific antibodies against the protein of 70 kDa, mostly of the IgG1 and IgG3 isotypes when using a soluble extract with proteins in the range of 20–96 kDa, suggesting that gp70 induces a strong humoral response [51]. Moreover, passive immunization with specific monoclonal anti-gp70 antibodies modified the course of the infection caused by *S. schenckii* in BALB/c mice, decreasing the fungal load and increasing the production of IFN- γ , an effect observed even in mice deficient in T cells [50]. A more recent report indicates that not only IFN- γ is secreted during passive immunization, but IL-10 and IL-4 levels also increased during the infection period suggesting a mixed Th1/Th2 response pattern [19]. Pathogenic fungus opsonized with antibodies are recognized through the Fc receptor, which can trigger a Th2 response [66], but noticeably, opsonization of yeast-like cells of *S. schenckii* with antibodies

against the 70 kDa protein also suggests a Th1 response [29]. Even though the most interest is presently focused in the gp60-gp70 isoforms, recently Portuondo-Fuentes et al. [58] showed that passive transfer of sera from immunized mice containing antibodies against two *S. schenckii* proteins of 44 and 47 kDa has a protective role during experimental sporotrichosis.

Conclusion and Future Perspective

A number of studies dealing with the mechanisms of the infection caused by *S. schenckii* suggest that the cellular immune response plays an important role against this mycosis. However, recent findings indicate that innate, humoral, Th17, and Treg responses cannot be ruled out. In fact, it seems that the responses induced by different *S. schenckii* antigens are antigen-specific. Therefore, the surface receptors involved in the recognition of these antigens, the signaling pathways activated by the corresponding receptors, the type of immune cells involved during this recognition, as well as the *S. schenckii* morphotype interacting during immune cells priming or mice infection, become as important as the antigens themselves. These ideas are schematized in Fig. 1, which illustrates these variables in a hypothetical cell containing macrophage, keratinocyte, dendritic, and mast cell receptors. Finally, a complete understanding of the immunological mechanisms involved in the innate and adaptive immune responses induced by the different antigens, as well as a better knowledge of the nature of these antigens, should lead to the development of immune responses that may have a protective and therapeutic effect against sporotrichosis.

Acknowledgments This paper constitutes a partial fulfillment of the requirements of the Graduate Program in Biomedical Sciences at UJED. CAAF thanks the scholarship No. 201509 granted by the Consejo Nacional de Ciencia y Tecnología (CONACyT), Mexico.

Compliance with Ethical Standards

Conflict of interest The authors have no conflicting interests with any of the subjects discussed in this paper.

References

- Alberici F, Paties CT, Lombardi G, Allejo L, Kaufman L, Chandler F (1989) *Sporothrix schenckii* var. *luriei* as the cause of sporotrichosis in Italy. *Eur J Epidemiol* 5:173–177
- Alegranci P, de Ribeiro LC, Ferreira LS et al (2013) The predominance of alternatively activated macrophages following challenge with cell wall peptide-polysaccharide after prior infection with *Sporothrix schenckii*. *Mycopathologia* 176:57–65
- Almeida-Paes R, de Oliveira LC, Oliveira MME et al (2015) Phenotypic characteristics associated with virulence of clinical isolates from the *Sporothrix* complex. *Biomed Res Int*. doi:10.1155/2015/212308
- Almeida-Paes R, Bailao AM, Pizzini CV et al (2012) Cell free antigens of *Sporothrix brasiliensis*: antigenic diversity and application in an immunoblot assay. *Mycoses* 55:467–475
- Almeida-Paes R, Pimenta MA, Pizzini CV et al (2007) Use of mycelial-phase *Sporothrix schenckii* exoantigens in an enzyme-linked immunosorbent assay for diagnosis of sporotrichosis by antibody detection. *Clin Vaccine Immunol* 14:244–249
- Almeida-Paes R, Pimenta MA, Monteiro PCF, Nosanchuk JD, Zancopé-Oliveira RM (2007) Immunoglobulins G, M, and A against *Sporothrix schenckii* exoantigens in patients with sporotrichosis before and during treatment with itraconazole. *Clin Vaccine Immunol* 14:1149–1157
- Arrillaga-Moncrieff I, Capilla J, Fernandez AM, Fariñas F, Mayayo E (2010) Diferencias en la patogenicidad del complejo de especies *Sporothrix* en un modelo animal. *Patologia* 48:82–87
- Arrillaga-Moncrieff I, Capilla J, Mayayo E et al (2009) Different virulence levels of the species of *Sporothrix* in a murine model. *Clin Microbiol Infect* 15:651–655
- Bernardes-Engemann AR, de Lima Barros M, Zeitune T, Russi DC, Orofino-Costa R, Lopes-Bezerra L (2015) Validation of a serodiagnostic test for sporotrichosis: a follow up study of patients related to the Rio de Janeiro zoonotic outbreak. *Med Mycol* 53:28–33
- Bernardes-Engemann AR, Loureiro y Penha CV, Benvenuto F et al (2009) A comparative serological study of the SsCBF antigenic fraction isolated from three *Sporothrix schenckii* strains. *Med Mycol* 47:874–878
- Bernardes-Engemann AR, Costa RC, Miguens BP et al (2005) Development of an enzyme-linked immunosorbent assay for the serodiagnosis of several clinical forms of sporotrichosis. *Med Mycol* 43:487–493
- Carlos IZ, Sgarbi DB, Santos GC, Placeres MC (2003) *Sporothrix schenckii* lipid inhibits macrophage phagocytosis: involvement of nitric oxide and tumour necrosis factor- α . *Scand J Immunol* 57:214–220
- Carlos IZ, Sgarbi DB, Placeres MC (1999) Host organism defense by a peptide-polysaccharide extracted from the fungus *Sporothrix schenckii*. *Mycopathologia* 144:9–14
- Carlos IZ, Zini MM, Sgarbi DB, Angluster J, Alviano CS, Silva CL (1994) Disturbances in the production of interleukin-1 and tumor necrosis factor in disseminated murine sporotrichosis. *Mycopathologia* 127:189–194
- Carlos IZ, Sgarbi DBG, Angluster J, Alviano CS, Silva CL (1992) Detection of cellular immunity with the soluble antigen of the fungus *Sporothrix schenckii* in the systemic form of the disease. *Mycopathologia* 117:139–144
- Castro RA, Kubitschek-Barreira PH, Teixeira PA et al (2013) Differences in the cell wall morphometry, cell wall topography and Gp70 expression correlate with the virulence of *Sporothrix brasiliensis* clinical isolates. *PLoS ONE* 8:1–17
- Cruz Choappa RM, Vieille Oyarzo PI, Carvajal Silva LC (2014) Aislamiento de *Sporothrix pallida* complex en muestras clínicas ambientales de Chile. *Rev Argent Microbiol* 46:311–314
- da Silva AC, Bezerra LM, Aguiar TS, Tavares D, Araujo LM, Pinto CE, Ribeiro OG (2001) Effect of genetic modifications by selection for immunological tolerance on fungus infection in mice. *Microbes Infect* 3:215–222
- de Almeida JR, Kaihama GH, Jannuzzi GP, de Almeida SR (2015) Therapeutic vaccine using monoclonal antibody against a 70-kDa glycoprotein in mice infected with highly virulent *Sporothrix schenckii* and *Sporothrix brasiliensis*. *Med Mycol* 53:42–50
- de Beer ZW, Harrington TC, Vismer HF, Wingfield BD, Wingfield MJ (2003) Phylogeny of the *Ophiostoma stenoceras-Sporothrix schenckii* complex. *Mycologia* 95:434–444

21. de Hoog GS (1974) The genera *Blastobotrys*, *Sporothrix*, *Calcarisporium* and *Calcarisporiella* gen. nov. *Stud Mycol* 7:1–84
22. de Meyer EM, de Beer ZW, Summerbell RC et al (2008) Taxonomy and phylogeny of new wood- and soil-inhabiting *Sporothrix* species in the *Ophiostoma stenoceras-Sporothrix schenckii* complex. *Mycologia* 100:647–661
23. Dias NM, Oliveira MME, Portela MA, Santos C, Zancopé-Oliveira R, Lima N (2011) Sporotrichosis caused by *Sporothrix mexicana*, Portugal. *Emerg Infect Dis* 17:1975–1976
24. Dickerson CL, Taylor RT, Drutz DJ (1983) Susceptibility of congenitally athymic (nude) mice to sporotrichosis. *Infect Immun* 40:417–420
25. Donabedian H, O'Donnell E, Olszewski C, McArthur RD, Budd N (1994) Disseminated cutaneous and meningeal sporotrichosis in an AIDS patient. *Diagn Microbiol Infect Dis* 18:111–115
26. Fernandes GF, dos Santos PO, Rodrigues AM, Sazaki AA, Burger E, de Camargo ZP (2013) Characterization of virulence profile, protein secretion and immunogenicity of different *Sporothrix schenckii* sensu stricto isolates compared with *S. globosa* and *S. brasiliensis* species. *Virulence* 4:241–249
27. Fernandez-Silva F, Capilla J, Mayayo E, Guarro J (2012) Virulence of *Sporothrix luriei* in a murine model of disseminated infection. *Mycopathologia* 173:245–249
28. Ferreira LS, Gonçalves AC, Portuondo DL, Maia DC, Placeres MC, Batista-Duharte A, Carlos IZ (2015) Optimal clearance of *Sporothrix schenckii* requires an intact Th17 response in a mouse model of systemic infection. *Immunobiology* 220:985–992
29. Franco DL, Nascimento RC, Ferreira KS, Almeida SR (2012) Antibodies against *Sporothrix schenckii* enhance TNF- α production and killing macrophages. *Scan J Immunol* 75:142–146
30. Freitas FS, Santos SS, Almeida-Paes R et al (2015) Increase in virulence of *Sporothrix brasiliensis* over five years in a patient with chronic disseminated sporotrichosis. *Virulence* 6:112–120
31. Freitas FS, de Siqueira-Hoagland B, do Valle AC et al (2012) Sporotrichosis in HIV-infected patients: report of 21 cases of endemic sporotrichosis in Rio de Janeiro, Brazil. *Med Mycol* 50:170–178
32. Gonçalves AC, Maia DC, Ferreira LS, Monazzi LG, Alegranci P, Placeres MC, Batista-Duharte A, Carlos IZ (2014) Involvement of major components from *Sporothrix schenckii* cell wall in the caspase-1 activation, nitric oxide and cytokines production during experimental sporotrichosis. *Mycopathologia* 179:21–30
33. Gorman AA, Hamblett I, Rodgers MA (1987) Ergosterol (provitamin D2) triplet state: an efficient sensitizer of singlet oxygen, O₂ (¹ Δ g) formation. *Photochem Photobiol* 45:215–221
34. Guzman-Beltran S, Perez-Torres A, Coronel-Cruz C, Torres-Guerrero H (2012) Phagocytic receptors on macrophages distinguish between different *Sporothrix schenckii* morphotypes. *Microbes Infect* 14:1093–1101
35. Jason Niu Q, Mendenhall GD (1992) Yields of singlet molecular oxygen from peroxy radical termination. *J Am Chem Soc* 114:165–172
36. Li M, Chen Q, Sun J, Shen Y, Liu W (2012) Inflammatory response of human keratinocytes triggered by *Sporothrix schenckii* via toll like receptor 2 and 4. *J Dermatol Sci* 66:80–82
37. Lloyd KO, Bitton MA (1971) Isolation and purification of a peptidoglycan-like form of the yeast form of *Sporothrix schenckii*. Structural and immunochemical studies. *J Immunol* 107:663–671
38. Madrid H, Gené J, Cano J, Silvera C, Guarro J (2010) *Sporothrix brunneoviolacea* and *Sporothrix dimorphospora*, two new members of the *Ophiostoma stenoceras-Sporothrix schenckii* complex. *Mycologia* 102:1193–1203
39. Madrid H, Cano J, Gene J, Bonifaz A, Toriello C, Guarro J (2009) *Sporothrix globosa*, a pathogenic fungus with widespread geographical distribution. *Rev Iberoam Micol* 26:218–222
40. Maia DC, Gonçalves AC, Ferreira LS et al (2015) Response of cytokines and hydrogen peroxide to *Sporothrix schenckii* exoantigen in systemic experimental infection. *Mycopathologia*. doi:10.1007/s11046-015-9966-2
41. Maia DC, Sassá MF, Placeres MC, Carlos IZ (2006) Influence of Th1/Th2 cytokines and nitric oxide in murine systemic infection induced by *Sporothrix schenckii*. *Mycopathologia* 161:11–19
42. Marimon R, Gene J, Cano J, Guarro J (2008) *Sporothrix luriei*: a rare fungus from clinical origin. *Med Mycol* 46:621–625. doi:10.1080/13693780801992837
43. Marimon R, Serena C, Gené J, Cano J, Guarro J (2008) *In vitro* antifungal susceptibilities of five species of *Sporothrix*. *Antimicrob Agents Chemother* 52:732–734
44. Marimon R, Cano J, Gene J, Sutton DA, Kawasaki M, Guarro J (2007) *Sporothrix brasiliensis*, *S. globosa*, and *S. mexicana*, three new *Sporothrix* species of clinical interest. *J Clin Microbiol* 45:3198–3206
45. Marimon R, Gene J, Cano J, Trilles L, dos Santos Lazera M, Guarro J (2006) Molecular phylogeny of *Sporothrix schenckii*. *J Clin Microbiol* 44:3251–3256
46. Martinez FO, Gordon S (2014) The M1 and M2 paradigm of macrophage activation: time for reassessment. *F1000prime rep*. doi: 10.12703/P6-13.
47. Martinez FO, Helming L, Gordon S (2009) Alternative activation of macrophages: an immunologic functional perspective. *Annu Rev Immunol* 27:451–483
48. Mercadal-Peyri J, Bassas-Grau M, Sans-Macaré J, de Martin-Gasso C, Mercadal-Peyri JO (1965) Two very rare clinical diseases in our climate: cutaneous actinomycoses and blastomycosis of a vegetating type. *Mycopathol Mycol Appl* 27:68–74
49. Morrison AS, Lockhart SR, Bromley JG, Kim JY, Burd EM (2013) In environmental *Sporothrix* as a cause of corneal ulcer. *Med Mycol Case Rep* 2:88–90
50. Nascimento RC, Espíndola NM, Castro RA et al (2008) Passive immunization with monoclonal antibody against 70-kDa putative adhesin of *Sporothrix schenckii* induces protection in murine sporotrichosis. *Eur J Immunol* 30:3080–3089
51. Nascimento RC, Almeida SR (2004) Humoral immune response against soluble and fractionate antigens in experimental sporotrichosis. *FEMS Immunol Med Microbiol* 43:241–247
52. Negrini TC, Ferreira LS, Arthur RA et al (2014) Influence of TLR-2 in the immune response in the infection induced by fungus *Sporothrix schenckii*. *Immunol Invest* 43:370–390
53. Negrini TC, Ferreira LS, Alegranci P et al (2013) Role of TLR-2 and fungal surface antigens on innate immune response against *Sporothrix schenckii*. *Immunol Invest* 42:36–48
54. Oliveira DC, Markus Lopes PG, Spader TB, Mahl CD, Tronco-Alves GR, Lara VM, Santurio JM, Hartz Alves S (2011) Antifungal susceptibilities of *Sporothrix albicans*, *S. brasiliensis*, and *S. luriei* of the *S. schenckii* complex identified in Brazil. *J Clin Microbiol* 49:3047–3049
55. Oliveira MM, Santos C, Sampaio P, Romeo O, Almeida-Paes R, Pais C, Lima N, Zancopé-Oliveira RM (2015) Development and optimization of a new MALDI-TOF protocol for identification of the *Sporothrix* species complex. *Res Microbiol* 166:102–110
56. Padhye AA, Kaufman L, Durry E et al (1992) Fatal pulmonary sporotrichosis caused by *Sporothrix schenckii* var. *luriei* in India. *J Clin Microbiol* 30:2492–2494
57. Pludedeman A, Mukhopadhyay S, Gordon S (2011) Innate immunity to intracellular pathogens: macrophage receptors and responses to microbial entry. *Immunol Rev* 240:11–24
58. Portuondo-Fuentes DL, Batista-Duharte A, Ferreira LS et al (2015) A cell wall protein-based vaccine candidate offers protection in the *Sporothrix schenckii* infection. *Immunobiology* 221:300–309

59. Prompi boon P, Bhumiratana A, Ruchirawat S, Boucias DG, Wiwat C (2008) Isolation of ergosterol peroxide from *Nomuraea rileyi* infected larvae of tobacco cutworm. *World J Microb Biot* 24:2909–2917
60. Rodrigues AM, Fernandes GF, Araujo LM, Della Terra PP, dos Santos PO, Pereira SA, Schubach TM, Burger E, Lopes-Bezerra LM, de Camargo ZP (2015) Proteomics-based characterization of the humoral immune response in sporotrichosis: toward discovery of potential diagnostic and vaccine antigens. *PLoS Negl Trop Dis*. doi:10.1371/journal.pntd.0004016
61. Rodrigues AM, Kubitschek-Barreira PH, Fernandes GF, de Almeida SR, Lopes-Bezerra LM, de Camargo ZP (2015) Immunoproteomic analysis reveals a convergent humoral response signature in the *Sporothrix schenckii* complex. *J Proteomics* 115:8–22
62. Rodrigues AM, de Hoog GS, Zhang Y, de Camargo ZP (2014) Emerging sporotrichosis is driven by clonal and recombinant *Sporothrix* species. *Emerg Microbes Infect*. doi:10.1038/emi.2014.33
63. Rodrigues AM, de Hoog S, de Camargo ZP (2013) Emergence of pathogenicity in the *Sporothrix schenckii* complex. *Med Mycol* 51:405–412
64. Roets F, de Beer ZW, Wingfield MJ, Crous PW, Dreyer LL (2008) *Ophiostoma gemellus* and *Sporothrix variecibatus* from mites infesting *Protea infructescences* in South Africa. *Mycologia* 100:496–510
65. Romani L (2011) Immunity to fungal infections. *Nat Rev Immunol* 11:275–288
66. Romani L (2004) Immunity to fungal infections. *Nat Rev Immunol* 4:1–13
67. Romo-Lozano Y, Hernández-Hernández F, Salinas E (2014) *Sporothrix schenckii* yeasts induce ERK pathway activation and secretion of IL-6 and TNF- α in rat mast cells, but no degranulation. *Med Mycol* 52:862–868
68. Romo-Lozano Y, Hernández-Hernández F, Salinas E (2012) Mast cell activation by conidia of *Sporothrix schenckii*: role in the severity of infection. *Scand J Immunol* 76:11–20
69. Ruiz-Baca E, Hernández-Mendoza G, Cuéllar-Cruz M, Toriello C, López-Romero E, Gutiérrez-Sánchez G (2014) Detection of two immunoreactive antigens of the cell wall of *Sporothrix brasiliensis* and *S. globosa*. *Diagn Microbiol Infect Dis* 79:328–330
70. Ruiz-Baca E, Mora-Montes HM, López-Romero E, Toriello C, Mojica-Marín V, Urtiz-Estrada N (2011) 2D-immunoblotting analysis of *Sporothrix schenckii* cell wall. *Mem Inst Oswaldo Cruz* 106:248–250
71. Ruiz-Baca E, Toriello C, Pérez-Torres A, Sabanero-López M, Villagómez-Castro JC, López-Romero E (2009) Isolation and some properties of a glycoprotein of 70 kDa (Gp70) from the cell wall of *Sporothrix schenckii* involved in fungal adherence to dermal extracellular matrix. *Med Mycol* 47:185–196
72. Sassá MF, Ferreira LS, Ribeiro LC, Carlos IZ (2012) Immune response against *Sporothrix schenckii* in TLR-4 deficient mice. *Mycopathologia* 174:21–30
73. Sassá MF, Satri AE, Souza LF, Ribeiro LC, Sgarbi DB, Carlos IZ (2009) Response of macrophage Toll-Like receptor 4 to a *Sporothrix schenckii* lipid extract during experimental sporotrichosis. *Immunology* 128:301–309
74. Scott EN, Muchmore HG (1989) Immunoblot analysis of antibody responses to *Sporothrix schenckii*. *J Clin Microbiol* 27:300–304
75. Scott EN, Muchmore HG (1985) Activation of the alternative complement pathway. *Infect Immun* 51:6–9
76. Segal BH (2007) Role of macrophages in host defense against aspergillosis and strategies for immune augmentation. *Oncologist* 12:7–13
77. Sethi KK, Schwarz J (1965) Experimental cutaneous sporotrichosis. *Mykosen* 8:128–135
78. Sgarbi DB, da Silva AJ, Carlos IZ (1997) Isolation of ergosterol peroxide and its reversion to ergosterol in the pathogenic fungus *Sporothrix schenckii*. *Mycopathologia* 139:9–14
79. Shaw JC, Levinson W, Montanaro A (1989) Sporotrichosis in the acquired immunodeficiency syndrome. *J Am Acad Dermatol* 21:1145–1147
80. Shimonaka H, Noguchi T, Kawai K, Hasegawa I, Nasawa I, Ito Y (1975) Immunochemical studies on the human pathogen *Sporothrix schenckii*: effects of chemical and enzymatic modification of the antigenic compounds upon immediate and delayed reactions. *Infect Immun* 11:1187–1194
81. Shiraishi A, Nakagaki K, Arai T (1992) Role of cell mediated immunity in the resistance to experimental sporotrichosis in mice. *Mycopathologia* 120:15–21
82. Shiraishi A, Nakagaki K, Arai T (1979) Experimental sporotrichosis in congenitally athymic (nude) mice. *J Reticuloendothelial Soc* 26:333–336
83. Silva-Vergara ML, de Camargo ZP, Ferreira-Silva P et al (2012) Case report: disseminated *Sporothrix brasiliensis* infection with endocardial and ocular involvement in an HIV-infected patient. *Am J Trop Med Hyg* 86:477–480
84. Silva-Vergara ML, Maneira FRZ, Oliveira RM et al (2005) Multifocal sporotrichosis with meningeal involvement in a patient with AIDS. *Med Mycol* 43:187–190
85. Tachibana T, Matsuyama T, Mitsuyama M (1999) Involvement of CD4+T cells and macrophages in acquired protection against infection with *Sporothrix schenckii* in mice. *Med Mycol* 37:397–404
86. Téllez MD, Batista-Duarte A, Portuondo D, Quinello C, Bonne-Hernandez R, Carlos IZ (2014) *Sporothrix schenckii* complex biology: environment and fungal pathogenicity. *Microbiology* 160:2352–2365
87. Teixeira MM, de Almeida LGP, Kubitschek-Barreira P et al (2014) Comparative genomics of the major fungal agents of human and animal Sporotrichosis: *Sporothrix schenckii* and *Sporothrix brasiliensis*. *BMC Genom* 15:943
88. Teixeira PA, de Castro RA, Nascimento RC et al (2009) Cell surface expression of adhesins for fibronectin correlates with virulence in *Sporothrix schenckii*. *Microbiology* 155:3730–3738
89. Uenotsuchi T, Tekeuchi S, Matsuda T et al (2006) Differential induction of Th1-prone immunity by human dendritic cells activated with *Sporothrix schenckii* of cutaneous and visceral origins to determine their different virulence. *Int Immunol* 18:1637–1646
90. Ursini F, Russo E, Leporini C, Calabria M, Bruno C, Tripolino C, Naty S, Grembale RD (2015) Lymphocutaneous sporotrichosis during treatment with anti-TNF-alpha monotherapy. *Case Rep Rheumatol*. doi:10.1155/2015/614504
91. Verdan FF, Faleiros JC, Ferreira LS, Monazzi LG, Maia DC, Tansine A, Placeres MC, Carlos IZ, Santos-Junior RR (2012) Dendritic cell are able to differentially recognize *Sporothrix schenckii* antigens and promote Th1/Th17 response in vitro. *Immunobiology* 217:788–794
92. Zhang Y, Hagen F, Stielow B, Rodrigues AM, Samerpitak K, Zhou X, Feng P, Yang L, Chen M, Deng S, Li S, Liao W, Li R, Li F, Meis JF, Guarro J, Teixeira M, Al-Zahrani HS, de Camargo ZP, Zhang L, de Hoog GS (2015) Phylogeography and evolutionary patterns in *Sporothrix* spanning more than 14000 human and animal case reports. *Persoonia* 35:1–20
93. Zhang Z, Liu X, Lv X, Lin J (2011) Variation in genotype and higher virulence of a strain of *Sporothrix schenckii* causing disseminated cutaneous sporotrichosis. *Mycopathologia* 172:439–446
94. Zhou X, Rodrigues AM, Feng P, de Hoog GS (2014) Global ITS diversity in the *Sporothrix schenckii* complex. *Fungal Divers* 66:153–165

Research Article

Immune Response Induced by an Immunodominant 60 kDa Glycoprotein of the Cell Wall of *Sporothrix schenckii* in Two Mice Strains with Experimental Sporotrichosis

**Carlos A. Alba-Fierro,¹ Armando Pérez-Torres,² Conchita Toriello,³
Evelyn Pulido-Camarillo,² Everardo López-Romero,⁴ Yolanda Romo-Lozano,⁵
Gerardo Gutiérrez-Sánchez,⁶ and Estela Ruiz-Baca¹**

¹Facultad de Ciencias Químicas, Universidad Juárez del Estado de Durango, Avenida Veterinaria S/N, 34120 Durango, DGO, Mexico

²Departamento de Biología Celular y Tisular, Facultad de Medicina, Universidad Nacional Autónoma de México, 04510 Ciudad de México, DF, Mexico

³Departamento de Microbiología y Parasitología, Facultad de Medicina, Universidad Nacional Autónoma de México, 04510 Ciudad de México, DF, Mexico

⁴Departamento de Biología, División de Ciencias Naturales y Exactas, Universidad de Guanajuato, Campus Guanajuato, Noria Alta S/N, 36050 Guanajuato, GTO, Mexico

⁵Departamento de Microbiología, Centro de Ciencias Básicas, Universidad Autónoma de Aguascalientes, Avenida Universidad No. 940, 20131 Aguascalientes, AGS, Mexico

⁶Department of Biochemistry and Molecular Biology and Complex Carbohydrate Research Center, University of Georgia, 315 Riverbend Road, Athens, GA 30602-4712, USA

Correspondence should be addressed to Estela Ruiz-Baca; eruiz@ujed.mx

Received 16 November 2015; Accepted 21 January 2016

Academic Editor: Enrico Maggi

Copyright © 2016 Carlos A. Alba-Fierro et al. This is an open access article distributed under the Creative Commons Attribution License, which permits unrestricted use, distribution, and reproduction in any medium, provided the original work is properly cited.

Cell wall (CW) components of fungus *Sporothrix schenckii* are the major inductors antigens of immune responses. The immunodominant 60 kDa glycoprotein (gp60) has been shown to be associated with the virulence of this fungus but its role in experimental sporotrichosis is unknown. In this work, the immunological effects of CW-purified gp60 were investigated in a model of experimental subcutaneous sporotrichosis in normal and gp60-preimmunized C57BL/6 and BALB/c mice strains which were then infected with *S. schenckii* conidia. Results showed that both mice strains use different cytokine profiles in order to fight *S. schenckii* infection; C57BL/6 mice seem to use a Th17 response while BALB/c mice tend to depend on a Th1 profile. Preimmunization with gp60 showed a downregulatory effect on the immune response since cytokines levels were diminished in both strains. There were no significant differences in the magnitude of dorsoplantar inflammation between gp60-preimmunized and nonimmunized mice of both strains. However, skin lesions due to the infection in gp60-preimmunized mice were more severe in BALB/c than in C57BL/6 mice, suggesting that the antigen exerts a higher downregulatory effect on the Th1 response.

1. Introduction

Sporotrichosis is a chronic mycosis that affects skin and subcutaneous tissues, but it also can spread to other organs through the lymph vessels [1–4]. It is acquired by traumatic implantation of the etiologic agent, the dimorphic fungus *Sporothrix schenckii*. The mycelial morphotype is found in

soil, wood, and plants [5], while the yeast morphotype is found in host tissues [6, 7]. Surface components of *S. schenckii* cell wall (CW) have a possible role in its pathogenicity. Accordingly, ergosterol peroxide helps the organism to evade the host's immune response, promoting fungal infection [8]. Also, a lipid antigen has been shown to decrease the production of proinflammatory cytokines such as TNF- α , IL-1 β , and

also IL-12 and IL-10 in experimental models of sporotrichosis [9, 10]; moreover, it is capable of inhibiting macrophage phagocytosis in *in vitro* assays [11].

One of the most studied CW components of *S. schenckii* is a peptide-polysaccharide known as peptide-rhamnomannan, a glycoconjugate molecular complex with a wide range of molecular weights composed of 33.5% rhamnose, 57% mannose, and 14.2% protein [12]. In murine models of sporotrichosis, the peptide-rhamnomannan is involved in the anti-inflammatory response diminishing the production of IL-1 β and TNF- α [10], and in *in vitro* lymphoproliferation assays have shown that it contains components with different mitogenic activities [13–15].

Recently, a 70 kDa glycoprotein (gp70) isolated from the CW of the yeast morphotype of *S. schenckii* has become a relevant cell surface component [16]. This molecule has an isoelectric point (IP) of 4.1 and about 5.7% of its molecular weight (MW) corresponds to carbohydrate residues. Some important features of gp70 are its ability to adhere to extracellular matrix proteins [16] and to induce a specific humoral response in *S. schenckii* infected mice [17]. Interestingly, administration of anti-gp70 monoclonal antibodies appears to have protective effect against fungal infection in mice [18]. In addition to the antigenic gp70, *S. schenckii* strains also express a 60 kDa immunodominant glycoprotein (gp60) [19, 20], and both have been proposed as potential virulence factors since they are expressed by the most virulent strains of the *Sporothrix* complex [21]. Recent studies seem to indicate that gp70 and gp60 share the same peptide but differ in glycosylation pattern, IP, and MW [22].

In order to shed light on the role of the gp60 during infection by *S. schenckii*, the antigen was purified by isoelectric focusing and continuous elution electrophoresis, and its effect on the immune response in two mice strains with experimental cutaneous sporotrichosis was evaluated.

2. Materials and Methods

2.1. Bioethical Statements. All procedures carried out in animals were approved by the Animal Ethics Committee, Facultad de Medicina, Universidad Nacional Autónoma de México, and followed the Mexican Official Guide (NOM 062-ZOO-1999) for the care and use of laboratory animals.

2.2. Animals. Male C57BL/6 and BALB/c mice, 8–10 weeks old, were purchased from Harlan (Mexico City, Mexico). The animals were free of parasites or pathogens and were fed mouse chow (Purina de México, México) and water *ad libitum*. Mice were housed in separate cages with wood shavings as nesting material, and five individuals were housed per cage. They were maintained in a 12/12 h light/dark cycle in a room thermostatically maintained at $24 \pm 2^\circ\text{C}$ throughout the study. Groups of ten experimental animals by mice strain and each corresponding control group of five mice were conformed. Two 12-week-old male New Zealand rabbits weighing 3.21 and 3.35 Kg were used to obtain hyperimmune serum.

2.3. Organism and Culture Conditions. *S. schenckii* strain ATCC 58251 was used for this study. Conidia were obtained from the mycelial morphotype prepared from a 10-day-old culture grown at 28°C in YPG medium [0.3% (w/v) yeast extract, 1% (w/v) peptone, and 2% (w/v) glucose] at pH 4.5. The yeast morphotype was obtained in YPG medium, pH 7.2, inoculated with 5×10^5 conidia mL^{-1} , and incubated for 10 days at 37°C with shaking (120 rpm). The harvested cells (centrifugation at 7000 g for 10 min) were washed twice with lysis buffer [50 mM Tris-HCl, pH 7.5, supplemented with 1 mM phenylmethylsulfonyl fluoride (PMSF)] and maintained at -20°C until used.

2.4. Extraction of CW Proteins. Yeast cells were resuspended in lysis buffer and broken with glass beads (0.45–0.5 mm in diameter) in an MSK cell homogenizer (Braun Melsungen, Germany) by alternate periods of breaking (40 s) and cooling (60 s) until all cells were broken. To isolate the CW, the cell homogenate was centrifuged at 1300 g for 15 min at 4°C , and the pellet was washed thrice with lysis buffer to remove any intracellular component associated with the CW during the cell-breaking process. CW proteins were extracted with hot 2% (w/v) sodium dodecyl sulfate (SDS) as described previously [16], precipitated with 70% ethanol for 2 h at -20°C , and stored at -70°C until use. CW proteins were quantified with the DC kit (Bio-Rad).

2.5. Two-Dimensional Gel Electrophoresis (2D-PAGE). CW proteins were analyzed by 2D-PAGE gels as described by Ruiz-Baca et al. [19]. Briefly, the extracted proteins were cleaned with the ReadyPrep 2D Cleanup kit (Bio-Rad) following the manufacturer's instructions. Samples of 160 μg of protein were resuspended in hydration buffer [7 M urea, 2 M thiourea, 4% (w/v) 3-[(3-cholamidopropyl)dimethylammonio]-1-propanesulfonate (CHAPS), 20 mM dithiothreitol (DTT), 0.5% (w/v) ampholytes, and 0.002% (w/v) bromophenol blue] and applied on immobilized pH 4–7 gradient strips (7 cm, Bio-Rad). The samples were hydrated for 16 h at 4°C . Isoelectric focusing (IEF) was performed in a Protean IEF system (Bio-Rad) using the following conditions: 250 volts (V) for 20 min, 4000 V for 2 h until 10000 V/h was reached. After IEF, the strips were incubated sequentially for 15 min in equilibrium buffer I [50 mM Tris/HCl, pH 8.8, 6 M urea, 30% (v/v) glycerol, 2% (w/v) SDS, and 0.5% (w/v) DTT] and equilibrium buffer II [50 mM Tris/HCl, pH 8.8, 6 M urea, 30% (v/v) glycerol, 2% (w/v) SDS, and 2% (w/v) iodoacetamide] under constant stirring. For the second dimension, the strips were mounted on 10% SDS-PAGE gels and run at 95 V for 2 h in a Mini-Protean 3 system (Bio-Rad). The gels were either stained by Coomassie Blue G-250 or transferred to nitrocellulose membranes.

2.6. Production of Polyclonal Anti-gp60 Antibodies. To this purpose, the same methodology reported by Ruiz-Baca et al. [19] was followed. Briefly, several samples of the gp60 antigen from 2D-PAGE gels stained with Coomassie Blue were obtained. The gel pieces were macerated with the help of a mortar and resuspended in sterile distilled water. A dose was

intramuscularly injected every 7 days for 4 weeks into male New Zealand rabbits. Each dose contained approximately 12.5 μg of gp60 suspended in a volume of 1 mL (50% distilled water and 50% adjuvant). The first and three last doses contained complete and incomplete Freund's adjuvant (Sigma), respectively. One week after the last dose, rabbits were sacrificed and bled to death, the serum was collected, and immunoglobulins were fractionated with 50% ammonium sulfate.

2.7. Western Blot. Immunodetection was carried out as previously described by Ruiz-Baca et al. [20]. Briefly, the membrane was blocked for 1 h with a skim milk solution (5%, w/v) in phosphate-buffered saline (PBS), pH 7.2. After washing thrice with PBS, membrane was incubated overnight with either anti-gp60 rabbit polyclonal antibody diluted 1:2000 or sera from nonimmunized or preimmunized mice with gp60 diluted 1:100 in PBS supplemented with 0.05% (v/v) Tween 20, as primary antibodies. Membrane was then washed thrice with the same buffer and incubated in anti-rabbit IgG or anti-mouse IgG, both goat horseradish peroxidase-conjugated secondary antibodies, diluted 1:1000 in PBS with gentle shaking for 2 h. After washing with PBS, enzyme activity was revealed with a solution containing 3-3'-diaminobenzidine (DAB, 1 mg/mL) and 0.01% (v/v) H_2O_2 . As a positive control for the presence of anti-gp60 antibodies in mice, anti-gp60 polyclonal antibodies were used.

2.8. Immunofluorescence to gp60 in Yeast Cells. Yeast cells were obtained from a 10-day-old culture, washed thrice with PBS, and centrifuged for 5 min at 7000 g. The resultant cell pellet was fixed for 30 min in 2% (w/v) paraformaldehyde diluted in PBS at 4°C and washed four times with cold PBS. Fixed cells were incubated for 1 h at room temperature (RT) with the anti-gp60 polyclonal antibody diluted 1:100 in PBS solution containing 5% (w/v) bovine serum albumin (BSA). After washing thrice with PBS, cells were incubated for 1 h at RT in the dark with a goat anti-rabbit antibody conjugated to fluorescein isothiocyanate (FITC), diluted 1:50 in PBS solution containing 0.1% (w/v) BSA. Finally, yeast cells were washed thrice with PBS and analyzed using the Axio-observer Z1 LSM 700 Carl Zeiss confocal microscope. Yeast cells processed as described above but incubated either with preimmune serum or with the secondary antibody conjugated to FITC only were used as control. Other cells fixed only in paraformaldehyde were used to assess the potential autofluorescence.

2.9. Purification of gp60. For the purification of gp60, CW proteins were extracted as described above. Approximately 6 mg of proteins was resuspended in 18 mL of hydration buffer at a concentration of 7% (v/v) ampholytes with a pH gradient of 3–10. The suspension of proteins was loaded onto a Rotofor preparative IEF cell (Bio-Rad) and ran for 4 h at a constant power of 12 watts (W) using a Powerpac Universal Power Supply (Bio-Rad). Subsequently, fractions enriched in gp60 were pooled and mixed with hydration buffer to reach 18 mL without further addition of ampholytes. This

sample was run on the same equipment for 2.5 h at a constant power of 12 W. Fractions enriched in gp60 were precipitated with 70% (v/v) ethanol at -20°C for 24 h and centrifuged and the resulting pellets were resuspended in 2x buffer [0.125 M Tris-HCl, pH 6.8; 4% (w/v) SDS, 20% (v/v) glycerol, 200 mM β -mercaptoethanol, and 0.002% (w/v) bromophenol blue]. The samples were separated by continuous elution electrophoresis for 6 h at 1 W in a Mini-Prep Cell (Bio-Rad). Fractions enriched in gp60 were pooled and kept in elution buffer [0.3% (w/v) Tris-HCl, 1.4% (w/v) glycine, and 1% (w/v) SDS]. The glycoprotein was monitored along the steps of purification by SDS-PAGE electrophoresis and Western blot using anti-gp60 as primary antibody.

2.10. gp60 Peptide Identification by LC-MS/MS Analysis. The gp60 was purified and manually excised from Coomassie Blue-stained electrophoresis gels. The gel pieces were washed and reduced with DTT and alkylated with iodoacetamide and in gel-digested with trypsin. LC-MS/MS analysis was performed on an Orbitrap Fusion Tribrid (Thermo Scientific) utilizing a nanospray ionization source. An instrument method was used to collect full mass spectrum every three seconds and continuously fragment the most intense ions with 38% collision-induced dissociation (CID) and record the resulting MS/MS spectra. Raw tandem mass spectra were converted to mzXML files and then to Peak List files (PKL) via the Transproteomic Pipeline (Seattle Proteome Center, Seattle, WA). PKL were searched using Mascot (Matrix Scientific, Boston, MA) against separate target and decoy databases containing dimorphic fungi proteins (*Sporothrix*, *Coccidioides*, *Blastomyces*, *Paracoccidioides*, *Lacazia*, and *Penicillium marneffeii*) downloaded June 17, 2014, from the Dimorphic Fungal Database from Broad Institute and National Center for Biotechnology Information (NCBI). Mascot settings were as follows: tryptic enzymatic cleavages allowing for up to 2 missed cleavages, peptide tolerance of 800 ppm, fragment ion tolerance of 0.8 Da, fixed modification due to carboxyamidomethylation of cysteine (+57 Da), and variable modifications of oxidation of methionine (+16 Da) and deamidation of asparagine or glutamine (+0.98 Da). Statistically significant protein was determined at a 1% protein false discovery rate applied via ProteoIQ (NuSep, Bogart, GA) by loading Mascot.DAT target and decoy search files into the software program.

2.11. Effect of gp60 on the Mice Immune Response during *S. schenckii* Infection. To evaluate the effect of gp60, BALB/c and C57BL/6 mice strains were injected intramuscularly with 100 μL (50% elution buffer and 50% adjuvant) containing 2 μg of gp60 every 7 days for three weeks (gp60-preimmunized mice groups); the first and subsequent doses were administered in complete and incomplete Freund adjuvant, respectively. Animals of each strain received the same treatment protocol without adding gp60 (nonimmunized mice groups). One week after treatment completion, blood samples from each mouse were collected in 500 μL tubes by facial vein phlebotomy to determine the anti-gp60 antibodies using the anti-gp60 polyclonal antibodies as a positive control.

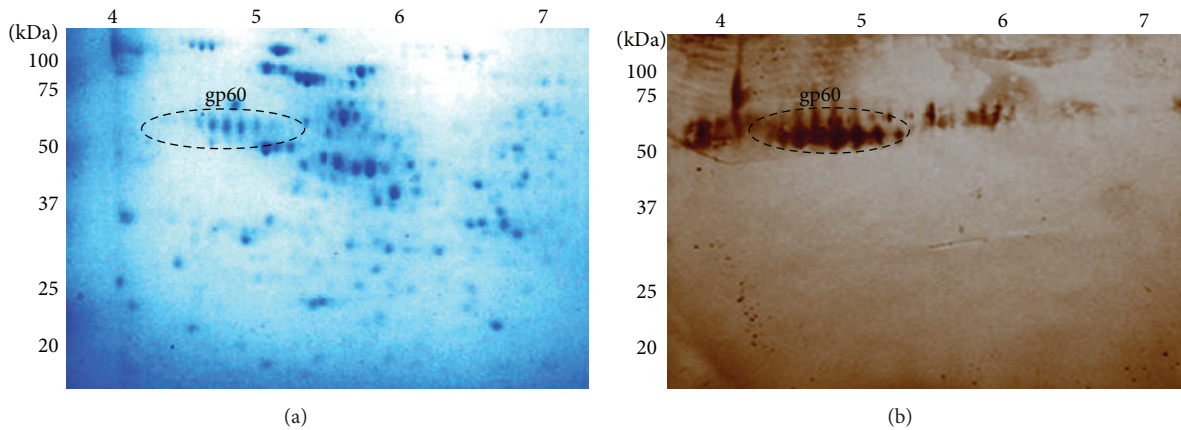


FIGURE 1: Cell wall proteins of yeast-like cells of *S. schenckii* were separated on 2D-PAGE gels and detected with Coomassie Blue (a) and Western blot using polyclonal anti-gp60 primary antibodies and peroxidase-conjugated secondary antibodies (b). Signal was revealed with a DAB-peroxidase substrate solution. Dotted circles represent gp60 antigen (pH 4.5–5.5) showing several isoforms. The position of molecular weight standards is indicated on the left.

Thereafter, all mice were infected subcutaneously by injecting 100 μL of PBS containing 5×10^5 conidia of *S. schenckii*. Mice were examined every three days during three weeks by evaluating the thickness of dorsoplantar inflammation with a Mitutoyo[®] micrometer and the presence of skin ulceration or scarring in foot dorsum. Additionally, five animals of each strain neither infected nor treated with gp60 were used as control groups. 19 days after infection, the mice were bled to determine anti-gp60 antibodies and some cytokines of Th1 and Th2 responses.

2.12. Determination of Cytokines. The cytokines IL-1 β , TNF- α , IL-12p40, IL-12p70, MIP-2, and IFN- γ from the Th1 response and IL-6, IL-4, and IL-10 from Th2 response were determined using the Luminex xMAP Milliplex Analyst Platform technology (Millipore kit) according to the manufacturer's instructions. Briefly, the serum samples were diluted in the assay buffer contained in the kit at 1:1 (v/v) ratio. The quality controls and the cytokine standards provided by the kit were also prepared. Afterwards, a 96-well ELISA plate was washed with washing buffer and 25 μL of each standard, control, and sample was added to the respective wells followed by 25 μL of assay buffer and 25 μL of magnetic beads. The plate was stirred at RT and after 2 h, it was washed twice with washing buffer and 25 μL of detection antibody was added to each well. Following this, the plate was stirred at RT and after 1 h, 25 μL of streptavidin and phycoerythrin was added and incubated for 30 min at RT. Finally, after two additional washes the plate was read on a Magpix reader after adding 150 μL of driving fluid to each well.

2.13. Statistical Analysis. Data from cytokine levels are expressed as mean \pm SD and analyzed by ANOVA followed by Tukey test. Data from ulceration are expressed as percentages and analyzed by Fisher's test. GraphPad Prism 6 was used to perform all analysis.

3. Results

3.1. Production of Polyclonal Antibodies. Anti-gp60 polyclonal antibodies were produced to monitor the reactivity of the yeast cell to this antigen and to track gp60 during the purification process. Figure 1 shows the separation of the CW proteins in 2D-PAGE gels, where at least six isoforms of the glycoprotein are seen in a pH range between 4.5 and 5.5 (Figure 1(a)). These isoforms were cut from different 2D-PAGE gels and used to inoculate a rabbit intramuscularly. One week after the last immunization dose, the rabbit was bled to obtain hyperimmune serum which was analyzed by Western blot (Figure 1(b)). Antibodies titers were up to 1/10000 (data not shown).

3.2. Confocal Microscopy. Immunofluorescence and confocal microscopy confirmed the expression of gp60 in the yeast morphotype of the fungus. This morphotype was observed with phase contrast microscopy (Figures 2(a) and 2(c)). Images indicate that gp60 is located on the cell surface of yeast cells (Figure 2(b)). Controls incubated with preimmune sera and paraformaldehyde-associated autofluorescence were negative (Figure 2(d)).

3.3. Purification of gp60. In order to obtain sufficient amounts of purified gp60 to determine its effect on the immune response, we standardized a purification protocol based on liquid phase IEF and continuous elution electrophoresis. The protein was monitored through the various purification steps by Western blot assays using the anti-gp60 antibodies. Results from liquid phase IEF showed that most of the pollutant proteins were in fractions 3 and 4, and despite the fact that gp60 was detected in every fraction, results showed a higher antigen concentration in fractions corresponding to lanes 5 through 11 (Figures 3(a) and 3(b)). These fractions were pooled and again subjected to IEF, which showed a higher concentration of gp60 in fractions

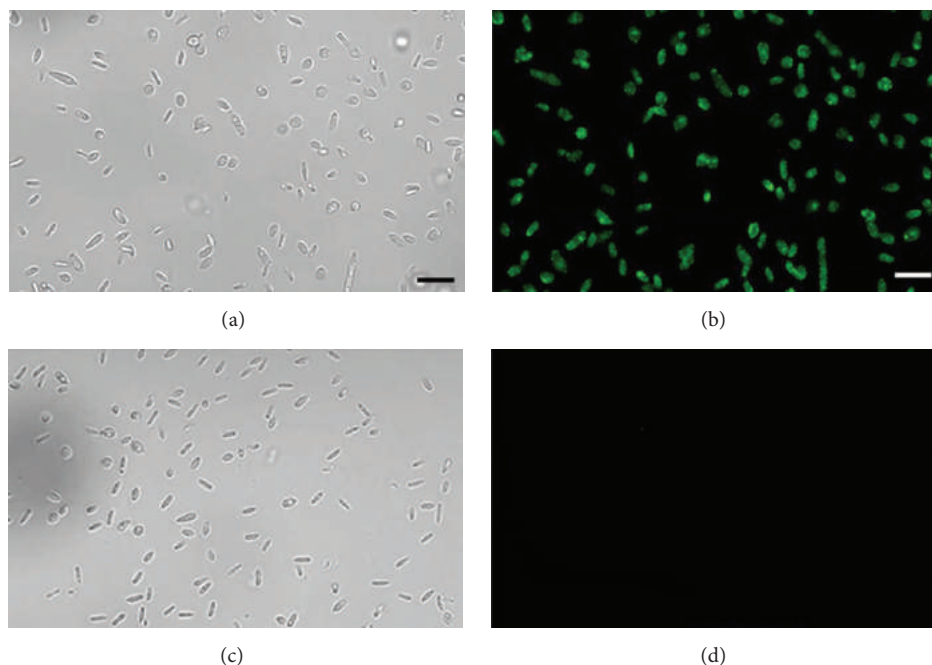


FIGURE 2: Immunolocalization of gp60 by confocal microscopy in the yeast morphotype of *S. schenckii*. Cells were incubated with polyclonal anti-gp60 antibodies ((a) and (b)) or preimmune sera ((c) and (d)). Bars = 10 μ m.

TABLE 1: Analysis of gp60 by LC-MS/MS.

Protein name	Molecular weight (kDa)	Protein score	Peptide sequence	# of spectra	Sequence coverage (%)
Carboxy- <i>cis</i> , <i>cis</i> -muconate cyclase [<i>S. schenckii</i>]	43.3	1171.6	LVEMSLVNAEIIGEPIDLTTFNTDPGLTEIR AGVSCASYSWYGLGPFDEL TVIPGQDATCWVAICPATHTAFVTDIR AVYVTSNTEHNSVVAIPIAR GGNGINPR NGSLLLNHATSTATGGR KPVQHALLTPLGLDR VTVVGEPALPGEFPTTVGASDKFNLVCVGLTGAK	185	42

Mass spectra were analyzed with Mascot and validated with ProteoIQ software.

Protein name: protein name as deduced by comparing peptide sequences via the software BLAST.

Molecular weight (kDa): theoretical molecular mass predicted from the amino acid sequence of the identified protein.

Protein score: sum of Mascot ion scores of all nonredundant peptides belonging to the protein.

Peptide sequence: peptides identified after LC-MS/MS analysis.

of spectra: total number of spectra matched to the protein.

Sequence coverage: coverage of the amino acid sequence of the identified protein.

corresponding to lanes 11 through 14 (Figures 3(c) and 3(d)). Subsequently, enriched fractions obtained after the second IEF were pooled and the pool was purified by continuous elution electrophoresis. This step yielded 5 fractions containing gp60 with a high degree of purity (Figures 3(e) and 3(f), lanes 2, 3, 4, 5, and 6) with the different isoforms ranging from 55 to 65 kDa.

3.4. Peptide Sequencing of gp60. The spots of the different gp60 isoforms separated in 2D-PAGE gels stained with Coomassie Blue were cut from the gel and exposed to tryptic digestion. The resulting peptides were analyzed by mass

spectrometry (LC-MS/MS) and gp60 was identified as a carboxy-*cis*, *cis*-muconate cyclase of *S. schenckii* (Table 1).

3.5. Effect of gp60 on the Mice Immune Response during *S. schenckii* Infection. The gp60-preimmunized C57BL/6 and BALB/c groups were subsequently infected with *S. schenckii*. Only gp60-preimmunized C57BL/6 mice showed the presence of anti-gp60 antibodies prior to infection, although detection was very low as can be seen in Figure 4 (lanes 3 and 4). Nonimmunized groups of both strains did not produce anti-gp60 antibodies (Figure 4, lanes 2 and 5). However, 21 days after infection, gp60-preimmunized mice

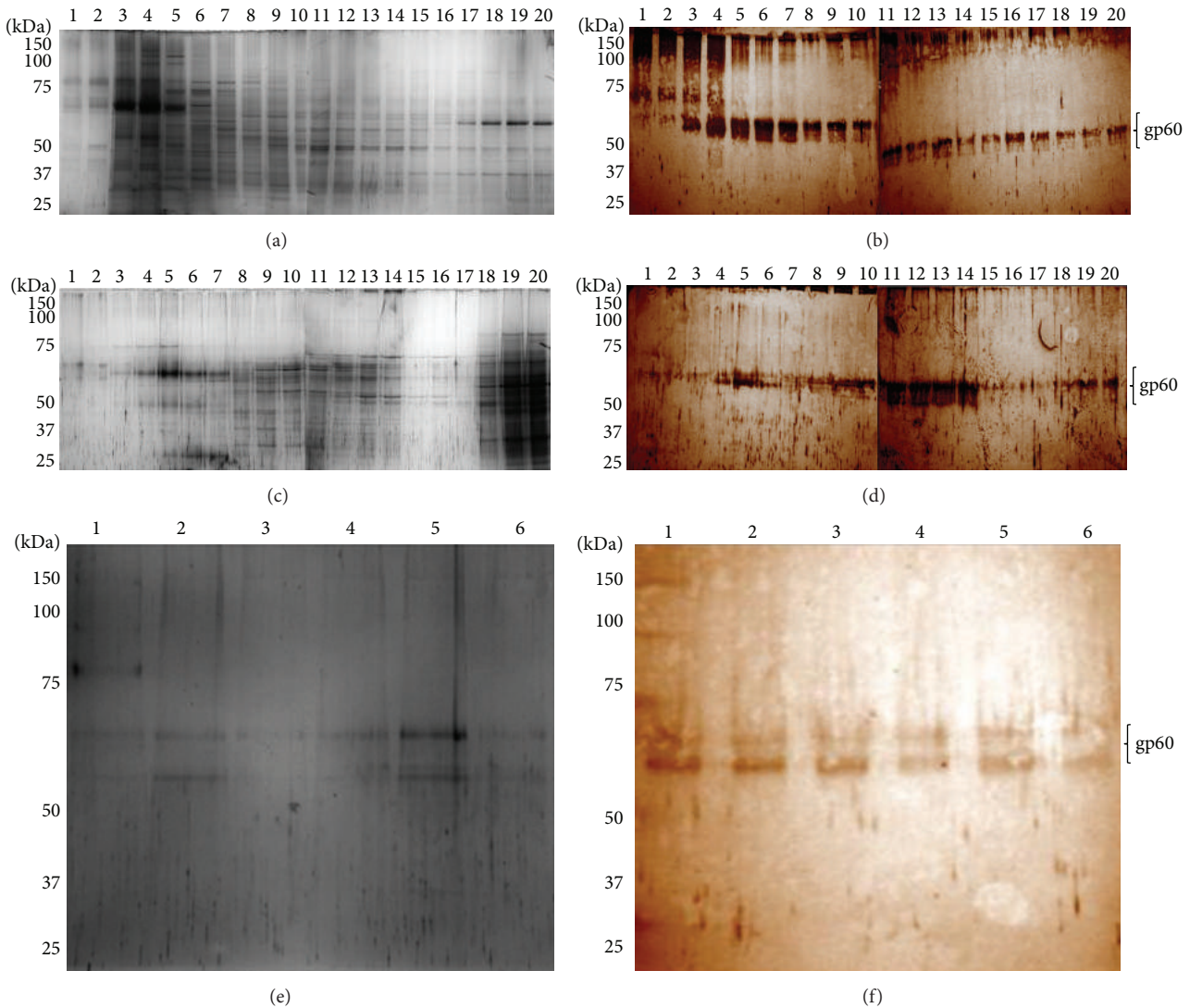


FIGURE 3: Purification of gp60. Cell wall proteins of yeast-like cells of *S. schenckii* were separated by sequential steps of liquid phase isoelectric focusing and electrophoresis with continuous electroelution as described in Materials and Methods. After each step, fractions were analyzed by SDS-PAGE ((a), (c), and (e)) and Western blot ((b), (d), and (f)) using polyclonal anti-gp60 primary antibodies and peroxidase-conjugated secondary antibodies. Signal was revealed with a DAB-peroxidase substrate solution. Fractions separated after the first ((a) and (b)) and second ((c) and (d)) liquid phase isoelectric focusing steps and after electrophoresis with continuous electroelution ((e) and (f)).

of both strains, as well as those that were infected only (nonimmunized mice groups), showed anti-gp60 antibodies. A higher detection was shown by the groups that received gp60 before infection (Figure 5, lanes 4, 5, 6, 10, 11, and 12) compared to the nonimmunized groups (Figure 5, lanes 1, 2, 3, 7, 8, and 9), particularly the C57BL/6 strain (Figure 5, lanes 4, 5, and 6).

Nonimmunized mice of both strains seemed to heal faster than those preimmunized with gp60 prior to infection (Figure 6); however, nonimmunized C57BL/6 mice (Figure 6(a)) did not show significant differences in foot dorsum ulceration (Figure 7(a)) as compared to those of the same strain that received gp60 prior to infection (Figure 6(b)), contrary to nonimmunized BALB/c mice (Figure 6(c)) which showed significant differences (Figure 7(b)) compared to

gp60-preimmunized mice of the same strain (Figure 6(d)). A lower susceptibility to *S. schenckii* was noted in C57BL/6 mice, since nonimmunized C57BL/6 mice showed lower ulceration than nonimmunized BALB/c mice (Figure 7(c)). Also, a different effect induced by gp60 was noted between the strains since gp60-preimmunized C57BL/6 mice showed a significant lower ulceration than gp60-preimmunized BALB/c mice (Figure 7(d)). No statistical differences in inflammation were detected between nonimmunized and gp60-preimmunized groups (data not shown).

3.6. Cytokine Profiles during Infection by *S. schenckii*. The cytokine profiles expressed by C57BL/6 and BALB/c mice strains were different in the baseline levels and during infection with *S. schenckii*. Control C57BL/6 mice showed

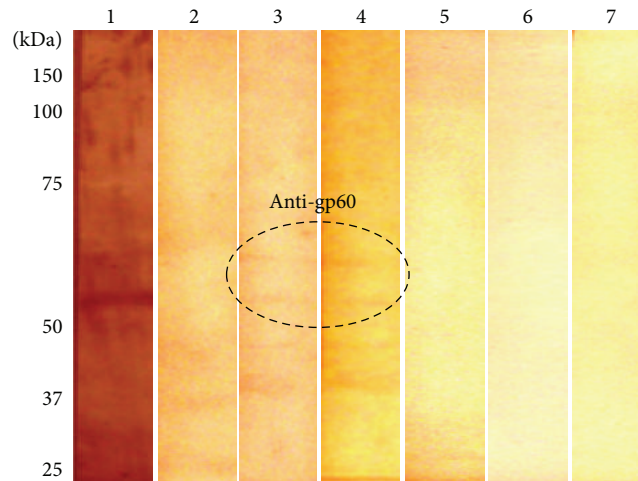


FIGURE 4: Presence of anti-gp60 antibodies in mice prior to infection. Cell wall proteins of yeast-like cells of *S. schenckii* were analyzed by Western blot using sera from nonimmunized and gp60-preimmunized mice and peroxidase-conjugated secondary antibodies. Signal was revealed with a DAB-peroxidase substrate solution. Positive control (lane 1), nonimmunized C57BL/6 (lane 2), gp60-preimmunized C57BL/6 (lanes 3 and 4), nonimmunized BALB/c (lane 5), and gp60-preimmunized BALB/c (lanes 6 and 7) mice.

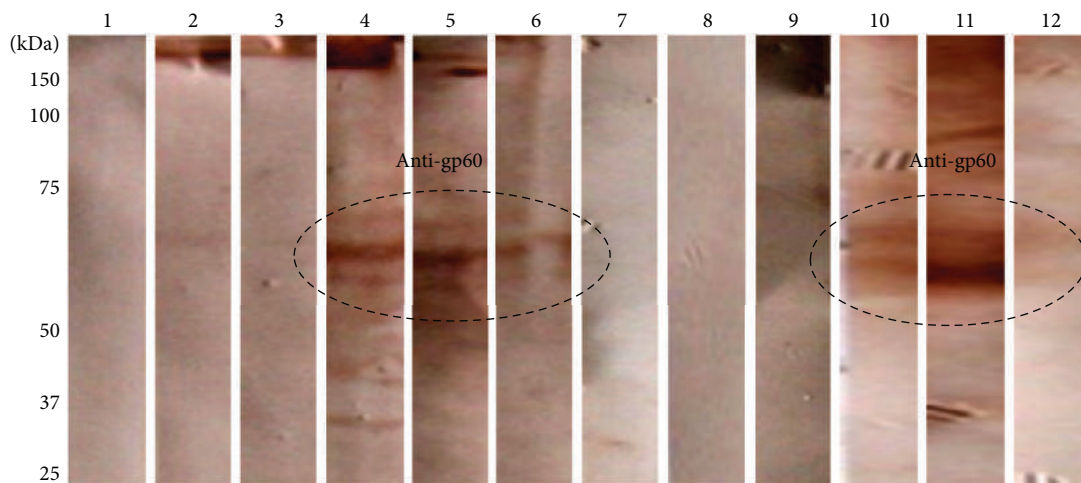


FIGURE 5: Presence of anti-gp60 antibodies in nonimmunized and gp60-preimmunized mice after 19 days after infection. Cell wall proteins of yeast-like cells of *S. schenckii* were analyzed by Western blot using sera from nonimmunized and gp60-preimmunized mice and peroxidase-conjugated secondary antibodies. Signal was revealed with a DAB-peroxidase substrate solution. Nonimmunized C57BL/6 (lanes 1-3), gp60-preimmunized C57BL/6 (lanes 4-6), nonimmunized BALB/c (lanes 7-9), and gp60-preimmunized BALB/c (lanes 10-12) mice.

lower levels of cytokines such as $\text{TNF-}\alpha$, $\text{IL-1}\beta$, and IL-12 (p70) compared with control group of BALB/c (Figure 8), which suggests a predisposition towards the inflammatory or Th1 response in BALB/c mice.

The nonimmunized C57BL/6 group showed significantly higher levels of $\text{TNF-}\alpha$ and $\text{IL-1}\beta$ as compared to the control group. Likewise, the level of MIP-2 was 5-fold higher in nonimmunized mice compared to the control group (Figure 8(a)). In the case of nonimmunized BALB/c mice, the levels of $\text{TNF-}\alpha$ and $\text{IL-1}\beta$ increased 45- and 8-fold over the control value, respectively (Figure 8(b)), that is, much more than in nonimmunized C57BL/6 group. On the contrary, the levels of MIP-2 increased about 2-fold over the baseline levels (Figure 8(b)), which is about half the increase observed in nonimmunized C57BL/6 mice. In nonimmunized C57BL/6

mice, the IL-12 (p70)/ IL-12 (p40) ratio decreased as compared to the control group (Figure 9(a)), contrary to the levels of $\text{IFN-}\gamma$, which increased significantly (Figure 8(c)). In contrast to C57BL/6, nonimmunized BALB/c mice showed an increase of almost twice in the IL-12 (p70)/ IL-12 (p40) ratio as compared to the control group (Figure 9(b)), and the same occurred with $\text{IFN-}\gamma$ (Figure 8(d)). Regarding the cytokines of the Th2 response, nonimmunized C57BL/6 mice showed a significant decrease in the levels of IL-10 and IL-4 with respect to the control group, but the levels of IL-6 increased almost 5-fold (Figure 8(e)). In nonimmunized BALB/c group, the levels of IL-10 and IL-6 increased almost twice, whereas the level of IL-4 increased more than twice over the control group (Figure 8(f)); however, although the levels of the Th2 response increased in nonimmunized BALB/c mice,

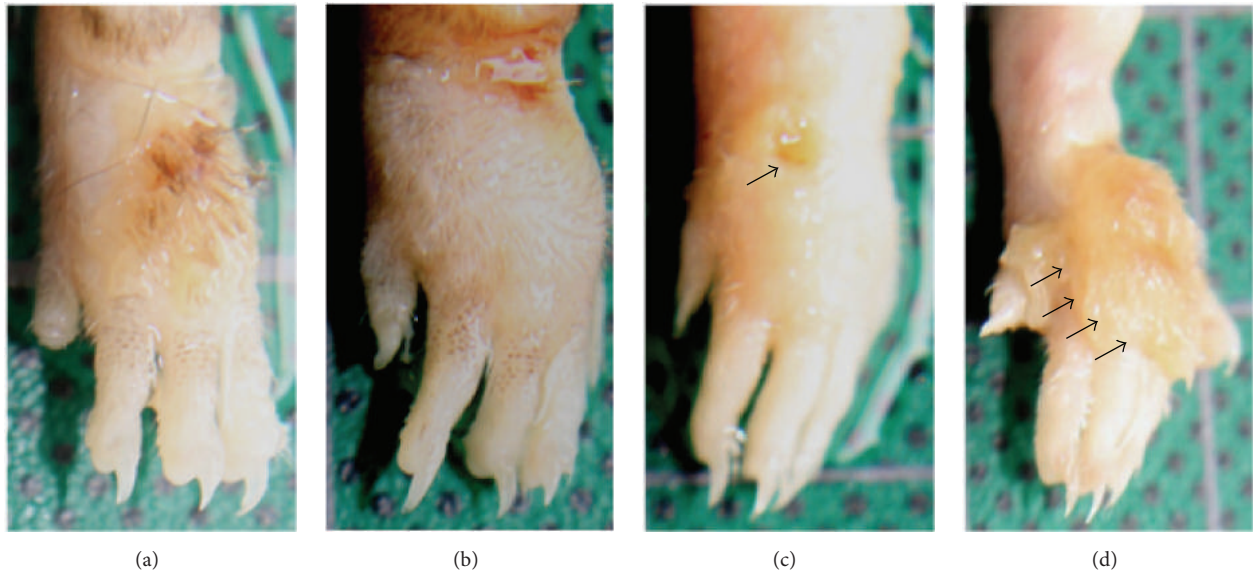


FIGURE 6: Ulceration at the foot dorsum in nonimmunized and gp60-preimmunized mice. Nonimmunized C57BL/6 (a), gp60-preimmunized C57BL/6 (b), nonimmunized BALB/c (c), and gp60-preimmunized BALB/c (d). Arrows indicate ulceration sites.

the increase was not as high as that of the cytokines characteristic of Th1.

3.7. Effect of gp60 on Cytokine Profiles during Infection with *S. schenckii*. In the gp60-preimmunized C57BL/6 group, the levels of TNF- α and IL-1 β decreased significantly when compared to the nonimmunized group; accordingly, the amount of TNF- α reached baseline levels in the control group, while that of IL-1 β was below the control value (Figure 8(a)). On the other hand, MIP-2 remained in the same level as the nonimmunized group; significant differences were observed only after comparing with the control group (Figure 8(a)). Cytokine levels in gp60-preimmunized BALB/c mice decreased more markedly. The levels of TNF- α dropped more than 100-fold with respect to the nonimmunized group, falling even below the control levels, yet no significant differences were observed when compared with the control group. The level of IL-1 β decreased almost 12-fold as compared to nonimmunized mice whereas the level of MIP-2 was unaffected as compared to the nonimmunized group, remaining above the level of the control group (Figure 8(b)). It is noteworthy that in both strains the levels of MIP-2 did not change in any of the gp60-preimmunized groups compared to the nonimmunized groups.

In gp60-preimmunized C57BL/6 mice, the IL-12 (p70)/IL-12 (p40) ratio decreased compared to the nonimmunized and control groups (Figure 9(a)). IFN- γ also decreased significantly (to control levels) compared to nonimmunized group (Figure 8(c)). In gp60-preimmunized BALB/c mice, the IL-12 (p70)/IL-12 (p40) ratio decreased 4-fold and 2-fold compared to the nonimmunized and control groups, respectively (Figure 9(b)), and the level of IFN- γ also decreased, though not significantly compared to nonimmunized group (Figure 8(d)). Although a slight decrease in IFN- γ was

observed in gp60-preimmunized mice, gp60 appears to have a greater effect on the IL-12 (p70)/IL-12 (p40) ratio, decreasing the heterodimeric form and increasing the homodimeric one. Furthermore, the levels of IL-10 decreased significantly in gp60-preimmunized C57BL/6 mice compared to nonimmunized group, falling even below that control level. The level of IL-6 also decreased, yet it remained above the control level. The level of IL-4 also decreased significantly compared to nonimmunized and control groups (Figure 8(e)). It is worth noting that although the levels of both Th1 and Th2 cytokines decreased in gp60-preimmunized C57BL/6 mice, they were not very affected in terms of ulceration (Figures 6(b) and 7(a)) being as damaged as nonimmunized C57BL/6 mice (Figure 6(a)). In gp60-preimmunized BALB/c mice, the level of IL-10 decreased over 17-fold as compared to nonimmunized group, reaching levels below baseline values. The levels of IL-6 and IL-4 also decreased to the control level (IL-6) and below the control level (IL-4) (Figure 8(f)).

4. Discussion

In the present work, gp60 from CW of *S. schenckii* was purified by isoelectric focusing and continuous elution electrophoresis, and its effects over the immune response in an experimental subacute sporotrichosis model in two mice strains were evaluated.

To isolate this glycoprotein as a single antigenic peptide, a purification protocol which takes advantage of the IP and molecular mass was used. The purified gp60 was sequenced by tandem mass spectrometry, yielding a sequence homologous to secreted gp70 [22], a carboxy-*cis*, *cis*-muconate cyclase involved in the β -ketoadipate pathway required for the catabolism of aromatic compounds [23]. However, unlike gp60, which was sequenced from the form present in the cell

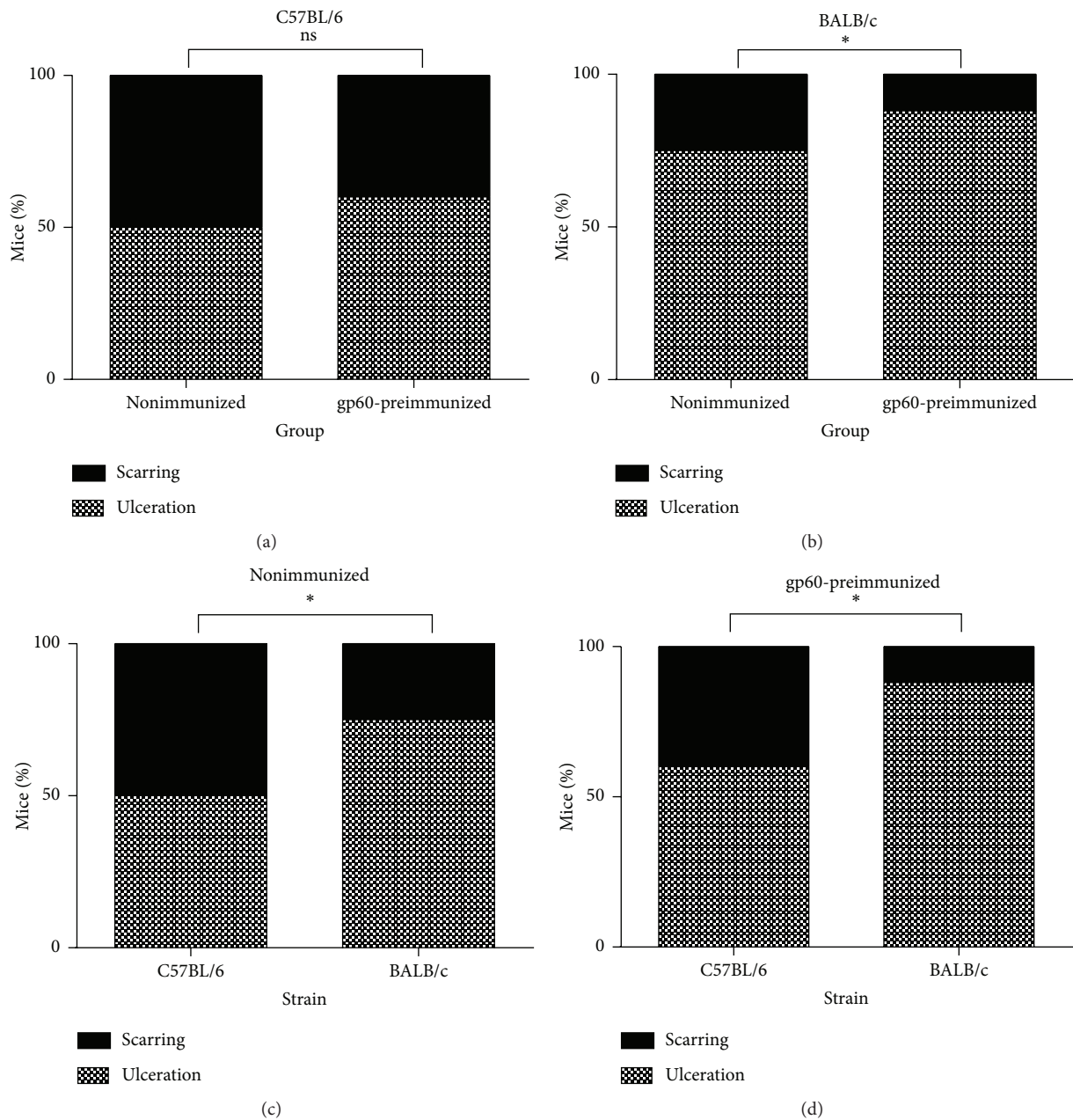


FIGURE 7: Statistical analysis of foot dorsum ulceration in mice. Nonimmunized and gp60-preimmunized C57BL/6 groups (a), nonimmunized and gp60-preimmunized BALB/c groups (b), nonimmunized groups (c), and gp60-preimmunized groups (d). Data are presented as percentages. ns: no significant differences; *significant differences between groups ($P < 0.05$).

surface, the sequence of gp70 was obtained from the secreted, extracellular protein, which might confer differences in the immune mechanisms induced by each antigen, as it has been demonstrated with the BAD-1 protein of *Blastomyces dermatitidis*; accordingly, the CW form induces regulatory mechanisms of the immune response through the production of TGF- β , whereas the secreted counterpart independently regulates from this cytokine [24].

The identification of gp60 as an enzyme complicates its implication in the immunological mechanisms. However, several CW enzymes such as the β -1,3-glucosyltransferase of

Coccidioides posadasii [25] and glyceraldehyde-3-phosphate dehydrogenase (GAPDH) from *Paracoccidioides brasiliensis* [26], altogether with other enzymes of pathways such as glycolysis and the Krebs and glyoxylate cycles, are classified as moonlight or multifunctional proteins due to their participation in pathogenic processes independently of their metabolic activities [27].

Confocal microscopy, using a rabbit polyclonal antibody against gp60 (Figure 1(b)), demonstrated that this protein is distributed along the cell surface of the yeast morphotype (Figure 2(b)). Location of gp60 implicates that it could be

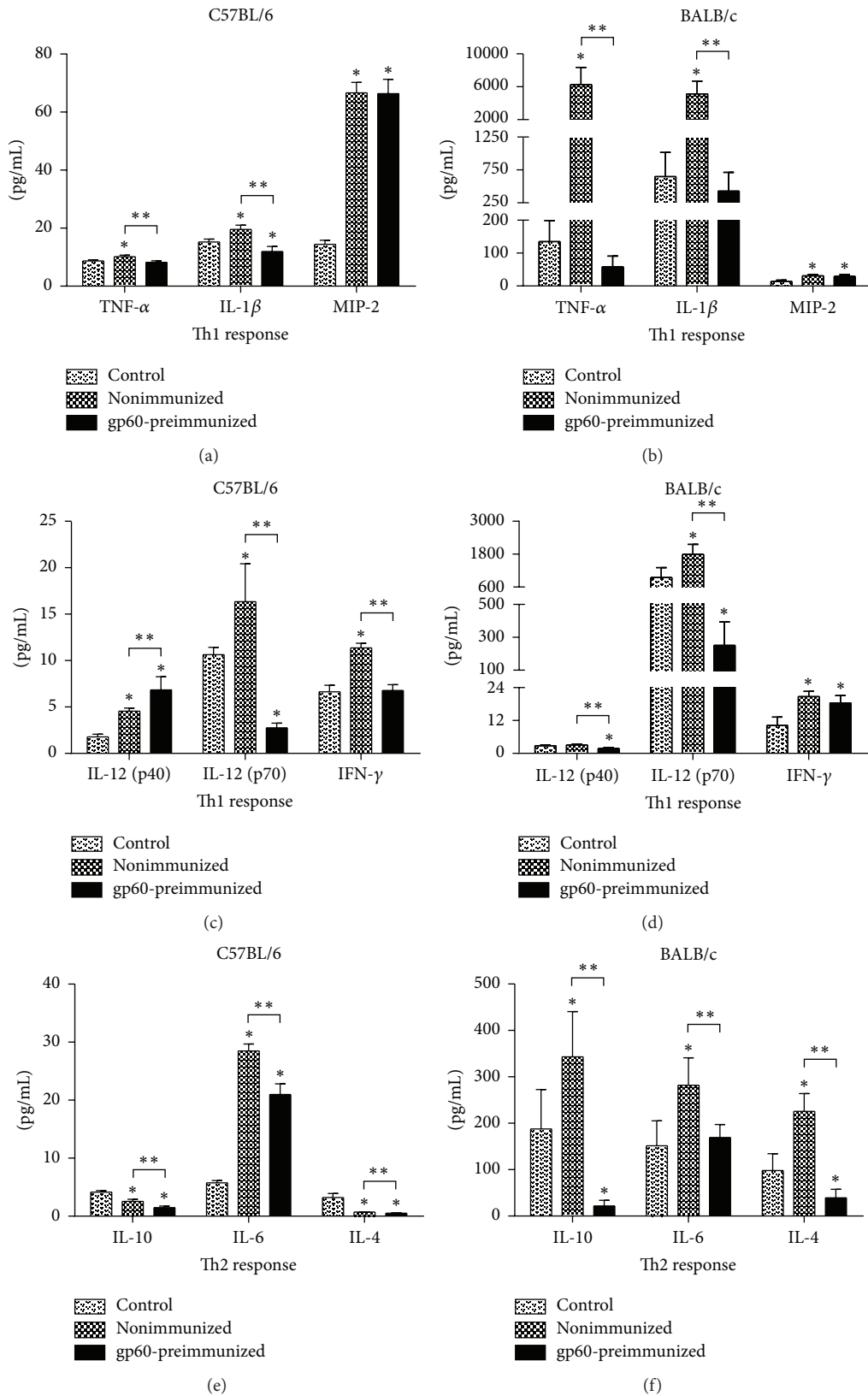


FIGURE 8: Cytokine profiles of control, nonimmunized, and gp60-preimmunized groups. C57BL/6 Th1 ((a) and (c)), BALB/c Th1 ((b) and (d)), C57BL/6 Th2 (e), and BALB/c Th2 (f). Data show mean values \pm SD ($n = 10$ for each group and $n = 5$ for controls). * Significant differences compared to control ($P < 0.05$). ** Significant differences between groups ($P < 0.05$).

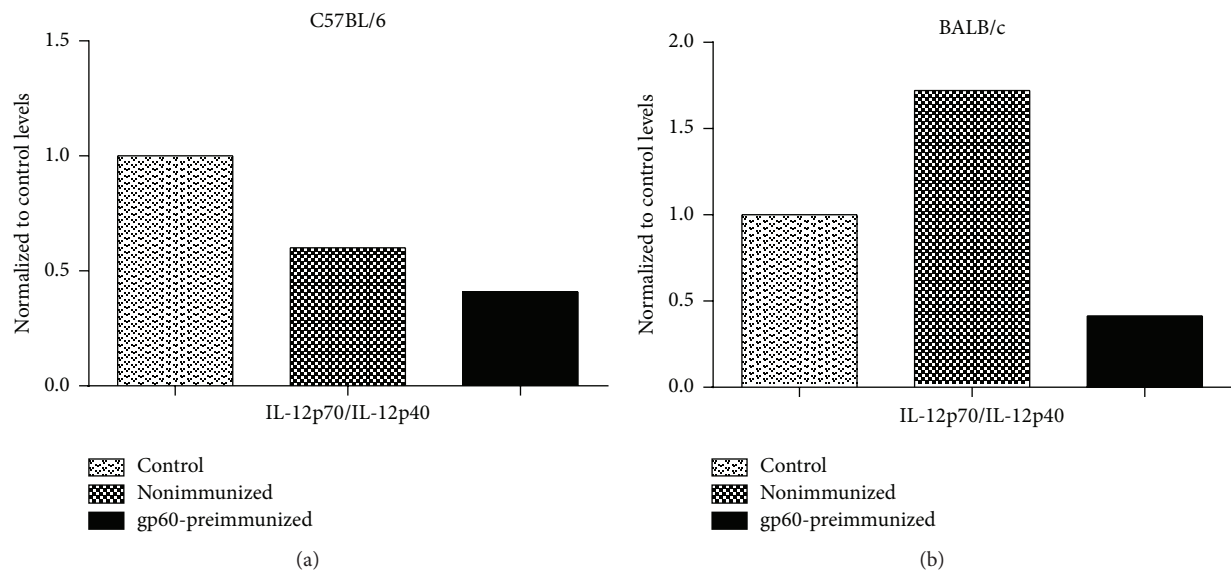


FIGURE 9: IL12-p70/IL-12p40 ratios. Values of C57BL/6 (a) and BALB/c (b) groups were normalized to corresponding control levels.

involved in different potential roles as protective, immunosuppressive, immunostimulatory, or adhesive proteins. The 60 kDa heat shock protein (Hsp60) of *Histoplasma capsulatum* has been associated with protection against stress conditions, since it is expressed when the yeast is subjected to thermal stress, acting as chaperone of proteins with essential functions [28]. The 120 kDa protein present on the surface of *B. dermatitidis* has been proposed as a modulator of the immune response, since it is capable of inhibiting the inflammatory response through the production of TGF- β [29], contrary to the glycoprotein of the outer wall of the spherules of *C. immitis* and *C. posadasii*, which acts as an immunodominant antigen capable of inducing cellular and humoral responses during parasitic infections [30, 31]. *P. brasiliensis* GAPDH and a 30 kDa protein act as adhesins and have an important role in the interaction between the fungus and the host cells [26, 32]. In the same line, gp70 of *S. schenckii* has been reported to have a role as an adhesin associated with the virulence of *S. schenckii* strains [16, 33]. However, an increased expression of this glycoprotein has been associated with less virulent strains of *S. brasiliensis* [34]. Therefore, the presence of gp60 on the cell surface and the homology with gp70 suggest a role in immune and adhesion mechanisms.

In the present work, both mice strains expressed different cytokine profiles. Their analysis in nonimmunized, gp60-preimmunized, and control mice groups demonstrated that levels of Th1 and Th2 response cytokines in C57BL/6 mice remained low compared to those of BALB/c mice, except for MIP-2 which was slightly higher in C57BL/6 mice. The importance of MIP-2 lies in its ability to attract neutrophils to the infected areas in the early stages of the immune response, regardless of the type of pathogen [35]. Moreover, it is known that the levels of MIP-2 change as a proportional function of IL-6, with a direct relationship between them [36]. The concentration of IL-6 noticeably increased in non-immunized C57BL/6 mice compared to the controls. Besides

being associated with the Th1 response, IL-6 promotes the growth and differentiation of B lymphocytes stimulating the humoral response, which suggests a slight tendency of the C57BL/6 mice to the Th2 response, which probably explains the stronger antibody response in this strain. IL-6 is also involved in the activation of the Th17 response, characterized by neutrophil recruitment and inflammation [37]; thus, it is not entirely clear what type of immune response in C57BL/6 mice is relevant to confront infection by *S. schenckii*. On the other hand, nonimmunized BALB/c mice produced higher amounts of proinflammatory cytokines or Th1 response, as indicated by the levels of TNF- α , IL-1 β , and IL-12p70. These mice exhibited severe tissue damage at the foot dorsum. In fact, increased levels of TNF- α have been associated with the severity of sporotrichosis skin lesions in BALB/c mice [38]. Moreover, more severe skin lesions in BALB/c than in C57BL/6 mice correlate with higher IL-4 levels observed in BALB/c mice, according to models of *P. brasiliensis* infection in which elevated levels of IL-4 are related to a worsening of the infection. This is probably due to a decreased fungicide capacity of lung phagocytes from normal mice compared with that of phagocytes from IL-4-deficient mice [39].

The low levels of IL-10 observed in nonimmunized C57BL/6 mice compared to nonimmunized BALB/c may explain why lower tissue damage was noted in C57BL/6 mice, as has been reported in infections caused by *P. brasiliensis* where IL-10 deficiency leads to increased immunity and regressive infection without enhancing tissue pathology [40]. In this sense, it is worth noting that the amount of specific antibodies against gp60 was higher in the C57BL/6 strain than in the BALB/c strain. The gp60 isoforms ranged between 60 and 70 kDa. Accordingly, sera from patients with sporotrichosis contain antibodies recognizing *S. schenckii* antigens in a range of 40–70 kDa [41]. Furthermore, a seroprevalence of the 60–70 kDa antigen exists, and patients with this mycosis contain serum antibodies against such a protein [22].

This immunodominant 60–70 kDa antigen also has been demonstrated in feline sporotrichosis, suggesting its potential as a marker for diagnosis or as a candidate for the development of therapeutic vaccines [42]. Humoral response in mice infected with species from the *S. schenckii* complex shows an antibody production pattern similar to human and cat patterns, where 60–70 kDa recognition becomes a constant [21]. This suggests a convergent humoral response between the three mammals species hosts that may increase our understanding of the coevolution of these hosts with *S. schenckii* species [42]. Whereas the Th2 response is associated with fungal susceptibility, it is known that antibodies can affect the balance of cytokines and the induction of regulatory T cells that help to reduce tissue damage caused by exacerbated inflammatory responses [43].

The conidial morphotype was used in our model of *S. schenckii* infection. This fact should be considered in the interpretation of mice immune response, along with the route of infection, the concentration and virulence of the inoculum, the mouse strain used, and its genetic background. *S. schenckii* yeast and conidial morphotypes are recognized by different receptors [44]. The mannose receptor is the one that recognizes the conidial morphotype, so a different expression of this receptor in each mouse strain may determine a difference in immune response, even though this receptor can activate both inflammatory and regulatory pathways [37]. Furthermore, the magnitude of the response may also vary according to the morphotype, as yeasts coincubated with mast cells have been unable to induce degranulation in *in vitro* assays, contrary to what occurs in conidia, which supports the increased immunological activity of the conidial morphotype [45].

Results of the present study emphasize the lack of a detailed knowledge of the mechanisms of pathogenicity of the different species leading to the development of sporotrichosis. Preimmunization of C57BL/6 and BALB/c strains with gp60 resulted in a downregulation effect on both strains of mice whose cytokine levels were lower as compared to the nonimmunized, particularly in the case of BALB/c. These results could explain why monoclonal antibodies directed against other *S. schenckii* antigens such as gp70 have an immunoprotective effect in murine models [46]. Noteworthy, antibodies against gp70 are not the only ones which have a protective role against *S. schenckii* infection, since passive transference of sera from mice containing antibodies against a 44 kDa hydrolase and a 47 kDa enolase has shown a protective role during murine sporotrichosis [47].

It is worth noting that gp60-preimmunized C57BL/6 mice seemed to be able to resolve the infection as non-immunized mice. It has been demonstrated that dendritic cells from C57BL/6 mice incubated with *S. schenckii* promote combinations of Th1 and Th17 responses [48]. A recent *in vitro* assay suggests that Th1/Th17 combined responses against *S. schenckii* depend on IL-23 [49]. Notably, IL-17 is involved in neutrophil recruitment and in the production of MIP-2; a cytokine markedly increased in nonimmunized and gp60-preimmunized C57BL/6 mice. Thus, gp60 does not seem to have an effect on the Th17 response. Indirectly,

we may infer that C57BL/6 mice tend to assemble Th17 response after infection with *S. schenckii*. Dendritic cells increase IL-23 production after ligation of β -glucans by the dectin-1 receptor regulating fungal pathogenicity via Th-17 responses [50]. Furthermore, vaccination with attenuated yeast cells of primary pathogenic fungi such as *B. dermatitidis*, *C. posadasii*, and *H. capsulatum* induces protective Th17 responses against a lethal infection. Protection is impaired when IL-17 levels are decreased with specific monoclonal antibodies [51]. Galectin-3 receptor-deficient mice express higher levels of Th17 response cytokines as TGF- β 1, IL-23, IL-17, and IL-6, in a model of *H. capsulatum* infection [52]. Thus, it could be hypothesized that C57BL/6 immunity tendency towards Th17 response, as it was observed in our study, might be related to recognition of *S. schenckii* conidia through the differential expression between C57BL/6 and BALB/c mice of the galectin-3 receptor and its ligand.

BALB/c strain cytokine levels were greatly affected by gp60. Previous reports indicate that BALB/c mice infected with *S. schenckii* express a Th1 response mediated by ligation of TLR-2 and TLR-4 receptors [9, 10, 53, 54]. Probably, preimmunization with gp60 blocks one of these receptors and prevents activation signaling pathways that involve NF- κ B transcription factor. Additionally, gp60 may have interfered with caspase-1-dependent signaling pathways activation, which has proven to be important for the production of Th1 cytokines during experimental sporotrichosis [55, 56]. Resistance to paracoccidiodomycosis in mice is related to paracoccin TLRs activation that triggers a balanced Th1 immunity [57]. Furthermore, during *S. schenckii* antigens recognition, the lack of TLR-2 and TLR-4 receptors, combined with the presence of these surface antigens, stimulates TGF- β -mediated regulatory responses with inhibition of Th1 response [53, 54]. Decreased levels of Th1 cytokines observed in gp60-preimmunized mice could be related to these mechanisms whose balance determines the efficiency of Th1 immune response mediated by cytokines.

The IL-12-p70/IL-12-p40 ratio decreased in gp60-preimmunized mice, mainly in the BALB/c strain, indicating the presence of a downregulation effect compared with non-immunized mice since IL-12 p70 is considered the bioactive one. This cytokine is produced only after dendritic cells are primed with microbial stimuli that upregulate IL-12 p40, which stimulates CD40 expression. CD40 ligation induces IL-12 p35, which finally yields bioactive IL-12 p70 [58]. The relevance of IL-12 as a protective cytokine has been demonstrated in gerbils infected with *S. schenckii* [59] but also as linker between innate and adaptive responses mediated by dendritic cells after *S. schenckii* phagocytosis [60]. Thus, gp60 might block one of the steps that lead the production of the bioactive form of this cytokine, avoiding the development of a full Th1 response.

Finally, it seems that gp60 has a greater downregulation effect on the Th1 response, since C57BL/6, a strain that probably depends on a different response like Th17 to fight this fungus, was not as affected as BALB/c strain, which appears to be dependent on Th1 response in order to clear the infection with *S. schenckii*.

Conflict of Interests

All authors declare no conflict of interests.

Acknowledgments

This work was supported by Grant CB-2011 no. 167737 from the Consejo Nacional de Ciencia y Tecnología (CONACyT, México) to Estela Ruiz-Baca. Carlos A. Alba-Fierro is thankful for the scholarship no. 201509 granted by the Consejo Nacional de Ciencia y Tecnología (CONACyT, México).

References

- [1] M. L. Elgart, "Subcutaneous mycosis," in *Cutaneous Fungal Infections*, pp. 124–158, Igku-Shoin Medical Publishers, New York, NY, USA, 1992.
- [2] W. H. Radentz and B. E. Elewski, "Opportunistic mycosis," in *Cutaneous Fungal Infection*, B. E. Elewski, Ed., pp. 184–211, Igaku Shoin Medical Publishers, New York, NY, USA, 1992.
- [3] B. A. Davis, "Sporotrichosis," *Dermatologic Clinics*, vol. 14, no. 1, pp. 69–76, 1996.
- [4] C. J. Espinoza-Hernández, A. Jesús-Silva, S. Toussaint-Caire, and R. Arenas, "Disseminated sporotrichosis with cutaneous and testicular involvement," *Actas Dermo-Sifiliograficas*, vol. 105, no. 2, pp. 204–206, 2014.
- [5] S. Conias and P. Wilson, "Epidemic cutaneous sporotrichosis: report of 16 cases in Queensland due to mouldy hay," *Australasian Journal of Dermatology*, vol. 39, no. 1, pp. 34–37, 1998.
- [6] E. López-Romero, M. D. R. Reyes-Montes, A. Pérez-Torres et al., "Sporothrix schenckii complex and sporotrichosis, an emerging health problem," *Future Microbiology*, vol. 6, no. 1, pp. 85–102, 2011.
- [7] J. W. Rippon, *Micología Médica*, Nueva Editorial Interamericana, S.A. de C. V., Mexico City, Mexico, 1990.
- [8] D. B. da Graça Sgarbi, A. J. R. da Silva, I. Z. Carlos, C. L. Silva, J. Angluster, and C. S. Alviano, "Isolation of ergosterol peroxide and its reversion to ergosterol in the pathogenic fungus *Sporothrix schenckii*," *Mycopathologia*, vol. 139, no. 1, pp. 9–14, 1997.
- [9] M. F. Sassá, A. E. T. Saturi, L. F. Souza, L. C. De Abreu Ribeiro, D. B. Da Graça Sgarbi, and I. Z. Carlos, "Response of macrophage toll-like receptor 4 to a *Sporothrix schenckii* lipid extract during experimental sporotrichosis," *Immunology*, vol. 128, no. 2, pp. 301–309, 2009.
- [10] T. D. C. Negrini, L. S. Ferreira, P. Alegranci et al., "Role of TLR-2 and fungal surface antigens on innate immune response against *Sporothrix schenckii*," *Immunological Investigations*, vol. 42, no. 1, pp. 36–48, 2013.
- [11] I. Z. Carlos, D. B. G. Sgarbi, G. C. Santos, and M. C. P. Placeres, "Sporothrix schenckii lipid inhibits macrophage phagocytosis, involvement of nitric oxide and tumour necrosis factor- α ," *Scandinavian Journal of Immunology*, vol. 57, no. 3, pp. 214–220, 2003.
- [12] L. M. Lopes-Bezerra, "Sporothrix schenckii cell wall peptidoglycanomannans," *Frontiers in Microbiology*, vol. 2, article 243, 2011.
- [13] I. Z. Carlos, D. B. da Graça Sgarbi, J. Angluster, C. S. Alviano, and C. L. Silva, "Detection of cellular immunity with the soluble antigen of the fungus *Sporothrix schenckii* in the systemic form of the disease," *Mycopathologia*, vol. 117, no. 3, pp. 139–144, 1992.
- [14] I. Z. Carlos, M. M. C. Zini, D. B. D. G. Sgarbi, J. Angluster, C. S. Alviano, and C. L. Silva, "Disturbances in the production of interleukin-1 tumor and necrosis factor in disseminated murine sporotrichosis," *Mycopathologia*, vol. 127, no. 3, pp. 189–194, 1994.
- [15] I. Z. Carlos, D. B. D. G. Sgarbi, and M. C. P. Placeres, "Host organism defense by a peptide-polysaccharide extracted from the fungus *Sporothrix schenckii*," *Mycopathologia*, vol. 144, no. 1, pp. 9–14, 1998.
- [16] E. Ruiz-Baca, C. Toriello, A. Pérez-Torres, M. Sabanero-Lopez, J. C. Villagómez-Castro, and E. López-Romero, "Isolation and some properties of a glycoprotein of 70 kDa (Gp70) from the cell wall of *Sporothrix schenckii* involved in fungal adherence to dermal extracellular matrix," *Medical Mycology*, vol. 47, no. 2, pp. 185–196, 2009.
- [17] R. C. Nascimento and S. R. Almeida, "Humoral immune response against soluble and fractionate antigens in experimental sporotrichosis," *FEMS Immunology and Medical Microbiology*, vol. 43, no. 2, pp. 241–247, 2005.
- [18] R. C. Nascimento, N. M. Espíndola, R. A. Castro et al., "Passive immunization with monoclonal antibody against a 70-kDa putative adhesin of *Sporothrix schenckii* induces protection in murine sporotrichosis," *European Journal of Immunology*, vol. 38, no. 11, pp. 3080–3089, 2008.
- [19] E. Ruiz-Baca, H. M. Mora-Montes, E. López-Romero, C. Toriello, V. Mojica-Marín, and N. Urtiz-Estrada, "2D-immunoblotting analysis of *Sporothrix schenckii* cell wall," *Memórias do Instituto Oswaldo Cruz*, vol. 106, no. 2, pp. 248–250, 2011.
- [20] E. Ruiz-Baca, G. Hernández-Mendoza, M. Cuéllar-Cruz, C. Toriello, E. López-Romero, and G. Gutiérrez-Sánchez, "Detection of 2 immunoreactive antigens in the cell wall of *Sporothrix brasiliensis* and *Sporothrix globosa*," *Diagnostic Microbiology and Infectious Disease*, vol. 79, no. 3, pp. 328–330, 2014.
- [21] G. F. Fernandes, P. O. dos Santos, A. M. Rodrigues, A. A. Sasaki, E. Burger, and Z. P. de Camargo, "Characterization of virulence profile, protein secretion and immunogenicity of different *Sporothrix schenckii* sensu stricto isolates compared with *S. globosa* and *S. brasiliensis* species," *Virulence*, vol. 4, no. 3, pp. 241–249, 2013.
- [22] A. M. Rodrigues, P. H. Kubitschek-Barreira, G. F. Fernandes, S. R. de Almeida, L. M. Lopes-Bezerra, and Z. P. de Camargo, "Immunoproteomic analysis reveals a convergent humoral response signature in the *Sporothrix schenckii* complex," *Journal of Proteomics*, vol. 115, pp. 8–22, 2015.
- [23] A. M. MacLean, G. MacPherson, P. Aneja, and T. M. Finan, "Characterization of the β -ketoacid pathway in *Sinorhizobium meliloti*," *Applied and Environmental Microbiology*, vol. 72, no. 8, pp. 5403–5413, 2006.
- [24] B. Finkel-Jimenez, M. Wüthrich, and B. S. Klein, "BAD-1, an essential virulence factor of *Blastomyces dermatitidis*, suppresses host TNF- α production through TGF- β -dependent and -independent mechanisms," *The Journal of Immunology*, vol. 168, no. 11, pp. 5746–5755, 2002.
- [25] N. Delgado, J. Xue, J.-J. Yu, C.-Y. Hung, and G. T. Cole, "A recombinant β -1,3-glucanosyltransferase homolog of *Coccidioides posadasii* protects mice against coccidioidomycosis," *Infection and Immunity*, vol. 71, no. 6, pp. 3010–3019, 2003.
- [26] M. S. Barbosa, S. N. Bão, P. F. Andreotti et al., "Glyceraldehyde-3-phosphate dehydrogenase of *Paracoccidioides brasiliensis* is a cell surface protein involved in fungal adhesion to extracellular

- matrix proteins and interaction with cells," *Infection and Immunity*, vol. 74, no. 1, pp. 382–389, 2006.
- [27] C. M. Marcos, H. C. de Oliveira, J. D. F. da Silva, P. A. Assato, A. M. Fusco-Almeida, and M. J. S. Mendes-Giannini, "The multifaceted roles of metabolic enzymes in the *Paracoccidioides* species complex," *Frontiers in Microbiology*, vol. 5, article 719, 2014.
- [28] A. J. Guimarães, E. S. Nakayasu, T. J. P. Sobreira et al., "*Histoplasma capsulatum* heat-shock 60 orchestrates the adaptation of the fungus to temperature stress," *PLoS ONE*, vol. 6, no. 2, Article ID e14660, 2011.
- [29] M. X. Zhang, T. T. Brandhorst, T. R. Kozel, and B. S. Klein, "Role of glucan and surface protein BAD1 in complement activation by *Blastomyces dermatitidis* yeast," *Infection and Immunity*, vol. 69, no. 12, pp. 7559–7564, 2001.
- [30] C.-Y. Hung, N. M. Ampel, L. Christian, K. R. Seshan, and G. T. Cole, "A major cell surface antigen of *Coccidioides immitis* which elicits both humoral and cellular immune responses," *Infection and Immunity*, vol. 68, no. 2, pp. 584–593, 2000.
- [31] C.-Y. Hung, K. R. Seshan, J.-J. Yu et al., "A metalloproteinase of *Coccidioides posadasii* contributes to evasion of host detection," *Infection and Immunity*, vol. 73, no. 10, pp. 6689–6703, 2005.
- [32] J. F. da Silva, H. C. de Oliveira, C. M. Marcos et al., "*Paracoccidioides brasiliensis* 30 kDa adhesin: identification as a 14-3-3 protein, cloning and subcellular localization in infection models," *PLoS ONE*, vol. 8, no. 4, Article ID e62533, 2013.
- [33] P. A. C. Teixeira, R. A. de Castro, R. C. Nascimento et al., "Cell surface expression of adhesins for fibronectin correlates with virulence in *Sporothrix schenckii*," *Microbiology*, vol. 155, no. 11, pp. 3730–3738, 2009.
- [34] R. A. Castro, P. H. Kubitschek-Barreira, P. A. C. Teixeira et al., "Differences in cell morphometry, cell wall topography and Gp70 expression correlate with the virulence of *Sporothrix brasiliensis* clinical isolates," *PLoS ONE*, vol. 8, no. 10, Article ID e75656, 2013.
- [35] X. T. Yan, T. M. Tumpey, S. L. Kunkel, J. E. Oakes, and R. N. Lausch, "Role of MIP-2 in neutrophil and tissue injury in the herpes simplex virus-1-infected cornea," *Investigative Ophthalmology and Visual Science*, vol. 39, no. 10, pp. 1854–1862, 1998.
- [36] R. R. Fenton, S. Molesworth-Kenyon, J. E. Oakes, and R. N. Lausch, "Linkage of IL-6 with neutrophil chemoattractant expression in virus-induced ocular inflammation," *Investigative Ophthalmology and Visual Science*, vol. 43, no. 3, pp. 737–743, 2002.
- [37] L. Romani, "Immunity to fungal infections," *Nature Reviews Immunology*, vol. 11, no. 4, pp. 275–288, 2011.
- [38] Y. Romo-Lozano, F. Hernández-Hernández, and E. Salinas, "Mast cell activation by conidia of *Sporothrix schenckii*: role in the severity of infection," *Scandinavian Journal of Immunology*, vol. 76, no. 1, pp. 11–20, 2012.
- [39] A. Pina, R. C. Valente-Ferreira, E. E. W. Molinari-Madlum, C. A. C. Vaz, A. C. Keller, and V. L. G. Calich, "Absence of interleukin-4 determines less severe pulmonary paracoccidioidomycosis associated with impaired Th2 response," *Infection and Immunity*, vol. 72, no. 4, pp. 2369–2378, 2004.
- [40] T. A. Costa, S. B. Bazan, C. Feriotti et al., "In pulmonary paracoccidioidomycosis IL-10 deficiency leads to increased immunity and regressive infection without enhancing tissue pathology," *PLoS Neglected Tropical Diseases*, vol. 7, no. 10, Article ID e2512, 2013.
- [41] E. N. Scott and H. G. Muchmore, "Immunoblot analysis of antibody responses to *Sporothrix schenckii*," *Journal of Clinical Microbiology*, vol. 27, no. 2, pp. 300–304, 1989.
- [42] A. M. Rodrigues, G. F. Fernandes, L. M. Araujo et al., "Proteomics-based characterization of the humoral immune response in sporotrichosis: toward discovery of potential diagnostic and vaccine antigens," *PLoS Neglected Tropical Diseases*, vol. 9, no. 8, Article ID e0004016, 2015.
- [43] L. Romani, "Immunity to fungal infections," *Nature Reviews Immunology*, vol. 4, no. 1, pp. 11–23, 2004.
- [44] S. Guzman-Beltran, A. Perez-Torres, C. Coronel-Cruz, and H. Torres-Guerrero, "Phagocytic receptors on macrophages distinguish between different *Sporothrix schenckii* morphotypes," *Microbes and Infection*, vol. 14, no. 12, pp. 1093–1101, 2012.
- [45] Y. Romo-Lozano, F. Hernández-Hernández, and E. Salinas, "*Sporothrix schenckii* yeasts induce ERK pathway activation and secretion of IL-6 and TNF- α in rat mast cells, but no degranulation," *Medical Mycology*, vol. 52, no. 8, pp. 862–868, 2014.
- [46] J. R. F. de Almeida, G. H. Kaihama, G. P. Jannuzzi, and S. R. de Almeida, "Therapeutic vaccine using a monoclonal antibody against a 70-kDa glycoprotein in mice infected with highly virulent *Sporothrix schenckii* and *Sporothrix brasiliensis*," *Medical Mycology*, vol. 53, no. 1, pp. 42–50, 2015.
- [47] D. L. Portuondo, A. Batista-Duharte, L. S. Ferreira et al., "A cell wall protein-based vaccine candidate induce protective immune response against *Sporothrix schenckii* infection," *Immunobiology*, vol. 221, no. 2, pp. 300–309, 2016.
- [48] F. F. Verdan, J. C. Faleiros, L. S. Ferreira et al., "Dendritic cell are able to differentially recognize *Sporothrix schenckii* antigens and promote Th1/Th17 response in vitro," *Immunobiology*, vol. 217, no. 8, pp. 788–794, 2012.
- [49] L. S. Ferreira, A. C. Gonçalves, D. L. Portuondo et al., "Optimal clearance of *Sporothrix schenckii* requires an intact Th17 response in a mouse model of systemic infection," *Immunobiology*, vol. 220, no. 8, pp. 985–992, 2015.
- [50] G. Chamilos, D. Ganguly, R. Lande et al., "Generation of IL-23 producing Dendritic Cells (DCs) by airborne fungi regulates fungal pathogenicity via the induction of T_H-17 responses," *PLoS ONE*, vol. 5, no. 9, Article ID e12955, 2010.
- [51] M. Wüthrich, B. Gern, C. Y. Hung et al., "Vaccine-induced protection against 3 systemic mycoses endemic to North America requires Th17 cells in mice," *Journal of Clinical Investigation*, vol. 121, no. 2, pp. 554–568, 2011.
- [52] S.-Y. Wu, J.-S. Yu, F.-T. Liu, S.-C. Miaw, and B. A. Wu-Hsieh, "Galectin-3 negatively regulates dendritic cell production of IL-23/IL-17-axis cytokines in infection by *Histoplasma capsulatum*," *The Journal of Immunology*, vol. 190, no. 7, pp. 3427–3437, 2013.
- [53] T. D. C. Negrini, L. S. Ferreira, R. A. Arthur et al., "Influence of TLR-2 in the immune response in the infection induced by fungus *Sporothrix schenckii*," *Immunological Investigations*, vol. 43, no. 4, pp. 370–390, 2014.
- [54] M. F. Sassá, L. S. Ferreira, L. C. de Abreu Ribeiro, and I. Z. Carlos, "Immune response against *Sporothrix schenckii* in TLR-4-deficient mice," *Mycopathologia*, vol. 174, no. 1, pp. 21–30, 2012.
- [55] M. Li, Q. Chen, J. Sun, Y. Shen, and W. Liu, "Inflammatory response of human keratinocytes triggered by *Sporothrix schenckii* via toll-like receptor 2 and 4," *Journal of Dermatological Science*, vol. 66, no. 1, pp. 80–82, 2012.
- [56] A. C. Gonçalves, D. C. G. Maia, L. S. Ferreira et al., "Involvement of major components from *Sporothrix schenckii* cell wall in

the caspase-1 activation, nitric oxide and cytokines production during experimental sporotrichosis," *Mycopathologia*, vol. 179, no. 1-2, pp. 21-30, 2015.

- [57] A. C. Alegre-Maller, F. C. Mendonça, T. A. da Silva et al., "Therapeutic administration of recombinant paracoccin confers protection against *Paracoccidioides brasiliensis* infection: involvement of TLRs," *PLoS Neglected Tropical Diseases*, vol. 8, no. 12, Article ID e3317, 2014.
- [58] O. Schulz, A. D. Edwards, M. Schito et al., "CD40 triggering of heterodimeric IL-12 p70 production by dendritic cells in vivo requires a microbial priming signal," *Immunity*, vol. 13, no. 4, pp. 453-462, 2000.
- [59] A. Flores-García, J. S. Velarde-Félix, V. Garibaldi-Becerra et al., "Recombinant murine IL-12 promotes a protective Th1/cellular response in mongolian gerbils infected with *Sporothrix schenckii*," *Journal of Chemotherapy*, vol. 27, no. 2, pp. 87-93, 2014.
- [60] M. Kusuhara, H. Qian, X. Li et al., "Mouse bone marrow-derived dendritic cells can phagocytize the *Sporothrix schenckii*, and mature and activate the immune response by secreting interleukin-12 and presenting antigens to T lymphocytes," *The Journal of Dermatology*, vol. 41, no. 5, pp. 386-392, 2014.



Morphological changes and phagocytic activity during the interaction of human neutrophils with *Sporothrix schenckii*: An *in vitro* model

Vicente Curtiellas-Piñol^a, Javier Ventura-Juárez^a, Estela Ruiz-Baca^b, Yolanda Romo-Lozano^{a,*}

^a Centro de Ciencias Básicas, Universidad Autónoma de Aguascalientes, Av. Universidad No. 940, Aguascalientes, AGS, Mexico

^b Facultad de Ciencias Químicas, Universidad Juárez del Estado de Durango, Av. Veterinaria S/N, 34120, Durango, DGO, Mexico

ARTICLE INFO

Keywords:

Conidia
Cell morphology
Phagocytosis
Yeasts

ABSTRACT

Histopathological studies of human sporotrichosis lesions show pyogenic and granulomatous processes in which polymorphonuclear neutrophils (PMNs) play a central role. Few studies regarding the events associated with the interaction of human PMNs with *Sporothrix schenckii* have been made despite their importance in the clinical manifestations of the disease. In this study, human PMNs were co-cultured with conidia or yeast cells of *S. schenckii* to compare the phagocytic activity and morphological changes that could provide a clearer insight into the role of these phagocytes in the initial phase of sporotrichosis. PMNs showed increased cell size and separation of the nuclear lobes after phagocytosis. Through Scanning Electron Microscopy (SEM) analysis, an increase in cells with flattened filaments and vesicles on their surface was observed. Phagocytosed conidia showed a significant increase in width and size. The phagocytic activity was greater against yeasts than with conidia, but the viability of both *S. schenckii* cellular morphotypes was not drastically affected even after 2 h of co-culture. In conclusion, morphological changes in PMNs suggest that *S. schenckii* induces processes that may favor proinflammatory events. These phagocytes show a high ability to bind or ingest *S. schenckii* cells without affecting their viability. Morphological changes recorded in ingested conidia, suggest that this fungus could make the dimorphic switching in PMNs.

1. Introduction

Sporotrichosis is a subcutaneous mycosis caused by species of the genus *Sporothrix*; the main species that causes sporotrichosis in humans is *Sporothrix schenckii* [1]. *S. schenckii* is considered a complex of cryptic species including six phylogenetically related species: *S. brasiliensis*, *S. schenckii sensu stricto*, *S. globosa*, *S. mexicana*, *S. larei*, and *S. pallida* [2].

S. schenckii is a dimorphic fungus. In its saprophytic stage it presents a filamentous form and develops sympodial conidia and sessile conidia. Sympodial conidia are ovoid or pear shaped, and measure 2–8 µm long by 1.5–2.5 µm wide; sessile conidia are usually triangular to cuneiform, and measure 2–6 µm long by 2–3.5 wide [3]. In host tissues, this fungus is evident as budding yeast, which may be round or oval, with 2–6 µm diameters, and usually has elongated, cigar-shaped buds on a narrow base [4]. Clinical presentations of sporotrichosis may vary according to the immunological condition of the host and pathogenicity of the strain among other factors [5]. The immunological mechanisms involved in the pathogenesis of sporotrichosis have not been completely explained, but are known to include elements of both cellular and humoral responses [4,6]. Studies in mice suggest that the cellular response seems

to be induced by cell surface antigens, especially some lipids, which inhibit the phagocytosis processes and induce a high release of tumor necrosis factor alpha (TNF-α) and nitric oxide (NO) in macrophage cultures [7]. On the other hand, the humoral response is induced by secreted proteins, called exoantigens [6,8,9].

Polymorphonuclear neutrophils (PMNs) are the most abundant innate immunity cells in the blood, and one of the first cells to migrate to the site of infection [10]. PMNs are cells with spherical morphology, multiple membrane folds, and a nucleus with 2–5 lobes [11]. In the absence of any extracellular stimuli, circulating PMNs can suffer spontaneous apoptosis within 1–5 days, and are subsequently ingested by macrophages, providing the means to resolve the inflammatory response without releasing cytotoxic molecules that would otherwise damage host tissues [12]. It is expected that PMNs play a transcendental role in the early course of sporotrichosis due to a) the diversity of surface receptors they possess which are able to recognize multiple molecular patterns associated with pathogens, b) the large number of intracellular granules and vesicles containing antimicrobial molecules, among them is the myeloperoxidase (MPO), which participate in phagocytosis, and also can damaging host tissues during the inflammatory

* Corresponding author. Lab. de Microbiología, Edif. 204 A. Av. Universidad No. 940, Ciudad Universitaria, Aguascalientes, AGS, CP 20131, Mexico.
E-mail address: yromo@correo.uaa.mx (Y. Romo-Lozano).

process [13], and c) the various signal transduction pathways leading to important modifications in their own physiology and to inflammatory tissue damage [14]. PMNs have the potentiality to recognize both conidia and yeasts cells of *S. schenckii*, and upon activation, to secrete inflammatory mediators that enhance the overall immune response of the host against this fungus, as it has been shown to occur with other innate immunity cells, such as macrophages [15], and mast cells [16]. An *in vitro* study showed that human PMNs are able to phagocytose and kill *S. schenckii* yeasts in the presence of 10% non-inactivated human serum [17]. A subsequent *in vitro* study showed that human PMNs are able to kill *S. schenckii* hyphae, but not yeasts, thereby highlighting the importance of dimorphism as a fungal virulence factor [18]. In addition to these contradictory results obtained in previous *in vitro* models, there are no reports that indicate differences in the activity of human PMNs against conidia and yeast of *S. schenckii*, or the possible role of these phagocytes in the necessary dimorphic switching that this fungus makes in host tissues.

Elucidation of the mechanisms associated with the interactions of innate immune cells with *S. schenckii* are essential for an adequate management of sporotrichosis, whose current treatments are usually prolonged and associated with several adverse effects [19,20]. The present study evaluated the morphological changes and the phagocytic activity during the *in vitro* interaction of human PMNs with *S. schenckii*, to clear up the role of these phagocytes in the pathogenesis of sporotrichosis.

2. Materials and methods

2.1. Ethics statement

The Institutional Bioethics Committee of the Universidad Autónoma de Aguascalientes approved this study (Act: CIB-UAA-18) and all the adult volunteers signed an informed consent form prior to blood donation.

2.2. Strain and culture conditions

The *S. schenckii sensu stricto* strain UAA-307 was obtained from a human lymphocutaneous sporotrichosis case and was used in all experiments. This strain was identified by phenotypic and molecular approaches as described on previous studies [16]. Conidial suspensions were obtained by incubation at 28 °C in Sabouraud Dextrose Broth (BD Bioxon) under orbital agitation at 150 rpm (Shaker Lumistell, IR0-60, México) for 3 days, and yeast cells were grown in Brain Heart Infusion Agar (BD Bioxon) for 6 days at 37 °C. At the end of the incubation, both types of cells were harvested by centrifugation at 750g, and washed three times with phosphate-buffered saline (PBS) pH 7.4, and then were resuspended in RPMI 1640 medium without phenol red (Sigma-Aldrich) and supplemented with 5% fetal bovine serum (FBS, Invitrogen) and 1% penicillin / streptomycin (Sigma-Aldrich), (RPMI 1640). Quantification of conidia and yeast cells was performed in the Neubauer chamber verifying the viability by trypan blue staining (Sigma-Aldrich).

2.3. Neutrophil isolation

Human PMNs were obtained from venous blood samples from healthy donor volunteers. PMNs were purified by centrifugation for 45 min at 700 g at room temperature on a discontinuous density gradient [21] prepared with Lymphoprep (Fresenius Kabi Norge AS) and Histopaque-1119 (Sigma-Aldrich) media. Contaminating erythrocytes were lysed by osmotic shock in a 0.15 M NH₄Cl solution. Cells were washed twice with PBS, resuspended in RPMI 1640 for quantification, and determination of viability and purity. Quantification was performed in Neubauer chamber, and PMNs viability was determined by using the Trypan blue exclusion test, additionally, cellular viability was

measured with MTT assay. The purity was determined by morphological examinations of samples staining with Wright-Giemsa, and verified by immunostaining of cells labeled with anti-CD15 antibody (FUT4/1478R Novus) (see section 2.5). Only those cell suspensions whose purity and viability was greater than 95% were used.

2.4. Viability of neutrophils

In addition to Trypan blue exclusion test, cellular viability of PMNs was determined following the conversion of water soluble MTT (3-(4,5-dimethylthiazol-2-yl)-2,5-diphenyltetrazolium bromide, Sigma-Aldrich M2128) compound to an insoluble formazan product [22]. Cells (4×10^5) were placed in 1.5 mL microcentrifuge polypropylene tubes with 250 μ L of RPMI 1640, and left to stand at 37 °C. After 10, 30, 60 and 120 min, 0.5 mg/mL of MTT (Sigma-Aldrich M2128) were added to centrifuged cells at 300 g for 3 min, and the mixture was left to incubate for 1 h to reduce the tetrazolium salts. The medium was discarded, and 250 μ L of acid-isopropanol (0.04 N HCl in 2-propanol) was added and mixed thoroughly to dissolve the blue crystals. After 10 min at room temperature, samples were centrifuged at 300 g for 3 min to eliminate cell debris, and supernatants were placed in 96-well ELISA culture plates. The optical density (OD) of the MTT solution was recorded using a microplate reader (595 nm absorbance, Bio-Rad Laboratories, iMark, Japan). The values were expressed as a percentage of MTT with respect to the control of untreated cells (100% viability).

2.5. Immunofluorescence microscopy

Newly obtained human neutrophils (4×10^5) were seeded on sterile round glass coverslips for 30 min at 37 °C in 250 μ L of RPMI 1640 to allow its adhesion. The RPMI 1640 was eliminated from some of the cells and then these were fixed with 4% paraformaldehyde (PFA) (Sigma-Aldrich) in PBS for 30 min. The remaining cells were used for interaction experiments with or without *S. schenckii* (2×10^6 conidia or yeast cells) for 30 min at 37 °C in a humidified atmosphere containing 5% CO₂. Subsequently, the RPMI 1640 was eliminated of all cells and were fixed with 4% PFA solution for 30 min.

All fixed cells were washed with PBS and permeabilized or not with 0.1% triton X-100-PBS. Nonspecific binding sites were blocked with 5% fetal bovine serum-0.1% triton X-100 in PBS. Subsequently, the samples were incubated with the rabbit anti-CD15 (FUT4/1478R Novus) or anti-gp70 (kindly donated by Dra. Estela Ruiz Baca) diluted 1:200 in PBS solution containing 0.1% BSA. A gentle washing step in PBS was performed following incubation. Afterwards, samples were incubated with a secondary antibody, Alexa fluor 488 (green) goat anti-rabbit IgG (Abcam, 2 μ g/mL) diluted 1:500 in PBS solution containing 0.1% BSA. DNA staining was performed with Hoechst (1 μ g/mL; Life Technologies, Thermo Fisher Scientific). Finally, the specimens were mounted in mowiol mounting medium [23] (Mowiol 4–88, Aldrich), and examined with epifluorescence microscopy (Axioskop 40, Carl Zeiss, CoolSnap-Pro Digital camera). Images were processed using Image-Pro Plus 4.5.0.19 Media cybernetics. Non-permeabilized cells or without primary antibody were used as control.

2.6. Release of myeloperoxidase during interaction of PMNs with *S. schenckii*

In order to demonstrate that the PMNs were not activated before the interaction, and activated after interaction with the fungus, the release of myeloperoxidase (MPO) was measured using diaminebenzidine (DAB, Sigma) as substrate according to the modified method of Herzog and Fahimi [24]. Human PMNs (4×10^5) were challenged with *S. schenckii* (2×10^6 conidia or yeast cells) or not in 250 μ L of RPMI 1640 at 37 °C in a humidified atmosphere containing 5% CO₂ (fungi-to-PMNs ratio, 5:1) by 0, 30 and 120 min. Next, were centrifuged at 300 g for 3 min, at 4 °C, and 200 μ L of the supernatant were taken to which

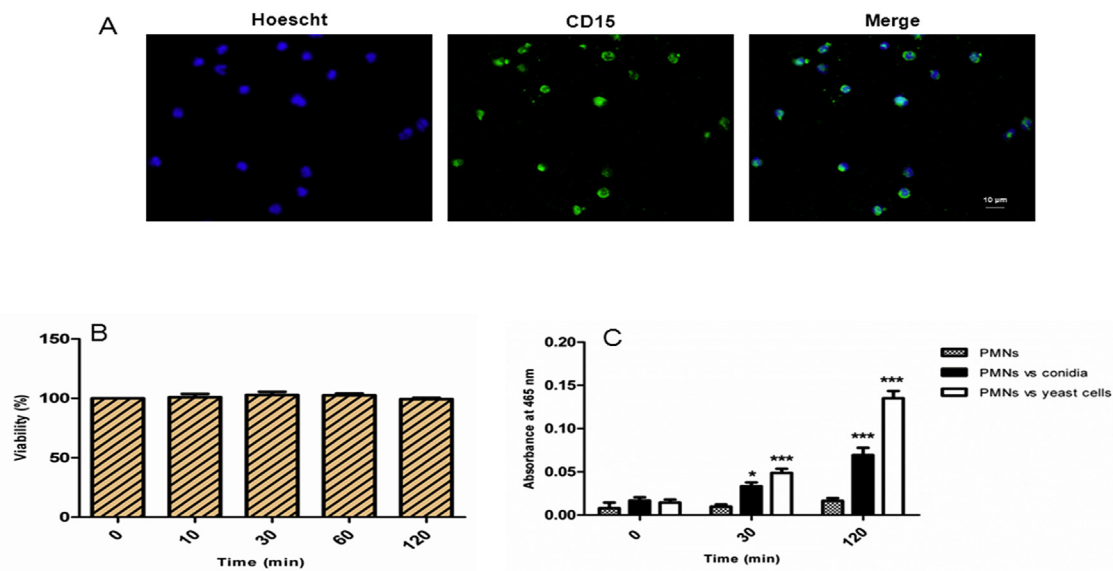


Fig. 1. Analysis of human neutrophil purity, viability and activation state. A) Cells were fixed, permeabilized and stained for adhesion molecule CD15 of PMNs (green) and nuclei of PMNs (Hoechst, blue); and the immunofluorescence images show a purity higher to 98% at time 0 min. B) The viability of PMNs evaluated by the MTT reduction assay and expressed as percentage with respect to basal value, did not change during the 10, 30, 60 and 120 min of incubation at 37 °C. C) To demonstrate that PMNs were not activated before co-culture with *S. schenckii*, the activity of MPO released by PMNs was determined at time 0, and after incubation for 30 min and 120 min at 37 °C. PMNs not challenged with *S. schenckii* were used as controls. PMNs exposed to *S. schenckii* showed an increase in the activity of MPO released to the culture medium after 30 min of co-incubation (mean \pm standard error of the mean, n = 3); ANOVA test. *p < 0.05; ***p < 0.001. Values compared with correspondent control.

800 μ L of a 0.25 mM DAB solution in 0.1 M potassium dihydrogenphosphate pH 4.5 were added. After this, the reaction was initiated with the addition of 50 μ L of 60 mM H₂O₂. After 30 min of incubation at room temperature, 20 μ L of 0.1 mM sodium azide was added to stop the reaction. Absorbances were measured at 465 nm (JENWAY 7305 Spectrophotometer, Bibby Scientific Ltd. Stone, USA).

2.7. Scanning electron microscopy

The Scanning Electron Microscopy (SEM) assay was performed according to the methods used in a previous study (16). Poly D-lysine-coated 24 well tissue culture plates were seeded with PMNs (4×10^5) challenged or not, with *S. schenckii* (2×10^6 conidia or yeast cells) in 250 μ L of RPMI 1640, and incubated for 30 min at 37 °C in a humidified atmosphere containing 5% CO₂. The medium was eliminated before the cells were fixed overnight at 4 °C with 2.5% glutaraldehyde in sterile PBS, and then the cells were washed twice. The samples were dehydrated with increasing concentrations of ethanol (50–100%); followed by critical point drying with liquid carbon dioxide (Samadri-PVT-3D, TOUSIMIS Research Corporation, Rockville, MD, USA). Samples were coated with gold (Denton Vacuum Desk II, NJ, USA), and analyzed by SEM (JEOL, Musashino, Tokyo, Japan).

2.8. Morphological analysis by light microscopy

The morphological analysis was realized after 30 and 120 min of interaction of PMNs (4×10^5) with *S. schenckii* (2×10^6 conidia or yeast cells) at 37 °C in 1.5 mL microcentrifuge polypropylene tubes. The cellular pellets, which were obtained by centrifugation at 300g for 3 min, were gently resuspended in 30 μ L of RPMI 1640 at 37 °C. Smears extended on sterile degreased slides were fixed in methanol, stained with Wright-Giemsa, and examined with light microscopy (LM). Images were captured by a microscope with a digital camera (Motic BA310, China) and were analyzed using the Motic Images Plus program, version 2.0. For each experimental condition, 200 cells of each type present in the interaction were analyzed on each slide (n = 3). The maximum and minimum diameters and areas of fungal cells and PMNs were

measured. From these values, the diameters ratio (minimum diameter/maximum diameter) was calculated for each cell. The nuclear morphology of PMNs was recorded and classified into two categories: normal (2–5 lobes bound by chromatin connections), and modified (loss of at least one characteristic of normal multi-lobulated nuclear morphology).

2.9. Phagocytic activity

Samples for phagocytic activity determination were prepared as detailed previously for the morphological analysis by LM. PMNs-Fungi (either conidia or yeast cells) co-cultures were performed for periods of 10, 30, 60 and 120 min. 200 PMNs were counted on each slide (n = 3), and the number of bound or internalized fungal cells was determined. From this data, the percentage of PMNs that bound or engulfed fungal cells (PPC), and the phagocytic index (PI) were determined. PI was calculated according to the following formula: (total number of bound or engulfed cells/total number of counted PMNs) \times (number of PMNs containing bound or engulfed cells/total number of counted PMNs).

2.10. *S. schenckii* viability assay

To determine the possible effect of PMNs on viability of conidia and yeast cells, PMNs-fungi interactions were performed under the same conditions and time-points established for the evaluation of phagocytic activity. After the interactions, the samples were diluted in sterile cold distilled water and mixed vigorously for 3 min to lyse the PMNs. Dilutions of the samples were seeded in Sabouraud Dextrose Agar and incubated for 72 h at 25 °C. Colony forming units (CFU) were then counted. The results were expressed as a percentage of the CFU obtained in samples of conidia or yeast cells of *S. schenckii* not challenged with PMNs and incubated for the same time-points.

2.11. Statistical analysis

Statistical analysis was carried out using an analysis of variance (ANOVA) test. In all cases, the values of the treatments (PMNs-S.

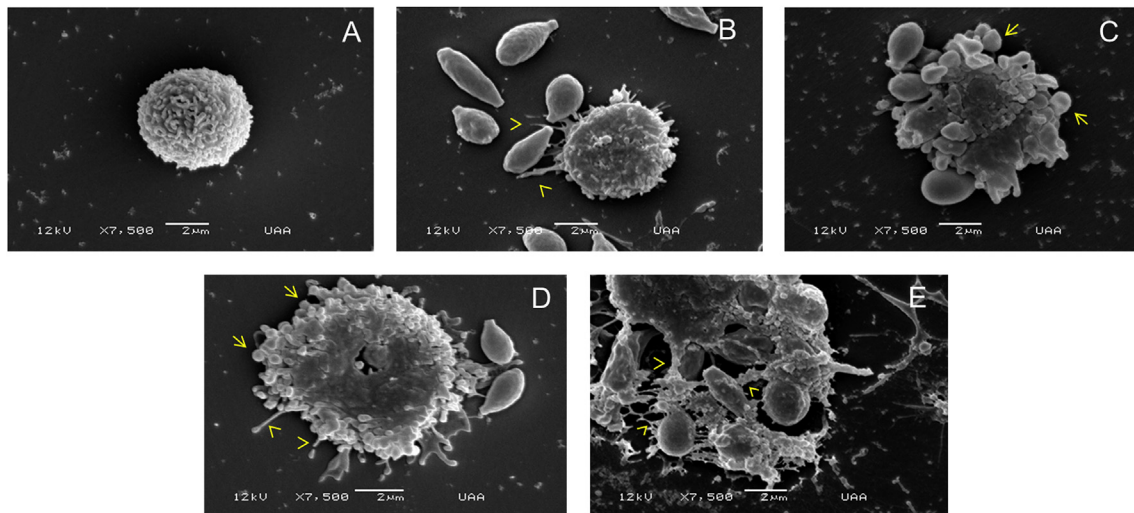


Fig. 2. Superficial deformations of human PMNs in response to *S. schenckii*. A) Quiescent PMN showing a rough surface and spherical morphology. B) PMN near to conidia of *S. schenckii*; reduction of roughness and the emission of flattened filaments (yellow arrowheads) are appreciated. C) PMN bound to yeast-like cells and showing vesicles on its membrane (yellow arrows). D) PMN in interaction with conidia. The increase in size, the formation of superficial vesicles (yellow arrows), and the emission of flattened filaments (yellow arrowheads) are appreciated. E) A PMN emitting long filaments similar to NETs (yellow arrowheads), in which several yeast-like cells of *S. schenckii* are trapped.

S. schenckii co-cultures) were compared with the values of control cells incubated during the same periods and environmental conditions. The IBM SPSS Statistics 17.0 program was used to perform all analysis. A *p* value of < 0.05 was considered statistically significant.

3. Results

3.1. Purity, viability and activation state of PMNs

The viability of PMNs, which purity was demonstrated by immunofluorescence (Fig. 1A) and Wright-Giemsa-stain (Fig. 2A), did not show significant changes from 0 to 120 min (Fig. 1B), neither did MPO activity was significantly modified ($p > 0.05$) in the same time period (Fig. 1C), which rules out the preactivation of these cells in our experimental conditions. On the other hand, MPO activity of PMNs challenged with conidia or yeast cells of *S. schenckii* showed significant increases since 30 min of co-culture, reaching a greater difference of this activity at 120 min in those cells challenged with yeasts than with conidia ($p < 0.001$) (Fig. 1C).

3.2. Morphological and morphometric changes following the interaction of PMNs with *S. schenckii*

SEM analysis showed that PMNs not exposed to the fungus maintained a spherical morphology and a normal roughened surface (Fig. 2A). After the co-culture with conidia or yeast cells of *S. schenckii*, the predominant surface deformations of PMNs were: a) flattened filaments (Fig. 2B), b) vesicles (Fig. 2C), and c) both type of deformation simultaneously (Fig. 2D). In PMNs exposed to yeast cells, filament emissions similar to neutrophil extracellular traps (NETs), were recorded (Fig. 2E), although this morphological deformation was observed at a very low frequency (< 2%).

The morphometric evaluation of quiescent PMNs showed cells with a diameters ratio of 0.90 ± 0.01 , and of minimum and maximum diameters of $7.83 \pm 0.08 \mu\text{m}$ and $8.73 \pm 0.02 \mu\text{m}$, respectively. PMNs not exposed to *S. schenckii* showed a decrease in size and diameters ratio of $0.88 \pm 0.01 \mu\text{m}$ after 2 h of incubation at 37°C (Table 1), indicating the predominance of a near-spherical morphology (Fig. 3A and B). Changes were observed in the diameters ratio and cellular areas of phagocytes that ingested or bound conidia or yeast cells; after 2 h of interaction, the increases in the area of phagocytes was 10% and 20.9%

with conidia and yeasts, respectively. Regarding nuclear changes, there was an increase in the percentage of cells that lost the typical multi-lobed morphology after interaction with *S. schenckii* (Table 1). The predominant nuclear morphological changes were: loss of the chromatin bridges between the lobes and condensation of the lobes. Lysis of PMNs was appreciated after 2 h of co-culture (Fig. 3C).

In order to evaluate the effect of PMNs on *S. schenckii*, the morphometric characteristics (minimum and maximum diameters, diameters ratio and cellular area) of conidia and yeast cells were determined by LM before their interaction with the phagocytes. Conidia measured $3.23 \pm 0.06 \mu\text{m}$ in length (mean \pm standard deviation) by $1.72 \pm 0.05 \mu\text{m}$ width. Yeasts measured $3.07 \pm 0.08 \mu\text{m}$ in length by $2.14 \pm 0.04 \mu\text{m}$. The diameters ratio was $0.53 \pm 0.03 \mu\text{m}$, and $0.70 \pm 0.04 \mu\text{m}$ for conidia and yeast cells, respectively. The morphometric characteristics evaluated in both *S. schenckii* cell morphotypes remained stable during the 2 h of incubation in the absence of PMNs (Table 2). Higher values in the minimum diameter and in the diameters ratio differentiate the conidia from yeast cells. Conidia that were ingested or remained bound to PMNs showed significant increases as compared to conidia not exposed to PMNs both for the lower diameter ($1.86 \pm 0.04 \mu\text{m}$ vs $1.73 \pm 0.04 \mu\text{m}$) and for the diameters ratio ($0.60 \pm 0.02 \mu\text{m}$ vs $0.55 \pm 0.01 \mu\text{m}$) at 30 min of incubation. These changes were accentuated after 2 h of co-incubation with PMNs, with a significant increase in the cellular area of the conidia (Table 2) (Fig. 3D). On the other hand, the yeast cells did not suffer morphometric changes after being phagocytosed or bound to PMNs.

3.3. Phagocytic activity of PMNs exposed to *S. schenckii*

Immunofluorescence staining with (Fig. 4A) and without permeabilization (Fig. 4B) to evaluate phagocytic activity against fungal cells expressing gp-70 showed that *S. schenckii* can be ingested by human PMNs; while the fungal cells outside the PMNs showed intense green fluorescence, those internalized showed negative fluorescence.

The phagocytic activity of the PMNs on conidia and yeast-like cells of *S. schenckii* was manifested from the first 10 min of incubation. PI (Fig. 5A) and PPC (Fig. 5B) were higher for PMNs exposed to yeast cells than for those exposed to conidia. Both indicators of phagocytic activity had gradual increases from 10 to 60 min of incubation. After 2 h incubation, PI and PPC registered decreases compared to the values reached at 60 min. These decreases were more pronounced for PMNs

Table 1
Morphometric data and nuclear morphological changes in human PMNs exposed to *S. schenckii*.^a

	PMNs (Control) ^b		PMNs with bound or ingested conidia		PMNs with bound or ingested yeast-like cells	
	30	120	30	120	30	120
Incubation time (min)	30	120	30	120	30	120
Minimum diameter (μm)	7.73 ± 0.03	7.61 ± 0.06	8.02 ± 0.08 ^e	8.18 ± 0.01 ^f	8.82 ± 0.06 ^f	8.50 ± 0.03 ^f
Maximum diameter (μm)	8.69 ± 0.02	8.63 ± 0.05	9.32 ± 0.01 ^e	9.27 ± 0.03 ^f	10.12 ± 0.07 ^f	9.63 ± 0.01 ^f
Diameters ratio ^c	0.89 ± 0.00	0.88 ± 0.01	0.87 ± 0.01 ^e	0.89 ± 0.00	0.87 ± 0.00 ^d	0.89 ± 0.00
Area (μm ²)	56.61 ± 2.67	52.74 ± 2.37	60.89 ± 1.13	58.02 ± 1.05 ^d	63.30 ± 1.74 ^f	63.77 ± 2.81 ^f
Cells with changes in nuclear morphology (%)	8.5 ± 1.5	12.5 ± 1.3	18.5 ± 2.0 ^e	33.0 ± 1.8 ^e	13.5 ± 1.8 ^d	28.0 ± 2.3 ^f

^a 200 cells were analyzed on each trial (mean ± standard deviation), n = 3.

^b Control: PMNs after 30 and 120 min of incubation in the absence of *S. schenckii*.

^c Diameters ratio = (minimum diameter/maximum diameter).

^d p < 0.05 compared with correspondent control.

^e p < 0.01 compared with correspondent control.

^f p < 0.001 compared with correspondent control.

exposed to yeast cells (> 50% for PI, and > 25% for PPC).

3.4. Effect of PMNs on the viability of *S. schenckii*

After 2 h of interaction with PMNs, the viability of *S. schenckii* did not decrease appreciably (Fig. 6). Cell viability remained above 95% for both fungal morphotypes after 2 h incubation.

4. Discussion

Histopathological studies of human sporotrichosis lesions show pyogenic and granulomatous processes in which PMNs play a central role [25]. Upon stimulation by molecules derived from pathogens or host damaged cells, PMNs become fully activated and suffer morphological changes associated to different types of death mechanisms; uncontrolled release of granule substances from the dead neutrophils can propagate the inflammatory response leading to tissue damage [26]. The nuclear morphological changes and membrane deformations in PMNs observed in our study, suggest that *S. schenckii* may induce processes in these phagocytes which could contribute to the inflammation-associated immunopathology of human sporotrichosis lesions. The loss of the chromatin bridges between the lobes and condensation of the nuclear lobes of phagocytes observed by LM in our study, are consistent with the initial steps of NETs formation and necrosis death mechanisms, which lead to the release of intracellular content [27]. Superficial

vesicles (Fig. 3C and D) are usually associated with an exocytosis process which allows the release of inflammatory mediators that can damage host tissue cells [11]. The release of MPO into the extracellular space is associated to PMNs activation [28,29], this could explain the significant increases in the activity of this enzyme observed during interactions of human PMNs with conidia or yeast cells of *S. schenckii*. In addition, it has been shown that PMNs can rapidly release MPO by degranulation [29]. The emission of flattened filaments observed in SEM images is an early event in phagocytosis, which allows surrounding and finally entrapping the particle [30]. On the other hand, PMNs not exposed to *S. schenckii* maintained a rough surface and a typical spherical morphology; nevertheless, they showed a reduction in cell size and altered nuclear morphology after 2 h of incubation. These phenotypic changes have been previously observed in *ex vivo* cultured PMNs; the nature of the factors that drive this process remains poorly understood [31].

NETs are neutrophil extracellular fibers that contain chromatin and granular enzymes [32]. A previous study demonstrated that NETs killed both hyphal and yeasts of *Candida albicans* [33]. They have also been associated with an effective defense against *Aspergillus nidulans* [34]. NETs formation was detected in a lung infection model against *A. fumigatus*; however, a direct effect of these structures in fungal killing could not be demonstrated [35]. As far as the authors know, there is no previous evidence of the NETs formation in response to *S. schenckii*. Boundaries of the fungal cells that remain attached to these web-like

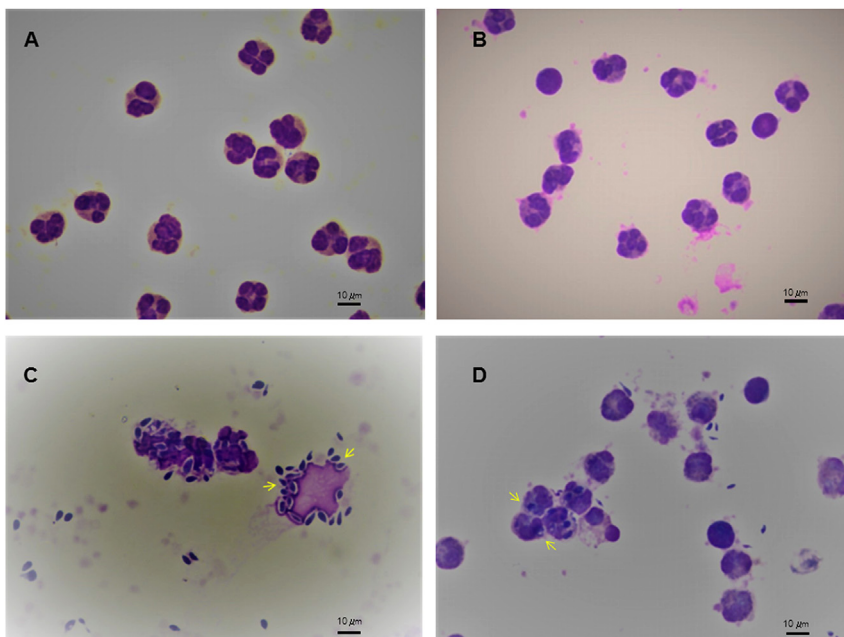


Fig. 3. Morphology of human PMNs and *S. schenckii*. The cells were cultured at 37 °C in RPMI medium and staining with Wright-Giemsa. A) PMNs showing normal multi-lobulated nuclei prior to incubation. B) Quiescent PMNs showing predominance of multi-lobulated morphology after 2 h of incubation. C) PMNs co-incubated with yeast-like cells of *S. schenckii* for 2 h. A cluster of yeast-like cells is seen on a lysed phagocyte (yellow arrows). D) PMNs co-incubated with conidia of *S. schenckii* for 2 h. Phagocytosed conidia (yellow arrows) show higher minimum diameter compared to non-phagocytosed.

Table 2
Cell morphometric alterations of *S. schenckii* phagocytosed by human PMNs.^a

	Conidia (control) ^b		Bound or ingested conidia		Yeast-like cells (control) ^b		Bound or ingested yeast-like cells	
	30	120	30	120	30	120	30	120
Incubation time (min)	30	120	30	120	30	120	30	120
Minimum diameter (μm)	1.73 ± 0.04	1.70 ± 0.03	1.86 ± 0.04 ^d	2.21 ± 0.01 ^e	2.12 ± 0.02	2.12 ± 0.01	2.17 ± 0.04	2.12 ± 0.01
Maximum diameter (μm)	3.23 ± 0.07	3.25 ± 0.04	3.18 ± 0.09	3.18 ± 0.05 ^d	3.05 ± 0.09	3.12 ± 0.01	3.11 ± 0.05	3.12 ± 0.01
Diameters ratio ^c	0.55 ± 0.01	0.54 ± 0.02	0.60 ± 0.02 ^d	0.70 ± 0.01 ^e	0.70 ± 0.02	0.68 ± 0.00	0.70 ± 0.01	0.68 ± 0.00
Area (μm ²)	3.39 ± 0.10	3.30 ± 0.01	3.33 ± 0.03	3.82 ± 0.05 ^e	4.19 ± 0.05	4.22 ± 0.01	4.25 ± 0.05	4.20 ± 0.03

^a 200 cells were analyzed on each trial (mean ± standard deviation), n = 3.

^b Control: *S. schenckii* cells after 30 and 120 min of incubation in the absence of PMNs.

^c Diameters ratio = (minimum diameter/maximum diameter).

^d p < 0.05 compared with correspondent control.

^e p < 0.001 compared with correspondent control.

fibers could not be clearly determined by SEM analysis performed in our study, so further essays are required to determine the particular effect of these structures on the morphology and viability of *S. schenckii*.

The morphological analysis by LM showed zones with remains of lysate phagocytes and several fungal cells around them. Therefore, we think that the ingestion of *S. schenckii* by PMNs may trigger mechanisms that lead to the early death of these phagocytes. This phenomena could be explained by the lysis of several PMNs which had ingested conidia or yeast like cells during the first hour of interaction. Receptors activating caspase 1 are present in human PMNs [14]. Caspase 1 has been shown to be associated with pyroptosis, a cell death mechanism which leads to the rupture of the cytoplasmic membrane and cell disintegration [36]. However, there are no previous reports regarding lysis of PMNs induced by phagocytosed conidia or yeast cells of *S. schenckii*. The histopathological manifestations of sporotrichosis show that the cutaneous disease typically presents with palisading granulomatous dermatitis surrounding a stellate suppurative abscess with the presence of a suppurative central zone composed of PMNs and few eosinophils [25]. This kind of inflammatory tissue reaction could be favored by the lysis of PMNs.

The morphometric analysis of phagocytosed conidia shows an increase in their diameters ratio and minimum diameter at 30 min of interaction, reaching a similar morphology to the yeast phase. The high survival rate of conidia after exposure to PMNs, suggests that these morphometric changes are not associated with an effective action of the toxic components of phagolysosomes, but would be related to the dimorphic switching necessary for colonization of host tissues [4,25]. In tissue cultures, germinating conidia of *S. schenckii* were found in the

cytoplasm of mice macrophages after 24 h; yeast-like cells formation resulted from changes in the hyphal elements formed by the germinating conidia [37]. Morphological transformation from mycelia to yeast-like cells at 37 °C in Brain Heart Infusion broth was observed to occur by direct formation of budlike structures at the tips and along the hyphae after 48 h, and by formations of conidia like structures and subsequent fragmentations of the chains into their constituent yeast-like cells after 72 h [38]. Direct transformation from conidia to yeasts has not been reported for *S. schenckii*. Transition from mycelia to yeast phase is fundamental in sporotrichosis, since unlike what happens with yeasts, hyphae of *S. schenckii* have shown a high susceptibility to the action of human PMNs [18]. A number of signaling pathways that induce the dimorphic switch in fungi have been identified. These pathways include two components and heterotrimeric G protein signaling systems as well as Ras and cAMP signaling and the downstream mitogen-activated protein kinase (MAPK) signaling cascades, which also frequently co-regulate processes important for adaptation to oxidative stress environments, such as those encountered in the intracellular environment of the host phagocytes [39]. Under this assumption, the PMNs phagolysosomes would provide the physiological environment required for a rapid dimorphic switching of the fungus, which would favor the survival and spread of this infectious agent. The mechanisms that regulate the dimorphic switch in *S. schenckii* remain unclear. It is known that α-subunit of the G protein of *S. schenckii*, SSG-2, (a major intracellular receptor of environmental signals) interacts with the cytosolic phospholipase A₂, participating in the control of the dimorphism in this fungus [40]. The MAPK cascades and cAMP pathways may also be involved in dimorphism of *S. schenckii*, and have been associated to

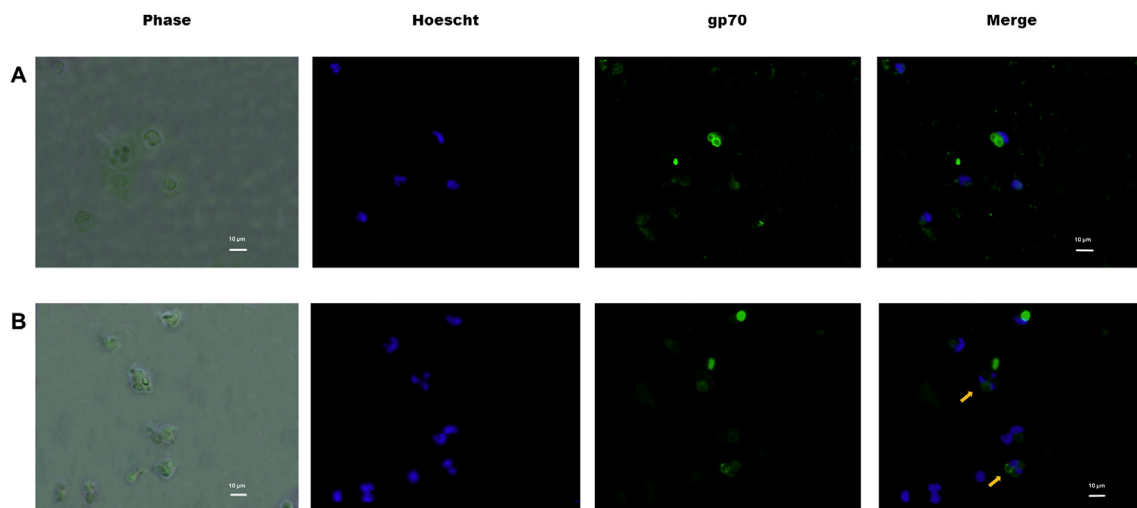


Fig. 4. Phagocytosis of *S. schenckii* by PMNs. Cells were fixed, permeabilized or no, and stained for glycoprotein gp70 of the *S. schenckii* cell wall (gp70, green) and nuclei of PMNs (Hoeschst, blue). In the images respective of phase contrast microscopy and immunofluorescence (merge) of A) permeabilized and B) non-permeabilized cells, phagocytized yeast cells within PMNs were observed at 30 min. The fluorescent staining was significantly reduced in ingested fungal cell of non-permeabilized samples (yellow arrows).

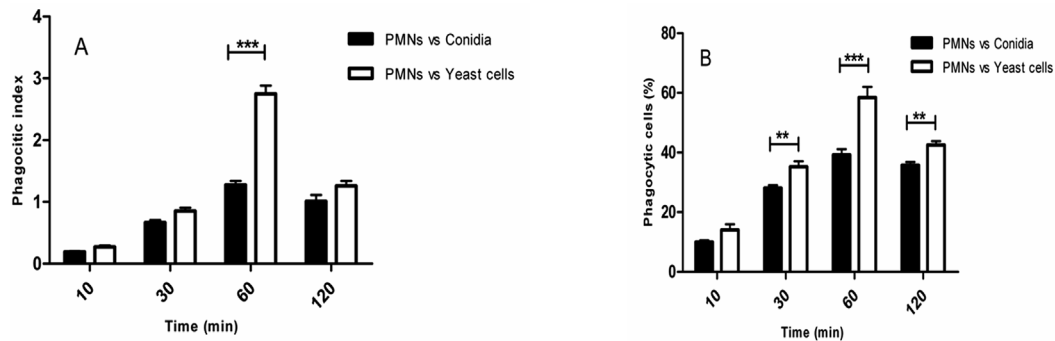


Fig. 5. Phagocytic activity of human PMNs against *S. schenckii*. Phagocytic index = (Total sum of bound or ingested fungal cells/total PMNs). Percentage of phagocytic cells = (PMNs with bound or ingested fungal cells/total PMNs) x 100. For each experimental condition 200 PMNs were evaluated (mean \pm standard deviation, n = 3). ANOVA test. **p < 0.01; ***p < 0.001.

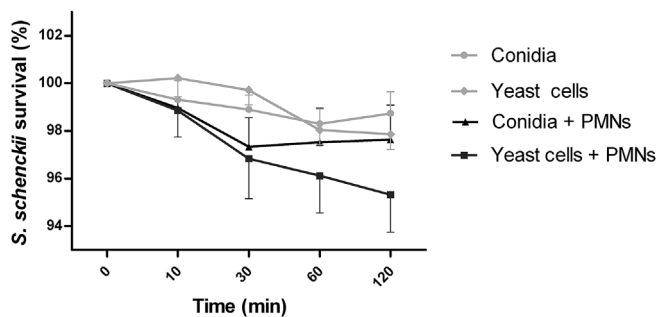


Fig. 6. Survival of *S. schenckii* after interaction with human PMNs. Viability is expressed as percentage of the CFU count in samples of conidia or yeast cells not exposed to PMNs. The quantity of viable fungal cells was estimated by plating the samples in Sabouraud Dextrose Agar at 25 °C for 72 h (mean \pm standard error of the mean, n = 5).

pathogenic development [41].

The absence of morphometric changes and the high survival rate of bound or ingested yeast cells are indicative that the pathogenic phase of *S. schenckii* possesses mechanisms to prevent damages caused by the oxidative and non-oxidative mechanisms of the human PMNs. An interaction study of human PMNs and yeasts of *S. schenckii* using Transmission Electron Microscopy, showed that after 3 h of co-incubation, only 6.3% of phagocytosed yeasts were lysed or partially damaged [18]. This result is similar to the yeast mortality rate obtained in this study using the CFU technique.

In conclusion, the interaction of human PMNs with conidia or yeast cells of *S. schenckii* induces changes in the nuclear morphology and membranes of the phagocytes that are compatible with processes that lead to the release of intracellular content and to the establishment of a pro-inflammatory environment. PMNs show a high capacity to bind or ingest *S. schenckii* cells without affecting fungal viability. The morphological changes recorded in phagocytosed conidia, suggest that this fungus could make the dimorphic switching within the PMNs, which would highlight the importance of these phagocytes for survival and dissemination of *S. schenckii* in host tissues.

Declarations of interest

None.

Funding

This work was supported by the Universidad Autónoma de Aguascalientes [grant number PIB17-2 to Romo-Lozano Yolanda]; and the Consejo Nacional de Ciencia y Tecnología, Mexico [grant number 450126/598367 to Curtiellas-Piñol Vicente].

Appendix A. Supplementary data

Supplementary data to this article can be found online at <https://doi.org/10.1016/j.micpath.2019.01.041>.

References

- [1] Y. Zhang, F. Hagen, B. Stielow, A.M. Rodrigues, K. Samerpitak, X. Zhou, et al., Phylogeography and evolutionary patterns in *Sporothrix* spanning more than 14 000 human and animal case reports, *Persoonia* 35 (2015) 1–20 <https://doi.org/10.3767/003158515X687416>.
- [2] O. Romeo, F. Scordino, G. Criseo, insight into molecular phylogeny and epidemiology of *Sporothrix schenckii* species complex based on calmodulin-encoding gene analysis of Italian isolates, *Mycopathologia* 172 (2011) 179–186 <https://doi.org/10.1007/s11046-011-9420-z>.
- [3] R. Marimon, J. Cano, J. Gene, D.A. Sutton, M. Kawasaki, J. Guarro, *Sporothrix brasiliensis*, *S. globosa*, *S. mexicana*, three new *Sporothrix* species of clinical interest, *J. Clin. Microbiol.* 45 (2007) 3198–3206 <https://doi.org/10.1128/JCM.00808-07>.
- [4] M.B. Barros, R. de Almeida Paes, A.O. Schubach, *Sporothrix schenckii* and Sporotrichosis, *Clin. Microbiol. Rev.* 24 (2011) 633–654 <https://doi.org/10.1128/CMR.00007-11>.
- [5] I. Arrillaga, J. Capilla, E. Mayayo, R. Marimon, M. Mariné, J. Gené, Different virulence levels of the species of *Sporothrix* in a murine model, *Clin. Microbiol. Infect.* 15 (2009) 651–655 <https://doi.org/10.1111/j.1469-0691.2009.02824.x>.
- [6] C. Alba, A. Pérez, C. Toriello, Y. Romo, E. Ruiz, Molecular components of the *Sporothrix schenckii* complex that induce immune response, *Curr. Microbiol.* 73 (2016) 292–300 <https://doi.org/10.1007/s00284-016-1045-5>.
- [7] I.Z. Carlos, D.B. Sgarbi, G.C. Santos, M.C. Placeres, *Sporothrix schenckii* lipid inhibits macrophage phagocytosis: involvement of nitric oxide and tumor necrosis factor- α , *Scand. J. Immunol.* 57 (2003) 214–220 <https://doi.org/10.1046/j.1365-3083.2003.01175.x>.
- [8] C. Alba, A. Pérez, E. López, M. Cuellar, E. Ruiz, Cell wall proteins of *Sporothrix schenckii* as immunoprotective agents, *Rev. Iberoam. De. Micol.* 31 (2014) 86–89 <https://doi.org/10.1016/j.riam.2013.09.017>.
- [9] I.Z. Carlos, M.F. Sassa, D.B. Sgarbi, M.C. Placeres, D.C. Maia, Current research on the immune response to experimental sporotrichosis, *Mycopathologia* 168 (2009) 1–10 <https://doi.org/10.1007/s11046-009-9190-z>.
- [10] R. Cascão, H.S. Rosário, J.E. Fonseca, Neutrophils: warriors and commanders in immune-mediated inflammatory diseases, *Acta Reumatol. Port.* 34 (2009) 313–326 <https://www.ncbi.nlm.nih.gov/pubmed/19727044>.
- [11] M. Faurischou, N. Borregaard, Neutrophil granules and secretory vesicles in inflammation, *Microb. Infect.* 5 (2003) 1317–1327 <https://doi.org/10.1016/j.micinf.2003.09.008>.
- [12] A.D. Kennedy, F.R. DeLeo, Neutrophil apoptosis and the resolution of infection, *Immunol. Res.* 43 (2009) 25–61 <https://doi.org/10.1007/s12026-008-8049-6>.
- [13] Y. Aratani Myeloperoxidase, Its role for host defense, inflammation, and neutrophil function, *Arch. Biochem. Biophys.* 640 (2018) 47–52 <https://doi.org/10.1016/j.abb.2018.01.004>.
- [14] K. Futosi, S. Fodor, A. Mócsai, Neutrophil cell surface receptors and their intracellular signals transduction pathways, *Int. Immunopharmacol.* 17 (2013) 638–650 <https://doi.org/10.1016/j.intimp.2013.06.034>.
- [15] D. Franco, R.C. Nascimento, K.S. Ferreira, S.R. Almeida, Antibodies against *Sporothrix schenckii* enhance TNF- α production and killing by macrophages, *Scand. J. Immunol.* 75 (2012) 142–146 <https://doi.org/10.1111/j.1365-3083.2011.02636.x>.
- [16] Y. Romo, F. Hernández, E. Salinas, *Sporothrix schenckii* yeasts induce ERK pathway activation and secretion of IL-6 and TNF- α in rat mast cells, but no degranulation, *Med. Mycol.* 52 (2014) 862–868 <https://doi.org/10.1093/mmy/myu055>.
- [17] K.M. Cunningham, G.S. Bulmer, E.R. Rhoades, Phagocytosis and intracellular fate of *Sporothrix schenckii*, *J. Infect. Dis.* 140 (1979) 815–817 <https://doi.org/10.1093/infdis/140.5.815>.

- [18] A. Schaffner, C.E. Davis, T. Schaffner, M. Markert, H. Douglas, A.I. Braude, *In vitro* susceptibility of fungi to killing by neutrophil granulocytes discriminates between primary pathogenicity and Opportunism, *J. Clin. Invest.* 78 (1986) 511–524 <https://doi.org/10.1172/JCI112603>.
- [19] J.B. Sterling, W.R. Heymann, Potassium iodide in dermatology: a 19th century drug for the 21st century—uses, pharmacology, adverse effects, and contraindications, *J. Am. Acad. Dermatol.* 43 (2000) 691–697 <https://doi.org/10.1067/mjd.2000.107247>.
- [20] C.A. Kauffman, B. Bustamante, S.W. Chapman, P.G. Pappas, Clinical Practice Guidelines for the management of sporotrichosis, 2007 update by the Infectious Disease Society of America, *Clin. Infect. Dis.* 45 (2007) 1255–1265 <https://doi.org/10.1086/522765>.
- [21] D. English, B.R. Andersen, Single-step separation of red blood cells. Granulocytes and mononuclear leukocytes on discontinuous density gradients of Ficoll-Hypaque, *J. Immunol. Methods* 5 (1974) 249–252 [https://doi.org/10.1016/0022-1759\(74\)90109-4](https://doi.org/10.1016/0022-1759(74)90109-4).
- [22] T. Mosmann, Rapid colorimetric assay for cellular growth and survival: application to proliferation and cytotoxicity assays, *J. Immunol. Methods* 65 (1983) 55–63 [https://doi.org/10.1016/0022-1759\(83\)90303-4](https://doi.org/10.1016/0022-1759(83)90303-4).
- [23] E. Harlow, D. Lane, Mounting samples in gelvatol or mowiol, *Cold Spring Harb. Protoc.* 1 (2006) pii: pdb.prot4461 <https://doi.org/10.1101/pdb.prot4461>.
- [24] V. Herzog, H.D. Fahimi, A new sensitive colorimetric assay for peroxidase using 3,3'-diaminobenzidine as hydrogen donor, *Anal. Biochem.* 55 (1973) 554–562 [https://doi.org/10.1016/0003-2697\(73\)90144-9](https://doi.org/10.1016/0003-2697(73)90144-9).
- [25] Y. Zhang, X. Xu, M. Zhang, P. Juang, Z. Zhou, Z. Li, et al., Sporotrichosis: clinical and histopathological manifestations, *Am. J. Dermatopathol.* 33 (2011) 296–302 <https://doi.org/10.1097/DAD.0b013e3181f5b622>.
- [26] T.N. Mayadas, X. Cullere, C.A. Lowell, The multifaceted functions of neutrophils, *Annu. Rev. Pathol.* 9 (2014) 181–218 <https://doi.org/10.1146/annurev-pathol-020712-164023>.
- [27] T. Iba, N. Hashiguchi, I. Nagaoka, Y. Tabe, M. Murai, Neutrophil cell death in response to infection and its relation to coagulation, *J. Intensive Care* 1 (2013) 13 <https://dx.doi.org/10.1186%2F2052-0492-1-13>.
- [28] D. Lau, H. Mollnau, J.P. Eiserich, B.A. Freeman, A. Daiber, U. Gehling, et al., Myeloperoxidase mediates neutrophil activation by association with CD11b/CD18 integrins, *Proc. Natl. Acad. Sci. U.S.A.* 102 (2004) 431–436 <https://doi.org/10.1073/pnas.0405193102>.
- [29] D. Odobasic, A. Richard, S.R. Holdsworth, Neutrophil-Mediated Regulation of Innate and Adaptive Immunity: The Role of Myeloperoxidase, *J. Immunol. Res.* 2016 (2016) 1–11 <https://doi.org/10.1155/2016/2349817>.
- [30] S. Greenberg, S. Grinstein, Phagocytosis and innate immunity, *Curr. Opin. Immunol.* 14 (2002) 136–145 [https://doi.org/10.1016/S0952-7915\(01\)00309-0](https://doi.org/10.1016/S0952-7915(01)00309-0).
- [31] J.M. Adrover, J.A. Nicolas-Ávila, A. Hidalgo, Aging: a temporal dimension for neutrophils, *Trends Immunol.* 37 (2016) 334–345 <https://doi.org/10.1016/j.it.2016.03.005>.
- [32] P. Naccache, M.J. Fernandes, Challenges in the Characterization of Neutrophil extracellular traps. The truth in details, *Eur. J. Immunol.* 46 (2016) 52–55 <https://doi.org/10.1002/eji.201546022>.
- [33] C. Urban, V. Relchard, V. Brinkmann, A. Zychlinsky, Neutrophil extracellular traps capture and kill *Candida albicans* yeast and hyphal forms, *Cell Microbiol.* 8 (2006) 668–676 <https://doi.org/10.1111/j.1462-5822.2005.00659.x>.
- [34] M. Bianchi, A. Hakkim, V. Brinkmann, U. Siler, R.A. Seger, A. Zychlinsky, et al., Restoration of NET formation by gene therapy in CGD controls aspergillosis, *Blood* 114 (2009) 2619–2622 <https://doi.org/10.1182/blood-2009-05-221606>.
- [35] M. Hasenberg, J. Behnsen, S. Krappmann, A. Brakhage, M. Gunzer, Phagocyte responses towards *Aspergillus fumigatus*, *Int. J. Med. Microbiol.* 301 (2011) 436–444 <https://doi.org/10.1016/j.ijmm.2011.04.012>.
- [36] G. Sollberger, G.E. Strittmatter, M. Garstkiewicz, J. Sand, H.D. Beer, Caspase-1: The inflammasome and beyond, *Innate Immun.* 20 (2014) 115–125 <https://doi.org/10.1177/1753425913484374>.
- [37] D.H. Howard, Dimorphism of *Sporotrichum schenckii*, *J. Bacteriol.* 81 (1961) 464–469 <https://www.ncbi.nlm.nih.gov/pmc/articles/PMC279030/>.
- [38] R.G. Garrison, K.S. Boyd, F. Mariat, Ultrastructural studies of the mycelium to yeast transformation of *Sporothrix schenckii*, *J. Bact.* 124 (1975) 59–68 <https://www.ncbi.nlm.nih.gov/pmc/articles/PMC235986/>.
- [39] K.J. Boyce, A. Andrianopoulos, Fungal dimorphism: The switch from hyphae to yeast is a specialized morphogenetic adaptation allowing colonization of a host, *FEMS Microbiol. Rev.* 39 (2015) 797–811 <https://doi.org/10.1093/femsre/fuv035>.
- [40] S. Valentin-Berrios, W. González-Velázquez, L. Pérez-Sánchez, R. González-Méndez, N. Rodríguez-del Valle, Cytosolic phospholipase A2: a member of the signalling pathway of a new G protein alpha subunit in *Sporothrix schenckii*, *BMC Microbiol.* 9 (2009) 100 <https://dx.doi.org/10.1186%2F1471-2180-9-100>.
- [41] M.D. Téllez, A. Batista-Duharte, D. Portuondo, C. Quinello, R. Bonne-Hernández, I.Z. Carlos, *Sporothrix schenckii* complex biology: environment and fungal pathogenicity, *Microbiol.* 160 (2014) 2352–2365 <https://doi.org/10.1099/mic.0.081794-0>.



El misterio del beso salado

Desde la antigüedad se ha otorgado a la sal una connotación mística; en particular, el sabor salado del sudor se ha asociado con la brujería o el mal de ojo, porque entre más salado fuera el sudor más pronto moría la gente. Ahora sabemos que ésta es una característica de los pacientes con fibrosis quística, una enfermedad genética y progresiva que produce afectaciones en las vías respiratorias e inclusive provoca la muerte a edad temprana. La presente revisión describe el mecanismo que lleva al surgimiento de dicha enfermedad; además, se presenta una breve introducción a las estrategias de rescate para restablecer la localización y función de la proteína implicada: el canal de cloro CFTR.

Un cristal denominado cloruro de sodio (cuya fórmula química es NaCl), también llamado sal común o sal de mesa, es posiblemente el condimento más antiguo. La sal ha influenciado el desarrollo de la historia económica y social de la humanidad; se ha usado como preservador de los alimentos e incluso como moneda de pago en algunas culturas (de ahí el origen de la palabra *salario*). Asimismo, la sal tiene un papel místico; la Biblia refiere que la mujer de Lot se convirtió en una estatua de sal y en muchas culturas vemos que la sal se usa en rituales de “pureza” o “desinfección” y sobre todo como “barrera contra el mal”.

De manera particular, en México es común usar el término *salado* para referirse a una persona con “mala suerte”, aunque en realidad no tengamos ni idea del origen de esta asociación. Se cree que esta relación se estableció a partir de la orden de algún emperador romano que como castigo al enemigo ordenaba tirar sal a los cultivos, de manera que la cosecha se secaba y la tierra se hacía infértil.

“¡Ay de aquel niño que al ser besado en la frente sabe salado! Él está embrujado y pronto debe morir”, reza un poema irlandés del siglo XV, haciendo referencia a

un niño enfermizo que moriría a temprana edad. De hecho, ésta es una descripción muy acertada para la enfermedad conocida como fibrosis quística (véase la figura 1). Sin duda, la cultura popular está llena de sabiduría.

La fibrosis quística

La fibrosis quística se caracteriza por la generación anormal de líquido espeso que se acumula en los órganos mucosos. Los síntomas se manifiestan desde edades tempranas y los más evidentes son los problemas respiratorios y digestivos. La expectativa de vida para los pacientes con fibrosis quística actualmente no supera los 40 años.

La fibrosis quística es una enfermedad que se hereda, pero para que un hijo la tenga es necesario que los dos padres hayan sido **portadores** del gen defectuoso. Esto se explica tomando en cuenta que la mitad de la información genética proviene del padre y la otra mitad, de la madre. Entonces, si se considera a unos padres portadores que tienen cuatro hijos, por probabilidad tendrían un hijo sano, dos hijos portadores del gen defectuoso y un hijo enfermo. A este tipo de herencia se le llama autosómica recesiva (véase la figura 2).

El gen afectado en pacientes con fibrosis quística es responsable de la generación de una proteína que se localiza en la membrana plasmática de las células que conforman las superficies mucosas, llamadas célu-

las apicales. Estas células se encuentran en pulmones, vías respiratorias, hígado, páncreas, intestinos y aparato reproductor, además de expresarse en la piel. La proteína relacionada con la fibrosis quística que se genera en dichas células se llama regulador de la conductancia transmembrana de la fibrosis quística (CFTR por sus siglas en inglés) y se encarga de mediar el flujo de iones cloro a través de la membrana de las células apicales, por lo que regularmente se le conoce como canal de cloro CFTR.

El CFTR

El transporte de iones (como sodio, calcio, cloro, etc.) entre el exterior y el interior de las células es muy importante en la fisiología de los organismos. Si las proteínas que regulan el paso unidireccional de iones —conocidas como canales iónicos— sufren algún defecto, pueden ocurrir muchos cambios en las células. Por ejemplo, en las vías aéreas, cuando el canal de cloro CFTR se descompone, afecta la función de otros canales y transportadores iónicos.

En las glándulas sudoríparas de la piel se expresan diferentes proteínas que regulan el transporte iónico; el canal CFTR es el principal mediador del transporte de cloro hacia el interior de las células. En condiciones normales, los iones sodio (Na^+) y cloro (Cl^-) fluyen hacia el interior a través del canal de sodio epitelial (ENaC) y el canal CFTR, respectivamente. Al estar el CFTR ausente o disfuncional en la membrana plasmá-



Figura 1. Fibrosis quística, la enfermedad del beso que sabe salado.

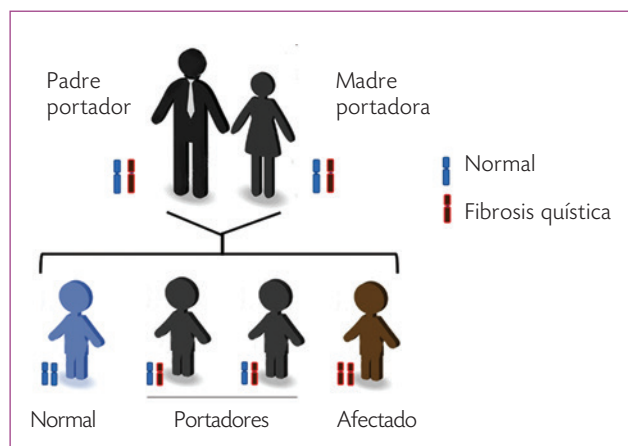


Figura 2. La fibrosis quística es una enfermedad que se hereda de manera autosómica recesiva.

tica, la entrada de Cl^- a la célula disminuye; como consecuencia, afecta la reabsorción del Na^+ (véase la figura 3). El resultado: hay un exceso de sales (NaCl) en el sudor.

La mayor expresión del canal CFTR se da en células apicales. Estas células están recubiertas con unas proyecciones móviles que parecen cabellos, denominadas cilios; los cilios están rodeados de una capa líquida viscosa llamada moco. En el pulmón, la superficie líquida de las vías aéreas proporciona un ambiente donde los cilios pueden moverse libremente, lo cual favorece la limpieza de pequeñas partículas inhaladas que han sido atrapadas en la mucosa y con ello se forma una barrera de protección contra agentes infecciosos. La consistencia del moco está regulada por la salida de Cl^- a través del canal CFTR y la entrada de Na^+ a las células apicales mediante el canal ENaC.

Cuando el canal CFTR es disfuncional, la salida de Cl^- disminuye, pero la entrada de Na^+ incrementa, lo que induce la absorción de agua en las células apicales. Como consecuencia de la disminución del líquido en la región extracelular, el moco se hace viscoso o pegajoso. Este evento hace que la capacidad del moco para limpiar disminuya, se bloqueen las vías aéreas y exista

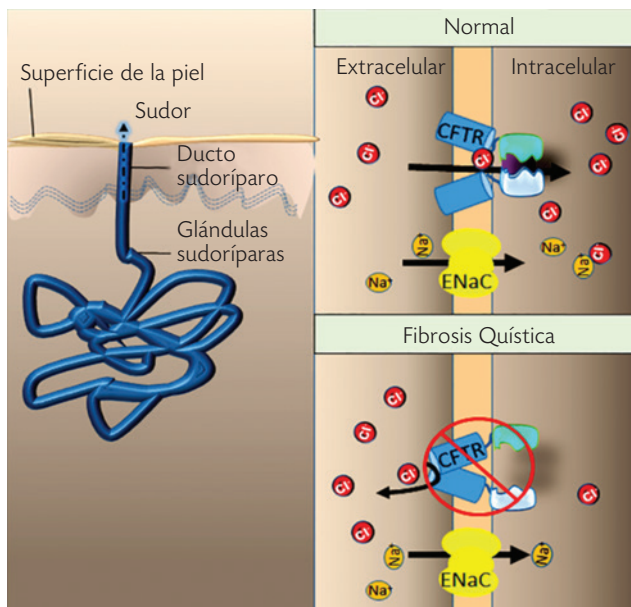


Figura 3. Expresión del canal CFTR en piel. En condiciones normales, en las glándulas sudoríparas los iones Cl^- y Na^+ entran a las células a través de los canales CFTR y ENaC. En la fibrosis quística, el canal CFTR en membrana plasmática está ausente o es disfuncional, lo que induce la acumulación de iones Cl^- y Na^+ en la región extracelular.

un ambiente favorable para la proliferación bacteriana, principalmente en pulmones (véase la figura 4).

La fibrosis quística es una enfermedad que causa la muerte

El conjunto de signos y síntomas de la fibrosis quística se hace evidente por la inflamación de los órganos afectados. La enfermedad llega a provocar esterilidad en hombres, además de que generalmente se puede presentar disfunción pancreática, bloqueo de intestinos y de vías respiratorias; esto último genera bronquiectasia –un padecimiento que induce la obstrucción de vías aéreas debido a la producción crónica de moco, manifestando dolor de pecho y sangrado al toser–. Finalmente la fibrosis quística induce la muerte.

Resulta muy importante detectar esta enfermedad en edades tempranas, en espera de que el tratamiento oportuno incremente la expectativa de vida del paciente. Es por esta razón que en algunos países, entre los métodos de detección temprana de enfermedades en neonatos –o perfil neonatal–, ya se incluye a la fibrosis quística.

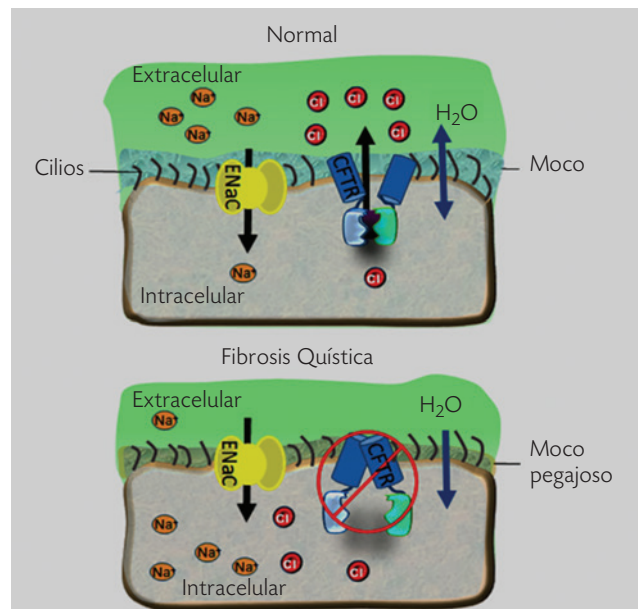


Figura 4. Expresión del canal CFTR en células del pulmón. Las células apicales del pulmón están cubiertas por una capa de moco y cilios que protegen de las partículas infecciosas inhaladas. La consistencia de este moco está regulada por el flujo de Cl^- hacia el exterior de la célula y el paso intracelular de Na^+ mediante los canales CFTR y ENaC. Cuando el canal CFTR es disfuncional o está ausente, la salida de Cl^- se ve disminuida e incrementa la entrada de Na^+ ; esto induce la absorción de agua y la formación de moco pegajoso en el exterior de la célula.

Últimamente en México se ha hecho conciencia de este problema; en 2013 la Secretaría de Salud publicó la *Guía de práctica clínica: diagnóstico de fibrosis quística en la edad pediátrica*. Según la Asociación Mexicana para la Fibrosis Quística, actualmente se tiene reporte de que alrededor de 3 000 niños viven con esta enfermedad. Se calcula que en el país cada año nacen aproximadamente 400 niños afectados, de los cuales 15% son diagnosticados con vida y el resto fallece antes de los cuatro años. La expectativa de vida para pacientes con fibrosis quística en México no supera los 18 años.

Durante mucho tiempo se pensó que la fibrosis quística era una enfermedad exclusiva de la gente caucásica (blancos), pero esto no es completamente cierto. El análisis de la prevalencia de esta enfermedad muestra claramente que las personas caucásicas tienen mayor incidencia, pero no es el único grupo afectado, ya que la variabilidad génica se ha visto favorecida por la mezcla de razas.

A lo largo de la historia los síntomas de la fibrosis quística han sido malinterpretados y confundidos con enfermedades como neumonía y obstrucción intestinal, o incluso con el mal de ojo y hasta la brujería. Al ser una enfermedad de vías respiratorias que en la mayor parte de los casos se presenta con problemas estomacales, los primeros remedios incluían la limpieza de vías aéreas y la administración de enzimas pancreáticas. Posteriormente, con la aparición de los primeros antibióticos, éstos se utilizaron para combatir las infecciones; luego se incluyeron los antibióticos inhalados y se modificaron los hábitos alimentarios. Sin embargo, estos tratamientos eran dirigidos sólo a contrarrestar los síntomas; quizá incrementaban el pronóstico de vida, pero no curaban la enfermedad. Ahora se sabe que para poder combatir la fibrosis quística es necesario ir al origen del problema.

El gen y la proteína CFTR

En 1989 se descubrió el gen CFTR que codifica a la proteína implicada en el desarrollo de la fibrosis quística; dicha proteína está compuesta por 1 480 aminoácidos. Con el auge que ha tenido la secuenciación de genomas, en la actualidad se han reportado cerca de 2 000 mutaciones en el gen CFTR. La mutación que se

ha encontrado en aproximadamente 90% de los pacientes con fibrosis quística consiste en la falta del aminoácido fenilalanina en la posición 508 de la proteína CFTR (CFTR- Δ F508, léase: delección de la fenilalanina 508).

Una vez conocida la secuencia codificante de la proteína CFTR, se hicieron muchos experimentos en el laboratorio para saber cuál era el problema inducido por la proteína mutante (Δ F508). Por ejemplo, se expresó tanto la proteína silvestre (control) como la mutante en cultivos de células y se comparó su **localización** mediante técnicas inmunológicas y de microscopía, entre otras.

La mutación Δ F508 provoca que la proteína CFTR tenga un defecto en su **plegamiento**. Este defecto da lugar a que no se reconozca la señal que hace que la proteína llegue a la membrana de la célula. En otras palabras, la proteína se queda detenida en el tráfico... no puede llegar a su destino final en la membrana plasmática, donde cumpliría la función de permitir el flujo de Cl^- en la célula.

Los primeros indicios de que es posible rescatar la localización (o reubicar) el canal de cloro CFTR- Δ F508 se dieron tras expresar esta proteína en cultivos celulares mantenidos a temperaturas bajas (26 °C). Una vez que CFTR- Δ F508 fue localizado en membrana plasmática se realizaron estudios biofísicos que determinaron que la proteína es funcional aun cuando presenta una conductividad de Cl^- disminuida. Sin embargo, la reducción de la temperatura corporal a 26 °C no es un tratamiento viable para pacientes con fibrosis quística, debido a que la temperatura del cuerpo humano es en promedio 37 °C. No obstante, esto abrió una ventana de posibilidades para el descubrimiento de sustancias que asistan el plegamiento correcto del canal CFTR- Δ F508 con la finalidad de restablecer su correcto tráfico hasta la membrana plasmática.

En los trabajos de búsqueda de sustancias que favorezcan el plegamiento de proteínas de membrana se ha considerado el hecho de que las membranas están constituidas de lípidos (sustancias grasas), por lo que se abordó el uso de compuestos químicos como glicerol y dimetilsulfóxido (DMSO), con resultados positivos en el laboratorio. Basadas en estos resultados, las industrias farmacéuticas se dieron a la tarea de desarrollar compuestos que ayudaran a mejorar la expectativa de

vida; esto dio lugar a medicamentos como Lumacaftor e Ivacaftor, así como Orkambi (que es una combinación de Lumacaftor e Ivacaftor). Estos medicamentos han sido aprobados por la Agencia de Drogas y Alimentos de Estados Unidos (FDA) y son los que más se utilizan para el tratamiento de la fibrosis quística. Actualmente, diversos grupos de investigación continúan buscando alternativas más eficaces para restaurar la ubicación y la función del canal CFTR mutante.

Aunque ha aumentado la expectativa de vida para el *niño que al ser besado en la frente sabe salado*, aún no existe un medicamento que alivie la enfermedad, pero hay esperanza de que pronto se encuentre la cura para la fibrosis quística.

Roberto González-Reyes desarrolló el tema “Diseño de terapias basadas en los mecanismos moleculares de la fibrosis quística” como práctica especial para obtener el grado de Químico Farmacéutico Biólogo en la Facultad de Ciencias Químicas de la Universidad Juárez del Estado de Durango.

roberto_emisael@gmail.com

Guillermo Rojas-Chávez es pasante de la carrera de Químico Farmacéutico Biólogo de la Facultad de Ciencias Químicas de la Universidad Juárez del Estado de Durango; actualmente desarrolla su tesis para obtener el grado.

halo_gerch@hotmail.com

Estela Ruiz-Baca estudió la licenciatura en Químico Farmacéutico Biólogo en la Facultad de Ciencias Químicas de la Universidad de Guanajuato y el doctorado directo en Biología Experimental en el Instituto de Investigación en Biología Experimental de la Universidad de Guanajuato. Realizó una estancia posdoctoral en el Instituto de Neurobiología de la Universidad Nacional Autónoma de México. Desde 2007 es profesor investigador en la Facultad de Ciencias Químicas de la Universidad Juárez del Estado de Durango y es miembro del Sistema Nacional de Investigadores, nivel I.

eruiz@ujed.mx

Angélica López-Rodríguez es profesora investigadora de tiempo completo en la Facultad de Ciencias Químicas de la Universidad Juárez del Estado de Durango. Estudió la carrera de Químico Farmacéutico Biólogo en la Facultad de Ciencias Químicas de la Universidad Autónoma de Tamaulipas; la maestría en la Unidad de

Laboratorios de Ingeniería y Expresión Genética de la Universidad Autónoma de Nuevo León; y obtuvo el grado de doctor en Ciencias Biomédicas en el Instituto de Neurobiología de la Universidad Nacional Autónoma de México. Fue becaria de la Fundación Grass en una estancia de investigación en los Laboratorios de Investigación Marina (MBL, Woods Hole, Massachusetts, EUA). Posteriormente realizó su posdoctorado en los Institutos Nacionales de Salud (NIH) de Estados Unidos. Es miembro del Sistema Nacional de Investigadores. Su trabajo de investigación se basa en el análisis biofísico de los canales iónicos relacionados con patologías (canalopatías), con la finalidad de contribuir al diseño de nuevas estrategias terapéuticas.
angelica.lopez@ujed.mx

Glosario

Portadores de una enfermedad: personas que expresan una copia normal y una defectuosa del gen afectado, pero no manifiestan síntomas de la enfermedad.

Localización de las proteínas en las células: la fabricación (síntesis) y distribución de las proteínas son actividades vitales para la célula. Existen proteínas que sólo cumplen su función cuando se localizan en un determinado lugar, ya sea de manera fija en las membranas o de manera soluble dentro de la célula.

Plegamiento proteico: la interacción de los aminoácidos que codifican una proteína determina su arreglo conformacional, con giros, dobleces y empalmes, hasta generar su forma final.

Lecturas recomendadas

Asociación Mexicana de Fibrosis Quística, A. C. Disponible en: <<http://fq.org.mx/sitio/>>.

Escuela de Minas “Dr. Horacio Carrillo” (2007), *Historia de la sal*. Disponible en: <<http://www.oni.escuelas.edu.ar/2007/JUJUY/1310/historia.html>>.

Orozco, L., M. Chávez, Y. Saldaña, R. Velázquez, A. Carnevale, A. González-del Ángel y S. Jiménez (2006), “Fibrosis quística: la frontera del conocimiento molecular y sus aplicaciones clínicas”, *Rev. Invest. Clín.*, 58(2): 139-152.

Palma, A. G., B. A. Kotsias y G. I. Marino (2014), “Funciones de los canales iónicos CFTR y ENaC en la fibrosis quística”, *Medicina (Buenos Aires)*, 74(2): 133-139.

Secretaría de Salud (2013), *Guía de práctica clínica: diagnóstico de fibrosis quística en la edad pediátrica*. Disponible en: <http://www.cenetec.salud.gob.mx/descargas/gpc/CatalogoMaestro/IMSS_627_13_FIBROSISQUISTI-CAPEDIATRICA/627GER.pdf>.



Moonlighting proteins induce protection in a mouse model against *Candida* species

César Luis Medrano-Díaz^a, Arturo Vega-González^b, Estela Ruiz-Baca^c, Abel Moreno^{d,**},
Mayra Cuéllar-Cruz^{a,*}

^a Departamento de Biología, División de Ciencias Naturales y Exactas, Campus Guanajuato, Universidad de Guanajuato, Noria Alta S/N, Col. Noria Alta, C.P. 36050, Guanajuato, Guanajuato, Mexico

^b Departamento de Ingenierías Química, Electrónica y Biomédica, División de Ciencias e Ingenierías, Campus León, Universidad de Guanajuato, Guanajuato, Guanajuato, Mexico

^c Facultad de Ciencias Químicas, Universidad Juárez del Estado de Durango, Durango, Mexico

^d Instituto de Química, Universidad Nacional Autónoma de México, Av. Universidad 3000, Ciudad Universitaria, Ciudad de México, 04510, Mexico

ARTICLE INFO

Keywords:

C. albicans

C. glabrata

Vaccines

Fba1

Pk

Moonlighting proteins

ABSTRACT

In recent years, *C. albicans* and *C. glabrata* have been identified as the main cause of candidemia and invasive candidiasis in hospitalized and immunocompromised patients. In order to colonize the human host, these fungi express several virulence factors such as the response to oxidative stress and the formation of biofilms. In the expression of these virulence factors, the cell wall of *C. albicans* and *C. glabrata* is of fundamental importance. As the outermost structure of the yeast, the cell wall is the first to come in contact with the reactive oxygen species (ROS) generated during the respiratory outbreak, and in the formation of biofilms, it is the first to adhere to organs or medical devices implanted in the human host. In both processes, several cell wall proteins (CWP) are required, since they promote attachment to human cells or abiotic surfaces, as well as to detoxify ROS. In our working group we have identified moonlighting CWP in response to oxidative stress as well as in the formation of biofilms. Having identified moonlighting CWP in *Candida* species in response to two virulence factors indicates that these proteins may possibly be immunodominant. The aim of the present work was to evaluate whether proteins of this type such as fructose-bisphosphate aldolase (Fba1), phosphoglycerate kinase (Pkg) and pyruvate kinase (Pk), could confer protection in a mouse model against *C. albicans* and *C. glabrata*. For this, recombinant proteins His₆-Fba1, His₆-Pkg and His₆-Pk were constructed and used to immunize several groups of mice. The immunized mice were infected with *C. albicans* or *C. glabrata*, and subsequently the liver, spleen and kidney were extracted and the number of CFU was determined. Our results showed that Pk confers immunity to mice against *C. albicans*, while Fba1 to *C. glabrata*. This data allows us to conclude that the moonlighting CWP, Fba1 and Pk confer *in vivo* protection in a specific way against each species of *Candida*. This makes them promising candidates for developing specific vaccines against these pathogens.

1. Introduction

Candida species are part of the microbiota in healthy individuals. However, when the immune system of the human host is compromised, *Candida* became opportunistic pathogens (they easily adapt to different host niches) causing therefore, infections like candidemia and invasive candidiasis (IC) [1–6]. This invasive candidiasis is one of the main causes of morbidity and mortality in hospitalized and immunocompromised patients [7–10]. Of all the different species of *Candida* known so far, *C. albicans* is the main specie identified in

patients [11,12]. However, due to the uncontrolled use of broad spectrum antibiotics, prolonged periods of hospitalization, and the implantation of medical devices, *C. glabrata* has emerged as the second most common cause of IC [13,14], being the one most commonly found in patients with cancer [15,16]. In order to colonize human hosts, these fungi express several virulence factors such as dimorphic transition [17,18], adhesins expression, the synthesis of hydrolytic proteins, thigmotropism, formation of biofilms and the response to oxidative stress (OSR) [19–21]. The formation of biofilms is of special interest because it has been associated with high rates of hospital mortality.

* Corresponding author.

** Corresponding author.

E-mail addresses: carcamo@unam.mx (A. Moreno), mcuellar@ugto.mx (M. Cuéllar-Cruz).

<https://doi.org/10.1016/j.micpath.2018.08.024>

Received 11 May 2018; Received in revised form 13 August 2018; Accepted 14 August 2018

Available online 15 August 2018

0882-4010/ © 2018 Elsevier Ltd. All rights reserved.

Once *Candida* has formed a biofilm in a device or tissue in the host, the patient cannot respond adequately to antifungals, which leads to presenting IC [22,23]. Another important virulence factor of *C. albicans* and *C. glabrata* is the response to oxidative stress (OSR), due to the fact that during the infection process, these yeasts have to cope with the reactive oxygen species (ROS) generated during the respiratory burst by the phagocytic cells of the human host [24]. In the expression of these two virulence factors the cell wall (CW) of *C. albicans* and *C. glabrata* is fundamental. The cell wall, as the outer structure of the yeast, is the first contact with the ROS generated during the respiratory outbreak, and with the formation of biofilms. The latter is the first step to adhere to the organs or to the medical devices implanted in the human host [25]. In these processes, several cell wall proteins (CWP) are required, since they are the ones that promote the attachment to human cells or abiotic surfaces of medical devices. They also promote the detoxification of the ROS generated during the respiratory burst [2,26,27]. Our group have identified CWP in OSR and biofilm formation [2,26]. The identified proteins corresponded to moonlighting CWP. The main characteristic of these proteins is that they are not covalently bound to the CW, but they can also be dually located on it [28–30]. The identification of moonlighting CWP in *Candida* species, in response to two virulence factors, indicates that these proteins may possibly be immunodominant. This shows that these type of proteins, such as the enolase of *C. albicans*, are considered one of the main immunodominant proteins detected in body fluids of patients with IC [31,32]. Other proteins that have been identified in cytoplasm and CW of *C. albicans* are heat shock proteins such as the heat shock protein Hsp90, of which a 47 kDa antigen has been detected [33,34] and Hsp70 [35]. Thus, these studies show that certain antigens of CW and anti-CW antibodies can be used to protect the human host against candidiasis. In order to assess whether the moonlighting CWP (that we identified in *Candida* species) are apparently involved in OSR and biofilm formation, and whether they protect a murine model against *C. albicans* and *C. glabrata*, we chose three of these proteins: the fructose-bisphosphate aldolase (Fba1), the phosphoglycerate kinase (Pkg) and the pyruvate kinase (Pk), because they are of special interest due to their decreasing expression in the cell for both *C. albicans* or *C. glabrata* which are involved in OSR as well as the formation of biofilms [2,29]. The fact that expression of Fba1, Pkg or Pk decreases in response to two factors of virulence, indicates that these pathogens probably inhibit the synthesis of proteins involved in OSR. These pathogens use, instead, the available CWP to protect themselves from the host's immune system [2]. Thus, these moonlight-like proteins (CWP) are the first line of defense of *Candida* against ROS. These confer protection against the OSR generated during the respiratory burst of phagocytic cells by human host, thereby enabling these pathogens to adhere, infect and remain in the infected host. This makes Fba1, Pkg and Pk excellent candidates as immunodominant proteins. In order to assess whether these proteins were immunodominant, the three moonlighting CWP: Fba1, Pkg and Pk of *C. glabrata* were overexpressed in the expression vector pET 19b. Finally, groups of BALB/c mice (Taconic) were immunized with the recombinant proteins His₆-Fba1, His₆-Pkg and His₆-Pk, and subsequently infected with *C. albicans* or *C. glabrata*.

2. Materials and methods

2.1. Strains and culture conditions

The strains and plasmids used in this study are listed in Table 1. The media for growing the strains of *E. coli* was LB liquid LB [36], which contains NaCl, 5 g/L; Peptone biotripcase, 10 g/L; yeast extract, 5 g/L. The solid media was supplemented with 15 g/L of bacteriological agar. In the selected samples, kanamycin 10 µg/mL and/or ampicillin 100 µg/mL were added to the media. The cultures were incubated with agitation at 250 rpm a 37 °C.

The strains of *C. albicans* (ATCC 10231) or *C. glabrata* (CBS 138)

Table 1

Identification by MALDI-TOF of the proteins corresponding to the cut bands on 12% SDS-PAGE gels.

Protein	Protein identity	Mass	pI	Organism/ reference	Peptide matching	Sequence coverage (%)
~ 40 kDa	Fructose-bisphosphate aldolase	40	6.2	<i>Candida glabrata</i>	664	Over 95%
~ 46 kDa	Phosphoglycerate kinase	45	6.8	<i>Candida glabrata</i>	324	Over 95%
~ 55 kDa	Pyruvate kinase	55	6.9	<i>Candida glabrata</i>	1019	Over 95%

were used throughout this study to infect different groups of mice. Yeast strains were cultured on yeast peptone (YPD: yeast extract 1%; peptone 2%; glucose 2%) [37].

2.2. Design and construction of plasmids to overexpress Fba1, Pkg and Pk

The recombinant proteins were designed from the genome of *C. glabrata*, based on the following considerations: i) These CWP are downregulated in both *C. albicans* and *C. glabrata*. ii) For non-*C. albicans* species (NCAC) such as *C. glabrata*, it has not been reported, if these proteins can be immunoprotective against this fungus. We need to mention that iii) Fba1, Pkg and Pk de *C. glabrata* are three proteins that show an identity ranging from 75 to 81% with orthologs proteins in *C. albicans*, which is what also enables their immunoprotective role against this pathogen. Fba1, Pkg and Pk of *C. glabrata* have a size of 361 aa, 417 aa, and 501 aa respectively, as the codons used for the synthesis of the correct protein may be different in *E. coli* since it is a gene that corresponds to *C. glabrata*. This work was focused on optimizing the reading frame of the gene of these proteins for its correct expression in *E. coli*. The optimized gene was sent to the GenScript Co. (Piscataway, New Jersey, USA) according to the original sequence of the protein to be over-expressed (reference sequence of *C. glabrata* CBS138 in *Candida* Genome Database). The restriction sites recognized by the enzymes *XhoI* and *BamHI* at the 5' and 3' ends, respectively, were added to the synthesized sequences, in order to use the mentioned enzymes to sub-clone the genetic sequence in the expression vector pET19b, which added a 6-histidine tag (His₆X) to the recombinant protein. The sequences of the optimized genes were received inserted into the expression plasmid pET19b. Subsequently, the three constructs obtained, pET19b-Fba1, pET19b-Pkg, and pET19b-Pk, were introduced by transformation to the *E. coli* strain BL21 (DE3). After transformation, the transforming BL21 cells were obtained in solid medium LB-ampicillin (100 µg/mL). Subsequently, some transformed colonies that grew in the culture medium were selected and the plasmid DNA extraction was performed in a similar procedure to de one described above. To verify the identity of the BL21 strains with the recombinant plasmids, a restriction analysis was carried out with the enzymes *XhoI* and *BamHI*. The restriction products were analyzed on a 1% agarose gel by electrophoresis at 80 V for 1 h. Finally, each of the strains whose size of the amplified one (corresponding to the size of the complete gene) were reseeded in liquid LB medium and then transferred to sterile cryopreservation vials with 15% sterile glycerol. The cryovials of each recombinant strain were stored at – 80 °C.

2.3. Induction of synthesis of recombinant proteins Fba1, Pkg and Pk

In order to overexpress the *FBA1*, *PKG*, and *PK* genes, and to evaluate the production of the His₆-Fba1 (~ 40 kDa), His₆-Pkg (~ 46 kDa) and His₆-Pk (~ 55 kDa) proteins, a colony of each recombinant strain was inoculated in five sterile test tubes containing 5 mL of LB medium with the indicated antibiotic. The first four tubes were supplemented

with isopropyl- β -D-1-thiogalactopyranoside (IPTG, Promega, Madison WI) at a concentration of 0.1, 0.25, 0.5 and 1 mM, respectively, and the fifth tube was the control that had no added IPTG. They were centrifuged at 250 rpm and incubated at 37 °C. Then aliquots were taken at every 0, 1, 2, 4, 6, 8, 12, 16 and 24 h. The cells were collected by centrifugation at $4800 \times g$, at 4 °C for 10 min and washed three times. The cell pellet was resuspended in lysis buffer (Tris-HCl 50 mM, NaCl 300 mM, imidazole 10 mM, 0.03% of tween 20, pH 7.5). The cells were lysed with the help of glass beads and vortexes. The homogenate was centrifuged for 10 min at $4800 \times g$, at 4 °C, and the supernatant (soluble fraction) was separated from the insoluble one (tablet). The soluble fraction protein extracts were used for trials of SDS-PAGE and western blot analysis. Aliquots of 20 μ L of the soluble and insoluble fraction of the lysates of each strain were taken and treated with sample buffer Laemmli 2 \times ; all aliquots were subjected to SDS-PAGE on a 12% polyacrylamide gel in a miniProtean II chamber (BioRad) for 1 h at 120 V, to evaluate the induction, as well as the purity of the obtained protein [38]. The overexpression conditions chosen for each of the recombinant proteins were: Fba1 at 37 °C, 8 h induction, and 0.5 mM IPTG; Pkg at 37 °C, 6 h induction, and 0.5 mM IPTG; Pk at 37 °C, 24 h induction, and IPTG 0.5 mM.

2.4. Preparation of Fba1, Pkg and Pk for immunity tests

The overexpressed recombinant proteins His₆-Fba1, His₆-Pkg and His₆-Pk were separated by preparative SDS-electrophoresis in 10% gels. After identification by Coomassie blue staining, each of the proteins were sliced out and used as an immunization protein against *C. albicans* or *C. glabrata*. The gel fragments cut with recombinant proteins were placed in a glass tube for electroelution (Model 422 Electro-Eluter, BIORAD), to which a membrane retention was bond, to be subsequently subjected to 12 mA during 5 h with buffer (Tris-Glicina-SDS pH 8.0). The eluted proteins were recovered from the membrane with a micropipette and were then analyzed in a polyacrylamide gel 10%. They were observed by staining with Coomassie blue. To confirm that it was the protein of interest, the cut protein bands were identified by MALDI-TOF.

2.5. MALDI-TOF

The identification of the proteins from the cut bands of the polyacrylamide gels was carried out according to the protocol reported by Serrano-Fujarte et al. (2016) and Ramírez-Quijas et al., 2015 [2,26].

2.6. Protein identification

Protein database searches were performed using Mascot 2.3 (Matrix Science) against *Candida*. The mass tolerance for precursor ions was set to 10 ppm and for fragment ions to 0.5 Da. The enzyme specified was trypsin and two missed cleavages were allowed. Cysteine carbamidomethylation was specified as a fixed modification, and methionine oxidation was specified as variable modification.

2.7. Immunization tests in a mouse model with Fba1, Pkg and Pk

Five groups of BALB/c mice (Taconic) were used, each group with 14 mice of 6 weeks of age. Groups of mice were immunized in the following manner: Group A control group inoculated with adjuvant and saline; Group B with the recombinant protein Fba1; Group C with the Pkg protein; group D with Pk; and finally group E with the combination of the three proteins Fba1, Pkg and Pk. The immunization was carried out by inoculating 10 μ g of each protein resuspended in 200 μ L of solution prepared with complete Freund's adjuvant (first inoculation) and incomplete (rest of the immunizations). Four immunizations were performed (1 every 15 days). We performed ocular bleeding during the first and the third immunization, and one more after the last

immunization, then we separated the serum from the samples and stored it at -20 °C. The experiments were carried out in triplicate.

2.8. Infection of the mice with *C. albicans* or *C. glabrata*

The 5 groups of male mice (each group consisting of 14 mice) previously immunized with each of the proteins or with the mixture of the three. The mice were again rearranged in two groups, leaving a total of 10 groups of 7 mice each. The first 5 groups of 7 mice immunized, as indicated in the previous section, were infected with 2.2×10^7 cells of *C. albicans* in a volume of 100 μ L in the tail vein. Following the same infection procedure, we infected with *C. glabrata* the rest of the 5 groups also previously immunized. The groups of mice infected with *C. albicans* and the groups infected with *C. glabrata*, were closely monitored to observe whether there was any death caused by the development of IC. Seven days after infection, the mice were sacrificed, and their kidneys, livers, and spleens were retrieved, and the organs were homogenized. Dilutions were made with the homogenates, which were plated onto YPD-penicillin-streptomycin plates. The CFU were counted at 24 h and the respective statistical analysis was performed. The experiments were performed in triplicate. The mice were treated according to the Declaration of Helsinki, as revised in 2013, and the International Guiding Principles for Biomedical Research Involving Animals, as revised by the International Council for Laboratory Animal Science (ICLAS) and the Councils for International Organizations of Medical Sciences (CIOMS) in 2012.

2.9. Statistical analysis

Data were statistically analyzed using one-way analysis of variance (ANOVA) when experiments implied one independent variable (protein) followed by a Dunnett's multiple comparison post hoc test or a two-way ANOVA when implied two independent variables (protein and species), followed by a Bonferroni post hoc test. On both cases an $\alpha = 0.05$ was considered (*?? < 0.05, **?? < 0.01, and ***?? < 0.001). The statistical analyses were performed with the GraphPad Prism software (GraphPad, USA).

2.10. Western blot

To evaluate the immunogenicity of Fba1, Pkg or Pk in a candidiasis process, two groups of male mice were considered (each group consisting of 7 mice) that were infected with 2.2×10^7 cells of *C. albicans* or *C. glabrata*, groups of mice were monitored to observe whether death was caused by the development of IC. Seven days after the infection, mice underwent eye bleeding, and the sera containing antibodies against *C. albicans* or *C. glabrata* was separate and stored at -20 °C. Bacterial protein extracts were obtained according to the methodology described above. The extracts of the CWP of *C. albicans* or *C. glabrata* were used as positive control, which were obtained according to the protocol used by Ramírez-Quijas et al. (2015) [2]. Once the proteins were transferred to the nitrocellulose membrane, the membrane was blocked for 1 h with a skim milk solution (5% w/v) in phosphate-buffered saline (PBS), pH 7.2. After washing it three times with PBS, the membrane was incubated overnight with sera from the infected mice with *C. albicans* and *C. glabrata* diluted 1:200 in PBS supplemented with 0.05% (v/v) Tween 20, as primary antibodies. Membrane was then again washed three times with the same buffer, and incubated in anti-mouse IgG, goat horseradish peroxidase-conjugated secondary antibodies, diluted in 1:1000 in PBS with gentle shaking for 2 h. After washing with PBS, enzyme activity was revealed with Clarity™ Western ECL substrate (Bio-Rad) using a molecular imager Chemi-Doc XRS + system (Bio-Rad).

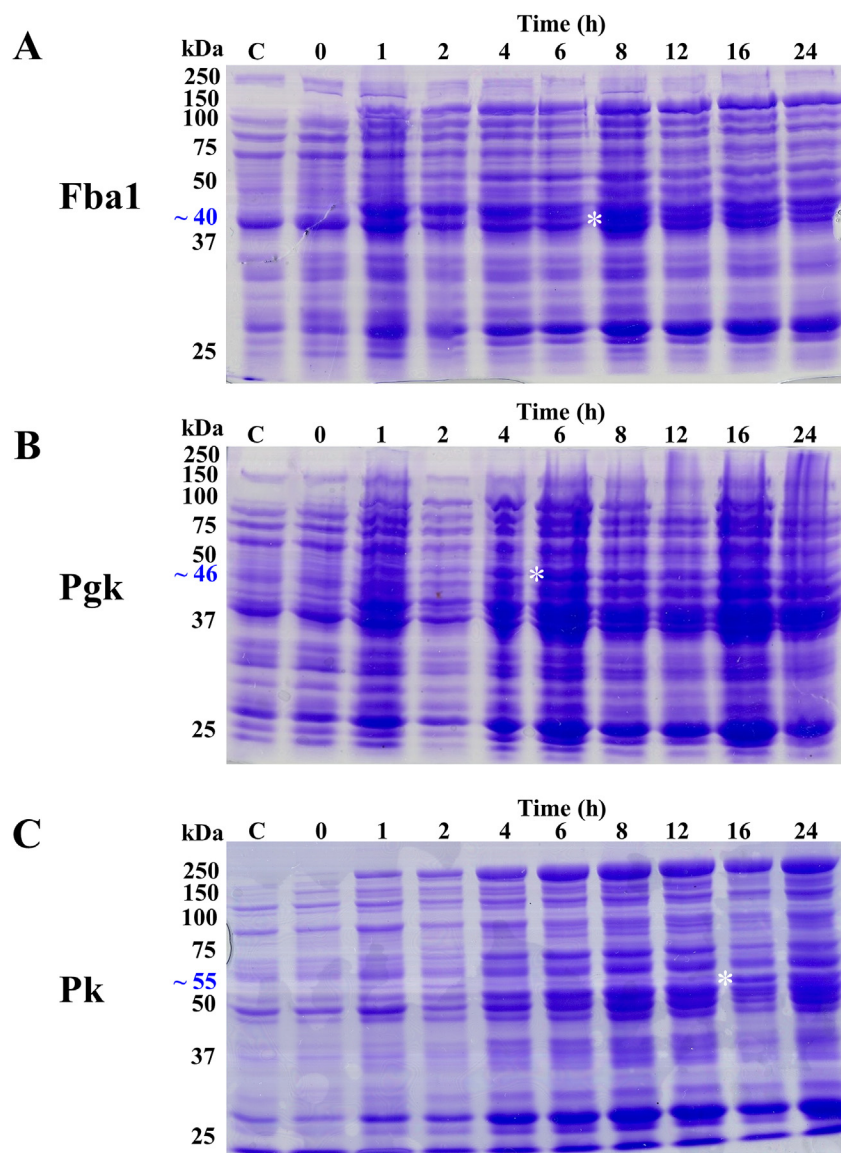


Fig. 1. Polyacrylamide gel with Coomassie blue staining to evaluate the induction of the recombinant protein. A) His₆-Fba1; B) His₆-Pgk; C) His₆-Pk. C: Fraction without IPTG. 0 a 24 h: Soluble fractions induced with 0.5 mM of IPTG. Asterisk indicates the chosen time of induction for each recombinant protein. (For interpretation of the references to colour in this figure legend, the reader is referred to the Web version of this article.)

3. Results

3.1. Overexpression and obtaining Fba1, Pgk and Pk

In order to find the optimal conditions for overexpression of the recombinant proteins Fba1, Pgk and Pk, the chosen clones were induced at 8 different times, with four concentrations of IPTG and at two different temperatures 30 and 37 °C, according to materials and methods. In Fig. 1 a representative gel is shown in the condition where the overexpression of all the recombinant proteins was found. As shown in Fig. 1A, for Fba1, the highest expression of the recombinant protein was found at 8 h. For Pgk, the highest induction was found at 6 h (Fig. 1B), and for Pk, the expression of the protein was observed at 16 h. However, the highest expression was found at 24 h (Fig. 1C). In all three proteins overexpression was carried out at 37 °C, and at a concentration of 0.5 mM IPTG (Fig. 1). The induced recombinant proteins were found in the soluble fraction (supernatant). These data indicate that the optimization of the genes was adequate (supplemental material), because none of the proteins was found in the insoluble part, so no inclusion bodies were formed. Once the appropriate induction conditions were

found, Fba1, Pgk and Pk were separated by preparative SDS-electrophoresis in 10% gels. After identification by Coomassie blue staining, each of the proteins were sliced out and used as an immunization protein against *Candida*. To confirm that it was the protein of interest, the cut protein bands were identified by MALDI-TOF. The results by MALDI-TOF confirmed that these were the corresponding proteins (Table 1). Subsequently, the different groups of mice were immunized with the bands corresponding to Fba1, Pgk or Pk.

3.2. Pk confers immunity to mice against *C. albicans*, while Fba1 confers immunity to *C. glabrata*

In order to evaluate whether Fba1, Pgk and Pk could be considered as immunodominant proteins that confer protection to mice against *C. albicans* or *C. glabrata*, mice were subsequently immunized with each of the proteins individually, as well as with a mixture of the three. After this immunization, mice were accordingly infected either with *C. albicans* or *C. glabrata*. Mice were then sacrificed, their kidneys, livers, and spleens retrieved, and the organs were homogenized. Dilutions were made with the homogenates according to the protocol indicated in

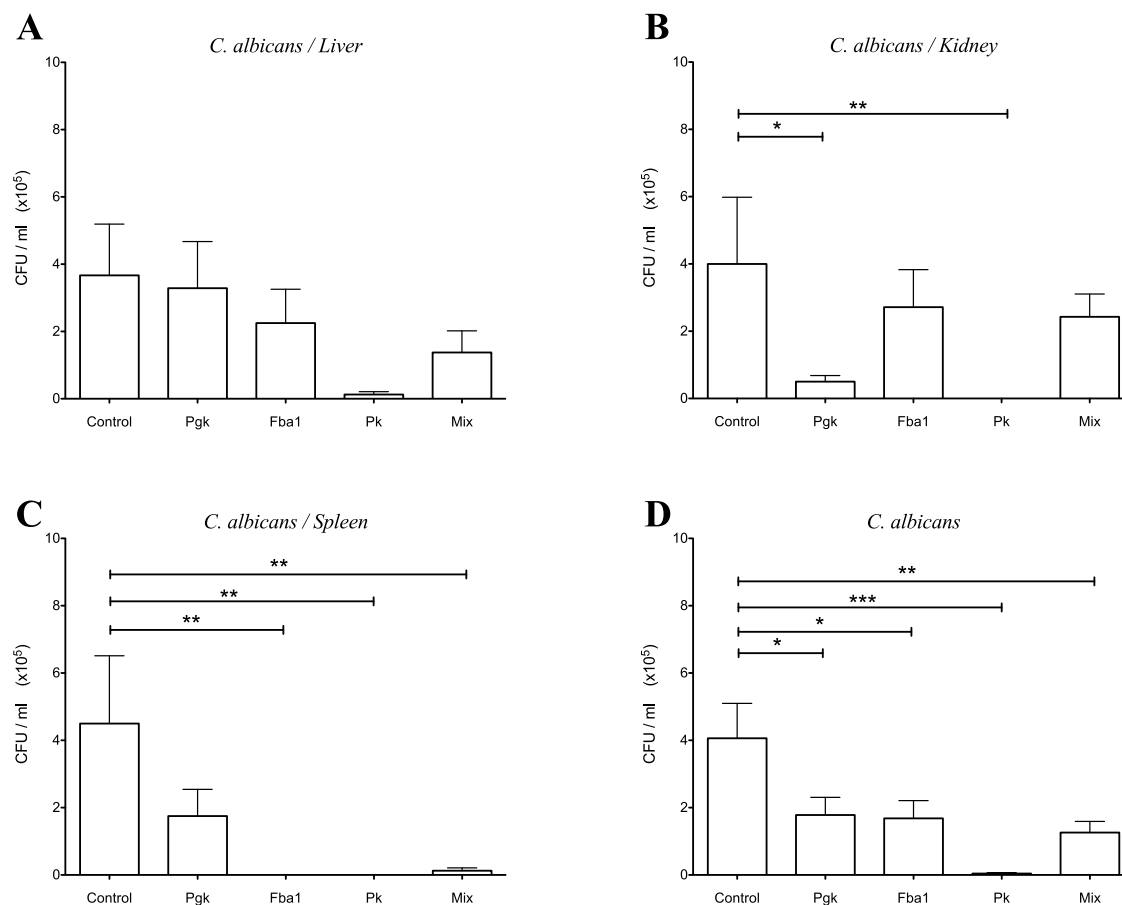


Fig. 2. Pk confers protection to mice against *C. albicans*. The CFU numbers are shown in tissues collected and homogenized from A) liver, B) kidney, C) spleen, 7 days after infection with mice previously immunized with Fba1, Pkg, Pk or the mixture of the three proteins. D) Statistical analysis considering the CFU of the three organs studied (A, B, C). The reference points represent the results of groups of 7 mice from three independent experiments. The statistical analysis performed is indicated in Materials and Methods.

materials and methods, and the CFU count per organ was performed for each protein (Figs. 2 and 3). In the groups infected with *C. albicans* for the liver the group of mice immunized with Pk had the greatest protection against this pathogen, followed by Fba1 and Pkg with respect to the control group (Fig. 2). In the analyses of the kidneys, the mice immunized with Pk showed the greatest immunity against *C. albicans*, followed by Pkg and Fba1 (Fig. 2). In the analyses of spleens, the groups immunized with Fba1 or Pk had the greatest immunity against this fungus, followed by the group immunized with Pkg (Fig. 2). The results after analyzing the three organs, showed that the moonlighting CWP that conferred total protection against *C. albicans* was Pk (Fig. 2). Interestingly enough, in the liver of the mice infected with *C. glabrata*, but previously immunize with Fba1, we found that it was in this organ where the mice presented the greatest protection against this yeast, followed by the group immunized with the mixtures of the three proteins and then the group immunized with Pk and Pkg (Fig. 3). In the case of the kidney, the greatest protection was found in the mice immunized with Fba1 and Pkg followed by Pk (Fig. 3). Finally, in the analyses of the spleen, the greatest protection against *C. glabrata* was found in the group of mice immunized with Pkg, followed by the group immunized with Fba1, and finally by the group immunized with Pk and the mixture of the three proteins (Fig. 3). As shown in Fig. 3, the mice immunized with Fba1 had the greatest protection against *C. glabrata*. In order to analyze whether one of these moonlighting CWP conferred specific protection against one or another species of *Candida*, we compared *C. albicans* against *C. glabrata*, and we found that the mice immunized with Pk showed the greater immunity against *C. albicans*, while the group immunized with Fba1 presents the greater protection

against *C. glabrata* (Fig. 4). The trials of immunization and infection showed that Fba1 and Pk are immunoprotective proteins (Figs. 2–4), not only we validated the immunoprotective role of these proteins against candidiasis, but also their immunogenicity. For this reason, an analysis of western blot from sera of mice infected either with *C. albicans* or *C. glabrata*, that were not previously immunized with neither Fba1 nor Pkg or Pk, was performed. Fig. 5 shows the results of two sera of mice infected with each of the pathogens. In the case of mice infected with *C. albicans* (Fig. 5A), we identified mainly Pk and Fba in the presence of the CWP of *C. albicans*, with Pk featuring the highest immunogenicity (Fig. 5A, lines 1). Even when using only extracts with either Fba1, Pkg or Pk, we still found that Pk had the highest immunogenicity followed by Fba1 (Fig. 5A, lines 3, 5), whereas Pkg presented an almost undetectable immunogenicity (Fig. 5A, line 4). In the case of sera obtained from the infected mice with *C. glabrata* (Fig. 5B), we found that the extract of CWP of *C. glabrata*, the protein with increased immunogenicity was Fba1, followed by Pk. Interestingly, Pkg was not detected (Fig. 5B, line 1). For the extracts of Fba1, Pkg or Pk, we also observed that the protein with increased immunogenicity for *C. glabrata* was Fba1 (Fig. 5B, line 5), followed by Pk (Fig. 5B, line 3). In contrast with Pkg in which only a faint band was detected, indicating that Pkg is the protein with the lowest immunogenicity against *C. glabrata* (Fig. 5B, line 4). These data show that these moonlighting CWP, previously identified in OSR and biofilm formation, are also immunodominant proteins, since they not only confer protection *in vivo* against *C. albicans* and *C. glabrata*, but also do it in a very specific way (Figs. 2–5).

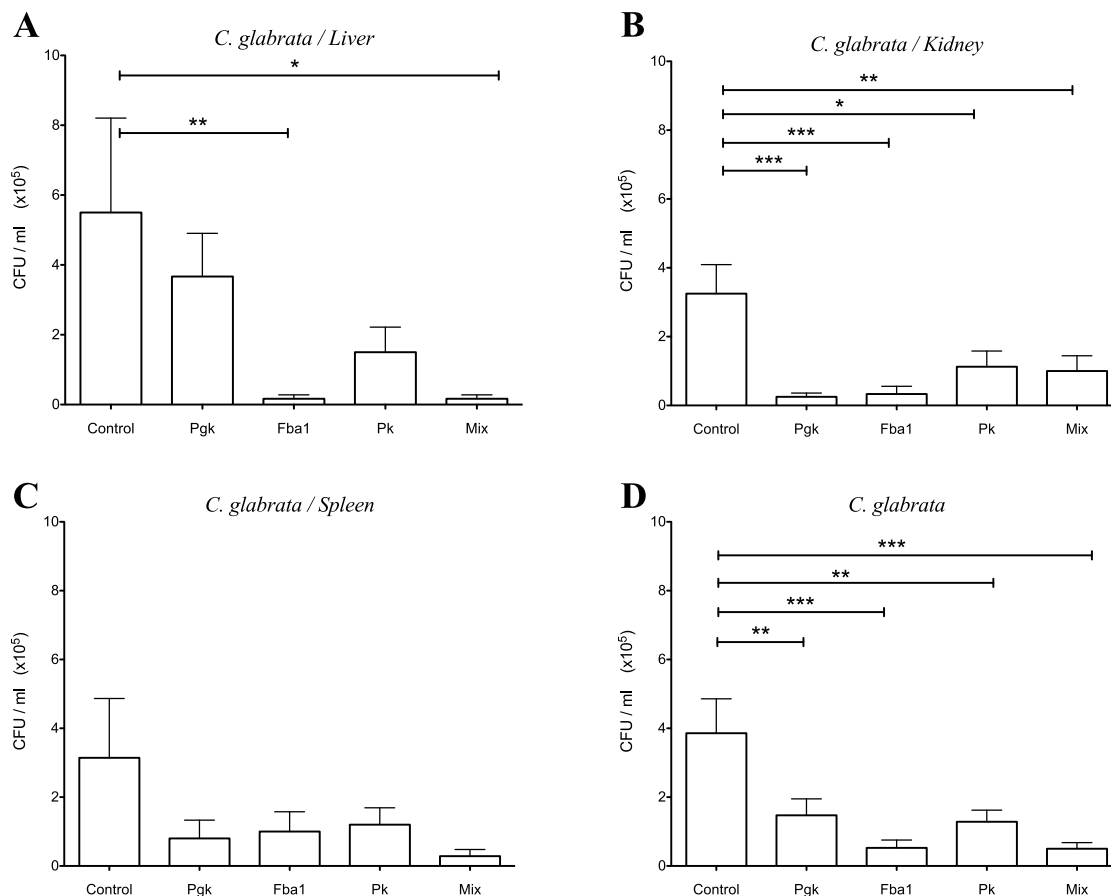


Fig. 3. Fba1 is indispensable in protecting mice against *C. glabrata*. The CFU numbers are shown in tissues collected and homogenized from A) liver, B) kidney, C) spleen, 7 days after infection with mice previously immunized with Fba1, Pkg, Pk or the mixture of the three proteins. D) Statistical analysis considering the CFU of the three organs studied (A, B, C). The reference points represent the results of groups of 7 mice from three independent experiments. The statistical analysis performed is indicated in Materials and Methods.

4. Discussion

For years, scientists have striven to obtain a vaccine against candidiasis without much success. However, in this respect, we have listed a number of proteins that have been tested as immunodominant proteins capable of protecting murine models against candidiasis. These proteins are: aspartyl proteinase2 (Sap2), agglutinin-like sequence proteins (Als1p, Als3p), Mp65, Enolase 1 (Eno1p), malate dehydrogenase (Mdh1p), fructose-bisphosphate aldolase (Fba), glyceraldehyde-3-phosphate dehydrogenase (Gap1p), phosphoglycerate kinase (Pkg1p), 5-methyltetrahydropteroyltrimethylglutamate homocysteine methyltransferase (Met6), heat shock protein 90 (Hsp90) and glycosyl phosphatidylinositol (GPI)-anchor mannoprotein (Hyr1p) [39–49]. According to our results, they are all capable of protecting the murine models against different types of candidiasis. We must emphasize that, even though scientists have already found and evaluated a protein against IC, this protein works only against *C. albicans* [39–49], whereas our aim is to identify immunodominant proteins that protect against other species of *Candida*, such as *C. glabrata*, currently found in patients with cancer. *C. glabrata* was first to be identified, followed by *C. albicans* [15,16]. In general, *C. glabrata* occupies the second place in causing IC [13,14], a fact that makes it necessary to find potential immunodominant proteins against these species. Our working group has identified moonlighting CWP in *Candida* species, which are involved in two virulence factors such as OSR and biofilm formation [2,26]. This result indicates that these proteins could have an immunodominant role. For this reason, we chose to evaluate Fba1, Pk and Pkg to see whether they protected the murine model against IC. Interestingly, we

found that Pk was the moonlighting CWP that conferred greater protection against *C. albicans* (Figs. 2, 4 and 5). This agrees with previous studies reporting moonlighting proteins as potential candidates for vaccines against *C. albicans* [44,45,49]. However, none of these studies have contemplated Pk so far. For this reason, we have studied Pk as a candidate against IC and have found relevant results. As we already know, Fba1 is an immunodominant protein against *C. albicans* (Figs. 2 and 5) as all the moonlighting CWP are. However, our data showed that the protection of mice against *C. albicans* under Pk was even greater than under Fba1 [49,50] (Figs. 2, 4 and 5). Finally, we studied Pkg (Figs. 2, 4 and 5) to confirm that this protein conferred the lowest protection against *C. albicans*. This result is consistent with other investigations [49,50]. Based on our studies we can, therefore, conclude that Pk is the promising candidate for future vaccines against *C. albicans*. However, we also studied a group of mice that were first immunized with Pk, Pkg or Fba1 respectively, and then infected with *C. glabrata*, to find that mice immunized with Fba1 showed the highest protection, followed by the group immunized by Pk (Figs. 3 and 4). In the literature, Fba1 was not reported as a possible immunodominant protein against *C. glabrata*. Other studies have also reported that the cell wall adhesin (rAls1p-N) of *C. albicans* confers protection to mice against *C. glabrata* [47]. In addition, as mentioned above, moonlighting proteins have been described in *C. albicans* as candidates for a vaccine against this pathogen [43–45,49], but they have not been reported as candidates against *C. glabrata*. According to our results Pkg (Figs. 2–5), is the only protein that protects neither against *C. albicans* nor *C. glabrata*.

Additionally, in this work we showed that mice that were not

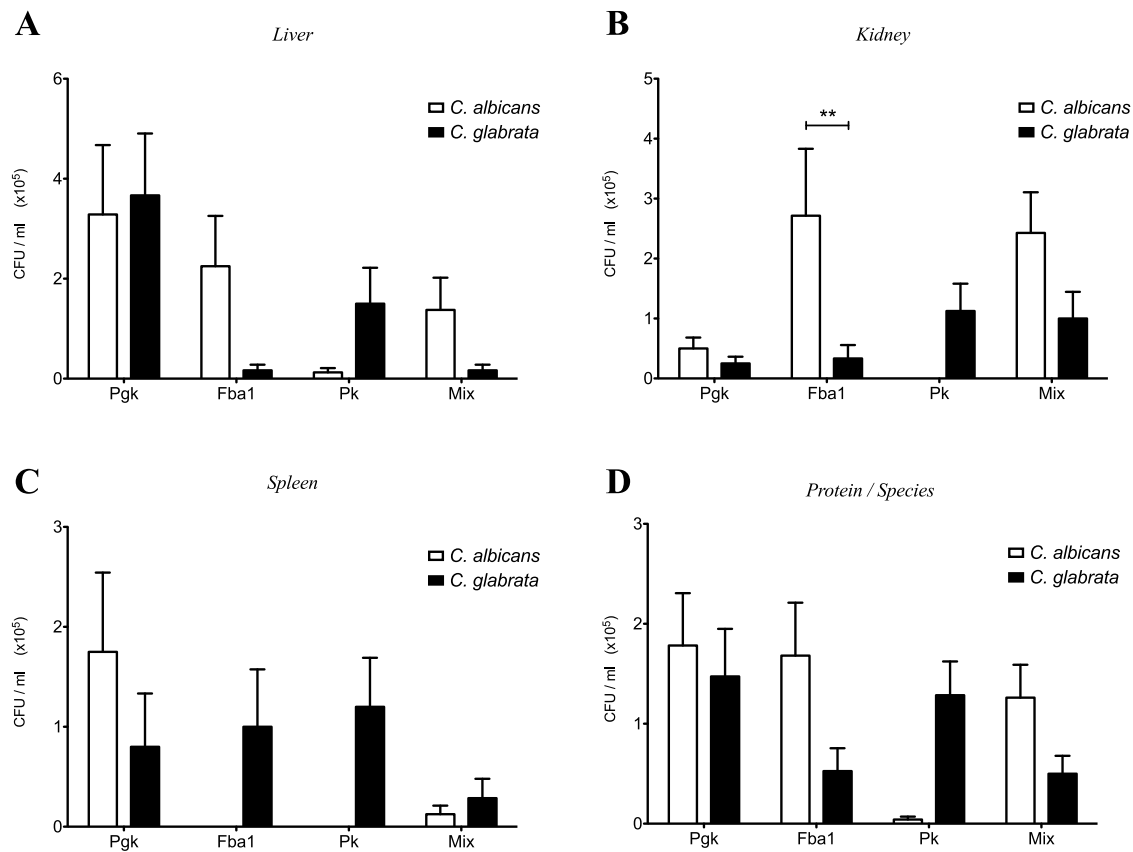


Fig. 4. Pk protects against *C. albicans*, and Fba1 against *C. glabrata*. The CFU numbers are shown in tissues collected and homogenized from A) liver, B) kidney, C) spleen from *C. albicans* or *C. glabrata*, 7 days after infection with mice previously immunized with Fba1, Pgk, Pk or the mixture of the three proteins. D) Statistical analysis considering the CFU of the three organs studied (A, B, C). The reference points represent the results of groups of 7 mice from three independent experiments. The statistical analysis performed is indicated in Materials and Methods.

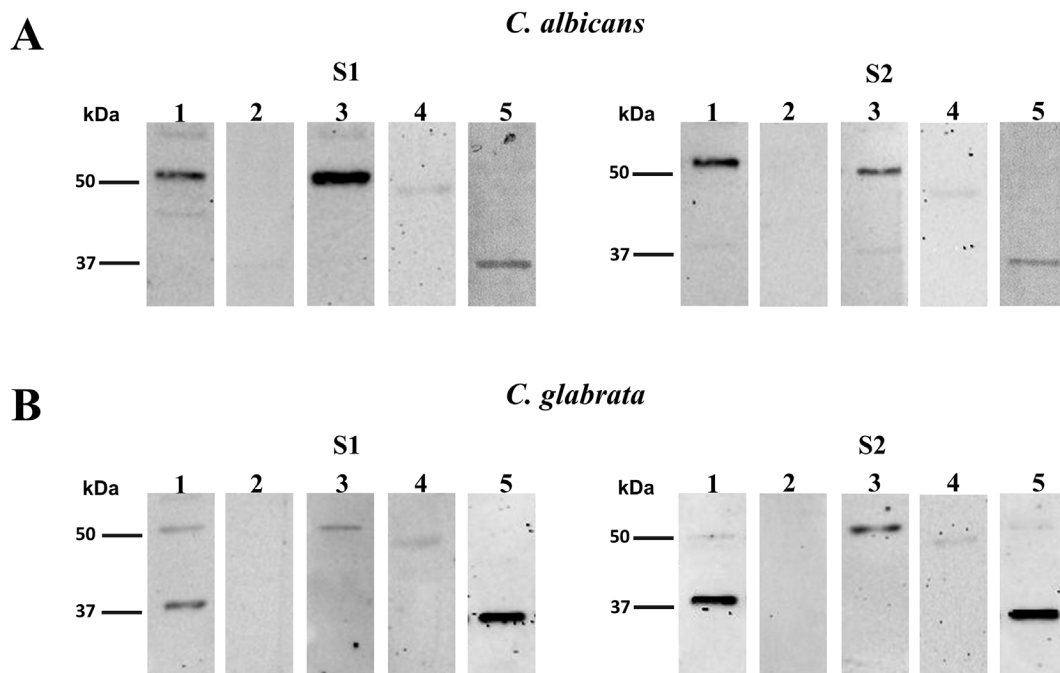


Fig. 5. Fba1 and Pk are the main immunogenic proteins in a process of IC. Western blot analysis of two representative sera (S1, S2) obtained from infected mice with: A) *C. albicans* or B) *C. glabrata*. Lines: 1 (positive control): extract of CWP of *C. albicans* (5A) or *C. glabrata* (5B); 2: protein extract from *E. coli* (negative control); 3: protein extract His₆-Pk; 4: protein extract His₆-Pgk; 5: protein extract His₆-Fba1.

previously immunized with Fba1, Pkg or Pk, but were equally exposed to candidiasis, presented the lowest protection against IC. We have also shown, that the proteins with major immunodominant roles are Fba1 and Pk (Figs. 2–5), whereas the role of Pkg as immunodominant or immunoprotective protein was almost null (Fig. 5). These findings are relevant as they help us to understand the shared mechanisms of protection of *C. albicans* and *C. glabrata* against the immune system of human host. These results are consistent with other works in which Fba1 was reported to induce protection against disseminated candidiasis caused by *C. albicans*, while Pkg was the only protein with the lowest protection against this disease [49,51]. Our results also suggest that Fba1 and Pk confer specific protection to each of the *Candida* species. This research will facilitate the development of specific vaccines for both *C. albicans* and *C. glabrata*, as well as for other *Candida* species. In the near future desirable studies will be needed to assess whether Pk and Fba1 can also confer protection against other NCAC. These studies will also need to identify whether Fba1 is the main immunodominant protein present in patients with IC caused by *C. glabrata*. Finally, to our understanding, this is the first report showing that moonlighting CWP are immunodominant proteins and can confer protection *in vivo* against both *C. albicans* and *C. glabrata*.

Conflicts of interest

The authors declare that they have no competing interest. All authors have submitted the ICMJE Form for Disclosure of Potential Conflicts of Interest.

Acknowledgements

This work was carried out with the financial support granted to Dr. M. Cuéllar-Cruz by Proyecto Institucional/IDCIC-44/2018 from University of Guanajuato, Mexico. We appreciate the technical support of Cristina León-García QFB, Carmen Sánchez-Leyva M.S., Maritza Almanza-Villegas QFB and assistant Juan Pedro Galván-Chia for handling the mice. The authors acknowledge Prof. John Dye and Ms. Antonia Sánchez-Marín for the English revision of this contribution.

Appendix A. Supplementary data

Supplementary data related to this article can be found at <https://doi.org/10.1016/j.micpath.2018.08.024>.

References

- [1] M. Rasheed, A. Battu, R. Kaur, Aspartyl proteases in *Candida glabrata* are required for suppression of the host innate immune response, *J. Biol. Chem.* (2018), <https://doi.org/10.1074/jbc.M117.813741>.
- [2] M.D. Ramírez-Quijas, E. López-Romero, M. Cuéllar-Cruz, Proteomic analysis of cell wall in four pathogenic species of *Candida* exposed to oxidative stress, *Microb. Pathog.* 87 (2015) 1–12.
- [3] R.A. Calderone, *Candida* and Candidiasis, ASM Press, Washington, DC, 2002.
- [4] R.A. Calderone, W.A. Fonzi, Virulence factors of *Candida albicans*, *Trends Microbiol.* 9 (7) (2001) 327–335.
- [5] C.J. Barelle, C.L. Priest, D.M. MacCallum, N.A. Gow, F.C. Odds, A.J. Brown, Niche-specific regulation of central metabolic pathways in a fungal pathogen, *Cell Microbiol.* 8 (6) (2006) 961–971.
- [6] I.V. Ene, C.J. Heilmann, A.G. Sorgo, L.A. Walker, C.G. de Koster, C.A. Munro, F.M. Klis, A.J. Brown, Carbon source-induced reprogramming of the cell wall proteome and secretome modulates the adherence and drug resistance of the fungal pathogen *Candida albicans*, *Proteomics* 12 (21) (2012) 3164–3179.
- [7] A. Le, D. Farmakiotis, J.J. Tarrand, D.P. Kontoyiannis, Initial treatment of cancer patients with fluconazole-susceptible dose-dependent *Candida glabrata* fungemia: better outcome with an echinocandin or polyene compared to an azole? *Antimicrob. Agents Chemother.* 61 (8) (2017) e0063117.
- [8] A. Gullo, Invasive fungal infections: the challenge continues, *Drugs* 69 (2009) 65–73.
- [9] A. Jain, S. Jain, S. Rawat, Emerging fungal infections among children: a review on its clinical manifestations, diagnosis, and prevention, *J. Pharm. BioAllied Sci.* 2 (4) (2010) 314–320.
- [10] C.Y. Low, C. Rotstein, Emerging fungal infections in immunocompromised patients, *F1000 Medicine Reports* 3 (2011) 14.
- [11] S.G. Whaley, K.E. Caudle, L. Simonicova, Q. Zhang, W.S. Moye-Rowley, P.D. Rogers, Jj1 is a negative regulator of Pdr1-Mediated fluconazole resistance in *Candida glabrata*, *mSphere* 3 (1) (2018) e0046617.
- [12] E. Marín, C.M. Parra-Giraldo, C. Hernández-Haro, M.L. Hernández, C. Nombela, L. Monteoliva, C. Gil, *Candida albicans* shaving to profile human serum proteins on hyphal surface, *Front. Microbiol.* 6 (2015) 1343.
- [13] M.A. Pfaller, P.R. Rhombert, S.A. Messer, R.N. Jones, M. Castanheira, Isavuconazole, micafungin, and 8 comparator antifungal agents' susceptibility profiles for common and uncommon opportunistic fungi collected in 2013: temporal analysis of antifungal drug resistance using CLSI species-specific clinical breakpoints and proposed epidemiological cutoff values, *Diagn. Microbiol. Infect. Dis.* 82 (4) (2015) 303–313.
- [14] M.A. Pfaller, D.J. Diekema, Epidemiology of invasive mycoses in North America, *Crit. Rev. Microbiol.* 36 (1) (2010) 1–53.
- [15] D. Farmakiotis, J.J. Tarrand, D.P. Kontoyiannis, Drug-resistant *Candida glabrata* infection in cancer patients, *Emerg. Infect. Dis.* 20 (11) (2014) 1833–1840.
- [16] R. Hachem, H. Hanna, D. Kontoyiannis, Y. Jiang, I. Raad, The changing epidemiology of invasive candidiasis: *Candida glabrata* and *Candida krusei* as the leading causes of candidemia in hematologic malignancy, *Cancer* 112 (11) (2008) 2493–2499.
- [17] Y. Lu, C. Su, H. Liu, *Candida albicans* hyphal initiation and elongation, *Trends Microbiol.* 22 (12) (2014) 707–714.
- [18] L. Yan, C. Yang, J. Tang, Disruption of the intestinal mucosal barrier in *Candida albicans* infections, *Microbiol. Res.* 168 (7) (2013) 389–395.
- [19] S.C. Deorukhkar, S. Saini, S. Mathew, Virulence Factors Contributing to pathogenicity of *Candida tropicalis* and its antifungal susceptibility profile, *Int. J. Microbiol.* 2014 (2014) 1–6.
- [20] J.C. Sardi, L. Scorzoni, T. Bernardi, A.M. Fusco-Almeida, M.J. Mendes Giannini, *Candida* species: current epidemiology, pathogenicity, biofilm formation, natural antifungal products and new therapeutic options, *J. Med. Microbiol.* 62 (Pt 1) (2013) 10–24.
- [21] H. Kusch, S. Engelmann, D. Albrecht, J. Morschhäuser, M. Hecker, Proteomic analysis of the oxidative stress response in *Candida albicans*, *Proteomics* 7 (5) (2007) 686–697.
- [22] Ch R. Cruz, L.E. Piontelli, Invasive fungal disease in patients from five hospitals in the Valparaíso region, Chile: 2004 to 2009, *Rev. Chilena Infectol.* 28 (2) (2011) 123–129.
- [23] S. Silva, M. Negri, M. Henriques, R. Oliveira, D.W. Williams, J. Azeredo, *Candida glabrata*, *Candida parapsilosis* and *Candida tropicalis*: biology, epidemiology, pathogenicity and antifungal resistance, *FEMS Microbiol. Rev.* 36 (2) (2012) 288–305.
- [24] D. Kaloriti, A. Tillmann, E. Cook, et al., Combinatorial stresses kill pathogenic *Candida* species, *Med. Mycol.* 50 (7) (2012) 699–709.
- [25] F.M. Klis, G.J. Sosinska, P.W. de Groot, S. Brul, Covalently linked cell wall proteins of *Candida albicans* and their role in fitness and virulence, *FEMS Yeast Res.* 9 (7) (2009) 1013–1028.
- [26] I. Serrano-Fujarte, E. López-Romero, M. Cuéllar-Cruz, Moonlight-like proteins of the cell wall protect sessile cells of *Candida* from oxidative stress, *Microb. Pathog.* 90 (2016) 22–33.
- [27] A. Núñez-Beltrán, E. López-Romero, M. Cuéllar-Cruz, Identification of proteins involved in the adhesion of *Candida* species to different medical devices, *Microb. Pathog.* 107 (2017) 293–303.
- [28] C. Nombela, C. Gil, W.L. Chaffin, Non-conventional protein secretion in yeast, *Trends Microbiol.* 14 (1) (2006) 15–21.
- [29] M. Martínez-Gomariz, P. Perumal, S. Mekala, C. Nombela, W.L. Chaffin, C. Gil, Proteomic analysis of cytoplasmic and surface proteins from yeast cells, hyphae, and biofilms of *Candida albicans*, *Proteomics* 9 (8) (2009) 2230–2252.
- [30] W.L. Chaffin, *Candida albicans* cell wall proteins, *Microbiol. Mol. Biol. Rev.* 72 (3) (2008) 495–544.
- [31] A. Lain, N. Elguezabal, E. Amutio, I. Fernández de Larrinoa, M.D. Moragues, J. Pontón, Use of recombinant antigens for the diagnosis of invasive candidiasis, *Clin. Dev. Immunol.* 2008 (2008) 721950.
- [32] A.Y. Jong, S.H. Chen, M.F. Stins, K.S. Kim, T.L. Tuan, S.H. Huang, Binding of *Candida albicans* enolase to plasminogen results in enhanced invasion of human brain microvascular endothelial cells, *J. Med. Microbiol.* 52 (Pt8) (2003) 615–622.
- [33] R. Matthews, C. Wells, J.P. Burnie, Characterisation and cellular localisation of the immunodominant 47-kDa antigen of *Candida albicans*, *J. Med. Microbiol.* 27 (1988) 227–232.
- [34] N.A. Strockbine, M.T. Largen, H.R. Buckley, Production and characterisation of three monoclonal antibodies to *Candida albicans* proteins, *Infect. Immun.* 43 (3) (1984) 1012–1018.
- [35] J.L. López-Ribot, H.M. Alloush, B.J. Masten, W.L. Chaffin, Evidence for presence in the cell wall of *Candida albicans* of a protein related to the hsp70 family, *Infect. Immun.* 64 (8) (1996) 3333–3340.
- [36] J.H. Miller, Experiments in Molecular Genetics, Cold Spring Harbor Laboratory Press, Cold Spring Harbor, N.Y., 1972, p. 433.
- [37] F. Ausubel, R. Brent, R.E. Kingston, et al., Current Protocols in Molecular Biology, John Wiley & Sons, Inc., New York, NY, 2003.
- [38] U.K. Laemmli, Cleavage of structural proteins during the assembly of the head of bacteriophage T4, *Nature* 227 (1970) 680–685.
- [39] S. Sandini, R. La Valle, S. Deaglio, F. Malavasi, A. Cassone, F. De Bernardis, A highly immunogenic recombinant and truncated protein of the secreted aspartic proteases family (rSap2p) of *Candida albicans* as a mucosal anticandidal vaccine, *FEMS Immunol. Med. Microbiol.* 62 (2) (2011) 215–224.
- [40] B.J. Spellberg, A.S. Ibrahim, V. Avanesian, Y. Fu, C. Myers, Q.T. Phan, et al., Efficacy of the anti-*Candida* rAls3p-N or rAls1p-N vaccines against disseminated and mucosal candidiasis, *J. Infect. Dis.* 194 (2) (2006) 256–260.

- [41] A.S. Ibrahim, B.J. Spellberg, V. Avenissian, Y. Fu, S.G. Filler, J.E. Edwards Jr., Vaccination with recombinant N-terminal domain of Als1p improves survival during murine disseminated candidiasis by enhancing cell-mediated, not humoral, immunity, *Infect. Immun.* 73 (2) (2005) 999–1005.
- [42] A. Zito, C. Bromuro, G. Mandili, P. Chiani, A.L. Horenstein, F. Malavasi, et al., A murine, bispecific monoclonal antibody simultaneously recognizing β -Glucan and MP65 determinants in *Candida* species, *PLoS One* 11 (2) (2016) e0148714.
- [43] S. Shibasaki, W. Aoki, T. Nomura, A. Miyoshi, S. Tafuku, T. Sewaki, M. Ueda, An oral vaccine against candidiasis generated by a yeast molecular display system, *Pathog. Dis.* 69 (3) (2013) 262–268.
- [44] S. Shibasaki, W. Aoki, T. Nomura, M. Karasaki, T. Sewaki, M. Ueda, Evaluation of Mdh1 protein as an antigenic candidate for a vaccine against candidiasis, *Biocontrol Sci.* 19 (1) (2014) 51–55.
- [45] S. Shibasaki, M. Karasaki, S. Tafuku, W. Aoki, T. Sewaki, M. Ueda, Oral immunization against candidiasis using *Lactobacillus casei* displaying Enolase 1 from *Candida albicans*, *Sci. Pharm.* 82 (3) (2014) 697–708.
- [46] B.J. Spellberg, A.S. Ibrahim, V. Avenissian, S.G. Filler, C.L. Myers, Y. Fu, J.E. Edwards Jr., The anti-*Candida albicans* vaccine composed of the recombinant N terminus of Als1p reduces fungal burden and improves survival in both immunocompetent and immunocompromised mice, *Infect. Immun.* 73 (2005) 6191–6193.
- [47] A.S. Ibrahim, B.J. Spellberg, V. Avanesian, Y. Fu, J.E. Edwards Jr., The anti-*Candida* vaccine based on the recombinant N-terminal domain of Als1p is broadly active against disseminated candidiasis, *Infect. Immun.* 74 (2006) 3039–3041.
- [48] M. Raska, J. Belakova, N.K. Wudattu, L. Kafkova, K. Ruzickova, M. Sebestova, Z. Kolar, E. Weigl, Comparison of protective effect of protein and DNA vaccines hsp90 in murine model of systemic candidiasis, *Folia Microbiol.* 50 (1) (2005) 77–82.
- [49] H. Xin, J.E. Cutler, Vaccine and monoclonal anti-body that enhance mouse resistance to candidiasis, *Clin. Vaccine Immunol.* 18 (10) (2011) 1656–1667.
- [50] H. Xin, Double chimeric peptide vaccine and monoclonal antibodies that protect against disseminated candidiasis, *J. Vaccines Vaccin.* 5 (2014) 241.
- [51] H. Xin, S. Dziadek, D.R. Bundle, J.E. Cutler JE, Synthetic glycopeptide vaccines combining beta-mannan and peptide epitopes induce protection against candidiasis, *Proc. Natl. Acad. Sci. U.S.A.* 105 (36) (2008) 13526–13531.

Bioreduction of precious and heavy metals by *Candida* species under oxidative stress conditions

Abel Moreno,¹  Nicola Demitri,² Estela Ruiz-Baca,³ Arturo Vega-González,⁴ Maurizio Polentarutti² and Mayra Cuéllar-Cruz^{1,5,*} 

¹Instituto de Química, Universidad Nacional Autónoma de México, Ciudad Universitaria, Av. Universidad 3000, Ciudad de México 04510, México.

²Elettra – Sincrotrone Trieste, S.S. 14 km 163.5 in Area Science Park, 34149 Basovizza – Trieste, Italy.

³Facultad de Ciencias Químicas, Universidad Juárez del Estado de Durango, Av. Veterinaria S/N, 34120 Durango, México.

⁴Departamento de Ingenierías Química, Electrónica y Biomédica, División de Ciencias e Ingenierías, Universidad de Guanajuato, Campus León, Guanajuato, México.

⁵Departamento de Biología, División de Ciencias Naturales y Exactas, Universidad de Guanajuato, Campus Guanajuato, Noria Alta S/N, Col. Noria Alta, C.P. 36050 Guanajuato, México.

Summary

The aim of the present work was to evaluate whether *Candida* species can reduce both precious and toxic pure metals from the respective molecular ions. From these results, the nanoparticles formed were studied using scanning electron microscopy with energy-dispersive spectroscopy, Raman spectroscopy, X-ray fluorescence spectroscopy and synchrotron radiation. Our results showed that the metal ions were reduced to their corresponding metallic nanoconglomerate or nanoparticles by *Candida* species. This is the first report on how yeasts of this genus are capable of achieving homeostasis (resilience) in the presence of metal ions of both precious and toxic metals by reducing them to a metallic state.

Received 14 September, 2018; revised 8 December, 2018; accepted 12 December, 2018. *For correspondence. E-mail mcuelar@ugto.mx; Tel. +52 (473) 732 0006; Fax +52 (473) 732 0006. *Microbial Biotechnology* (2019) 0(0), 1–16
doi:10.1111/1751-7915.13364

Funding Information

This work was carried out with the financial support granted to Dr. M. Cuéllar-Cruz by Proyecto-Institucional-IDCIIC-44/2018 from Universidad de Guanajuato, Mexico.

Introduction

For thousands of years, metallic minerals have been of great value to mankind, since they are widely used from tools making to the construction of buildings and houses, and even to generate energy and to manufacture jewellery (Cuéllar-Cruz *et al.*, 2017). Among these minerals we find precious metals such as gold and silver, as well as other widely used metals, like mercury, lead, copper, nickel, iron, aluminium. Nowadays, the obtainment of pure metals by high-cost mineral treatments such as pyrometallurgical and hydrometallurgical processes (Marchant, 1985) has been substituted by less expensive biological procedures known as bioleaching (Vera *et al.*, 2013). These procedures make use of a large diversity of microorganisms such as bacteria, archae and yeasts (Kelly *et al.*, 1979; Hutchins *et al.*, 1986; Norris and Parrott, 1986; Wiegel and Ljungdahl, 1986; Biryuzova *et al.*, 1987; Kelly and Harrison, 1989; Rawlings and Kusano, 1994; Clark and Norris, 1996; Karamushka and Gadd, 1999; Norris *et al.*, 2000; Brandl *et al.*, 2001; Vera *et al.*, 2013; Madrigal-Arias *et al.*, 2015) resulting in the isolation of macroscopic forms of minerals. Contrary to macroscopic metals, nanoparticles (NPs) exhibit physical and chemical characteristics such as optical, electrical, magnetic, colligative and catalytic properties, that depend from the form, size and method of isolation (Lu *et al.*, 2013). Gold and silver NPs (AuNPs, AgNPs) are particularly important as some of their properties have allowed their use as therapeutic alternatives (Mandal *et al.*, 2006; Asharani *et al.*, 2010, 2011). AuNPs, for instance, are potentially useful as carriers of therapeutic agents and in gene therapy and also as a phototherapeutic aid in the early detection, diagnoses and treatment of cancer (Paciotti *et al.*, 2004, 2006; Chen *et al.*, 2008; Jain *et al.*, 2008). In the same line, AgNPs have been used as antimicrobial compounds, topic creams and as anticancer products (Firdhouse and Lalitha, 2015). Several laboratories have recently focused their interest on the obtainment of NPs of toxic metals such as lead and mercury by biological synthesis from their molecular ions present in waste waters from the mining industry to prevent further contamination of water bodies and arable lands. Microorganisms such as bacteria, yeasts and filamentous fungi are able to synthesize these nanostructures (Mandal *et al.*, 2006; ; Kharissova

et al., 2013), which tend to oxidize by giving up their electrons to reduce the metal to zero valence.

We have recently used species the genus *Candida* that are able to form nanocrystals of lead sulphide, mercury and cadmium (Cuéllar-Cruz *et al.*, 2017). However, it has not been evaluated whether these yeasts are capable of synthesizing micro- or nanoparticles (MPs, NPs) of precious and heavy metals. The aim of the present work was to evaluate the capacity of *C. albicans*, *C. dubliniensis* and *C. glabrata* to synthesize NPs of precious metals (gold and silver) or heavy metals (mercury and lead), by reducing their corresponding molecular ions. The formation of the metallic NPs was carried out with the three *Candida* species, for which the yeasts were grown in YPD (yeast extract, 1%; peptone and glucose, 2%) in the presence of 1.0 mM of the metal ions and 100 mM of hydrogen peroxide (H₂O₂) for 48 h at 28°C. In this case, the addition of an oxidizing agent was necessary, because *Candida* species are not capable of reducing the cations of precious or heavy metals in non-oxidizing conditions (Cuéllar-Cruz *et al.*, 2017). The NPs formed were evaluated using scanning electron microscopy with energy-dispersive spectroscopy (SEM-EDS), Raman spectroscopy, X-ray fluorescence spectroscopy and synchrotron radiation. Our results showed that the metal ions of Au³⁺, Ag⁺, Pb²⁺ or Hg²⁺ are reduced to their corresponding NPs by *Candida* species. This is the first report that shows that yeasts of this genus are able to achieve a homeostasis (resilience) in the presence of metal ions of both precious and toxic metals, by reducing them to a metallic state. These data indicate that *Candida* species have developed mechanisms that enable them to adapt to different habitats.

Results

Candida species tolerate precious and heavy metals

Candida cells were exposed to different concentrations of each of the metals in the presence of 100 mM of the oxidizing agent, hydrogen peroxide (H₂O₂). The chosen concentration of the oxidizing agent does not alter the cellular viability of the *Candida* species used (Cuéllar-Cruz *et al.*, 2008; Ramírez-Quijas *et al.*, 2015). As observed in Fig. 1A, in the presence of Au³⁺ or Ag⁺ the cells exposed to oxidizing conditions are able to tolerate up to 2.0 mM of these elements. *C. albicans* and *C. dubliniensis*, in the presence of Hg²⁺, at a concentration of 2.0 mM are susceptible. Nonetheless, *C. glabrata* at this concentration is unable to survive (Fig. 1B). Regarding Pb²⁺, the three *Candida* species are able to tolerate up to a concentration of 2.0 mM (Fig. 1B). Based on these results, we decided to assess whether *C. albicans*, *C. dubliniensis* and *C. glabrata* could reduce the cations of both the precious and the heavy

metals up to 1.0 mM concentration (Fig. 1). At this concentration, *Candida* cells are viable. These results agree with those published results from different groups that have shown that yeasts possess mechanisms that have allowed them to survive in different habitats, from the human body to soil and water contaminated with precious or heavy metals (Hagler and Mendonca-Hagler, 1981; Suihko and Hoekstra, 1999; Lopez-Archilla *et al.*, 2004; Harrison *et al.*, 2006; Cuéllar-Cruz *et al.*, 2017).

Biosynthesis of precious metal nanoparticles: gold and silver

In order to evaluate whether the *Candida* species were able to synthesize NPs from the gold, or silver ions in solution, 100 mM of H₂O₂ were added to favour oxidizing conditions. In this way, the ions in solution were reduced by each of the *Candida* species. In addition to the oxidizing conditions, it has been reported that those microorganisms that perform the synthesis process are characterized by growing in acidic environments (Vanderrest *et al.*, 1995; Muhlschlegel and Fonzi, 1997; Gupta *et al.*, 2000). In the case of the *Candida* species, this is shown below as they reach an acidic pH (Cuéllar-Cruz *et al.*, 2017). As illustrated in Fig. 2, control cells in the presence of only the oxidant agent do not form NPs of any type. Notwithstanding, cells treated with Au³⁺ or Ag⁺ showed scarce or a lack of extracellular particles (Fig. S1). Therefore, in order to perform an adequate analysis of the metallic particles of these elements it was necessary to subject the cells to lysis. Representative microphotographs, taken through SEM, of the obtained results in the three *Candida* species in the presence of Au³⁺ are shown in Fig. 3 and S2. *Candida* cells, in the presence of Au³⁺, can reduce this cation to gold NPs (AuNPs, see Fig. 3 and S2). As seen in Fig. 3A, B and S2 the Au⁰ nanoparticles (AuNPs) are grouped in clusters. Under higher magnification, we can see the AuNPs, which have a completely spherical shape (Fig. 3B). Analysing the samples under SEM, AuNPs clusters were found in all the analysed fields, which shows that the *Candida* species have the ability to efficiently reduce Au³⁺ to Au⁰. Additionally, to corroborate that the AuNPs observed through SEM corresponded to Au⁰, the analysis of the elements present in the sample was carried out by means of EDS. Additionally, the percentage of these elements present in the sample was determined. As shown in the representative figure, in the analysed AuNPs, only Au⁰ was found (Fig. 3C–F). However, in order to confirm this result, the AuNPs were afterwards analysed through X-ray fluorescence and synchrotron radiation. The very small percentage of carbon and oxygen shown by the EDS analysis is due to the sample processing to be analysed by SEM-EDS and/or due to

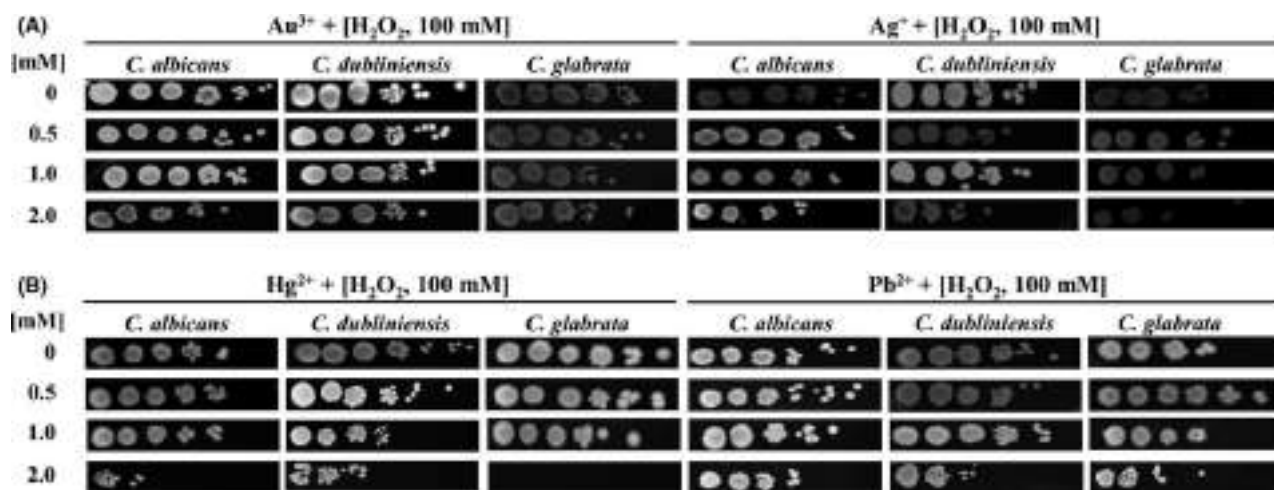


Fig. 1. Susceptibility assays in *C. albicans*, *C. dubliniensis* and *C. glabrata* in the presence of (A) precious metals Au^{3+} or Ag^+ , or (B) heavy metals Hg^{2+} , Pb^{2+} . Cultures of treated cells with any of the precious or heavy metals were under oxidizing conditions. Control cells were not treated with any cation.

the cell residues present in the samples (Fig. 3E, F). After finding that *Candida* species were able to reduce molecular ions of gold, we wondered if these microorganisms could also reduce silver. The three species of *Candida* were exposed to the Ag^+ ion under the same conditions as we did for gold. Interestingly enough, when observing the samples through SEM, we found that, unlike gold (which formed clusters), silver formed 'nanorocks' or 'nanoclusters' (Fig. 4A and S3). In a microphotograph at a higher magnification, it is remarkable to see how these nanorocks or nanoclusters of silver nanoparticles (AgNPs) were formed (Fig. 4B). These AgNPs appear in the form of elongated bars (Fig. 4B), but are smaller than the AuNPs (Fig. 3A, B). To corroborate that the nanorocks or nanodeposits effectively corresponded to elemental silver, the analysis was carried out by EDS. The analysis revealed that they actually corresponded to Ag^0 (Fig. 4C–F). These data were then confirmed with X-ray fluorescence and synchrotron radiation. Through EDS applied on these samples, we also found a very small percentage of carbon and oxygen due, as mentioned before, to the processing and/or cell residues present in the samples (Fig. 4E, F).

Obtaining heavy metal particles: mercury and lead

In order to evaluate whether the *Candida* species, apart from reducing precious metals, could also reduce toxic metals such as lead and mercury, the cells of these yeasts were exposed to Pb^{2+} or Hg^{2+} . The treated cells were observed through SEM. *Candida* cells exposed to Hg^{2+} , a minimal presence of extracellular microdrops was found (Fig. S1). The largest concentration of these microdrops was found intracellularly; thus, the cells were

lysed. Observing the microphotographs of the lysed samples exposed to Hg^{2+} , Hg^0 , we found micrometre diameter droplets in practically the entire sample (Fig. 5A–C and S4). The mercury microdrops displayed the cohesion property characteristic of Hg in liquid form, when we placed close to one another these drops, both drops of liquid mercury bound to each other forming a larger drop (Fig. 5C). The drops formed were analysed through EDS, which corroborated that they were formed of Hg^0 (Fig. 5D, E, F, G and S4).

When observing cells exposed to Pb^{2+} , we found scarce or a lack of extracellular metallic particles (Fig. S1); thus, we decided to disrupt the cells. In the case of the lysed samples from the cells exposed to Pb^{2+} , 'nanodeposits' were found (Fig. 6A and S5). Looking closely at these nanodeposits and taking microphotographs it was observed that the particles of Pb^0 were perfectly ordered, forming perfect squares with a particle of Pb^0 (Fig. 6B, C) in each vertex. These lead-treated samples were analysed through EDS, which revealed that the nanodeposits were formed by Pb^0 (Fig. 6D–G). The low percentage of oxygen and carbon present in both mercury and lead samples (Figs 5F, G and 6F, G) is due to the same causes mentioned for gold and silver.

Characterization of Au, Ag, Pb and Hg by Raman spectroscopy and X-ray powder diffraction (XRPD)

Gold, silver and lead NPs and mercury drops synthesized by *C. albicans*, *C. dubliniensis* and *C. glabrata* were characterized by Raman spectroscopy and XRPD as described in the *materials and methods* section, based on the fact that NPs exhibit unique physicochemical properties that depend on their shape and size

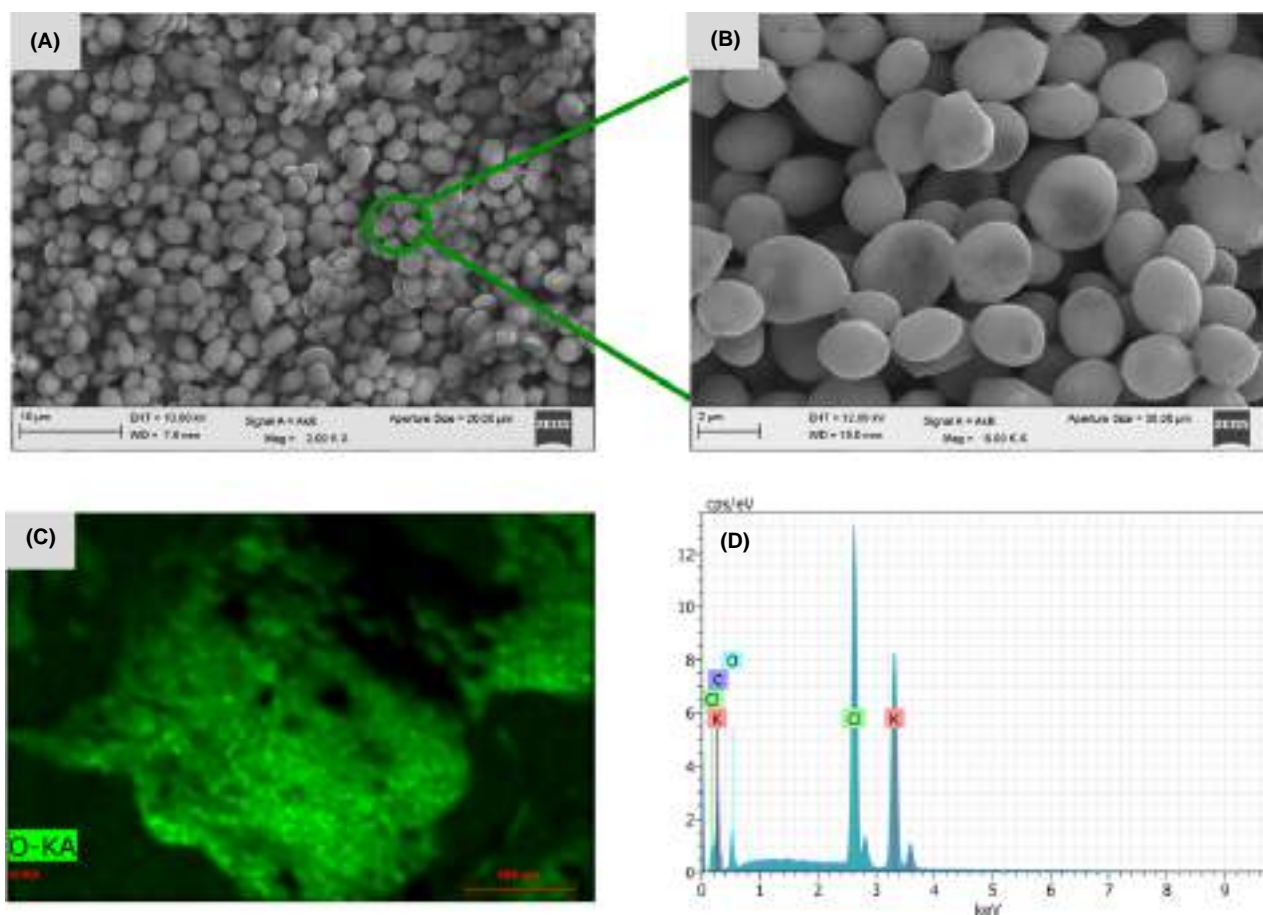


Fig. 2. Control cells of *Candida* species in absence of precious or heavy metals.

A, B. The control cells were analysed by means of SEM as described in the *methods* section. Scale bar is indicated in each photomicrograph to show the size of the cells.

C, D. Qualitative analysis of the elements present in the control cells by means of energy-dispersive spectroscopy (EDS).

(Poulose *et al.*, 2014; Firdhouse and Lalitha, 2015). These characteristics of the nanometric dimension are due to the surface/volume ratio and quantum confinement of NPs, which are displayed as a consequence of an increase in the space between the levels of electronic energy due to a decrease in particle size (Daniel and Astruc, 2004). Raman spectroscopy helps to identify molecules through spectral information, which is considered a molecular fingerprint. This technique has been widely used for the identification of NPs of different chemical composition (Lu *et al.*, 2013; Chen *et al.*, 2017). Raman spectroscopy, as observed in Table 1, when used for the characterization of AuNPs, revealed two peaks at 589 and 1102 nm wavelengths, which are close to those previously reported for gold nanospheres (Kalmodia *et al.*, 2013). For AgNPs, three peaks at 437, 1594 and 1646 nm were identified, corresponding to values essentially similar to those found for silver nanoparticles (Lu *et al.*, 2013; Tu and Chung, 2017). These results strongly indicate that *Candida* species are able to

synthesize AgNPs. We detected three peaks for NPs of lead at 445, 1096 and 4396 nm. For mercury drops, three peaks at 254, 3843 and 4168 nm were also detected. However, due to the size of AuNPs and AgNPs, the intensity of the peaks was not highly enough to be characterized by Raman spectroscopy. This led us to corroborate these results by synchrotron radiation setting up a powder diffraction in capillary tubes to collect data from each *Candida* species.

X-ray fluorescence spectroscopy confirmed the presence of gold in *C. albicans*, *C. dubliniensis* and *C. glabrata*, with superimposable patterns among different cell lines (Fig. 7B and Table 2). Nonetheless, endogenous zinc and other common metals (K, Fe) were found, even in blank samples (Fig. 7A). Spectra obtained from silver loaded samples (Fig. 7C) are not informative due to heavy air absorption of emission peaks at photon energies below 3.5 keV and peak overlaps with widespread bioelements like potassium, calcium, chlorine and atmospheric argon.

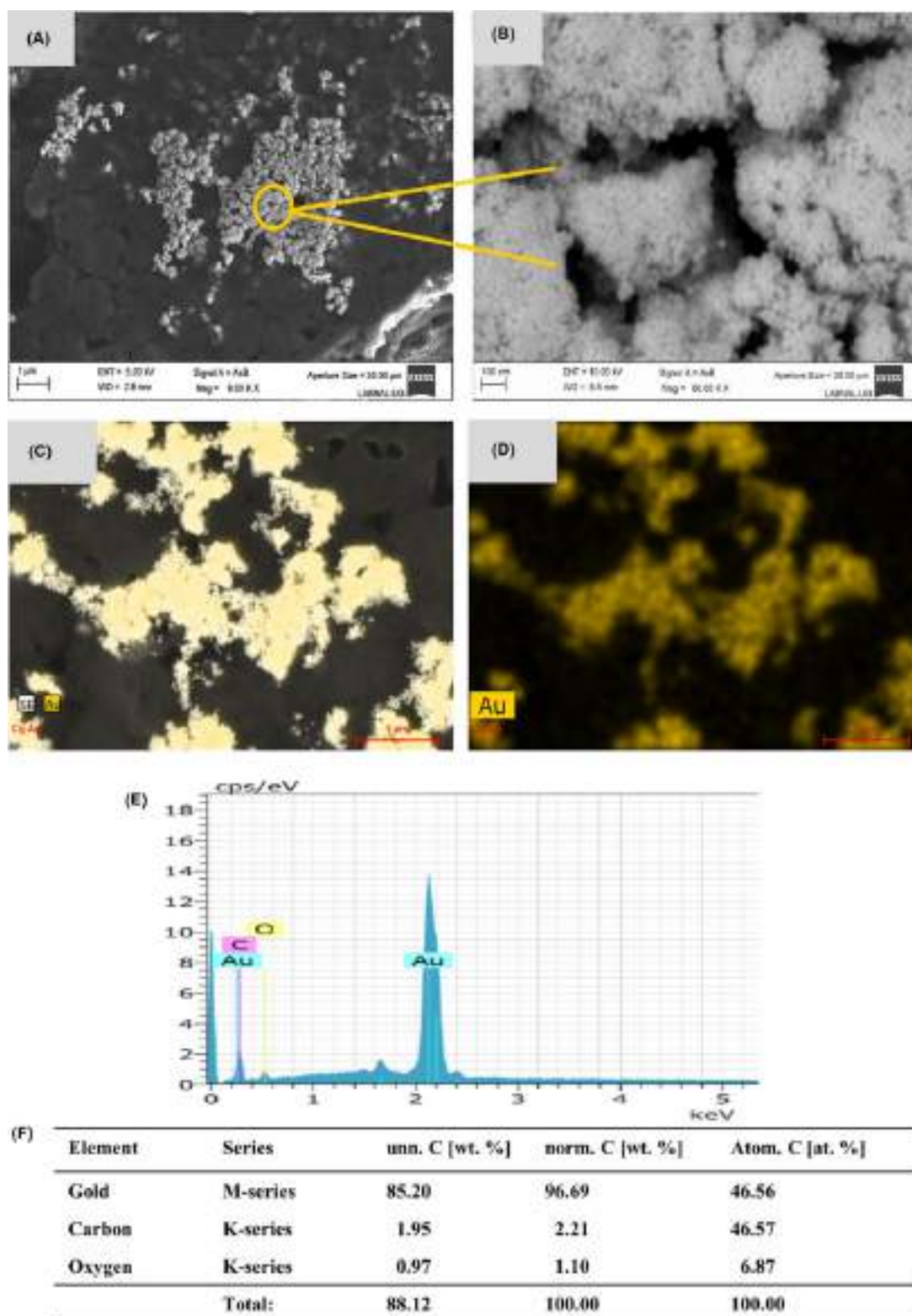


Fig. 3. Formation of gold nanoparticles formed by the *Candida* species in the presence of Au^{3+} . A, B. The AuNPs were analysed by means of SEM as described in the *methods* section. Scale bar is indicated in each photomicrograph. Yellow arrows and circle indicate the NPs formed. C–E. Energy-dispersive spectroscopy (EDS) qualitative analysis of the elements present in the AuNPs. F. Percentage of the element present in the sample. As shown in the EDS plot, the NPs are formed from the reduced metal.

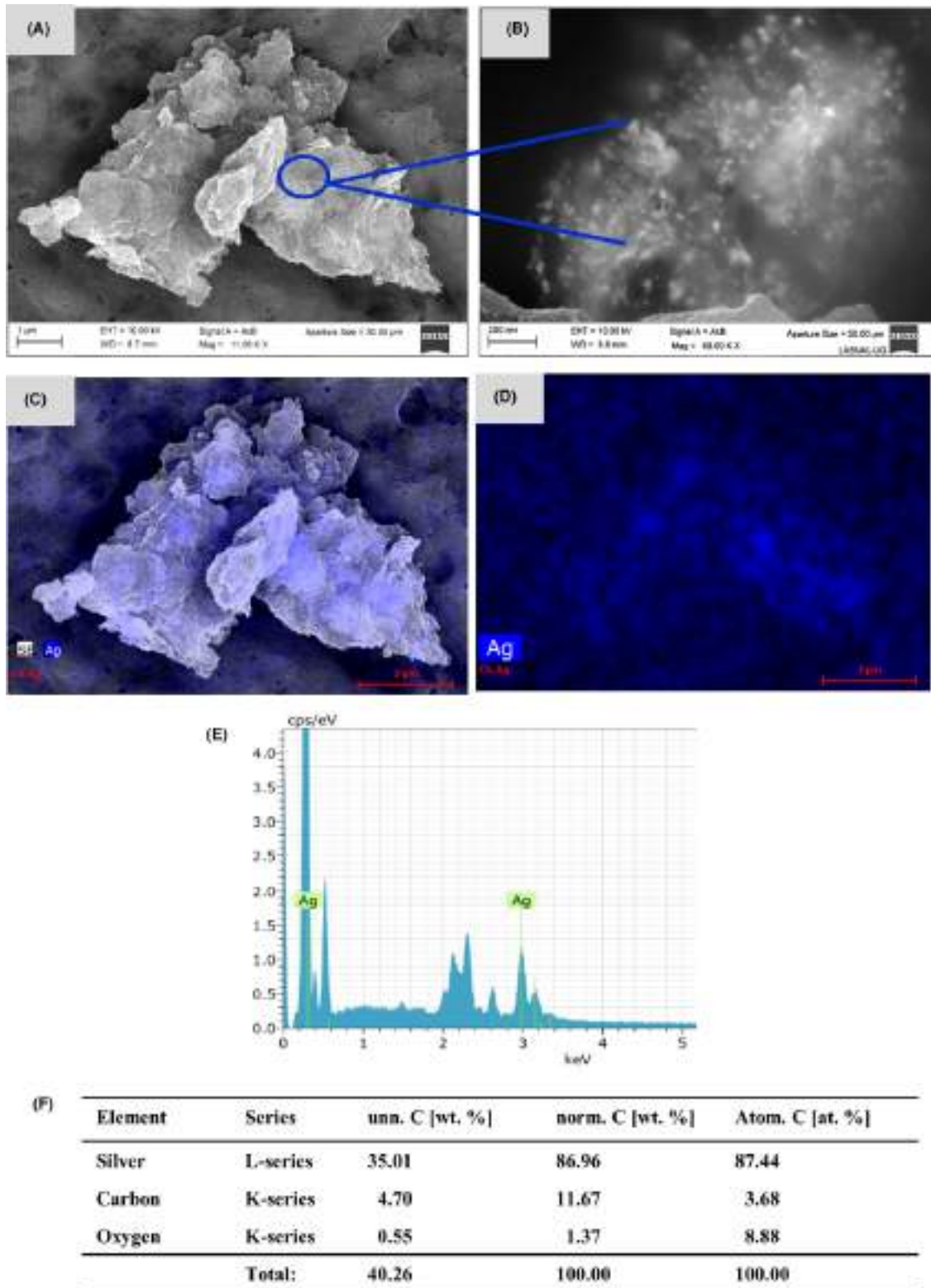


Fig. 4. Formation of silver nanoparticles formed by the *Candida* species in the presence of Ag^+ . A, B. The AgNPs were analysed by means of SEM as described in the *methods* section. Scale bar is indicated in each photomicrograph. Blue arrows and circle indicate the silver nanoconglomerates. C–E. Qualitative analysis of the elements present in the Ag nanoconglomerates through energy-dispersive spectroscopy (EDS). F. Percentage of the element present in the sample. As shown in the EDS plot, the nanoconglomerates are formed from the reduced metal.

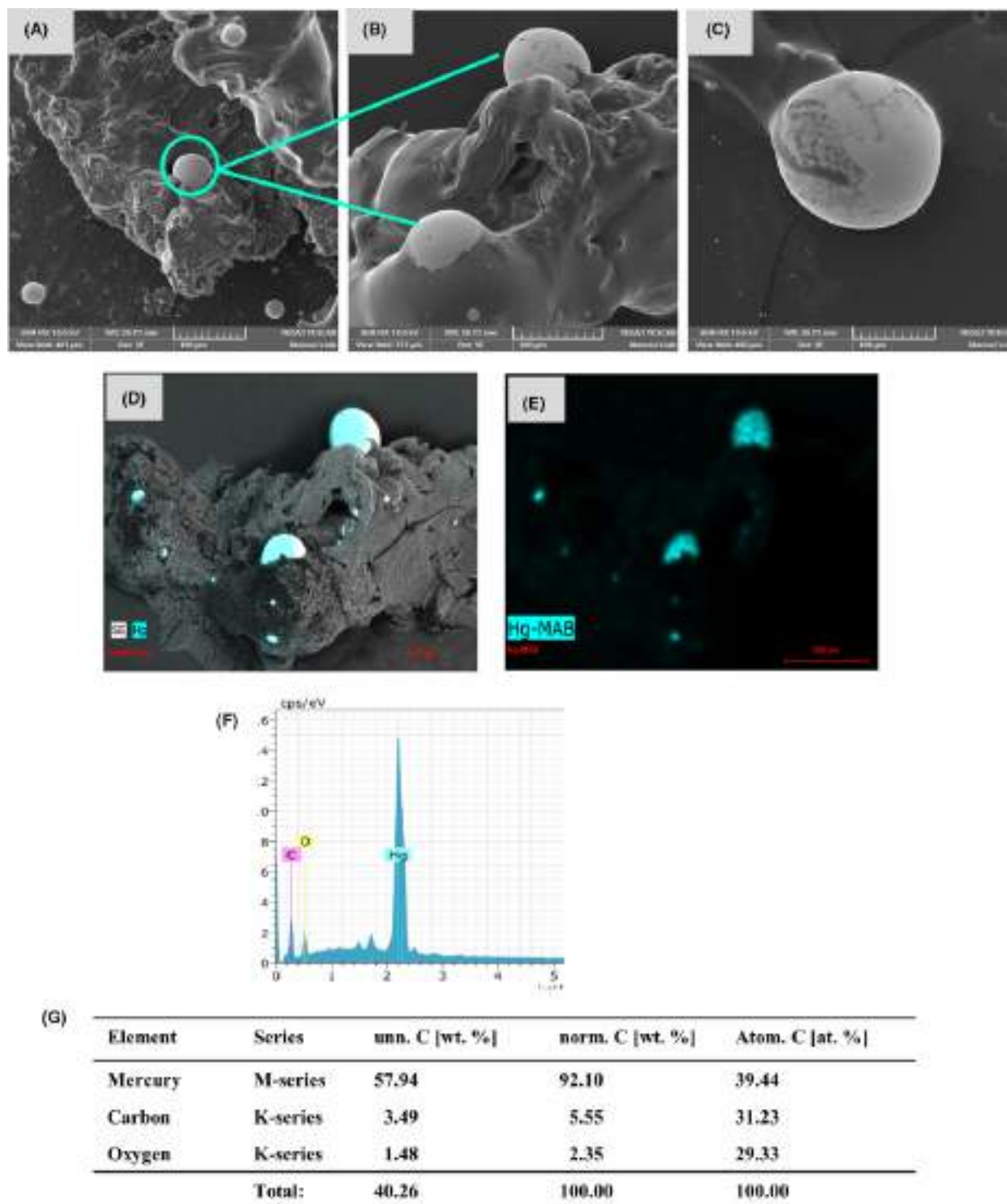


Fig. 5. Formation of mercury drops by the *Candida* species in the presence of Hg^{2+} . A–C. The Hg drops were analysed by means of SEM as described in the *methods* section. Scale bar is indicated in each photomicrograph. Green arrows and circle indicate the drops formed. D–F. Qualitative analysis of the elements present in the HgNPs through energy-dispersive spectroscopy (EDS). G. Percentage of the element present in the sample.

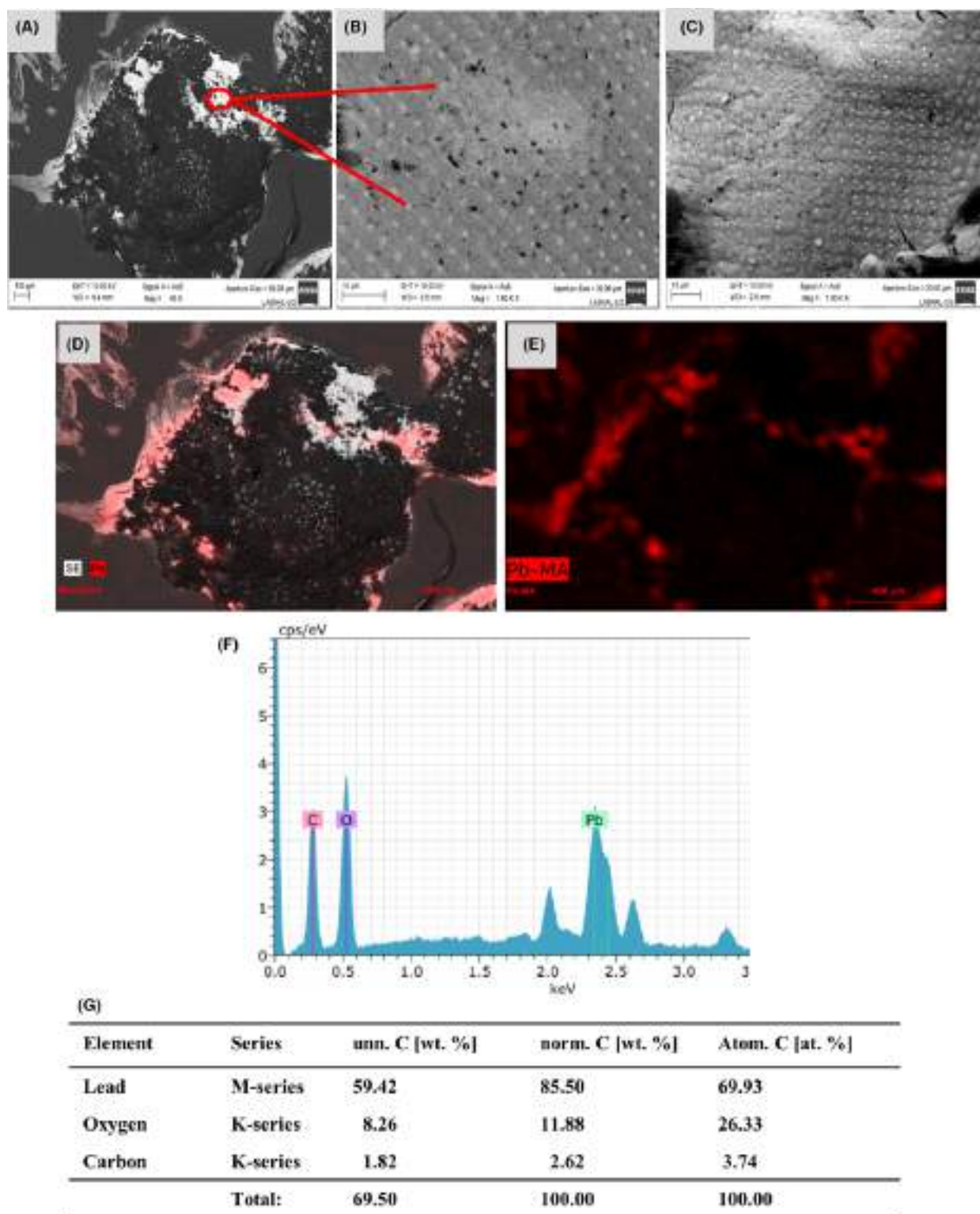


Fig. 6. Formation of lead nanoparticles formed by the *Candida* species in the presence of Pb^{2+} .

A–C. The PbNPs were analysed by means of SEM as described in the *methods* section. Scale bar is indicated in each photomicrograph. Red arrows and circle indicate the NPs formed.

D–F. Qualitative analysis of the elements present in the PbNPs through energy-dispersive spectroscopy (EDS).

G. Percentage of the element present in the sample.

Table 1. Identification of the chemical composition of the nanocrystals formed by Raman.

Metal	λ cm ⁻¹	<i>Candida</i> specie
<i>Candida</i> without metal	ND	<i>C. albicans</i> , <i>C. dubliniensis</i> , <i>C. glabrata</i>
Au ⁰	589, 1102	<i>C. albicans</i> , <i>C. dubliniensis</i> , <i>C. glabrata</i>
Ag ⁰	437, 1594, 1646	<i>C. albicans</i> , <i>C. dubliniensis</i> , <i>C. glabrata</i>
Pb ⁰	445, 1096, 4396	<i>C. albicans</i> , <i>C. dubliniensis</i> , <i>C. glabrata</i>
Hg ⁰	254, 3843, 4168	<i>C. albicans</i> , <i>C. dubliniensis</i> , <i>C. glabrata</i>

NA, Not applicable; ND, no signal detected.

The samples and data obtained were analysed as described in the methods section.

X-ray powder patterns collected from *Candida* cells not exposed to heavy metals (Fig. 8A) show broad peaks that agree with previous data published for glucans extracted from cell walls (Lowman *et al.*, 2014) and 'poorly ordered' lipidic phases (giving a broad peak at ~4.3 Å; Tyler *et al.*,

Table 2. Elements detected in sample fluorescence spectra using 16 keV excitation energy.

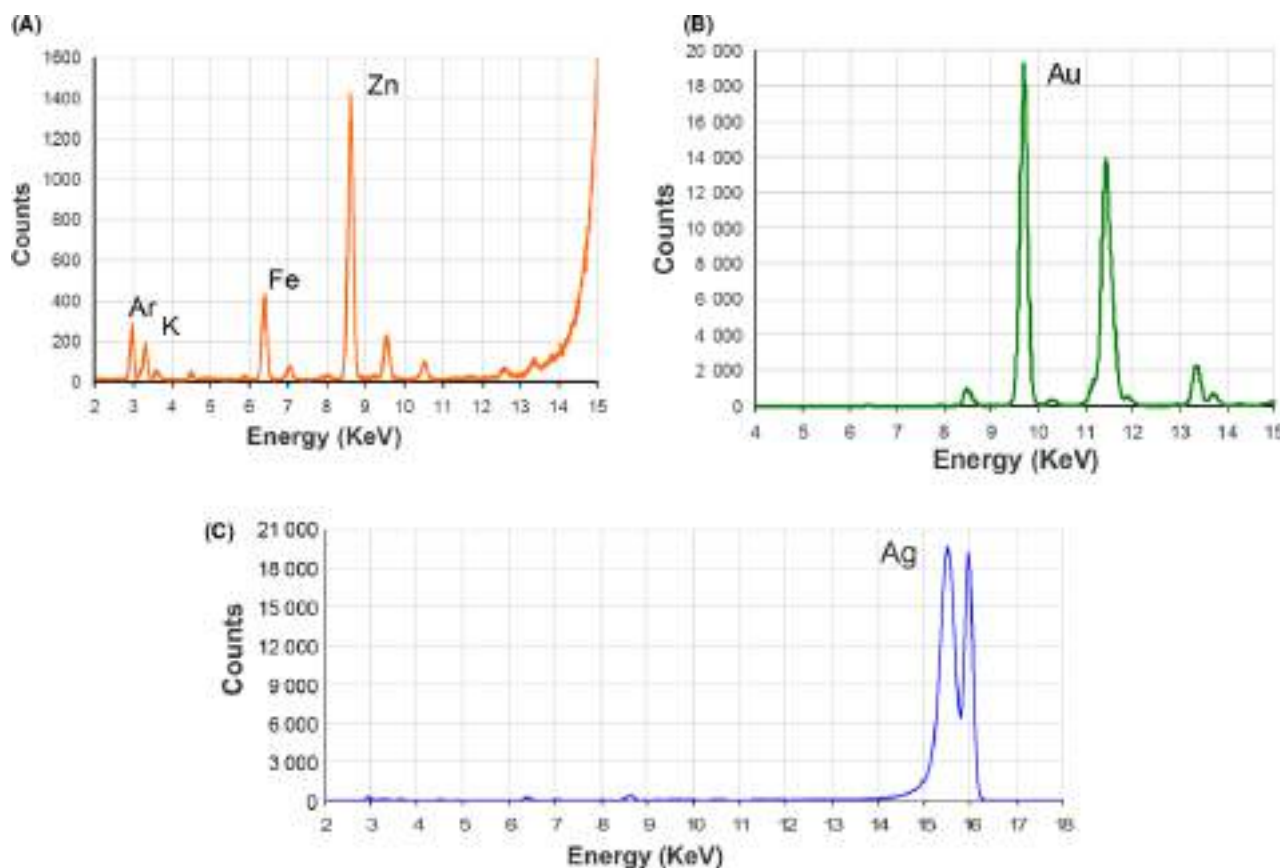
	<i>C. albicans</i>	<i>C. glabrata</i>	<i>C. dubliniensis</i>
Capillary blank	[Ar], K, Fe, [Cu], Zn, [Pb], [Br]		
Au loaded	[Ar], [K], [Fe], Zn, Au		
Ag loaded ^a	[Ag-Ar], [K], [Fe], Zn, Ag		

Elements reported in square parenthesis seem present as traces and could be due to environmental contamination – bolded symbols refer species estimated as more abundant from elemental analysis and, qualitatively from fluorescence intensities.

^aAg peaks cannot be clearly assigned, due to heavy air absorption of photons below 3.5 keV and peak overlaps with widespread bioelements like K, Ca, Cl and Ar.

2014). Blank background patterns of the three *Candida* species analysed are superimposable.

The presence of heavy atoms in the cells introduces sharper signals that belong to crystalline metallic nanoparticles. For AuNPs (Fig. 8B), sharp signals match nicely the peak positions expected for crystalline cubic closest packed (ccp) metallic gold *F m3m* phase (Wyckoff, 1963)

**Fig. 7.** Fluorescence peaks interpretation for: (A) *Candida* blank sample packed in capillary (16 keV excitation energy) – elements labelled on corresponding K_{*x*} lines.

(B) Peaks for a *Candida* gold loaded sample, belong to Au⁰; element is labelled on its L_{*x*} lines.

(C) Peaks for a *Candida* silver loaded sample, belong to Ag⁰; element is labelled on its L_{*x*} lines.

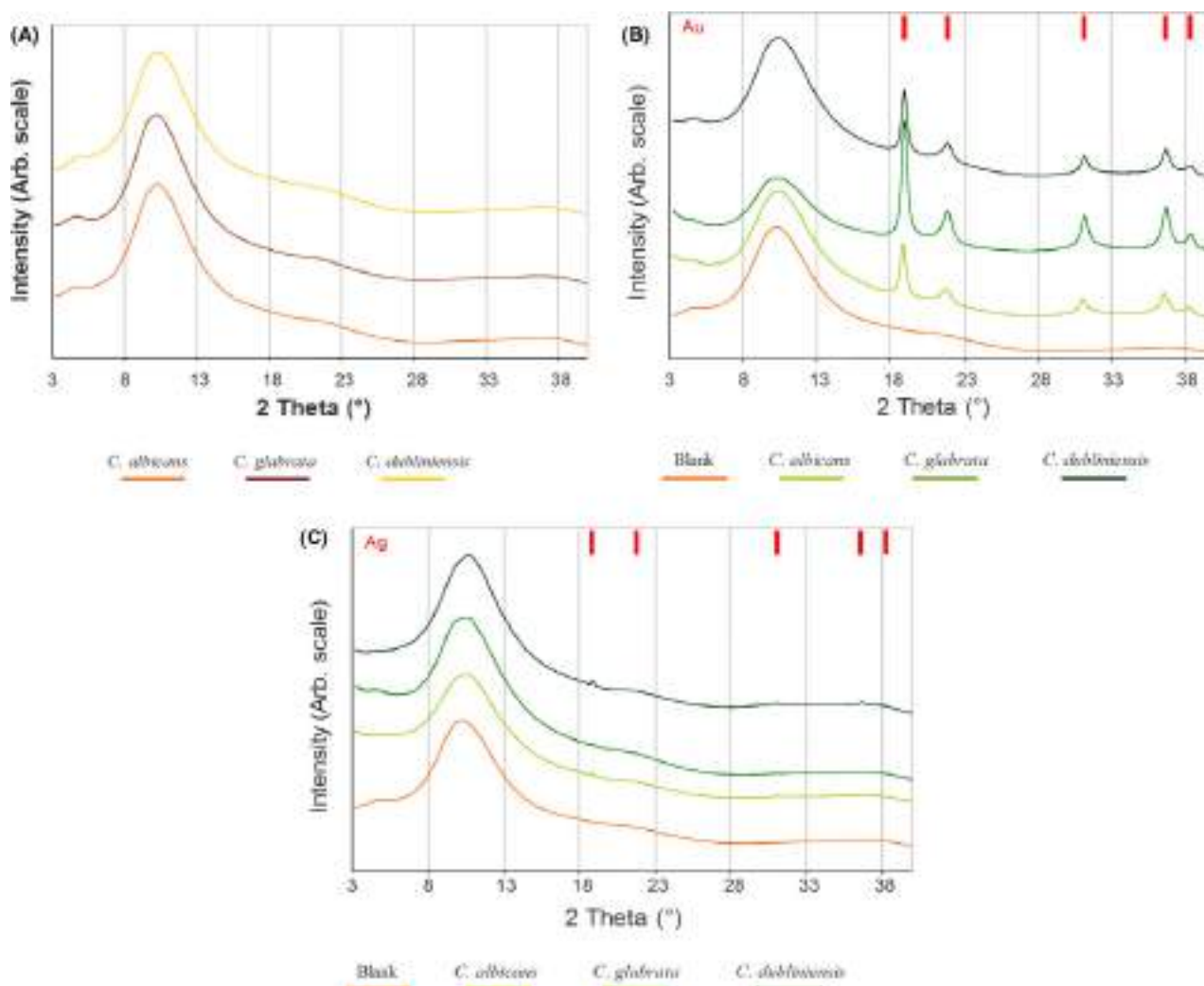


Fig. 8. X-Ray powder patterns of Au⁰ or Ag⁰.

A. *Candida* cells not exposed to heavy metals (blanks).

B. *Candida* cells exposed to gold. Red bars represent expected positions of ccp *F m3m* Au (Wyckoff, 1963).

C. *Candida* cells exposed to silver. Red bars represent expected positions of ccp *F m3m* Ag (Wyckoff, 1963). All samples had diffraction peaks at 16 keV, calculated using CCDC Mercury (Macrae *et al.*, 2008). Patterns are vertically shifted for clarity.

samples from different cell lines are equivalent. The same result is found in cell lines loaded with silver, where the crystalline silver *F m3m* phase is found (Wyckoff, 1963) in all the cell lines considered (Fig. 8C). Taken together, these results indicate that in the presence of an oxidant, such as H₂O₂, *Candida* species are able to reduce ions of both precious and heavy metals (Figs 3–6).

Discussion

Nanoparticles can be synthesized by chemical and biological methods, the latter using mostly bacteria, fungi and plants. In both methods, conditions are optimized to carefully control the size and form to obtain

monodisperse nanoparticles of identical crystalline structure and chemical composition. Numerous studies have found that many microorganisms can synthesize NPs (Li *et al.*, 2011; Zhang *et al.*, 2011; Moghaddam *et al.*, 2015). These works show that each microorganism is able to synthesize either a corresponding metal sulphide nanocrystal or metallic NPs but not both (Zhang *et al.*, 2011). The *Candida* species can synthesize nanocrystals of lead sulphide, mercury or cadmium (Cuéllar-Cruz *et al.*, 2017) and reduce cations of precious or heavy metals to the corresponding NPs (Figs 3–8, Tables 1 and 2). The latter indicates that these microorganisms have developed specific mechanisms under specific conditions, which allow them to achieve homeostasis with the metals to which they are exposed, and thus adapt to

the different habitats that they encounter. *Candida* species have been identified in different habitats from soils and water contaminated with heavy metals to organs or bloodstream of humans (Hagler and Mendonca-Hagler, 1981; Suihko and Hoekstra, 1999; Lopez-Archilla *et al.*, 2004; Cuéllar-Cruz *et al.*, 2017). A condition required in the formation of metallic NPs, in addition to an oxidizing condition, is an acidic medium (Agnihotri *et al.*, 2009). We added H₂O₂ to the culture medium to achieve an oxidizing condition. It is important to remark that without adding the oxidizing agent, the *Candida* species are not able to reduce the ions of precious or toxic metals. Interestingly, in the absence of H₂O₂, *Candida* synthesizes sulphur nanocrystals of the corresponding metal (Cuéllar-Cruz *et al.*, 2017; Moreno *et al.*, 2019). This shows that *Candida*, unlike other fungi, has specific mechanisms to synthesize nanocrystals or NPs, a characteristic of *Candida* species that make them an excellent model to use as producers of nanocrystals of lead sulphide, mercury or cadmium (Cuéllar-Cruz *et al.*, 2017) or of NPs of gold, silver or lead, as well as mercury drops (Figs 3–8).

Regarding AuNPs, the microorganisms widely used to synthesize these NPs are bacteria, where *Bacillus subtilis* 168 has been reported to be able to reduce Au³⁺ to AuNPs with a size ranging between 5 and 25 nm (Southam and Beveridge, 1996). *Halomonas salina* is another bacterium that synthesizes AuNPs, only that the morphology of these NPs varies according to whether it is found in acid or basic medium. In fungi, *Verticillium* sp. are reported to be able to synthesize AuNPs, with the disadvantage that the NPs must be extracted from the interior of the fungal biomass (Zhang *et al.*, 2011). Extremophilic yeast has been reported to synthesize AuNPs that show irregular shapes (Mourato *et al.*, 2011). In the case of *Candida* species, they have advantages over the bacteria and fungi described above, since *Candida* synthesizes fully spherical, uniform, and stable AuNPs (Fig. 3 and S2).

AgNPs are of special interest due to different uses in medicine and as a microbicide. In the synthesis of AgNPs, it has been described that most of the microorganisms are not capable of producing them due to their toxicity. However, bacteria that are resistant to silver have been identified (Silver, 2003). The bacterium *Pseudomonas stutzeri* AG259 produces AgNPs with a size ranging between 35 and 46 nm. Another bacterium that synthesizes AgNPs is *Idiomarina* sp., which produces NPs with an average size of 26 nm (Slawson *et al.*, 1994). In yeasts, *Pichia capsulta* is reported to be able to synthesize AgNPs in an extracellular manner (Srivastava and Kowshik, 2015). Another fungus that has been reported to be able to synthesize AgNPs is the filamentous fungus *Verticillium* sp. This fungus is able to synthesize spherical intracellular AgNPs

with an average size of 25 nm, but the disadvantage is that they must be recovered from the fungal mass. Halophilic fungi such as *Thraustochytrium* sp. and *Aspergillus niger* have also been reported to synthesize AgNPs (Mandal *et al.*, 2006).

Another element of interest in this study was Hg²⁺, which was evaluated to determine whether it could be reduced by *Candida* species. The fact that mercury droplets are formed by *Candida* species makes it a rather interesting finding as mercury is toxic to mammals and microorganisms (Clarkson, 1997; Diamond and Zalups, 1998; Westwater *et al.*, 2002). However, *Candida* cells were not only able to survive in the presence of Hg²⁺ ions, but they were also able to reach homeostasis with these toxic ions by reducing them and forming the Hg⁰ drops (Fig. 5 and S4). It has been reported in *Saccharomyces cerevisiae* that the toxicity of mercury is due to the binding of mercury to thiol-containing compounds, such as glutathione, resulting in oxidative stress (Kungolos *et al.*, 1999; Miura *et al.*, 1999). Probably, the fact that mercury generates oxidative stress, coupled to the stress that H₂O₂ had already generated in the sample, enables the *Candida* species to reduce the Hg²⁺ ions to form the Hg⁰ drops (Fig. 5). It has been recently reported that *Candida* species can form mercury nanocrystals (Cuéllar-Cruz *et al.*, 2017), but it has not been shown whether these yeasts are capable of producing HgNPs or not.

Finally, we also decided to evaluate Pb²⁺. In the case of the PbNPs synthesized by *Candida* (Fig. 6 and S5) this is the first report, to our knowledge, where the reduction of Pb²⁺ to Pb⁰ has been reported in a microorganism. In other studies, the formation of lead sulphide nanocrystals has been reported in both bacteria and yeasts (Ingale and Chaudhari, 2013; Cuéllar-Cruz *et al.*, 2017) but not the synthesis of PbNPs.

Although the mechanism of biological synthesis of NPs has not been fully elucidated, fungi in general have several characteristics that are advantageous for the synthesis of metal NPs. It has been shown that fungi are able to synthesize NPs by two routes, intracellular and extracellular, through reduction by enzymes (Moghaddam *et al.*, 2015; Cuéllar-Cruz *et al.*, 2017). In the case of *Candida* species, the mechanisms by which they can reduce the cations of precious or heavy metals are probably similar to those reported for other yeasts (Gericke and Pinches, 2006; Agnihotri *et al.*, 2009; Sanghi and Verma, 2009; Mourato *et al.*, 2011). It is generally proposed that these mechanisms are dependent on enzymes and that the genes for resistance to metals, proteins, peptides, reducing cofactors and organic molecules have significant roles as reducing agents. In addition, they provide NPs with a natural coating, preventing aggregation, stabilizing them for a long time. One proposed mechanism is that metal cations interact with the negatively charged groups

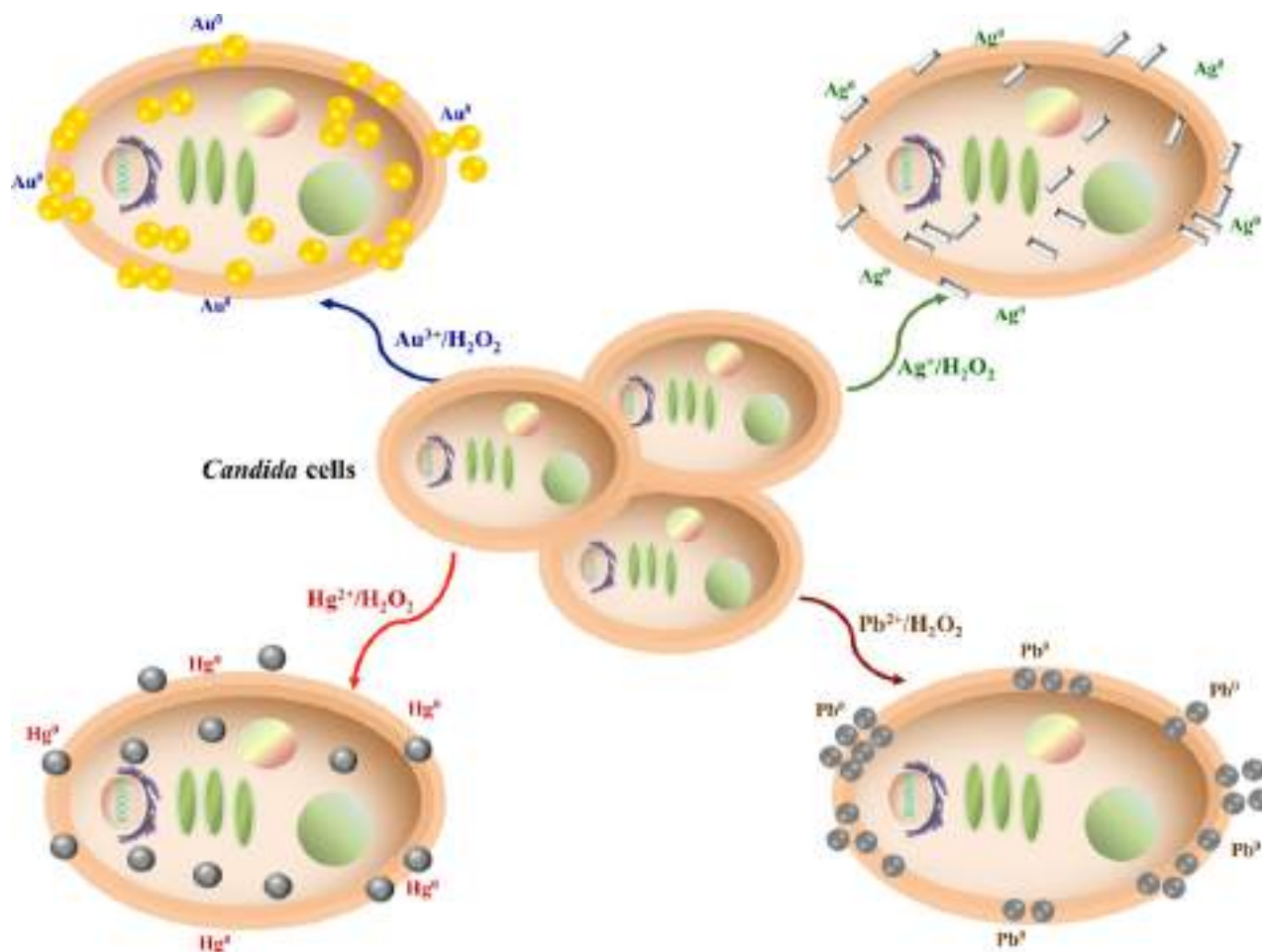


Fig. 9. Proposed mechanism through which *Candida* species synthesize NPs of gold, silver and lead, as well as mercury drops.

of enzymes or polypeptides of the cell wall (CW; Ulberg *et al.*, 2010). Another mechanism reported is that, after the ions are trapped in the CW, they are reduced by the enzymes present there (Sastry *et al.*, 2003). A third mechanism that has been proposed is that metal ions can diffuse into the cytoplasm and be reduced by the enzymes present in the cytoplasmic membrane and within the cytoplasm (Gericke and Pinches, 2006; Agnihotri *et al.*, 2009; Sanghi and Verma, 2009). Even though it has not been described which of the proposed mechanisms is the one followed by microorganisms, it has been reported that the formation of NPs of the different metals is favoured by an acidic pH. A mechanism by which *Candida* species achieve an extracellular acid pH involving the CW is by forming a bond between the metal ions with some component of the wall (Cuéllar-Cruz *et al.*, 2017). An acidic pH is generated because during the formation of the coordinated covalent bond, it can be accompanied by proton dislocation depending on the degree of protonation of the CW (Gupta *et al.*, 2000). Another mechanism reported in the maintenance of acid pH is through

the *PHR2* gene, which codes for a CW protein involved in the binding of β -1,3 and β -1,6 glucans and is expressed in acidic conditions (Muhlschlegel and Fonzi, 1997). In *C. albicans*, it has also been shown that about 500 genes are regulated in response to changes in pH (Bensen *et al.*, 2004). Another way that *Candida* species assure an extracellular acid environment is through the membrane ATPase Pma1, which has been reported in *S. cerevisiae* that has a proton export activity (Vanderrest *et al.*, 1995). Possibly, by means of these mechanisms, *Candida* species can reduce the metal ions to NPs or drops (Fig. 9). Although the synthesis mechanism of NPs in *Candida* has not been fully elucidated, our working group is working in this direction.

Conclusions

To our knowledge, this is the first report showing that *Candida* species are able to reduce ions of gold and silver to metallic forms, as well as ions of heavy metals, such as mercury or lead, to their corresponding NPs.

Based on these results, we can infer that *Candida* species have developed specific mechanisms that allow them to achieve homeostasis in the presence of metal ions. Therefore, *Candida* can be used in the near future for the bioleaching of different types of water and soil.

Experimental procedures

Strains and culture conditions

The strains of *C. albicans*, *C. dubliniensis* and *C. glabrata* used in this study are clinical isolates from the collection of the Department de Microbiology, ENCB-IPN, Mexico. Yeast strains were cultured on yeast peptone (yeast extract, 1%; peptone and glucose, 2%) and 2% agar was added to solidify the media (Ausubel *et al.*, 2003). Obtainment of the precious or heavy metals was induced by the addition to the cell culture of 1.0 mM of hydrogen tetrachloroaurate trihydrate (HAuCl₄), silver nitrate, lead nitrate or mercury nitrate (all obtained from Sigma-Aldrich) and 100 mM of hydrogen peroxide (H₂O₂).

Susceptibility assays of Candida strains to Au³⁺, Ag⁺, Pb²⁺, Hg²⁺ in oxidizing conditions

Candida albicans, *C. dubliniensis* and *C. glabrata* at OD_{600 nm} 1.0 were cultured in 50 ml of YPD medium with 1.0 mM of hydrogen tetrachloroaurate trihydrate (HAuCl₄), silver nitrate, lead nitrate or mercury nitrate, and 100 mM of hydrogen peroxide (H₂O₂), as oxidizing agent, for 48 h at 28°C under constant agitation. Afterwards, cells in stationary stage were removed from the culture medium containing the metals and the oxidizing agent by centrifugation at 10 000 *g* during 5 min. Then, the cells were resuspended in 1 ml of sterile deionized water, obtaining an OD_{600 nm} of 0.5. According to calculations, serial exponential dilutions were made in 96-well plates. Additionally, cells were seeded by dripping in plates with YPD medium and incubated at 28°C during 48 h. Plates were photographed with the GeneGenius Bioimaging system (Syngene, Cambridge, UK). Experiments were performed in a triplicate. Control samples were not treated with any metal.

Obtaining precious or heavy metals from lysis of Candida

To isolate the precious or heavy metals, yeast protoplasts were obtained as follows: cells of the three *Candida* species treated with each of the different salts of the metal were pelleted by centrifuging at 3500 *g* for 15 min at 4°C, the pellets were washed four times with sterile deionized water, resuspended in water and counted. Aliquots of the cell suspension were resuspended at a final OD_{600 nm} of 1.0 in 1.0 ml of lysis buffer containing 50 mM Tris-HCl, pH 7.2, 0.8 M sorbitol, 0.8 M KCl, 10 mM MgSO₄, 15 mM β-

mercaptoetanol and 0.25 mg ml⁻¹ lyticase (all reagents from Sigma-Aldrich, St Louis, MO, USA) and incubated at 37°C. After 3 h, cells were observed with a Zeiss Axiostar microscope (Carl Zeiss, Germany) to assess protoplast formation. This was about 90%. Protoplasts were collected and gently lysed by resuspending in 500 μl of sterile deionized water and the metallic particles formed *in vivo* were pelleted and separated from cellular debris by centrifugation at 120 *g* for 3 min.

Scanning electron microscopy (SEM)

After the metallic particles were separated from cellular debris, the particles of gold, silver, lead or mercury were thoroughly washed four times with sterile deionized water. Subsequently, the metal particles were lyophilized in a Tousimis auto Samdri 815 critical point dryer for 4 h. The dried samples were covered with a layer of colloidal gold, except for the samples treated with gold. Subsequently, the samples were observed with the scanning electron microscope, model EVO HD15, high definition ZEISS®. Finally, the samples were photographed using the secondary electron detector (SE1) at 15 kV under high vacuum conditions and at a working distance of 4 mm. Treated and without treatment *Candida* cells were visualized under the same conditions as the metallic particles.

Analysis of elements contained in the metals by energy-dispersive spectroscopy (EDS)

The metallic particles were observed with SEM and analysed qualitatively and quantitatively to determine their main components. EDS-JEOL Model JSM-6010PLUS was used for all analyses.

Raman spectroscopy

Control and exposure to heavy metals of the previously lyophilized cells were used to analyse the formation of NPs using Raman spectrophotometry. Raman spectra of wetted samples on a silicon wafer (001) oriented surface were performed with a WITec Alpha300 microscope (Ulm, Germany) using a 633 nm laser for excitation. The integration time per Raman spectrum was between 10 and 60 s, which gives a sufficient signal-to-noise ratio without destroying the samples. The data were evaluated using the software program WITec project 2.10 (Ulm, Germany).

X-Ray powder diffraction (XRPD)

X-Ray powder diffraction (XRPD) analysis was performed at the X-ray diffraction beamline (XRD1) of the Elettra Synchrotron, Trieste, Italy (Lausi *et al.*, 2015).

Powder diffraction patterns were collected in transmission mode, at room temperature (25°C) with a monochromatic wavelength of 0.77491 Å (16 keV) and 200 × 200 μm² spot size, using a Pilatus 2M hybrid-pixel area detector. *Candida* cells exposed to precious and heavy metals were packed in 700-μm diameter borosilicate capillaries (10 μm wall thickness). Blank samples were analysed in the same way, collecting data of lyophilized cells not exposed to heavy metals but treated with the same protocol (same growth parameters, washing and lyophilisation steps) as described by Cuéllar-Cruz *et al.* (2017). Two-dimensional powder patterns were integrated using Fit2D program (Hammersley, 2016), after preliminary calibration of the hardware setup, using a capillary filled with LaB₆ standard reference powder (NIST 660a). Fluorescence spectra were recorded for all the samples, during diffraction data acquisition on a Silicon drift Amptek X-123SDD detector, perpendicular to the X-rays beam.

Acknowledgements

Mayra Cuéllar-Cruz thanks the sabbatical leave support from SEP-PRODEP (Oficio No. 511-6/18-5929). The authors (M.C.C. and A.M.) acknowledge the XRD1-Hard X-ray Diffraction Beamline and Structural Biology Laboratory of the Elettra Synchrotron, in Italy, for the support and beamtime awarded to collect data from the different NPs. We are grateful to Dr. Jorge Delgado-García from the *Laboratorio de Materiales Blandos, Universidad de Guanajuato*, Mexico, for the facilities and technical assistance with Raman spectra, and to Dr. Ricardo Navarro and Dr. Paulina Lozano-Sotomayor from the *Laboratorio Nacional, Universidad de Guanajuato*, Mexico, for the facilities and technical assistance with the SEM photographs. The authors acknowledge Prof. John Dye for the English revision and editing of this contribution.

Conflict of interest

None declared.

References

- Agnihotri, M., Joshi, S., Kumar, R., Zinjarde, S., and Kulkarni, S. (2009) Biosynthesis of gold nanoparticles by the tropical marine yeast *Yarrowia lipolytica* NCIM 3589. *Mat Lett* **63**: 1231–1234.
- Asharani, P.V., Sethu, S., Vadukumpully, S., Zhong, S., Lim, C.T., Hande, P., and Valiyaveetil, S. (2010) Investigations on the structural damage in human erythrocytes exposed to silver, gold, and platinum nanoparticles. *Adv Funct Mater* **20**: 1–10.
- Asharani, P.V., Lianwu, Y., Gong, Z., and Valiyaveetil, S. (2011) Comparison of the toxicity of silver, gold and platinum nanoparticles in developing zebrafish embryos. *Nanotoxicology* **5**: 43–54.
- Ausubel, F., Brent, R., Kingston, R.E., Moore, D.D., Seidman, J.G., Smith, J.A., *et al.* (2003) *Current Protocols in Molecular Biology*. New York, NY: John Wiley & Sons.
- Bensen, E.S., Martin, S.J., Li, M., Berman, J., and Davis, D.A. (2004) Transcriptional profiling in *Candida albicans* reveals new adaptive responses to extracellular pH and functions for Rim101p. *Mol Microbiol* **54**: 1335–1351.
- Biryuzova, V.I., Korobushkina, Y.D., Pozmogova, I.N., and Karavaiko, G.I. (1987) Gold uptake by *Candida utilis* cells. *Microbiologia* **56**: 209–216.
- Brandl, H., Bosshard, R., and Wegmann, M. (2001) Computer-munching microbes: metal leaching from electronic scrap by bacteria and fungi. *Hydrometallurgy* **59**: 319–326.
- Chen, P.C., Mwakwari, S.C., and Oyelere, A.K. (2008) Gold nanoparticles: from nanomedicine to nanosensing (Review). *Nanotechnol Sci Appl* **1**: 45–66.
- Chen, L., Yan, H., Xue, X., Jiang, D., Cai, Y., Liang, D., *et al.* (2017) Surface-Enhanced Raman Scattering (SERS) active gold nanoparticles decorated on a porous polymer filter. *Appl Spectrosc* **71**: 1543–1550.
- Clark, D.A., and Norris, P.R. (1996) *Acidimicrobium ferrooxidans* gen. nov., sp. nov.: mixed-culture ferrous iron oxidation with *Sulfobacillus* species. *Microbiol* **142**: 785–790.
- Clarkson, T.W. (1997) The toxicology of mercury. *Crit Rev Clin Lab Sci* **34**: 369–403.
- Cuéllar-Cruz, M., Briones-Martin del Campo, M., Cañas-Villamar, I., Montalvo-Arredondo, J., Riego-Ruiz, L., and De Las Peñas, A. (2008) High resistance to oxidative stress in the fungal pathogen *Candida glabrata* is mediated by the single catalase, Cta1p, and controlled by the transcription factors Yap1p, Skn7p, Msn2p and Msn4p. *Eukaryot Cell* **7**: 814–825.
- Cuéllar-Cruz, M., Lucio-Hernández, D., Martínez-Ángeles, I., Demitri, N., Polentarutti, M., Rosales-Hoz, M.J., and Moreno, A. (2017) Biosynthesis of micro- and nanocrystals of Pb (II), Hg (II) and Cd (II) sulfides in four *Candida* species: a comparative study of in vivo and in vitro approaches. *Microb Biotechnol* **10**: 405–424.
- Daniel, M.C., and Astruc, D. (2004) Gold Nanoparticles: assembly, supramolecular chemistry, quantum-size-related properties, and applications toward biology, catalysis and nanotechnology. *Chem Rev* **104**: 293–346.
- Diamond, G.L., and Zalups, R.K. (1998) Understanding renal toxicity of heavy metals. *Toxicol Pathol* **26**: 92–103.
- Firdhouse, M.J., and Lalitha, P. (2015) Biosynthesis of silver nanoparticles and its applications. *J Nanotechnol* **2015**: 1–18.
- Gericke, M., and Pinches, A. (2006) Microbial production of gold nanoparticles. *Gold Bulletin* **39**: 22–28.
- Gupta, R., Ahuja, P., Khan, S., Saxena, R.K., and Mohapatra, H. (2000) Microbial biosorbents: meeting challenges of heavy metal pollution in aqueous solutions. *Curr Sci* **78**: 967–973.
- Hagler, A.N., and Mendonca-Hagler, L.C. (1981) Yeasts from marine and estuarine waters with different levels of pollution in the state of rio de janeiro, Brazil. *Appl Environ Microbiol* **41**: 173–178.
- Hammersley, A.P. (2016) FIT2D: a multi-purpose data reduction, analysis and visualization program. *J Appl Crystallogr* **49**: 646–652.

- Harrison, J.J., Rabiei, M., Turner, R.J., Badry, E.A., Sproule, K.M., and Ceri, H. (2006) Metal resistance in *Candida* biofilms. *FEMS Microbiol Ecol* **55**: 479–491.
- Hutchins, S.R., Davidson, M.S., Brierley, J.A., and Brierley, C.L. (1986) Microorganisms in reclamation of metals. *Annu Rev Microbiol* **40**: 311–336.
- Ingale, A.G. and Chaudhari, A.N. (2013) Biogenic synthesis of nanoparticles and potential applications: an eco-friendly approach. *J Nanomed Nanotechnol* **4**: 4–7. <https://doi.org/10.4172/2157-7439.1000165>
- Jain, P.K., Huang, X., El-Sayed, I.H., and El-Sayed, M.A. (2008) Noble metals on the nanoscale: optical and photothermal properties and some applications in imaging, sensing, biology and medicine. *Acc Chem Res* **41**: 1578–1586.
- Kalmodia, S., Harjwani, J., Rajeswari, R., Yang, W., Barrow, C.J., Ramaprabhu, S., *et al.* (2013) Synthesis and characterization of surface-enhanced Raman-scattered gold nanoparticles. *Int J Nanomedicine* **8**: 4327–4338.
- Karamushka, V.I., and Gadd, G.M. (1999) Interaction of *Saccharomyces cerevisiae* with gold: toxicity and accumulation. *Biometals* **12**: 289–294.
- Kelly, D.P. and Harrison, A.P. (1989) Genus *Thiobacillus*, Beijerinck 1904b. In *Bergey's Manual of Systematic Bacteriology*, Vol. **3**. Staley, J.T., Bryant, M.P., Pfennig, N., and Holt, J.G. (eds). Baltimore: The Williams & Wilkins, Co., **597**, pp. 1842–1858.
- Kelly, D.P., Norris, P.R., and Brierley, C.L. (1979) Microbiological methods for the extraction and recovery of metals. In *Microbial Technology: Current State*. Bull, A.T., Elwood, D.C., and Ratledge, C. (eds). Cambridge, U.K: Future Prospects, Cambridge University Press, pp. 969–989.
- Kharisova, O.V., Rasika-Dias, H.V., Kharisov, B.I., Olvera-Pérez, B. and Jiménez-Pérez, V.M. (2013) The greener synthesis of nanoparticles. *Trends Biotechnol* **31**: 240–248.
- Kungolos, A., Aoyama, I., and Muramoto, S. (1999) Toxicity of organic and inorganic mercury to *Saccharomyces cerevisiae*. *Ecotoxicol Environ Saf* **43**: 149–155.
- Lausi, A., Polentarutti, M., Onesti, S., Plaisier, J.R., Busetto, E., Bais, G., *et al.* (2015) Status of the crystallography beamlines at Elettra. *Eur Phys J Plus* **130**. <https://doi.org/10.1140/epjp/i2015-15043-3>
- Li, X., Xu, H., Chen, Z.S., and Chen, G. (2011) Biosynthesis of nanoparticles by microorganisms and their applications. *J Nanomater* **2011**: 1–16.
- Lopez-Archilla, A.I., Gonzalez, A.E., Terron, M.C., and Amils, R. (2004) Ecological study of the fungal populations of the acidic Tinto river in southwestern Spain. *Can J Microbiol* **50**: 923–934.
- Lowman, D.W., Greene, R.R., Bearden, D.W., Kruppa, M.D., Pottier, M., Monteiro, M.A., *et al.* (2014) Novel structural features in *Candida albicans* hyphal glucan provide a basis for differential innate immune recognition of hyphae versus yeast. *J Biol Chem* **289**: 3432–3443.
- Lu, Y., Feng, S., Liu, X., and Chen, L. (2013) Surface-Enhanced Raman scattering study of silver nanoparticles prepared by using MC as a template. *J Nanomat* **2013**: 1–8.
- Macrae, F., Bruno, I.J., Chisholm, J.A., Edgington, P.R., McCabe, P., Pidcock, E., *et al.* (2008) Mercury CSD 2.0 – new features for the visualization and investigation of crystal structures. *J Appl Crystallogr* **41**: 466–470.
- Madrigal-Arias, J.E., Argumedo-Delira, R., Alarcon, A., Mendoza-Lopez, M.R., Garcia-Barradas, O., Cruz-Sanchez, J.S., *et al.* (2015) Bioleaching of gold, copper and nickel from waste cellular phone PCBs and computer goldfinger motherboards by two *Aspergillus Niger* strains. *Braz J Microbiol* **46**: 707–713.
- Mandal, D., Bolander, M.E., Mukhopadhyay, D., Sarkar, G., and Mukherjee, P. (2006) The use of microorganisms for the formation of metal nanoparticles and their application. *Appl Microbiol Biotechnol* **69**: 485–492.
- Marchant, P.B. (1985) Plant scale design and economic considerations for biooxidation of an arsenical sulfide concentrate, in Internat. Symp. Complex Sulfides, San Diego, CIMAI ME.
- Miura, N., Kaneko, S., Hosoya, S., Furuchi, T., Miura, K., Kuge, S., and Naganuma, A. (1999) Overexpression of L-glutamine-D-fructose-6-phosphate amidotransferase provides resistance to methylmercury in *Saccharomyces cerevisiae*. *FEBS Lett* **458**: 215–218.
- Moghaddam, A.B., Namvar, F., Moniri, M., Tahir, P.M., Azizi, S., and Mohamad, R. (2015) Nanoparticles biosynthesized by fungi and yeast: a review of their preparation, properties, and medical applications. *Molecules* **20**: 16540–16565.
- Moreno, A., Lucio-Hernández, D. and Cuéllar-Cruz, M. (2019) Biosynthesis of chemical compounds by *Candida albicans* and *Candida glabrata*. *Rev Iberoam Micol* (in press).
- Mourato, A., Gadanho, M., Lino, A.N. and Tenreiro, R. (2011) Biosynthesis of crystalline silver and gold nanoparticles by extremophilic yeast. *Bioinorg Chem Appl* **2011**: 1–8. <https://doi.org/10.1155/2011/546074>
- Muhlschlegel, F.A., and Fonzi, W.A. (1997) PHR2 of *Candida albicans* encodes a functional homolog of the pH-regulated gene PHR1 with an inverted pattern of pH-dependent expression. *Mol Cell Biol* **17**: 5960–5967.
- Norris, P.R. and Parrott, L.M. (1986) High temperature mineral concentrate dissolution with *Sulfolobus*. In *Fundamente and Applied Biohydrometallurgy*. Lawrence, R.W., Branion, R.M.R. and Ebner, H.E. (eds). New York: Elsevier, pp. 355–365.
- Norris, P.R., Burton, N.P., and Foulis, N.A.M. (2000) Acidophiles in bioreactor mineral processing. *Extremophiles* **4**: 71–76.
- Paciotti, G.F., Myer, L., Weinreich, D., Goia, D., Pavel, N., McLaughlin, R.E., and Tamarkin, L. (2004) Colloidal gold: a novel nanoparticle vector for tumor directed drug delivery. *Drug Deliv* **11**: 169–183.
- Paciotti, G.F., Kingston, D.G.I., and Tamarkin, L. (2006) Colloidal gold nanoparticles: a novel nanoparticle platform for developing multifunctional tumor-targeted drug delivery vectors. *Drug Dev Res* **67**: 47–54.
- Poulose, S., Panda, T., Nair, P.P., and Theodore, T. (2014) Biosynthesis of silver nanoparticles. *J Nanosci Nanotechnol* **14**: 2038–2049.
- Ramírez-Quijas, M.D., Zazueta-Sandoval, R., Obregón-Herrera, A., López-Romero, E., and Cuéllar-Cruz, M. (2015) Effect of oxidative stress on cell wall morphology in four pathogenic *Candida* species. *Mycol Progress* **14**: 1–15.
- Rawlings, D.E., and Kusano, T. (1994) Molecular genetics of *Thiobacillus ferrooxidans*. *Microbiol Rev* **58**: 39–55.

- Sanghi, R., and Verma, P. (2009) Biomimetic synthesis and characterization of protein capped silver nanoparticles. *Bioresour Technol* **100**: 501–504.
- Sastry, M., Ahmad, A., Khan, M.I., and Kumar, R. (2003) Biosynthesis of metal nanoparticles using fungi and actinomycete. *Curr Sci* **85**: 162–170.
- Silver, S. (2003) Bacterial silver resistance: molecular biology and uses and misuses of silver compounds. *FEMS Microbiol Rev* **27**: 341–353.
- Slawson, R.M., Lohmeier-Vogel, E.M., Lee, H., and Trevors, J.T. (1994) Silver resistance in *Pseudomonas stutzeri*. *Biomaterials* **7**: 30–40.
- Southam, G., and Beveridge, T.J. (1996) The occurrence of sulfur and phosphorus within bacterially derived crystalline and pseudocrystalline octahedral gold formed *in vitro*. *Geochim Cosmochim Acta* **60**: 4369–4376.
- Srivastava, P. and Kowshik, M. (2015) Biosynthesis of nanoparticles from halophiles. In *Halophiles: Biodiversity and Sustainable Exploitation*, 6th edn. Maheshwari, D.K. and Saraf, M. (eds). Switzerland: Springer Cham, pp. 145–161.
- Suihko, M.L., and Hoekstra, E.S. (1999) Fungi present in some recycled fibre pulps and paperboards. *Nor Pulp Pap Res J* **14**: 199–203.
- Tu, K.T., and Chung, C.K. (2017) Enhancement of surface Raman spectroscopy performance by silver nanoparticles on resin nanorods arrays from anodic aluminum oxide template. *J Electrochem Soc* **164**: B3081–B3086.
- Tyler, A.I.I., Law, R.V. and Seddon, J.M. (2015) X-Ray Diffraction of Lipid Model Membranes. In *Methods in Membrane Lipids. Methods in Molecular Biology (Methods and Protocols)*, Owen, D. (ed). New York, NY: Humana Press, Vol **1232**, pp. 199–225.
- Ulberg, Z.R., Podolskaya, V.I., Voitenko, E.Y., Grishchenko, N.I., and Yakubenko, L.N. (2010) Formation and biological activity of preparations based on microorganisms and colloidal silver. *Colloid J* **72**: 66–73.
- Vanderrest, M.E., Kamminga, A.H., Nakano, A., Anraku, Y., Poolman, B., and Konings, W.N. (1995) The plasma membrane of *Saccharomyces cerevisiae* – structure, function, and biogenesis. *Microbiol Rev* **59**: 304–322.
- Vera, M., Schippers, A., and Sand, W. (2013) Progress in bioleaching: fundamentals and mechanisms of bacterial metal sulfide oxidation—part A. *Appl Microbiol Biotechnol* **97**: 7529–7541.
- Westwater, J., McLaren, N.F., Dormer, U.H., and Jamieson, D.J. (2002) The adaptive response of *Saccharomyces cerevisiae* to mercury exposure. *Yeast* **19**: 233–239.
- Wiegel, J., and Ljungdahl, L.G. (1986) The importance of thermophilic bacteria in biotechnology. *Crit Rev Microbiol* **3**: 39–108.
- Wyckoff, R.W.G. (1963) Second edition. Interscience Publishers, New York, New York Crystal Structures, 1: 85–237.
- Zhang, X., Yan, S., Tyagi, R.D., and Surampalli, R.Y. (2011) Synthesis of nanoparticles by microorganisms and their application in enhancing microbiological reaction rates. *Chemosphere* **82**: 489–494.

Supporting information

Additional supporting information may be found online in the Supporting Information section at the end of the article.

Fig. S1. Cells of *C. albicans*, *C. dubliniensis*, and *C. glabrata* in presence of precious or heavy metals. Scale bar is indicated in each photomicrograph to show the size of the cells.

Fig. S2. Formation of gold nanoparticles by the *Candida* species in the presence of Au^{3+} .

Fig. S3. Formation of silver nanoparticles by the *Candida* species in the presence of Ag^+ .

Fig. S4. Formation of mercury drops by the *Candida* species in the presence of Hg^{2+} .

Fig. S5. Formation of lead nanoparticles by the *Candida* species in the presence of Pb^{2+} .

IL-2 Expression and T lymphocyte Phenotyping in Young Children Suffering from Upper Respiratory Tract Infection with *Streptococcus Pyogenes*

Eda Guadalupe Ramirez-Valles¹, Verónica Dayali Gutierrez-Martinez¹,
Maribel Cervantes-Flores¹, Estela Ruiz-Baca¹, Cosme Alvarado-Esquivel²

¹Faculty of Chemical Sciences, Juárez University of Durango State. Avenida Universidad S/N. 34000 Durango, Dgo, Mexico;

²Faculty of Medicine and Nutrition, Juárez University of Durango State. Avenida Universidad S/N. 34000 Durango, Dgo, Mexico

ABSTRACT

T cells are components of adaptive immunity and are involved in the resolution of respiratory infections, which are a major cause of morbidity and mortality in young children worldwide. Activation and differentiation of T cells is given mostly by the cytokine IL-2. This study aimed to determine the phenotype of T cells and IL-2 expression in children suffering from upper respiratory tract infection with *Streptococcus pyogenes* (*S. pyogenes*). For this purpose, IL-2 expression at its gene and protein levels and quantitation of CD4⁺ and CD8⁺ T lymphocytes were assessed in children aged 0-5 years old suffering from upper respiratory tract infection with *S. pyogenes* and healthy children of the same age. Children with *S. pyogenes* infection had a higher expression of IL-2 gene and a lower level of this cytokine expression at protein level than healthy children. The numbers of CD4⁺ T lymphocytes were similar among the groups. In contrast, difference in the numbers of CD8⁺ T lymphocytes among the groups was found. We conclude that infections by *S. pyogenes* in young children lead to an increased expression of IL-2 mRNA. (*Int J Biomed Sci* 2016; 12 (2): 53-57)

Keywords: IL-2 expression; phenotyping; T lymphocytes; *Streptococcus pyogenes*; infection

INTRODUCTION

T cells belong to the adaptive immune system and perform a wide range of functions in immune regulation, inflammation and protective immune response (1). The maturation of these cells is subjected to positive and negative selection to produce CD4⁺ and CD8⁺ lymphocytes. At maturation, lymphocytes leave the thymus, in that moment are considered naive cells until they are activated by signals, then they start to proliferate and differentiate into effector cells (helper and cytotoxic). The activation of na-

Corresponding author: Dr. Cosme Alvarado-Esquivel, Laboratorio de Investigación Biomédica. Facultad de Medicina y Nutrición. Avenida Universidad S/N. 34000 Durango, Dgo, México. Tel/Fax: 0052-618-8130527. E-mail: alvaradocosme@yahoo.com.

Received December 22, 2015; **Accepted** March 3, 2016

Copyright: © 2016 Eda Guadalupe Ramirez-Valles et al. This is an open-access article distributed under the terms of the Creative Commons Attribution License (<http://creativecommons.org/licenses/by/2.5/>), which permits unrestricted use, distribution, and reproduction in any medium, provided the original author and source are credited.

ive T cells in the peripheral immune system is the first step of the adaptive immune response (2).

The balance between the differentiations of T cells may be influenced by the types of dendritic cells that initially respond to infections, the cytokines they secrete when are activated by the microorganisms and thus, the type of effector T cell induced (3).

Interleukin 2 (IL-2) is a cytokine secreted by T cells, it regulates the proliferation, differentiation and survival for the cells that produce it (4) also stimulates growth and differentiation of B lymphocytes, NK cells ("natural killer"), LAK cells ("lymphokine-activated killers"), monocytes, macrophages and oligodendrocytes (5).

Streptococcus pyogenes (*S. pyogenes*) is a pathogen responsible for at least 616 million cases of respiratory tract infections per year worldwide and 111 million infections in the skin (6), causes 700,000 cases of invasive infections (7) and, in total, cause 163,000 deaths per year (8). The bacteria are phagocytized and destroyed by the macrophages and dendritic cells, is processed into small fragments, attached to MHC II and presented to helper T lymphocytes (ThL) (9).

In this study, the expression of IL-2 at its gene and protein levels and the phenotyping of CD4⁺ and CD8⁺ T lymphocytes were investigated in children aged 0-5 years old with *S. pyogenes* infection and healthy children of the same age.

MATERIALS AND METHODS

Selection and description of participants

Through a case-control study, the expression of IL-2 and phenotyping of CD4⁺ and CD8⁺ T lymphocytes were examined in children with *S. pyogenes* infection (cases) and children without *S. pyogenes* infection (controls). The children studied attended the Hospital "Santiago Ramón y Cajal" of the Institute for Security and Social Services of the State Workers and the Health Center No. 1 "Dr. Carlos León de la Peña" of the Secretary of Health in Durango, City, Mexico from June 2012 to September 2013. Inclusion

criteria for cases were children with *S. pyogenes* infection, aged 0-5 years old, of any gender. Inclusion criteria for controls were healthy children without *S. pyogenes* infection, aged 0-5 years old (age-matched with cases), of any gender. During the study period, 604 children aged 0-5 years old were tested for *S. pyogenes* infection in the participating Hospital and Health Center. A throat swap sample was obtained from each participant and cultured on a sheep blood agar plate. Identification of *S. pyogenes* was performed by using the VITEK 2 automatic system (bioMérieux, Marcy l'Etoile, France). Of these 604 children, 31 were positive for *S. pyogenes* infection.

Children with *S. pyogenes* infection were aged 0.5-5 years old and included 16 male and 15 female. The control group included 31 clinically healthy children without *S. pyogenes* infection matched for age and sex with cases. Peripheral blood samples from cases and controls were collected by venipuncture using EDTA vacuum tubes (Vacutainer). Whole blood and plasma aliquots were obtained and stored at 4°C and -20°C, respectively until analyzed.

Expression of IL-2 at gene level

This expression was assessed by RT-qPCR. To achieve this, total RNA was extracted using protocols by Chomczynski and Sacchi (10) TRIzol extraction (Ambion). The RT-qPCR was performed from extracted RNA using the RT-PCR System™ (Promega) commercial kit under supplier conditions. Gene expression of IL-2 was compared to the expression of a constitutive gene (GAPDH) showing relative expression. The oligonucleotides used in this study are shown in Table 1, oligonucleotides for the amplification of IL-2 were designed using the primer quest tool from IDT page using the identification number of the gene bank K02056.1; oligonucleotides for amplification of GAPDH were designed according to sequences reported by Chen *et al.* (11).

Quantification of IL-2 at protein level

To quantify IL-2, the commercial ELISA kit PeproTech human IL-2 was used under supplier conditions. Readings

Table 1. Sequences of the oligonucleotides used for RT-qPCR

Target mRNA	Sequence	Amplicon length (bp)
IL-2	5' TCC CAA ACT CCA TCA CCT TTC 3' 5' CAC CTG AGT CCC TTG CAT ATT 3'	355
GAPDH	5' TGA ACG GGA AGC TCA CTG G 3' 5' TCC ACC ACC CTG TTG CTG TA 3'	306

at 5 minute intervals were performed from 0 to 45 minutes after adding the enzyme substrate. Readings were taken at 405 nm and 650 nm.

Phenotyping of T CD4⁺ and CD8⁺ lymphocytes

These two populations of cells were quantified from whole blood samples by flow cytometry, using reagents, controls and BD FACSCount™ software for whole blood, searching the surface antigens CD3⁺/CD4⁺ and CD3⁺/CD8⁺, according to the supplier conditions.

Ethical aspects

This study was approved by the Ethics Committee of the Hospital “Santiago Ramón y Cajal” of the Institute for Security and Social Services of the State Workers in Durango City. Information about the study procedures was given to the parents of the children. An informed consent was obtained from all parents of the participants.

Statistical analysis

The normality of data was assessed by the Kolmogorov-Smirnov test. F test was used for analysis of variance and finally, the data were analyzed using the student's *t* test. Statistically significance was set at a $p < 0.05$.

RESULTS

IL-2 expression

Quantitative analysis by RT-qPCR revealed that the expression of IL-2 was lower (1.16 ± 0.23) in *S. pyogenes* infected individuals than in controls (1.46 ± 0.17) ($p < 0.001$) (Figure 1A). The protein expression of IL-2, analyzed by ELISA, shown an increased expression in uninfected individuals compared to infected individuals (0.72 ± 0.5 and 0.51 ± 0.39 ng/ml, respectively; $p = 0.032$) (Figure 1B).

CD4⁺ and CD8⁺ T lymphocyte phenotyping

No difference in the numbers of CD4⁺ T cells in subjects with *S. pyogenes* infection and controls (1258.3 ± 422.9 and 1257.7 ± 403.4 cells/ μ l, respectively; $p = 0.48$) was found (Figure 2A). In contrast, cases had a higher number of CD8⁺ T cells than controls (824.5 ± 306.3 and 674.1 ± 269.6 cells/ μ l, respectively; $p = 0.022$) (Figure 2B).

DISCUSSION

In this study, according to the analysis results, there is evidence of a statistically significant difference in the rate of IL-2 gene expression, protein expression, and number

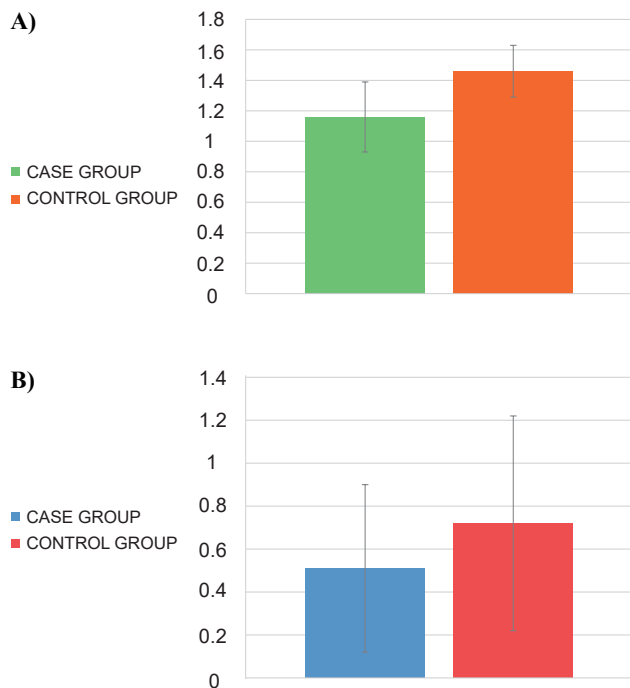


Figure 1. IL-2 expression in the study groups. A) Gene expression; B) Protein expression (ng/ml).

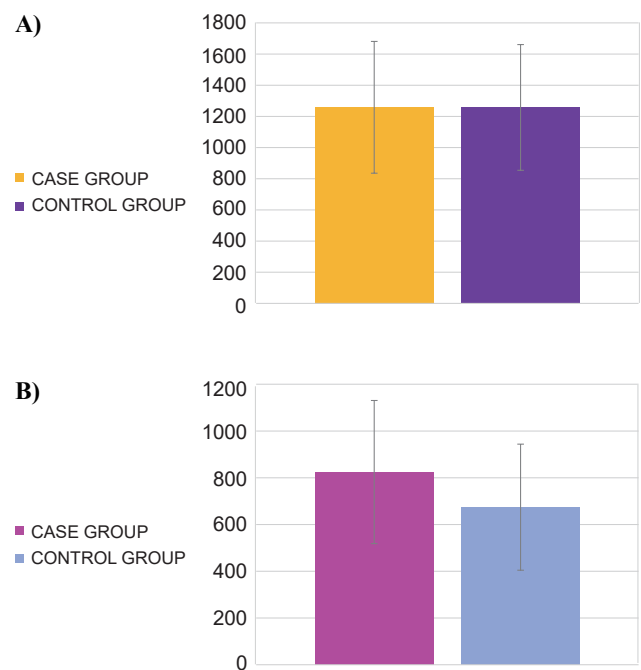


Figure 2. Results of T lymphocyte quantitation in the study groups. A) CD4⁺ T cells (cells/ μ l); B) CD8⁺ T cells (cells/ μ l).

of CD8⁺ T cells between infected children with *S. pyogenes* and control individuals. However, under the same statistical conditions, there is no significant difference in the quantitation of CD4⁺ T cells. A study carried out with monocytes from healthy donors which were stimulated with a strain of *S. pyogenes* isolated from children with bacteremia revealed that infection by this bacteria induces the expression of IL-2 messenger RNA (mRNA) and other cytokines (12). According to this finding, the present study shows an increased expression of this cytokine mRNA in samples of patients with this pathogen infection in comparison with those which were free of it. It is expected that because of this infection and with the results showing the expression of IL-2 mRNA had a higher product of protein expression in plasma, however, although a statistically significant difference was found, the highest expression of this cytokine in plasma was present in the infection-free samples. Gene expression can be controlled at various stages, which are divided into: “control at transcription level”, “control at processing level” and “control at translational level” (13). The control of gene activity has as general purpose: the organism can adapt to the properties of various cell types for their benefit (14). A key point in the regulation of gene expression is the control in the cytoplasm of the mRNA translation. In the last decade, micro-RNA (miRNA) and siRNA (small interfering RNA) have emerged as important regulators of translation and elimination of mRNAs (15), more than 800 individual miRNAs have been identified in humans, it is estimated that they regulate 74-92% of mRNAs (16) and these repress translation by several mechanisms including: inhibition of translation initiation, inhibition of elongation in the translation, premature translational termination and co-translational degradation of proteins, there is evidence of an expression of these miRNAs in bacterial infections (17). This may explain somehow the fact that in samples with *S. pyogenes* infection there is a smaller amount of protein in plasma in relation to the samples from healthy individuals, however, further studies are required to endorse these possible explanations for these results.

It has been documented that in infection with *S. pyogenes*, specifically by its toxin A, the major histocompatibility complex type II (MHC II) is expressed on cell lines involved in immunity (18). This molecule is expressed on B lymphocytes, dendritic cells and monocytes/macrophages and is responsible for presenting antigens to CD4⁺ T helper cells (Th cells) (19). Therefore, it was expected to find a greater number of these lymphocytes in samples from infected individuals. Besides, *S. pyogenes* is an ex-

tracellular bacterium (20, 21) and its protein antigens activate Th cells (3). However, in the present study, there was no difference in the numbers of CD4⁺ T cells between cases and controls.

Although *S. pyogenes* is considered as extracellular, it has mechanisms that allow it to be found within epithelial, endothelial and within neutrophil cells, this is due to its pathogenicity factors (fibronectin binding proteins), but these internalization factors have not been completely elucidated (22, 23), which explains only in part, the fact of a greater amount of cytotoxic CD8⁺ T cells (CTL). It was reported that when the microorganisms are in the interior of cell, the infection should be eradicated through CTL elimination of infected cells (3). Furthermore, in previous studies of children with pneumonia, researchers found bacterial-viral co-infections, especially respiratory syncytial virus, rhinovirus, human bocavirus, metapneumovirus, parainfluenza and influenza viruses co-existing with bacteria such as: *Streptococcus pneumoniae*, *Haemophilus influenzae*, *Moraxella catarrhalis*, and *S. pyogenes* (24). The samples of the present study were further analyzed to detect a co-infection with both respiratory syncytial virus and the human adenovirus (25), however, this coinfection was not found. A possible co-infection with influenza virus cannot be excluded. In a previous study, it was found that mortality by *S. pyogenes* was associated with an additional infection with influenza virus (7). Besides, in studies of mice, researchers also found this bacterial-viral co-infection (26). It has been reported that transmission of influenza virus requires certain characteristics of humidity and temperature and its incidence is related with wintertime and in rainy season (27). It is important to note that sample collection mostly occurred in the July to September period, corresponding to the rainy season. Therefore, it cannot be discarded the possible association of *S. pyogenes* with the influenza virus, due to the season; thus it could also explain the high amount of CTL in *S. pyogenes* infection. Two assumptions may explain the lower amounts of Th cells found: that *S. pyogenes* resides intracellularly, or a viral co-infection. In both cases, the response would be mostly by CD8⁺ T cells.

CONCLUSIONS

We conclude that infections by *S. pyogenes* in young children lead to an increased expression of IL-2 mRNA. Contrary to expectations, a lower protein expression of this cytokine was found in samples of children infected with *S. pyogenes*. In addition, there was a greater amount

of CD8⁺ T cells and a minor amount of CD4⁺ T cells. Certainly more studies to identify a possible control of mRNA translation and to reveal whether different viruses may be associated with infection by *S. pyogenes* are needed.

CONFLICT OF INTERESTS

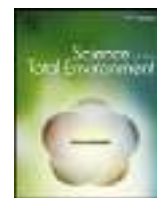
The authors declare that no conflicting interests exist.

ACKNOWLEDGEMENTS

This study was supported by Juárez University of Durango State, Durango, Mexico.

REFERENCES

- Gerner W, Käser, Saalmuller. Porcine T lymphocytes and NK cells, an update. *Dev. Comp. Immunol.* 2009; 33 (3): 310-320.
- Wang M, Windgassen D, Papoutsakis E. Comparative analysis of transcriptional profiling of CD3⁺, CD4⁺ and CD8⁺ T cells identifies novel immune response players in T-cell activation. *BMC Genomics.* 2008; 9 (1): 225.
- Abbas A, Lichtman A, Pillai S. Cellular and molecular immunology. 6th edition. Philadelphia, PA: Elsevier Saunders. 2008.
- INSIGHT-ESPRIT Study Group, SILCAAT Scientific Committee, Abrams D, Lévy Y, Losso MH, et al. Interleukin-2 therapy in patients with HIV infection. *N. Engl. J. Med.* 2009; 361 (16): 1548-1559.
- Leung AK, Kellner JD, Davies HD. Respiratory syncytial virus bronchiolitis. *J. Natl. Med. Assoc.* 2005; 97 (12): 1708-1713.
- Bessen DE. Population biology of the human restricted pathogen, *Streptococcus pyogenes*. *Infect. Genet. Evol.* 2009; 9 (4): 581-593.
- Dmitriev AV, Chaussee MS. The *Streptococcus pyogenes* proteome: maps, virulence factors and vaccine candidates. *Future Microbiol.* 2010; 5 (10): 1539-1551.
- Chiappini N, Seubert A, Telford JL, et al. *Streptococcus pyogenes* SpyCEP influences host-pathogen interactions during infection in a murine air pouch model. *PLoS One.* 2012; 7 (7): e40411.
- Paustian T. Through the microscope. 4th edition. Middleton: Consortia. 2012.
- Chomczynski P, Sacchi N. Single-step method of RNA isolation by acid guanidinium thiocyanate-phenol-chloroform extraction. *Analytical Biochemistry.* 1987; 162 (1): 156-159.
- Chen G, Kronenberger P, Teugels E, De Greve J. Influence of RT-qPCR primer position on EGFR interference efficacy in lung cancer cells. *Biol. Proced. Online.* 2010; 13: 1.
- Veckman V, Miettinen M, Pirhonen J, et al. *Streptococcus pyogenes* and *Lactobacillus rhamnosus* differentially induce maturation and production of Th1-type cytokines and chemokines in human monocyte-derived dendritic cells. *J. Leukoc. Biol.* 2004; 75 (5): 764-771.
- Schwanhauser B, Busse D, Li N, et al. Global quantification of mammalian gene expression control. *Nature.* 2011; 473 (7347): 337-342.
- Brawand D, Soumillon M, Necsulea A, et al. The evolution of gene expression levels in mammalian organs. *Nature.* 2011; 478 (7369): 343-348.
- Valencia-Sanchez MA, Liu J, Hannon GJ, Parker R. Control of translation and mRNA degradation by miRNAs and siRNAs. *Genes Dev.* 2006; 20 (5): 515-524.
- Kong YW, Cannell IG, de Moor CH, et al. The mechanism of microRNA mediated translation repression is determined by the promoter of the target gene. *Proc. Natl. Acad. Sci. USA.* 2008; 105 (26): 8866-8871.
- Singh PK, Singh AV, Chauhan DS. Current understanding on microRNAs and its regulation in response to mycobacterial infections. *J. Biomed. Sci.* 2013; 20: 14.
- Ulrich RG. Vaccine based on a ubiquitous cysteinyl protease and streptococcal pyrogenic exotoxin A protects against *Streptococcus pyogenes* sepsis and toxic shock. *J. Immune. Based Ther Vaccines.* 2008; 6: 8.
- Rocha N, Neefjes J. MHC class II molecules on the move for successful antigen presentation. *The EMBO journal.* 2007; 27 (1): 1-5.
- Li P, Li M, Lindberg MR, et al. PAD4 is essential for antibacterial innate immunity mediated by neutrophil extracellular traps. *J. Exp. Med.* 2010; 207 (9): 1853-1862.
- Abbot EL, Smith WD, Soiu GP, et al. Pili mediate specific adhesion of *Streptococcus pyogenes* to human tonsil and skin. *Cellular Microbiology.* 2007; 9 (7): 1822-1833.
- Thulin P, Johansson L, Low DE, et al. Viable group A streptococci in macrophages during acute soft tissue infection. *PLOS Medicine.* 2006; 3 (3): 371-379.
- Ogawa T, Terao Y, Okuni H, et al. Biofilm formation or internalization into epithelial cells enable *Streptococcus pyogenes* to evade antibiotic eradication in patients with pharyngitis. *Microbial pathogenesis.* 2011; 51 (1-2): 58-68.
- Honkinen M, Lahti E, Osterback R, et al. Viruses and bacteremia in sputum samples of children with community-acquired pneumonia. *Clin. Microbiol. Infect.* 2011; 18 (3): 300-307.
- Gutierrez-Martinez A. El papel del perfil proteómico como diagnóstico en co-infecciones bacteriano-virales en niños de 0 a 5 años [master thesis]. Durango, México: Facultad de Ciencias Químicas. 2014.
- Okamoto S, Kawabata S, Nakagawa I, et al. Influenza A virus-infected hosts boost an invasive type of *Streptococcus pyogenes* infection in mice. *J. Virol.* 2003; 77 (7): 4104-4112.
- Lowen AC, Mubareka S, Steel J, Palese P. Influenza virus transmission is dependent on relative humidity and temperature. *PLOS Pathogens.* 2007; 3 (10): 1470-1476.



Chemical and surface analysis during evolution of arsenopyrite oxidation by *Acidithiobacillus thiooxidans* in the presence and absence of supplementary arsenic



Hugo Ramírez-Aldaba^a, O. Paola Valles^{a,b}, Jorge Vazquez-Arenas^{c,1}, J. Antonio Rojas-Contreras^b, Donato Valdez-Pérez^d, Estela Ruiz-Baca^a, Mónica Meraz-Rodríguez^e, Fabiola S. Sosa-Rodríguez^f, Ángel G. Rodríguez^g, René H. Lara^{a,*}

^a Facultad de Ciencias Químicas, Departamento de Ciencia de Materiales, Universidad Juárez del Estado de Durango (UJED), Av. Veterinaria S/N, Circuito Universitario, Col. Valle del Sur, 34120 Durango, Dgo, Mexico

^b Instituto Tecnológico de Durango, UPIDET, Av. Felipe Pescador 1830 Ote. Col. Nueva Vizcaya, 34080 Durango, Dgo, Mexico

^c Departamento de Química, Universidad Autónoma Metropolitana-Iztapalapa, Av. San Rafael Atlixco 186, Col. Vicentina, Iztapalapa, México DF 09340, Mexico

^d Instituto Politécnico Nacional, UPALM, Edif. Z-4 3er Piso, CP 07738 México D.F, Mexico

^e Departamento de Biotecnología, Universidad Autónoma Metropolitana-Iztapalapa, Av. San Rafael Atlixco 186, Col. Vicentina, Iztapalapa, México DF 09340, Mexico

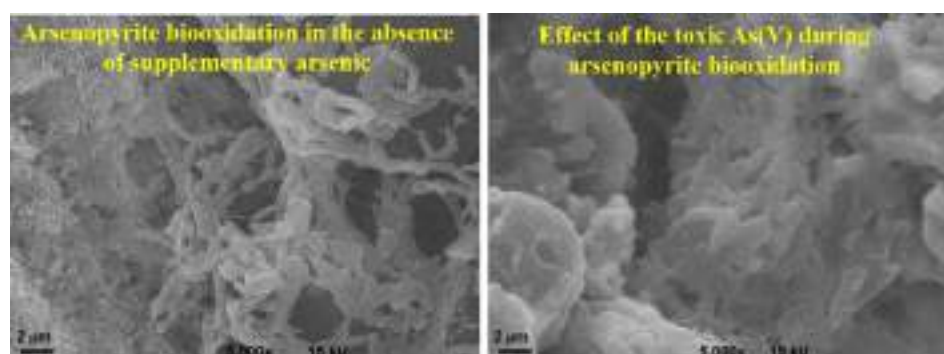
^f Universidad Autónoma Metropolitana-Azcapotzalco, Área de Crecimiento Económico y Medio Ambiente, Departamento de Economía, Av. San Pablo 180, Azcapotzalco, México DF 02200, Mexico

^g CIACyT, Universidad Autónoma de San Luis Potosí, Av. Sierra Leona 550, Lomas 2da sección, 78230 San Luis Potosí, SLP, Mexico

HIGHLIGHTS

- Biofilm structures occur as compact micro-colonies.
- Surface transformation reactions control arsenopyrite and cell interactions.
- Toxic arsenic does not limit biofilm formation but damage its evolution.
- Biofilm adhesion forces are lowered in the presence of supplementary arsenic.
- Synthesis of protein is mitigated in the presence of supplementary arsenic.

GRAPHICAL ABSTRACT



ARTICLE INFO

Article history:

Received 10 February 2016

Received in revised form 18 May 2016

Accepted 19 May 2016

Available online 14 June 2016

Editor: D. Barcelo

Keywords:

Arsenopyrite biooxidation

ABSTRACT

Bioleaching of arsenopyrite presents a great interest due to recovery of valuable metals and environmental issues. The current study aims to evaluate the arsenopyrite oxidation by *Acidithiobacillus thiooxidans* during 240 h at different time intervals, in the presence and absence of supplementary arsenic. Chemical and electrochemical characterizations are carried out using Raman, AFM, SEM-EDS, Cyclic Voltammetry, EIS, electrophoretic and adhesion forces to comprehensively assess the surface behavior and biooxidation mechanism of this mineral. These analyses evidence the formation of pyrite-like secondary phase on abiotic control surfaces, which contrast with the formation of pyrite (FeS₂)-like, orpiment (As₂S₃)-like and elementary sulfur and polysulfide (S_n²⁻/S⁰) phases found on biooxidized surfaces. Voltammetric results indicate a significant alteration of arsenopyrite due to (bio)oxidation. Resistive processes determined with EIS are associated with chemical and electrochemical

* Corresponding author.

E-mail addresses: lcrh75@ujed.mx, lcrh75@hotmail.com (R.H. Lara).

¹ CONACYT research fellow.

Acidithiobacillus thiooxidans
 Direct cell attachment
 Electrochemical impedance spectroscopy
 Toxic arsenic
 Biofilm modification

reactions mediated by (bio)oxidation, resulting in the transformation of arsenopyrite surface and biofilm direct attachment. Charge transfer resistance is increased when (bio)oxidation is performed in the presence of supplementary arsenic, in comparison with lowered abiotic control resistances obtained in its absence; reinforcing the idea that more stable surface products are generated when As(V) is in the system. Biofilm structure is mainly comprised of micro-colonies, progressively enclosed in secondary compounds. A more compact biofilm structure with enhanced formation of secondary compounds is identified in the presence of supplementary arsenic, whereby variable arsenopyrite reactivity is linked and attributed to these secondary compounds, including S_n^{2-}/S^0 , pyrite-like and orpiment-like phases.

© 2016 Elsevier B.V. All rights reserved.

1. Introduction

Arsenopyrite (FeAsS) is the most abundant arsenic-bearing sulfide mineral (SM) in lithosphere, whereby its reactivity has become important for bioleaching operations such as: mining industry (recovery of valuable metals, i.e. Au, Ag), environmental processes (bioremediation of arsenic-bearing soils, acid rock drainage (ARD), mine wastes, electrokinetic processes for soil cleaning) (Benzaazoua et al., 2007; Wang and Zhao, 2009; Kim et al., 2012; Ko et al., 2013). Bioleaching is based on the application of sulfur-oxidizing (SOM) and/or iron-oxidizing (IOM) microorganisms in tanks, heaps, and polluted soils (Tuovinen et al., 1994; Nguyen et al., 2015). *Leptospirillum ferrooxidans*, *Acidithiobacillus ferrooxidans* and *Acidithiobacillus thiooxidans* are included among the most significant mesophilic IOM and/or SOM used to achieve sustained bioleaching reactions (Rohwerder and Sand, 2007; Rawlings, 2008). Most bioleaching operations are focused on studying mineralogical aspects, bulk leaching parameters, among others, using *A. ferrooxidans* and mixed cultures containing this microorganism (Falco et al., 2003; Jin et al., 2012), since it efficiently utilizes the Fe^{2+}/Fe^{3+} cycle to directly oxidize reduced sulfur species from surface mineral (i.e. S^{2-} , S^0), acting concomitantly as IOM/SOM (Rohwerder et al., 2003). The single role of SOM *A. thiooxidans* is to carry out the oxidation of sulfur compounds (i.e. S_n^{2-}/S^0) from altered SM surface, producing bioacidification which maintains soluble Fe(III) as oxidant agent (Rodríguez et al., 2003; Jin et al., 2012). This process has received less attention in spite of its great potential for bioleaching operations of arsenic-bearing SM (i.e. FeAsS, As_2S_3 , As_2S_2) (Wang and Zhao, 2009; Ko et al., 2013). Thus, the study of SM biooxidation mechanisms by single *A. thiooxidans* would certainly enable a better understanding of its contribution in mixed cultures, since its metabolic conditions influencing complex reactions, coupled phenomena and rates are comprehensively isolated.

Bioleaching mechanisms (i.e. kinetics and transport phenomena) arising at the interface biofilm/SM strongly rely on transient biofilm properties (Sharma et al., 2003; Harneit et al., 2006; Devasia and Natarajan, 2010). The presence of toxic metals or metalloids (i.e. As, Cr, Hg) (Koechler et al., 2015) can modify the structure (i.e. proteins, lipids, exopolysaccharides) and performance of these biofilms (Ram et al., 2005; Dave et al., 2008; Ngoma et al., 2015). Most evaluations on arsenopyrite have been carried out using *A. ferrooxidans* (Sharma et al., 2003; Dave et al., 2008; Fantauzzi et al., 2011), whence there is a lack of information concerning reaction mechanisms associated to arsenopyrite oxidation by *A. thiooxidans*. This analysis requires attention to establish a comparison of its surface reactivity in the presence of these microorganisms (i.e. mixed culture), and to draw on the advantages of its use. Additionally, the biooxidation of arsenopyrite particles represents a high risk for human health in areas where mining activities occur near to human settlements (Razo et al., 2004), whereby understanding the mechanisms for biologically mediated arsenic release in the presence of *A. thiooxidans* is critical to assess its impact in the incidence of numerous cancers (i.e. skin, bladder, lungs) (Yoshida et al., 2004). A comprehensive examination of biofilm structure, chemical and surface analysis for arsenopyrite biooxidation by *A. thiooxidans* in the presence and absence of supplementary arsenic has not been conducted to our current state of knowledge. Furthermore, this information

is relevant to account for the role of stressing environments on attachment properties during arsenopyrite bioleaching, and its influence on biofilm organization, evolution and performance. An environment of this type simulating real bioleaching SM conditions includes the presence of supplementary arsenic in the system (Dopson et al., 2003; Hong et al., 2016), i.e. pentavalent species under oxidizing conditions (Chen et al., 2004; Leng et al., 2009), which can potentially affect SM and cell interaction. Thus, the aim of this study is to comprehensively assess the surface chemistry and mechanism of arsenopyrite biooxidation by SOM *A. thiooxidans*, and monitor its changes in the presence of supplementary arsenic. The analyses involve surface speciation and mineral reactivity using electrochemical (cyclic voltammetry, electrochemical impedance spectroscopy), spectroscopic (Raman) and microscopic (SEM-EDS, AFM) techniques at different stages of the biooxidation processes. Additionally, biochemical and biophysical methods are applied to quantify total protein production and its effect on cell adhesion forces. These parameters are indicative of structural and organization properties of biofilm to control environmental parameters inducing an optimal performance. It is expected that these results contribute to gain a better understanding of relevant factors influencing biofilm formation and performance during arsenopyrite biooxidation.

2. Experimental

2.1. Arsenopyrite sample

Pure arsenopyrite crystals were obtained from Velardeña in the State of Durango (Mexico), which is a well-known site for exploitation of auriferous ore bearing minerals such as arsenopyrite (Pinet and Tremblay, 2009). Selected crystals were digested in acid (HCl + HNO₃, 3:1 v/v), and the resultant solutions were analyzed by microwave plasma-atomic emission spectrometry (AES-MP, Agilent 4100 spectrometer) to evaluate mineral composition and impurities. Scanning electron microscopy (ZEISS-DSM950 coupled to EDX system) and X-ray diffraction (XRD, Rigaku DMAX 2200, 2 θ angle = 0.02, from 10 to 90°, using CuK α radiation) were used to examine impurities contained in crystals and corroborate arsenopyrite identity, respectively. Selected crystals were employed for the construction of massive arsenopyrite electrodes (MAE) with an exposed surface area ranging from ~0.8 to ~1.0 cm². MAE specimens were constructed using rectangular coupons (dimensions ~2 mm width, ~6 mm length and ~2 mm thickness), and subsequently polished to obtain a mirror-like surface prior to each experiment. The quality of MAE specimens is guaranteed by selecting specimens with only electrical resistivity lower than 50 Ω , bearing in mind the semiconductive features of some of the mineral phases.

2.2. Potentiostatic oxidation of arsenopyrite

Potentiostatic oxidation of MAE surfaces allows a rapid, significant and quasi-homogeneous generation of surface sulfur compounds (i.e. S_n^{2-}/S^0), thus, enhancing the development of a biofilm which generates surface products for their subsequent chemical and surface analyses. MAE specimens were successfully oxidized in ATCC-125 (American Type Culture Collection) solution (acidified with H₂SO₄ at pH 2.0) at a

potentiostatic anodic pulse (E_a) of 1.21 V vs. SHE during 1 h using a Biologic SP-150 potentiostat coupled to a personal computer. This E_a was selected according to previous voltammetric and chronoamperometric analyses conducted for pristine arsenopyrite samples in the same culture solution. Potentiostatic oxidation was carried out in a Pyrex™ glass three-electrode cell, using a working electrode of MAE, counter electrode of graphite rod (Alfa Aesar, 99.9995% purity), and a saturated sulfate electrode (0.615 V vs. the Standard Hydrogen Electrode, SHE) as reference. After potentiostatic alteration of MAE, the resultant surfaces (referred as eMAE along the text) were modified to S_n^{2-}/S^0 and pyrite (FeS_2)-like compounds (Figs. 1b and 4b). S_n^{2-}/S^0 phases act as electron donors (energy source) for *A. thiooxidans* during altered arsenopyrite biooxidation (Rohwerder et al., 2003; Jin et al., 2012), whereas pyrite-like structures can be further oxidized to S_n^{2-}/S^0 under acidified ATCC-125 conditions (ESM, Fig. S1c and S1d), and therefore, cell attachment will be stimulated and driven by the metabolic capability of *A. thiooxidans* (i.e. substrate for biooxidation) (Sampson et al., 2000; Harneit et al., 2006; Devasia and Natarajan, 2010).

2.3. Biofilm formation and biooxidation assays

The strain used in this study was *A. thiooxidans* ATCC no. 19377. It was aerobically cultivated at 28–30 °C in 50 mL of acidified ATCC-125

solution (pH 2.0). This medium contained per liter: 10 g S^0 , 3.0 g KH_2PO_4 , 0.4 g $(NH_4)_2SO_4$, 0.5 g $MgSO_4 \cdot 7H_2O$, 0.25 g $CaCl_2 \cdot 2H_2O$ and 0.01 g $FeSO_4 \cdot 7H_2O$ (JT Baker). The medium was distributed in 250 mL Erlenmeyer flasks and sterilized using an autoclave at 121 °C for 15 min, whereas S^0 and the eMAE were separately placed in glass Petri dishes and statically sterilized under UV irradiation for 2 h. *A. thiooxidans* cells were grown until exponential growth phase attained around 14 days with an average biomass concentration of $\sim 10^8$ cells per mL. Cell counting was carried out using UV-Vis technique (Hach 5500 spectrophotometer) by relating biomass content to absorbance measurements. 5 mL of this culture were used as inoculum in biotic experiments (biooxidation assays). Sterilized eMAE surfaces were placed in 50 mL ATCC-125 culture medium containing $\sim 10^7$ cells of *A. thiooxidans* per mL (pH 2.0) (batch system), under sterile conditions. Biooxidation assays were conducted in the presence and absence of supplementary arsenic (0.2 M $NaH_2AsO_4 \cdot H_2O$, JT Baker) (Collinet and Morin, 1990; Leng et al., 2009) and incubated aerobically at 28–30 °C. Abiotic control assays were also carried out to establish a comparison between chemical and biological oxidation. The selected supplementary As(V) concentration was chosen to induce biofilm stress, since *A. thiooxidans* possesses *Ars-A*, *Ars-B* and *Ars-C* genes that encode the enzymatic machinery to detoxify toxic As(V) via dissimilatory reduction to less toxic As(III) (Dopson et al., 2003; Bowen et al., 2013; Koehler et al.,

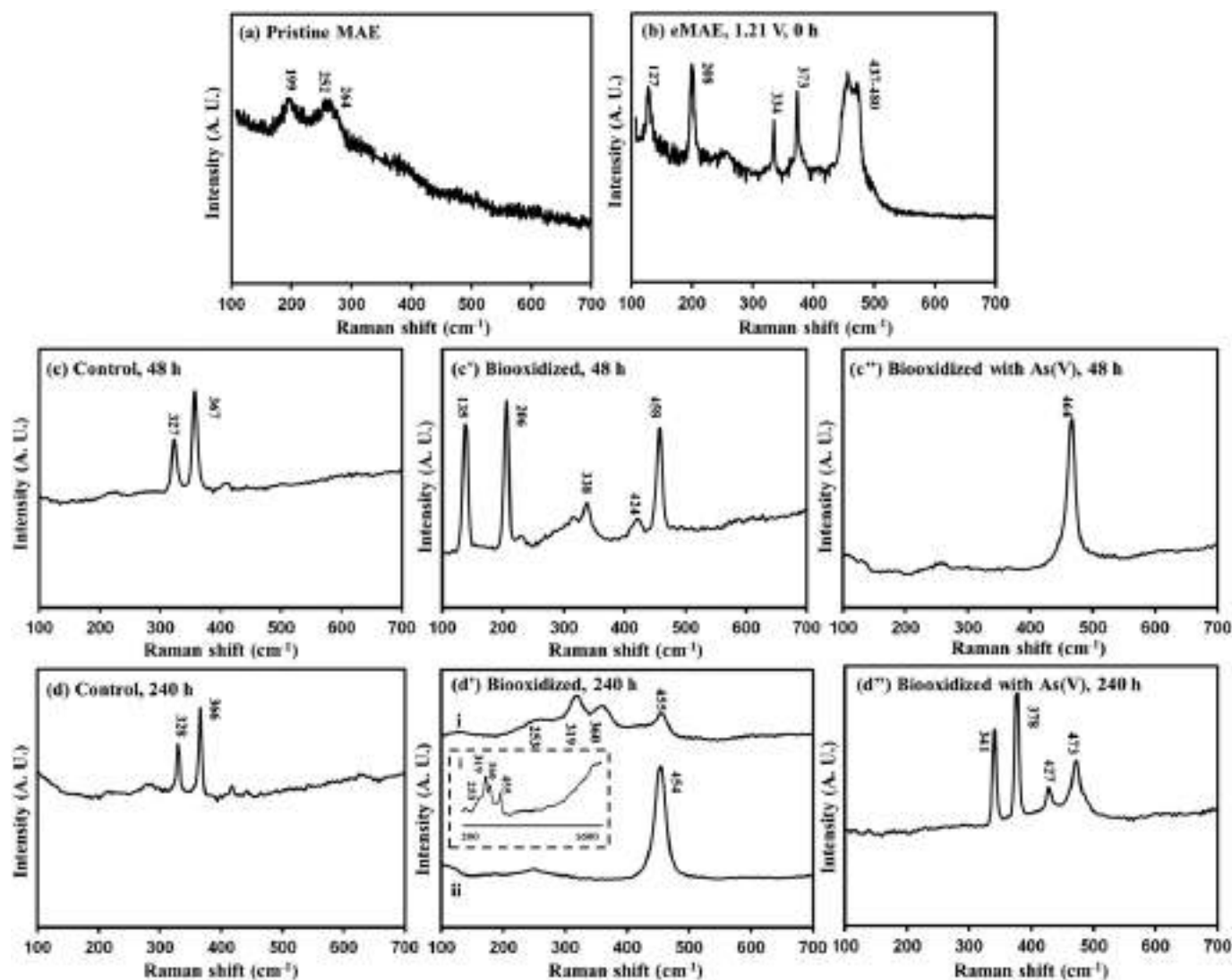


Fig. 1. Raman spectra of the pristine MAE (a), eMAE surface (b), abiotic control eMAE surfaces after 48 and 240 h of assay (c, d, respectively), biooxidized eMAE surfaces after 48 and 240 h of assay (c', d', respectively) and biooxidized eMAE surfaces with As(V) after 48 and 240 h of assay (c'', d'', respectively). 60 s of collection time. $\lambda = 514$ nm.

2015). Low or negligible effects of toxic As(V) are expected for planktonic cells at the beginning of biotic experiments, assuming that *A. thiooxidans* attach fast enough to surface as occurs for *A. ferrooxidans* (Nöel et al., 2010; Florian et al., 2011). The stability of As(V) compounds has been established according to thermodynamics and laboratory observations published in Lu and Zhu (2011). Resulting eMAE surfaces after biooxidation assays in the absence of supplementary arsenic are referred as 'biooxidized eMAE surfaces', whereas those after biooxidation assays in the presence of supplementary arsenic are referred as 'biooxidized eMAE surfaces with As(V)'. Resulting eMAE surfaces after abiotic experiments are referred as 'abiotic control eMAE surfaces'. Abiotic control, biooxidized and biooxidized eMCE surfaces with As(V) were collected at 1, 12, 24, 48, 72, 120 and 240 h, dried with a direct flow of chromatographic grade N₂ current, and maintained under inert conditions until further microscopic, spectroscopic and electrochemical characterizations. All control and biooxidation assays were carried out at least in duplicate.

2.4. Electrochemical study

All variants of eMAE surfaces were analyzed using Cyclic voltammetry (CV, negative scans) and Electrochemical Impedance Spectroscopy (EIS) in a Bio-logic SP-150 potentiostat which included a SP-150_Z FRA module. Voltammetric experiments were performed using a typical Pyrex™ three-electrode cell as described in section 2.2; the potential scan was conducted between -1.2 and 0.8 V vs. SHE and using 20 mV s⁻¹. Working electrodes of all variants of eMAE surfaces were characterized in acidified ATCC-125 solution (pH 2.0), which was previously deaerated by N₂ sparging during 20 min and an inert atmosphere of N₂ was kept throughout the experiments. For all electrochemical measurements, the open circuit potential (OCP_{i=0}) was monitored until reaching a steady-state value (± 20 mV), before conducting the CV and EIS measurements. Successively, EIS spectra (Nyquist plots) were collected under OCP mode using a small amplitude voltage of 10 mV from sine to sine, and scanning the frequency range from 0.01 Hz to 0.5 MHz. All EIS spectra were successfully fitted to equivalent electric circuits (EQs) to analyze the data (Boukamp, 1989; Liu et al., 2011).

2.5. Surface and spectroscopic analysis

All collected surfaces were analyzed using scanning electron microscopy (SEM-EDS), atomic force microscopy (AFM) and Raman spectroscopy. Raman spectra were recorded with a Horiba XploRA™ PLUS spectrometer coupled to a SWIFT™ v2 confocal imaging module. The samples were excited by a solid-state laser beam at $\lambda = 532$ nm. Raman performance was validated using a Si wafer disc by assuming a single sharp peak at 521 cm⁻¹. Raman backscattering showed a signal/noise ratio > 100 for Si analyses. The vibrational range was from 100 to 750 cm⁻¹ as S_n²⁻/S⁰ and main arsenic-bearing phases show their main active modes within this interval (Mycroft et al., 1990; Márquez et al., 2012). At least 10 Raman spectra were collected for each arsenopyrite surface. SEM analysis was carried out using a ZEISS-DSM950 coupled to an EDX system. Previously, biooxidized eMAE and biooxidized eMAE surfaces with As(V) (containing biofilm structures) were fixed by immersion in a 3% (m/m) of glutaraldehyde (grade I, Sigma Aldrich) phosphate buffer (pH 7.2) for 24 h at 4 °C. Subsequently, they were rinsed with a phosphate buffer at pH 7.2. Dehydration of biofilms was carried out by successive rinsing in solution with increasing ethanol (ultrapure, Sigma Aldrich) from 10 to 100% (v/v). Excess of ethanol was removed carefully from the samples and they were frozen instantly with liquid nitrogen and dried by lyophilization (Labconco FreeZone Freeze Dry System) at 0.13 mbar and -41 °C for 2 h; afterwards samples were kept in sealed glass vials. The dehydrated samples were mounted on a sample holder with a double-adhesive carbon tape and coated with an Au thin film. AFM analysis was carried out using a

Nanoscope AFM multimode IIIa microscope. Narrow and wide regions were visualized to obtain topographic images by tapping mode in air (scan rate of 0.5–1 Hz). The Si₃N₄ cantilever showed a free resonance frequency between 275 and 325 kHz and a constant between 31.18 and 44.54 N m⁻¹ during these experiments. Roughness (Ra, nm) and root mean square (Rq, nm) of samples were also evaluated to generate a complete description of surface behavior. Force-separation (F–Z) curves were also acquired using contact mode in air in 1 μm². At least 300 curves were taken from each specific surface, and 20% of the obtained curves were randomly analyzed. The Si₃N₄ cantilever showed a free resonance frequency between 90 and 115 kHz and a constant between 1.08 and 2.03 N m⁻¹ during the collection of these curves.

2.6. Total protein extraction in biofilms and SDS-PAGE

Quantification of total protein in *A. thiooxidans* biofilms in the presence and absence of supplementary As(V) was carried out using the Bradford protein assay (Bradford, 1976). For total protein extraction, different eluents (NaCl, NaOH, Na₂EDTA, buffer A [0.5% SDS, 10 mM DTT, 50 mM Tris-HCl pH = 7.5, 10 mM EDTA and 1 mM PMFS], and ATCC-125) were tested from which buffer A showed the highest extraction efficiency. Biofilms of *A. thiooxidans* were scraped from each biooxidized surface and placed on Eppendorf™ vials. The cells were washed with 0.15 M NaCl and centrifuged (7000g) for 15 min at 4 °C, then, obtained pellets were resuspended using 300 μL of sterile water. The cells were lysed with glass beads (0.45 mm of diameter) in 300 μL of buffer A by alternate periods of breaking (30 s) and cooling (60 s) for 5 min. The cell homogenate was centrifuged (13,000g) for 10 min at 4 °C. Proteins were precipitated with 70% ethanol (v/v) at -20 °C for 2 h and stored at -70 °C until further use. Protein concentration was determined using bovine serum albumin as standard and a UV-vis 50 Bio spectrophotometer. Electrophoretic analysis was also conducted to characterize protein size for biofilms in the presence and absence of supplementary arsenic. Proteins were separated by sodium dodecyl sulfate polyacrylamide gel electrophoresis (SDS-PAGE) according to Laemmli (1970) in a Mini-protean III Cell (Bio-Rad) and silver stained using Dodeca™ silver stain kit (Bio Rad). Images were captured using a ChemiDoc™ XRS + System (Bio-Rad).

3. Results and discussion

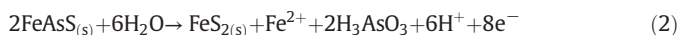
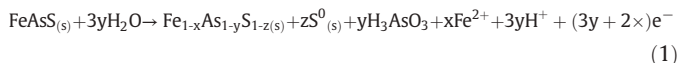
3.1. Chemical analysis of pristine arsenopyrite samples

Chemical analyses showed the following composition for pristine sample: 96.56 (± 0.2) wt% of FeAsS, 1.42 (± 0.3) wt% of PbS, 0.88 (± 0.1) wt% of ZnS and 1.16 (± 0.3) wt% of SiO₂. SEM-EDS indicated that these impurities occurred as inclusions in FeAsS crystals, which correspond to the diffraction pattern JCPDS card no. 14–218.

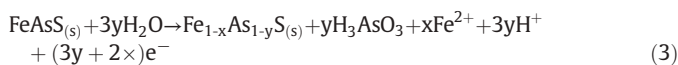
3.2. Spectroscopy analysis of pristine, abiotic control and biooxidized samples

Fig. 1a shows the Raman spectrum for pristine MAE, displaying typical broad peaks at ~ 199 , ~ 252 and ~ 264 cm⁻¹ (McGuire et al., 2001; Márquez et al., 2012). A summary of characteristic Raman transitions are described in Table S1 (electronic supplementary material, ESM) for pyrite (FeS₂), polysulfides (S_n²⁻), elemental sulfur (S⁰), orpiment (As₂S₃) and realgar (As₂S₂). Raman spectra for As₂S₃, S⁰, pristine and oxidized FeS₂ in acidified ATCC-125 culture solution (pH 2.0) are also shown for comparison purposes (ESM, Fig. S1). Abiotic control assays in the presence of supplementary arsenic were also performed; however, they are not included since identified secondary compounds were essentially the same as those observed in the absence of supplementary arsenic, thus, suggesting that supplementary arsenic does not significantly modify the stoichiometry of surface products resulting from chemical oxidation of arsenopyrite. This valuable information is used

to identify secondary (intermediate) compounds in this study. Under this consideration, the Raman spectrum of electrooxidized (altered) MAE specimen (eMAE surface, Fig. 1b) shows the formation of mainly S^0/S_n^{2-} (i.e. $Fe_{1-x}As_{1-y}S_{1-z}$, at 127, 208, 437–480 cm^{-1} , Table S1 and Fig. S1b) and pyrite-like compounds (at 334 and 373 cm^{-1} , Table S1 and Fig. S1c–d). The electrochemical formation of secondary compounds on eMAE surface can proceed according to the following overall reactions:



The eMAE surface (Fig. 1b) is then considered as the initial stage ($t = 0$ h) for abiotic control and biooxidation assays. Fig. 1c and 1d show abiotic controls for eMAE surfaces after 48 and 240 h of assay, respectively, where it is evident that arsenopyrite undergoes a slow chemical oxidation i.e. $Fe_{1-x}As_{1-y}S_{1-z}$ -like and S^0 compounds (Lara et al., 2010), particularly this reaction enhances the accumulation of refractory pyrite-like compounds as described by Eq. 2. The formation of pyrite-like compound is suggested instead of marcasite-like compound (a dimorph of pyrite) since Raman peak positions for this phase appear around 344 and 377 cm^{-1} , instead of 337 and 388 cm^{-1} for marcasite phase (Hope et al., 2001; White, 2009). Under the premise that As is heavier than Fe, the substitution of Fe atoms by As would rise the effective mass, resulting in a decrease of vibrational frequencies down to 334 and 373 cm^{-1} (i.e. the vibrational frequency of an harmonic oscillator is the square root of the elastic constant over the mass). Thus, both frequencies diminish for $Fe_{1-x}As_{1-y}S_{1-z}$ -like and pyrite-like compound, unlike marcasite possessing a similarly higher-frequency phonon. For the Raman analysis presented in this work, shifts of Raman peaks are expected due to mass changes in the structures of surface compounds, thus, modifying their vibrational frequencies. Fig. 1c' and 1d' present Raman spectra for biooxidized eMAE surfaces after 48 and 240 h of assay, respectively, which are the most relevant stages of arsenopyrite biooxidation. The formation of S^0 and pyrite-like phases in Fig. 1c' are evident after 48 h of assay (ESM, Table S1 and Figs. S1b–d); whereas two oxidized areas containing mainly S_n^{2-} and As_2S_3 -like compounds are identified after 240 h of assay for the same sample (Fig. 1d', i, ii, ESM, Table S1 and Fig. S1a). These results indicate a significant interaction between *A. thiooxidans* biofilms and arsenopyrite whereby specific secondary compounds are formed as a result of direct cell attachment to arsenopyrite surface (Liu et al., 2003; Devasia and Natarajan, 2010; Liu et al., 2011). After biooxidation of pyrite-like and S^0 compounds, resulting arsenopyrite surfaces are dominated by the formation of S_n^{2-} (i.e. $Fe_{1-x}As_{1-y}S$ -like, from 455 to 470 cm^{-1} , Fig. 1d', ii, Table S1) and As_2S_3 -like (Fig. 1d', i, Table S1 and Fig. S1a) species, according to the following overall reactions:



In the presence of supplementary arsenic in the system, the formation of S_n^{2-} (Fig. 1c'', Table S1, Eq. 4) and S_n^{2-} along with pyrite-like compounds (Fig. 1d'', Table S1) were observed after 48 and 240 h of assay, respectively, suggesting a significant arsenopyrite biooxidation by stressed *A. thiooxidans* biofilms. This behavior agrees with hazardous effects observed for toxic metal species (i.e. Cr, Hg, Ni) during cell attachment of leaching (Dave et al., 2008; Leng et al., 2009; Nguyen et al., 2015) and non-leaching bacteria (Lièvrement et al., 2009; Koechler et al., 2015). Note that arsenopyrite biooxidation by *A. ferrooxidans* under acidified M2 culture medium (pH 1.8) results in the formation

of realgar (As_2S_2)-like and ferric oxide compounds, thus limiting bacterial attachment to SM surface and enhancing the requirement of available Fe^{2+} species in the system (Liu et al., 2011). This is a different mechanism compared to the one performed by *A. thiooxidans* requiring direct cell attachment to SM (i.e. S_n^{2-}/S^0) (Harneit et al., 2006; Noël et al., 2010). These remarkable differences in the chemical surface speciation during arsenopyrite biooxidation by *A. ferrooxidans* and *A. thiooxidans* (refer to Eqs. 1 to 4) indicate the occurrence of more dynamic and complex interfacial processes occurring in the presence of *A. thiooxidans* due to substantial surface modifications and possible arsenic release, as described in the literature (Liu et al., 2011; Ko et al., 2013).

The pristine MAE and all variants of eMAE surfaces were also examined using AFM to evaluate the characteristics of cell attachment and biofilm structure (Fig. 2). A compilation of Ra and Rq data for these surfaces is given in Table 1 to obtain topographic information associated with secondary compounds; hence, these parameters are useful to examine further accumulation or depletion in surface structures (i.e. compounds, cells). Fig. 2a and 2b show images collected from pristine MAE and eMAE surfaces, respectively. The formation of quasi-homogeneous and well-distributed sub-micro sized S_n^{2-}/S^0 and pyrite-like compounds is evident on eMAE surface (Fig. 2b), and corroborated by the corresponding Ra and Rq values in Table 1, unlike the relative flat surface observed for pristine MAE (Fig. 2a). On the other hand, Fig. 2c and 2d show images collected from abiotic control eMAE surfaces after 48 and 240 h of assay, respectively. Ra and Rq obtained from these samples reveal that the highest values for abiotic control are observed at 48 h, whereas these parameters remain constant at longer times (Table 1), suggesting that no significant accumulation of secondary pyrite-like compounds occurs after 48 h of assay. This also confirms the presence of these refractory compounds during abiotic arsenopyrite oxidation, as a result of different surface roughness presented in the samples. As described in the Raman study (Fig. 1b–d) and Eq. 2, this process is attributed to chemical oxidation of potentiostatically generated S_n^{2-}/S^0 compounds by effect of the acidified ATCC-125 solution, leading to the formation of refractory pyrite-like structures. In contrast, Fig. 2c' and 2d', and Fig. 2c'' and 2d'' show typical AFM 3D images enhancing biofilm formation and details of specific cell and arsenopyrite interactions in the presence and absence of supplementary arsenic, respectively. Fig. 2c' reveals a clear response for attachment of *A. thiooxidans* cells (dimensions ~0.5 μm width, ~1–2 μm length, ~0.5 mm thickness) (Liu et al., 2003) to altered arsenopyrite surfaces, enabling the colonization of different S_n^{2-}/S^0 and pyrite-like compounds, in agreement with SEM-EDS analysis (see below). Another relevant feature observed are well-organized biofilms comprised of micro-colonies surrounded by secondary compounds after 48 h of assay (Fig. 2c'), whereas only attached cells partially or totally embedded in a profuse formation of secondary compounds are identified after 240 h of assay (Fig. 2d'). These observations are supported by Ra and Rq values which are higher in the biooxidized eMAE surfaces as time increases, likewise these parameters are higher than those obtained for abiotic control eMAE surfaces (Table 1). The significant formation and accumulation of secondary compounds is related to enhanced S_n^{2-}/S^0 and pyrite-like biooxidation by *A. thiooxidans* cells, regardless of the presence of toxic orpiment-like compound after 240 h of assay (Fig. 1d'). This significant stage for arsenopyrite biooxidation is related to a remarkable increase of cell density and abundant formation of secondary compounds (Fig. 1d', Table 1), enabling S_n^{2-}/S^0 modification, in agreement with Raman analysis (Fig. 1d'). A comparison of biofilms formed in the presence and absence of arsenic reveals that its formation is strongly affected by the availability of this element, generating a more compact biofilm structure in its presence, surrounded by secondary S_n^{2-} compounds after 48 h of assay on the biooxidized eMAE surface with As(V) (Fig. 2c''). However, none discernible biofilm but some spread attached cells are observed after 240 h of assay, accompanied by a profuse formation of secondary S_n^{2-} and pyrite-like compounds (Fig. 2d'', Table 1) enabling the partial covering

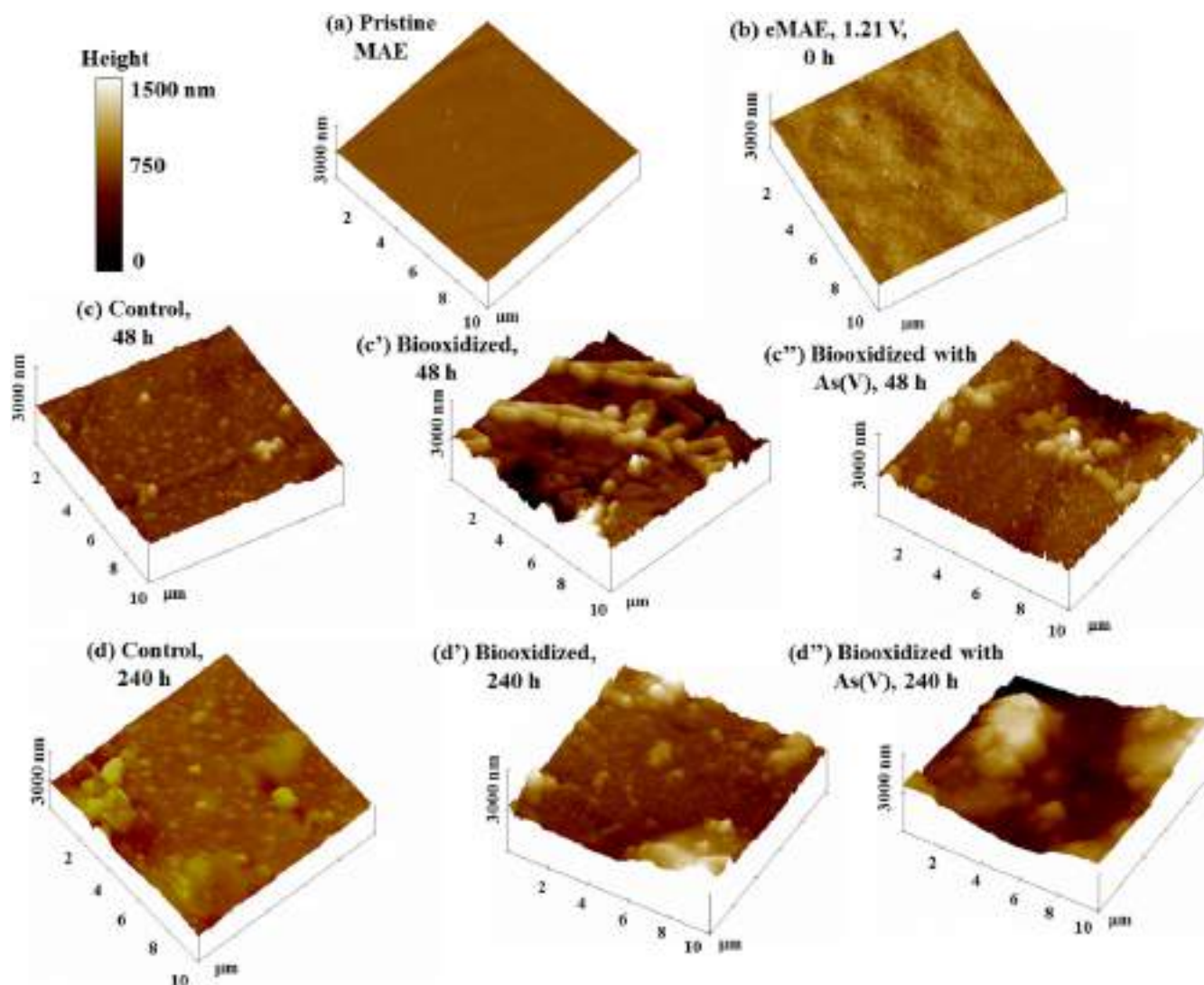


Fig. 2. Typical AFM 3D images of the pristine MAE surface (a), eMAE surface (b), abiotic control eMAE surfaces after 48 and 240 h of assay (c, d, respectively), biooxidized eMAE surfaces after 48 and 240 h of assay (c', d', respectively) and biooxidized eMAE surfaces with As(V) after 48 and 240 h of assay (c'', d'', respectively).

of *A. thiooxidans* cells in the presence of supplementary arsenic in the system, as indicated by Raman study (Fig. 1d''). A thick secondary/biofilm structure is formed after 240 h of assay in the presence of supplementary arsenic, as suggested by high Ra and Rq values (Fig. 2d'', Table 1). Additionally, the presence of orpiment-like compounds enables biofilm attachment and biooxidation process, as indicated in the Raman analysis (Fig. 1d'') and in agreement with literature review (Liu et al., 2011), thus suggesting that arsenic included in a solid phase is essentially innocuous to biofilm evolution (Fig. 2), in contrast with soluble species (Leng et al., 2009; Jin et al., 2012). However, it is necessary to further examine the specific biochemical effects of *A. thiooxidans* biofilms during their evolution (i.e. total proteins analysis, see below). *Acidithiobacillus* strains respond differently according to specific SM surface properties and physicochemical conditions (Devasia and Natarajan, 2010; Ngoma et al., 2015), since the absence of available ferrous concentrations in system allows starvation effects by *A. ferrooxidans* cells (Sharma et al., 2003; Tu et al., 2014), and because *A. thiooxidans* cells are able to perform sustained chalcopyrite biooxidation, in spite of cells partially covered by secondary covellite (CuS)-like compounds (Falco et al., 2003; Lara et al., 2013). Accordingly, biofilm and arsenopyrite interactions can be significantly modified in the presence and absence of supplementary arsenic in the system.

Complementary to AFM study, a compilation of adhesion forces measuring cell attachment of biofilms to surface is provided in Table 2 and displayed in Fig. 3. Note that adhesion forces are not intended to reflect 'real forces' of cell attachment in biofilms, instead, the curves of these forces illustrate extension (red lines, Fig. 3) and retraction (black lines, Fig. 3) between cantilever tip and substrate enabling indirect quantification of adhesion forces mediating cell attachment interaction to metal-SM surface. For the colonized surfaces, the cantilever tip is briefly trapped by cell surface in biofilms (i.e. EPS) inducing stronger tip and substrate interaction, respect to a flat or biofilm free substrate, allowing determination of adhesion forces (Kendall and Lower, 2004; Zhu et al., 2015). Force-separation curves show essentially similar behavior for all sampling times, examples of these experiments are shown in Fig. 3 for 48 h of assay. Adhesion forces for pristine MAE and eMAE ($t = 0$ h) are also obtained to assess the evolution of surface behavior (Fig. 3a, 3b, respectively, Table 2). The forces associated with interactions between eMAE and *A. thiooxidans* cells (spread and/or forming biofilms) are evaluated by comparing force data obtained for eMAE and those obtained after abiotic control and biooxidation experiments (with and without supplementary arsenic). The adhesion forces of pristine MAE surface is neglected due to its low value, in comparison with that obtained for eMAE, which exhibits an interaction force of

Table 1

Evolution of roughness (Ra, nm) and root mean square (Rq, nm) values, collected from pristine MAE, eMAE and all variants of eMAE surface areas in the ATCC-125 solution. Data average \pm standard deviation. Area of collection of $1 \mu\text{m}^2$.

Mineral sample	Ra, nm	Rq, nm
Pristine MAE	4.41 \pm 0.56	5.79 \pm 0.70
eMAE surface	10.28 \pm 1.54	13.52 \pm 1.32
Biooxidized eMAE surfaces		
1 h	9.52 \pm 0.67	11.90 \pm 0.18
12 h	14.95 \pm 2.21	15.43 \pm 3.25
24 h	33.89 \pm 3.24	38.90 \pm 4.69
48 h	41.03 \pm 2.67	43.90 \pm 5.18
72 h	51.93 \pm 2.98	56.12 \pm 6.57
120 h	71.23 \pm 5.71	75.90 \pm 5.19
240 h	90.38 \pm 8.41	112.5 \pm 9.10
Biooxidized eMAE surfaces with As (V)		
1 h	16.36 \pm 1.34	17.25 \pm 3.36
12 h	18.63 \pm 3.89	22.65 \pm 4.12
24 h	36.12 \pm 4.07	42.89 \pm 6.83
48 h	48.11 \pm 7.03	60.57 \pm 10.23
72 h	63.96 \pm 4.33	75.32 \pm 7.79
120 h	90.87 \pm 5.48	98.37 \pm 11.15
240 h	106.54 \pm 6.97	134.10 \pm 8.83
Abiotic control eMAE's		
1 h	10.36 \pm 1.34	11.25 \pm 3.36
12 h	13.63 \pm 3.89	15.65 \pm 4.12
24 h	16.12 \pm 4.07	17.89 \pm 6.83
48 h	28.11 \pm 7.03	30.57 \pm 10.23
72 h	23.96 \pm 4.33	26.32 \pm 7.79
120 h	25.87 \pm 5.48	24.23 \pm 11.15
240 h	21.70 \pm 7.84	26.71 \pm 2.24

\sim 0.93 nN (Fig. 3a–b and Table 2). Note the significant repulsive interaction associated with approaching the cantilever tip to the eMAE surface (extending curve, Fig. 3b); nevertheless, an attractive interaction is also identified (retracting curve, Fig. 3b) allowing quantification of force data (Kendall and Lower, 2004). The global interaction may then result from the combination of repulsive forces of the cantilever tip and the attractive force of semiconductive secondary phases (after chemical and biological oxidation), in agreement with analyses described above. Force data from abiotic control eMAE surfaces range from \sim 2.31 to \sim 2.68 nN (Fig. 3c, Table 2), which is related to the progressive accumulation of attractive pyrite-like compounds, in agreement with AFM (Figs. 2c–d and Table 1) and Raman (Figs. 1c–d and Table S1) studies. The highest interaction force is observed after 48 h of assay (Fig. 3c, Table 2), in agreement with the greatest accumulation of secondary compounds shown by AFM (Figs. 2c–d and Table 1). In contrast, interaction forces for biooxidized eMAE surfaces range from \sim 3.85 to \sim 3.52 nN, involving the highest interaction value after 48 h of assay, also indicating the best stage for biofilm attachment (Fig. 3c', Table 2). Differences between interaction forces for abiotic control and biooxidized surfaces indicate that cell adhesion forces are 1.75, 1.2, 1.48, 1.84, 1.11, 1.68 and 1.17 nN for 1, 12, 24, 48, 72, 120 and 240 h of biooxidation, respectively (Table 2). This information suggests that the highest adhesion forces are then observed for 48 and 120 h of assay, which can be attributed to greatest stages for total protein production (see Fig. 5 below), and therefore, mediating cell attachment (i.e. pili-type in EPS) (Bowen et al., 2013; Zhu et al., 2015). A correlation between cell adhesion forces and total protein production has been observed for SM and *A. ferrooxidans* (Zhu et al., 2012; Bowen et al., 2013), in agreement with our results. Note that adhesion forces ranging from \sim 1.1 to \sim 5 nN have been reported for interactions between *A. ferrooxidans* cells and chalcopyrite in the 9 K culture medium (Chandraprabha et al., 2010; Zhu et al., 2012), thus, our results (Fig. 3, Table 2) are in the same order of magnitude to these values. Nevertheless, such results were obtained with the bacterium-tip approaching strategy (Zeng et al., 2011; Zhu et al., 2015), suggesting that our indirect approach is adequate to

Table 2

Interaction (adhesion) forces acquired from pristine MPE, eMPE, and all variants of eMAE surfaces (data, $n = 30$). Area of collection of $1 \mu\text{m}^2$ (scan rate of 0.5–1 Hz). Contact mode in air. Data \pm standard deviation.

Mineral surface	Interaction forces (nN)			Experimentally calculated adhesion forces (nN)	
	Biooxidized eMAE	Biooxidized eMAE with As(V)	Control abiotic	Biooxidized eMAE	Biooxidized eMAE with As(V)
1 h	3.75 \pm 0.1	3.80 \pm 0.2	2.01 \pm 0.15	1.75	1.79
12 h	3.75 \pm 0.0	3.80 \pm 0.18	2.55 \pm 0.13	1.20	1.25
24 h	3.92 \pm 0.08	3.35 \pm 0.22	2.44 \pm 0.14	1.48	0.91
48 h	4.52 \pm 0.05	3.12 \pm 0.07	2.68 \pm 0.05	1.84	0.44
72 h	3.73 \pm 0.10	2.75 \pm 0.20	2.62 \pm 0.07	1.11	0.13
120 h	3.99 \pm 0.35	2.41 \pm 0.06	2.31 \pm 0.12	1.68	0.11
240 h	3.52 \pm 0.35	2.45 \pm 0.11	2.35 \pm 0.21	1.17	0.10

Pristine MAE = \sim 0.025 \pm 0.05 nN; eMAE surface (before experiments) = \sim 0.93 \pm 0.14 nN.

obtain close values of cell adhesion forces. On the other hand, interaction forces obtained from biooxidized eMAE surfaces with As(V) range from \sim 3.80 to \sim 2.41 nN (Fig. 3c' and Table 2) indicating that *A. thiooxidans* are weakly attached to arsenopyrite surfaces in the presence of supplementary arsenic, in comparison with those observed in the absence of arsenic, thus, confirming an important effect of toxic arsenic on the formation of *A. thiooxidans* biofilms and surface cell attachment properties (Harneit et al., 2006; Devasia and Natarajan, 2010). The cell adhesion forces for *A. thiooxidans* under this experimental scheme are 1.79, 1.25, 0.91, 0.44, 0.13, 0.11 and 0.1 nN for 1, 12, 24, 48, 72, 120 and 240 h of assay, respectively (Table 2). These significant differences between adhesion forces for biooxidation experiments (with and without supplementary arsenic in system) indicate that attachment of *A. thiooxidans* depends upon the protein production (Fig. 5 and Table 3) and biofilm structure (Figs. 2–4 and Table 2), as suggested for *A. ferrooxidans* and SM systems (Chandraprabha et al., 2010; Bowen et al., 2013). This finding indicates the disadvantageous effect of toxic arsenic in the biofilm performance (i.e. modifying biofilm evolution), as occurs in bioleaching operations. Indeed, if leaching acidophilic microorganisms are successfully adapted to toxic species (Bowen et al., 2013; Koechler et al., 2015), then biofilms structures induce protein production as survival strategy to metal-resistance and therefore, enabling the progress of SM bioleaching under different conditions (Dopson et al., 2003; Chen et al., 2004).

Fig. 4 shows SEM images of pristine MAE (Fig. 4a), eMAE (Fig. 4b), abiotic control eMAE (Fig. 4c–d), biooxidized eMAE (Fig. 4c'–d') and biooxidized eMAE surfaces with As(V) (Fig. 4c''–d''). A comparison between pristine MAE and eMAE surfaces confirms the formation of secondary S^0 and pyrite-like phases, in agreement with Raman (Fig. 1b, Table S1) and AFM (Fig. 2b, Table 1) studies. SEM-EDS images for abiotic control MAE surfaces confirmed further oxidation of S^0 and accumulation of pyrite-like compounds after 48 and 240 h of assay (Fig. 4c, 4d, respectively), as indicated by AFM (Fig. 2c–d and Table 2) and Raman (Fig. 1c–d) studies, probably due to the acidified ATCC-125 medium. EDS analyses (data not shown, $n = 10$) indicate the formation of mainly S^0 and S_n^{2-} compounds on these surfaces, in agreement with Raman study (Fig. 1). As suggested by AFM (Fig. 2), *A. thiooxidans* colonizes arsenopyrite surfaces to form well-structured biofilms with high density of cells, forming mainly macro-colonies after 48 h of assay (Fig. 4c'). However, a more compact biofilm was formed with abundant EPS production in the presence of supplementary arsenic in the system (Fig. 4c''), indicating that EPS acts as a protecting barrier against toxic metallic species such as As(V), and it is a bacterial survival strategy for non-leaching bacteria (Harrison et al., 2005; Vu et al., 2009). Note that bacterial EPS over-production is typically low for leaching SOM and IOM strains (Tu et al., 2014; Lara et al., 2013), in comparison with non-leaching bacteria (i.e. *Bacillus subtilis*, *Pseudomonas aeruginosa*) (Breed et al., 1996; Leng et al., 2009). A more abundant generation of secondary

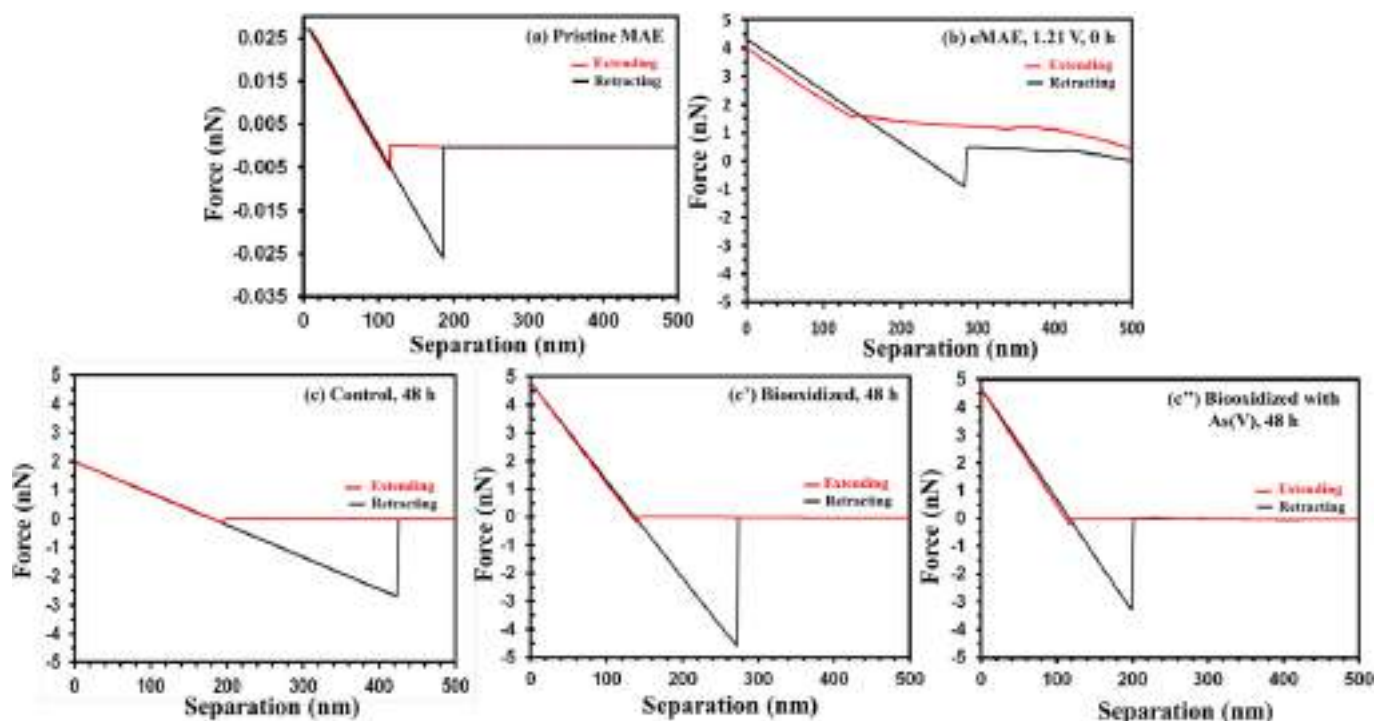


Fig. 3. Force separation (extending and retracting curves) in air using contact mode of pristine MAE (a), eMAE after 48 h (b), abiotic control eMAE surface after 48 h (c) biooxidized eMAE surface after 48 h (d), and biooxidized eMAE surface with As(V) after 48 h (e). Area of collection: $1 \mu\text{m}^2$. Scan rates from 0.5–1 Hz.

S_n^{2-} and orpiment-like compounds is observed after 240 h of assay, with partial or fully cell attachment (Fig. 4d'), particularly in the presence of supplementary arsenic (Fig. 4d''). These differences in secondary compounds (i.e. Eqs. 1 to 4) confirm that *A. thiooxidans* biofilms significantly modify the arsenopyrite biooxidation processes, depending upon the availability of toxic arsenic in the system and as a function of time, presumably as a strategy for cell survival (Leng et al., 2009; He et al., 2012). The incidence of partially embedded *A. thiooxidans* and/or *A. ferrooxidans* within secondary compounds matrix (i.e. S_n^{2-}/S^0 , $K_2Fe_3(SO_4)_2(OH)_6$) has been suggested to occur during biooxidation of some SM under different conditions (Sasaki et al., 1998; Lara et al., 2013), indicating that *A. thiooxidans* oxidizes altered SM regardless the presence of secondary compounds, in agreement with previous results, and highlighting the importance of *A. thiooxidans* in mixed cultures (i.e. *A. thiooxidans* and *A. ferrooxidans*) (Sasaki et al., 1998, 2009).

3.3. Total amount and size of proteins in biofilms

Some interesting works have studied protein production and its relationship to cell attachment during pyrite and chalcopyrite biooxidation mainly using *A. ferrooxidans* and/or *A. thiooxidans* planktonic cells exposed to toxic metals and environments (Chen et al., 2004; Bowen et al., 2013). However, there is a lack of information concerning the understanding of protein production during biofilm

formation and evolution during arsenopyrite biooxidation by SOM *A. thiooxidans* considering the role of arsenic. Fig. 5 shows SDS-PAGE gels of total protein extraction after 1, 12, 24, 48, 72, 120 and 240 h of biofilm and arsenopyrite interaction in the presence and absence of supplementary arsenic. Additionally, Table 3 shows the quantification of total protein extraction after 48 and 240 h of assay under the same experimental conditions above referred. A general increase of total protein with significant differences ($p < 0.05$ for data, $n = 3$) is clearly observed after 48 and 240 h of assay in the absence of supplementary arsenic (Table 3). However, an opposite behavior is observed in the presence of supplementary arsenic, lowering down the protein production after 48 h (Table 3), thus confirming the detrimental effect (damage) of toxic arsenic during biofilm evolution, in agreement with our previous analyses and reports in the literature (Dave et al., 2008; Leng et al., 2009; Koehler et al., 2015). According to the electrophoretic analysis (Fig. 5), the production of mainly 29, 40–50, 75, 100, 150 and 250 kDa proteins is described as a function of time. In fact, the highest production of total protein is observed after 24, 48 and 120 h of assay, involving a wide range of expressed proteins, as described by comparison with the molecular weight marker (Fig. 5), confirming the presence of attached biofilms and the effects of supplementary arsenic in the system (Figs. 2, 3, respectively). Note that the highest and lowest interaction forces agree with the highest and lowest protein production, respectively (Table 2 and Figs. 4–5). In summary, a significant influence of available toxic arsenic is clearly observed in the electrophoretic and quantification protein studies, these variables (i.e. 35–50 kDa) are generally lower in biofilms collected on biooxidized eMAE surfaces with As(V) (Fig. 5), confirming that available toxic arsenic in system allows biofilm formation. However, it affects (damages or modifies) biofilm structure and evolution, in agreement with all previous results. A precise description of the role of protein production to oxidize sulfur, cell attachment and arsenic resistance during arsenopyrite biooxidation by *A. thiooxidans* (i.e. 2D gels, proteomics and bioinformatics) in the presence and absence of supplementary arsenic will be the motivation of a forthcoming work. This research could account for changes in biofilm structure and function during its evolution.

Table 3

Quantification of total protein from *Acidithiobacillus thiooxidans* cells (ATCC no. 19,377) attached to biooxidized eMAE's and biooxidized eMAE's surfaces with As(V) (data, $n = 3$).

Time (h)	Proteins (mg/mL)	
	Biooxidized eMAE surface	Biooxidized eMAE surface with As(V)
0*	19.8	19.8
48	47.7	42.1
240	60.1	22.3

* Planktonic cells.

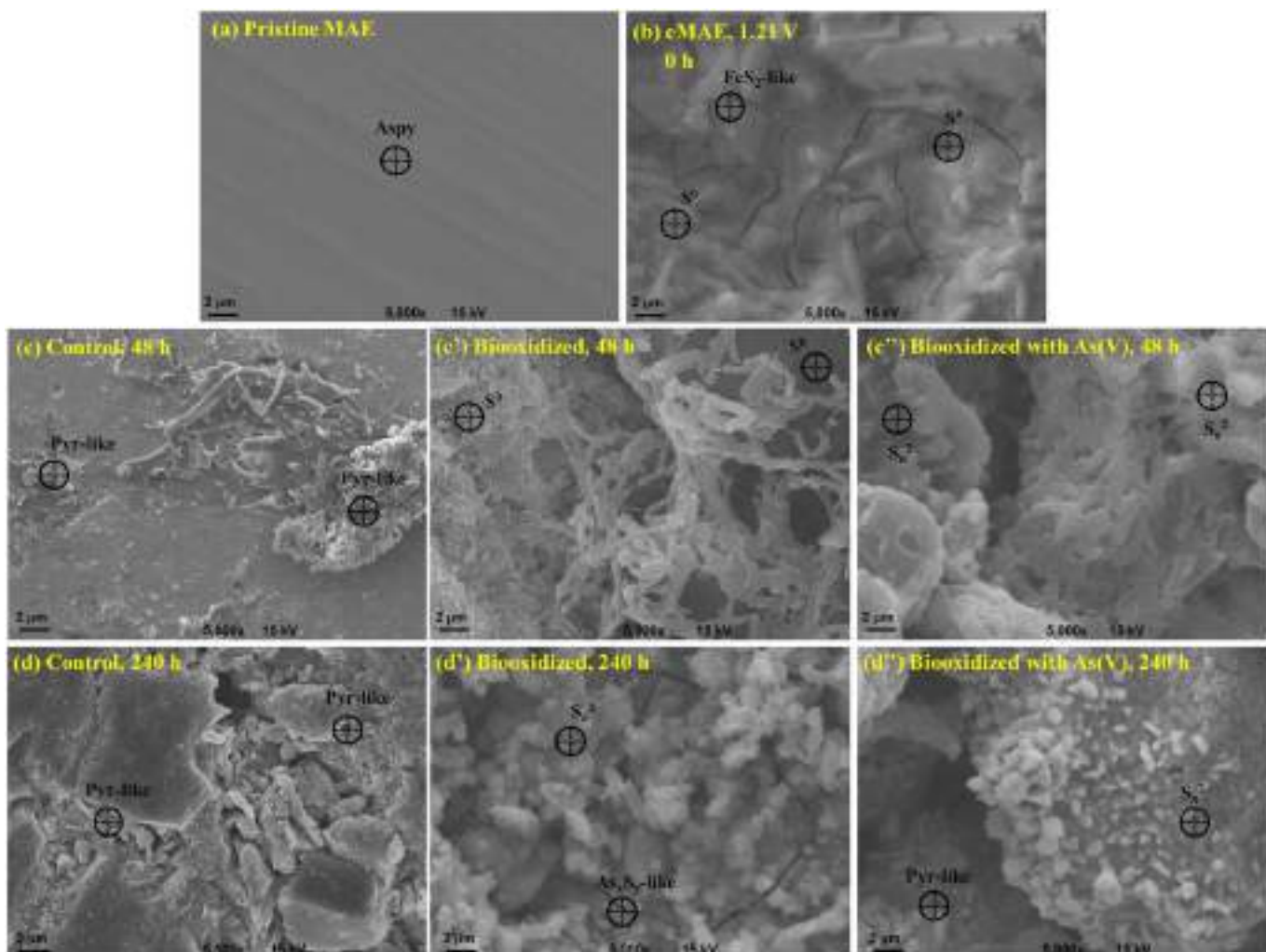


Fig. 4. Typical SEM images of the pristine MAE surface (a), eMAE surface (b), abiotic control eMAE surfaces after 48 and 240 h of assay (c, d, respectively), biooxidized eMAE surfaces after 48 and 240 h of assay (c', d', respectively) and biooxidized eMAE surfaces with As(V) after 48 and 240 h of assay (c'', d'', respectively). Aspy = FeAs; pyr-like = pyrite-like; As_xS_x -like = orpiment-like; S_n^{2-}/S^0 = polysulfide structures; S^0 = elementary sulfur (according to EDS analyses, $n = 10$).

3.4. Electrochemical analysis

Fig. 6 shows cyclic voltammograms (negative scans) for pristine MAE (Fig. 6a, i, black continuous line) and eMAE (initially containing S_n^{2-}/S^0 and pyrite-like compounds, Fig. 6b, ii, blue dot line) under stagnant conditions and 20 mV s^{-1} in ATCC-125 solution (pH 2.0). Two reduction processes of low intensity (C1 and C2) appear between -0.1 and -1.1 V for the pristine sample (Fig. 6a, i, black continuous line). Generally, these processes are attributed to reduction of mineral lattices to form non-stoichiometric metal-deficient and sulfur-rich layers (i.e. S_n^{2-}/S^0 in $Fe_{1-x}As_{1-y}S/Fe_{1-x}As_{1-y}S_{2-z}$ -like phases), which agrees with Raman (Fig. 1b) and SEM-EDS (Fig. 3b) studies, as well as reports in the literature (Almeida and Giannetti, 2003). Accordingly, the signal augmentation of C1 and C2 during eMAE voltammetric analysis (Fig. 6a, ii, blue continuous line) indicates the reduction of an increased amount of S_n^{2-}/S^0 and pyrite-like compounds.

Figs. 6b–e also show negative scans for all variants of eMAE surfaces after 1, 48, 72 and 240 h of assay. A summary of accumulated charge for these electrochemical processes is given in Table 4. An initial activation process is observed after 1 h in all experiments (Fig. 6b and Table 4), indicating some minor abiotic and biooxidation processes, which is caused by incipient chemical and biological arsenopyrite oxidation, driven by slow chemical mineral dissolution and initial stages of cell attachment (Nöel et al., 2010; Florian et al., 2011). Some reports have indicated low cell colonization (cell density) during incipient pyrite

oxidation by *A. ferrooxidans* cells (<1 h) under acidic 9 K culture conditions (Florian et al., 2010, 2011). Additionally, SEM and AFM analyses showed low cell density associated with arsenopyrite biooxidation after 1 h of assay in the presence and absence of supplementary arsenic (data not shown). In contrast, cyclic voltammograms after 48 h (Fig. 6c, i, gray continuous lines), 72 h (Fig. 6d) and 240 h (Fig. 6e) of assay for abiotic control eMAE (curves i, gray continuous lines), biooxidized eMAE surfaces (curves ii, green continuous lines) and biooxidized eMAE surfaces with As(V) (curves iii, red continuous lines) display significant differences in electrochemical responses, thus denoting variable mineral reactivity (Table 4). A comparison between abiotic control eMAE and biooxidized eMAE surfaces (with and without supplementary arsenic) suggests that biooxidation induces considerable modifications in the biofilm/arsenopyrite system (see peaks formed along the scan), in agreement with previous analyses. On the other hand, cyclic voltammetry suggests a higher arsenopyrite reactivity for abiotic control eMAE after 48 h of assay (Fig. 6c, i, black continuous line) as observed in the peak recorded around -0.9 V . This indicates a larger accumulation of secondary pyrite-like compounds in the system, also in agreement with previous evaluations. Note that after 120 h of assay in the presence of supplementary arsenic, biofilm production is low (Fig. 5), but surface reactivity is high compared to other times (Fig. 6d, iii, red continuous line, Table 4), suggesting that reactive properties of the biofilm/arsenopyrite system are achieved during previous stages of biooxidation (i.e. <120 h), demonstrating the transient correlation existing between

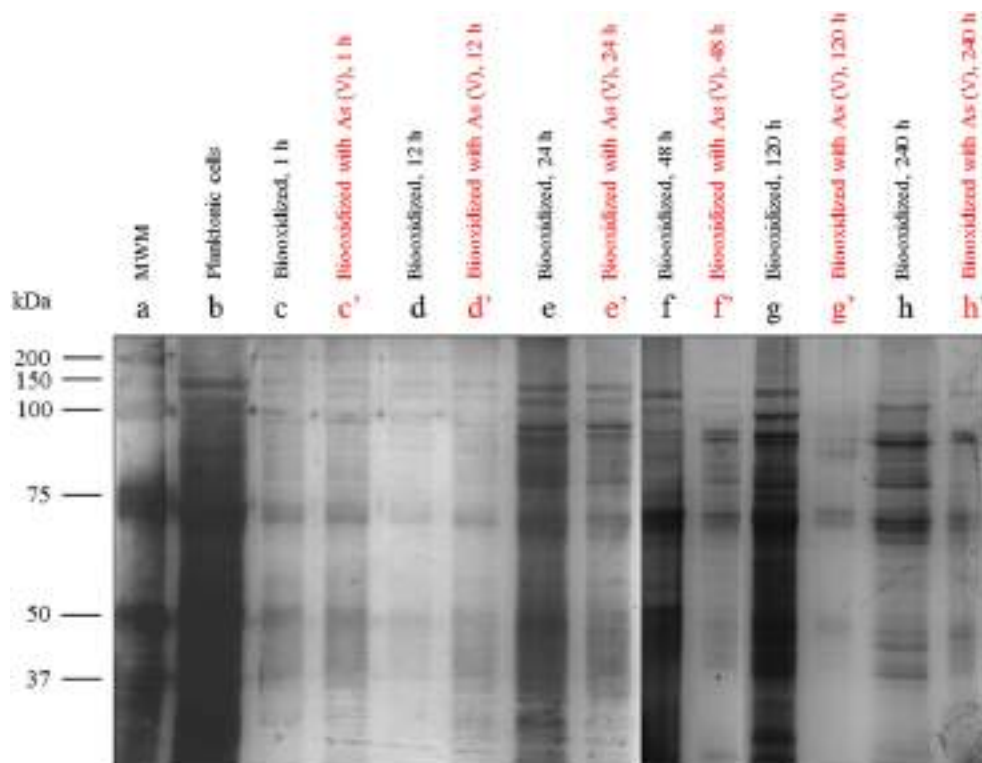


Fig. 5. SDS-PAGE analysis of total protein extraction after 1, 12, 24, 48, 120 y 240 h of *A. thiooxidans* biofilm and arsenopyrite interaction in the presence (red labels, c, d, e, f, g, h, respectively) and the absence (black labels, a, b, a', b', c', d', e', f', g', h', respectively) of supplementary arsenic in the system. MWM = molecular weight marker (b).

biochemical changes (i.e. total proteins production in Fig. 5) and reactivity of secondary compounds (Fig. 6 and Table 4). High reactivity of biofilm/arsenopyrite structure is achieved after 240 h of assay in the absence of supplementary arsenic (Fig. 6e, ii, green continuous line, Table 4), indicating that surface reactivity is progressively reached without the influence of toxic species. Voltammetric analysis indicates that most significant stages of arsenopyrite biooxidation are reached between 48 and 240 h of assay, as a combination of specific bacterial response (i.e. Figs. 2, 4, 5) and attachment properties affected by available arsenic (Fig. 3, Table 2).

Fig. 7 shows experimental and fitted Nyquist spectra obtained for pristine MAE (Fig. 7a) and eMAE surfaces (Fig. 7b) in acidified ATCC-125 solution (pH 2.0). As observed, a semi-circle with larger imaginary components compared to real ones is recorded for the pristine surface (Fig. 7a). Both components are moderately high, which suggests the presence of semiconductive phases in the mineral lattice, as described for other SM (Constantin and Chiriță, 2013). The diagram collected for pristine sample has been fitted to a simple $R_e(R_{ct} Q_{dl})$ electrical circuit denoting a single time constant in the EIS measurement (Fig. 7a), where R_e represents the solution resistance, while R_{ct} and Q_{dl} are the charge transfer resistance and the distributed capacitive behavior due to surface heterogeneities of the interface arsenopyrite/biofilm (i.e. Figs. 2, 4, Table 2), respectively (Constantin and Chiriță, 2013). On the other hand, Fig. 7 shows spectra collected for eMAE (Fig. 7b) after 48, 120 and 240 h of assay for abiotic control eMAE (Fig. 7c to 7e, respectively), biooxidized eMAE (Fig. 7c' to 7e', respectively) and biooxidized eMAE surfaces with As(V) (Fig. 7c'' to 7e'', respectively) are also included. Note that these latter experiments present a general EIS behavior (excepting Figs. 7d and 7d'') compared to the pristine MAE, the capacitive inputs considerably increase while the resistive contributions remain around the same values. Likewise, the capacitive components of impedance are higher in the biooxidized eMAE and some biooxidized eMAE surfaces with As(V) compared to the abiotic control samples. These observations are an indicative that more semi-conductive phases

(i.e. increasing passive features) arise on the surface of the biooxidized samples, as a result of the interactions with microorganisms. In addition, mass-transfer effects are not perceived in the EIS plots, whereby the charge transfer resistance in the interface arsenopyrite/biofilm controls the overall (bio)oxidation process. It is worthwhile mentioning that this resistance relies on several factors including pH, biofilm properties (i.e. cell attachment, structure), semiconductive phases on arsenopyrite (i.e. reactivity, type and amount of secondary products); and the role of some of them have been analyzed in former sections (Figs. 1–4). A similar equivalent circuit $R_e(R_{ct} Q_{dl})$ was used to fit the Nyquist diagrams for the above experiments. The proposed circuit (black dashed lines, Fig. 7) enables to obtain adequate fits for spectra collected for all variants of eMAE surfaces. It is worthwhile mentioning that prior to this EQ, additional EQs involving diffusive processes (i.e. solid-diffusion, Warburg type impedance) were tried, as indicated by Bevilaqua et al. (2004, 2009) to describe SM and leaching bacteria (i.e. *A. ferrooxidans*) interactions. However, this procedure did not succeed indicating the absence of diffusive processes in the controlling stages of the arsenopyrite/biofilm system. Note that diffusion mechanisms characterized with EIS measurements have been only reported for *A. ferrooxidans* and SM surface systems (i.e. cells, secondary compounds), which were attributed to specific requirements of Fe(II)/Fe(III) species (Bevilaqua et al., 2004, 2009; Liu et al., 2011), whereby this process is not required for SOM *A. thiooxidans* and therefore, instead, it requires direct cell attachment to SM surface to obtain its energy source throughout enzymatic mechanisms to attack i.e., S_n^{2-}/S^0 phases (Rohwerder et al., 2003; Devasia and Natarajan, 2010). Table 5 summarizes the parameters obtained from the fits to EIS data. The values of α are close to 1.0 for all spectra, which denote the formation of a capacitor when the voltage is modified in the interface arsenopyrite/biofilm. The capacitance of this element does not vary with sample ($\times 10^{-3}$ farad), probably due to its value depends on bulk properties of the mineral, or it is not dominant during the occurrence of charge transfer phenomena. On the other hand, the resistance values (R_{ct}) are sensitive in the analysis, standing out the importance

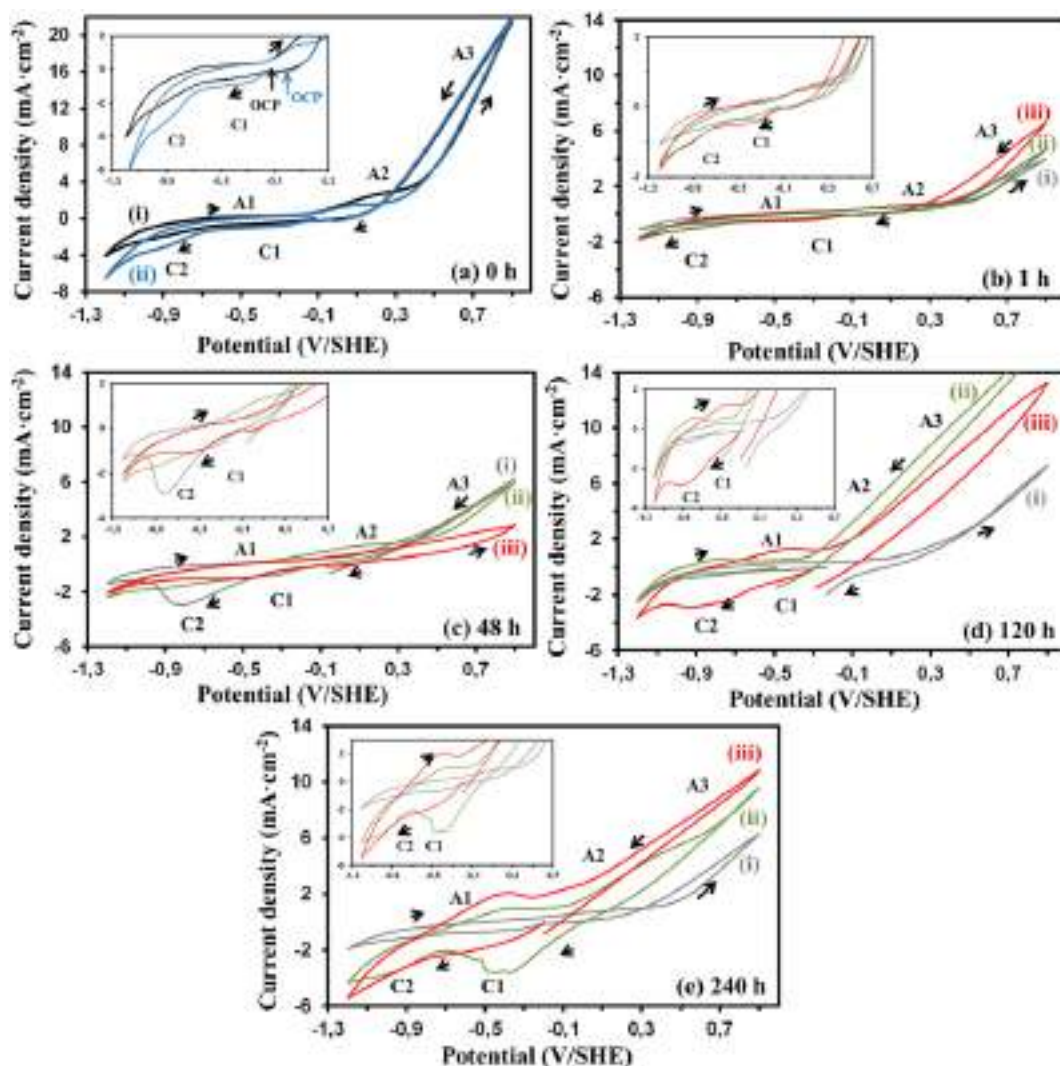


Fig. 6. Cyclic voltammograms initiated in the negative-going sweep in the acidified ATCC-125 culture solution (at pH 2.0) for abiotic control eMAE surfaces (gray continuous lines, curves i), biooxidized surfaces (green continuous lines, curves ii) and biooxidized eMAE surfaces with As(V) (red continuous lines, curves iii) after 1 h (b), 48 h (c), 120 h (d) and 240 h (e) of experimental assay. This figure includes cyclic voltammograms for pristine MAE sample (a, black continuous line, curve i) and eMAE sample (a, blue continuous line, curve ii) for comparison purposes. Insets show low overpotential regions. Quiescent solution. 20 mV s^{-1} .

of the products (i.e. electronic, conductive and structural properties) formed during (bio)oxidation on the capacity of the interface arsenopyrite/biofilm to transfer charge, and the surface changes due to (bio)oxidation processes (Eqs. 1 to 4). Charge transfer process is more facile in the abiotic control eMAE surfaces, in contrast with biooxidized eMAE and biooxidized eMAE surfaces with As(V) (Table 5), suggesting that secondary products and biofilms contained on the biooxidized

samples (with and without arsenic) are more resistive. This also indicates that chemical oxidation of pyrite-like compounds present on the abiotic control eMAE is chemically oxidized faster due to constant acid dissolution, in contrast with biooxidation reactions, which proceed slower due to difficulty to transform the arsenopyrite surface into different secondary products, in agreement with Raman (Fig. 1), AFM (Figs. 2, 3, Tables 2, 3) and SEM-EDS (Fig. 4) studies. In addition, R_{T1} values are in general higher for biooxidized eMAE surfaces with As(V) than in the absence of this element, indicating that more resistive surface products are formed when As(V) is present, as indicated by cyclic voltammetry (Fig. 6) and the surface behavior identified by AFM (Table 1, Fig. 2). As indicated by cyclic voltammetry, highest reactivity of abiotic control eMAE and biooxidized eMAE surfaces with As(V) are reached after 48 h and 120 h of assay (Fig. 6c, i, grey continuous line; Fig. 6d, ii, red continuous line, respectively), respectively, which are in agreement with a lower magnitude in impedance response and parameters for corresponding assays (Figs. 7c, 7d", Table 5). Thus, a high reactivity of abiotic control and biooxidized surface is occurring to transform mineral surface due to biofilm organization and chemical/electrochemical reactions (Eqs. 1 to 4). In summary, arsenopyrite biooxidation process is slow and driven by direct cell attachment, its continuous surface modifications, and toxic environment adaptation (Fig. 5, Tables 1–5).

Table 4

Accumulated charge associated to negative scans in cyclic voltammograms of Fig. 6 obtained for abiotic control eMAE and biooxidized eMAE surfaces.

Mineral sample	Accumulated charge (Q, mC)		
	Biooxidized eMAE	Biooxidized eMAE with As(V)	Control abiotic eMAE
1 h	21.1	24.7	20.8
12 h	41.7	40.1	10.6
24 h	60.4	63.5	10.8
48 h	92.2	76.9	98.2
72 h	101.5	252.8	95.6
120 h	77.4	185.6	72.5
240 h	203.9	181.9	66.1

Pristine MAE = 27.1 mC; eMAE = 35.87 mC.

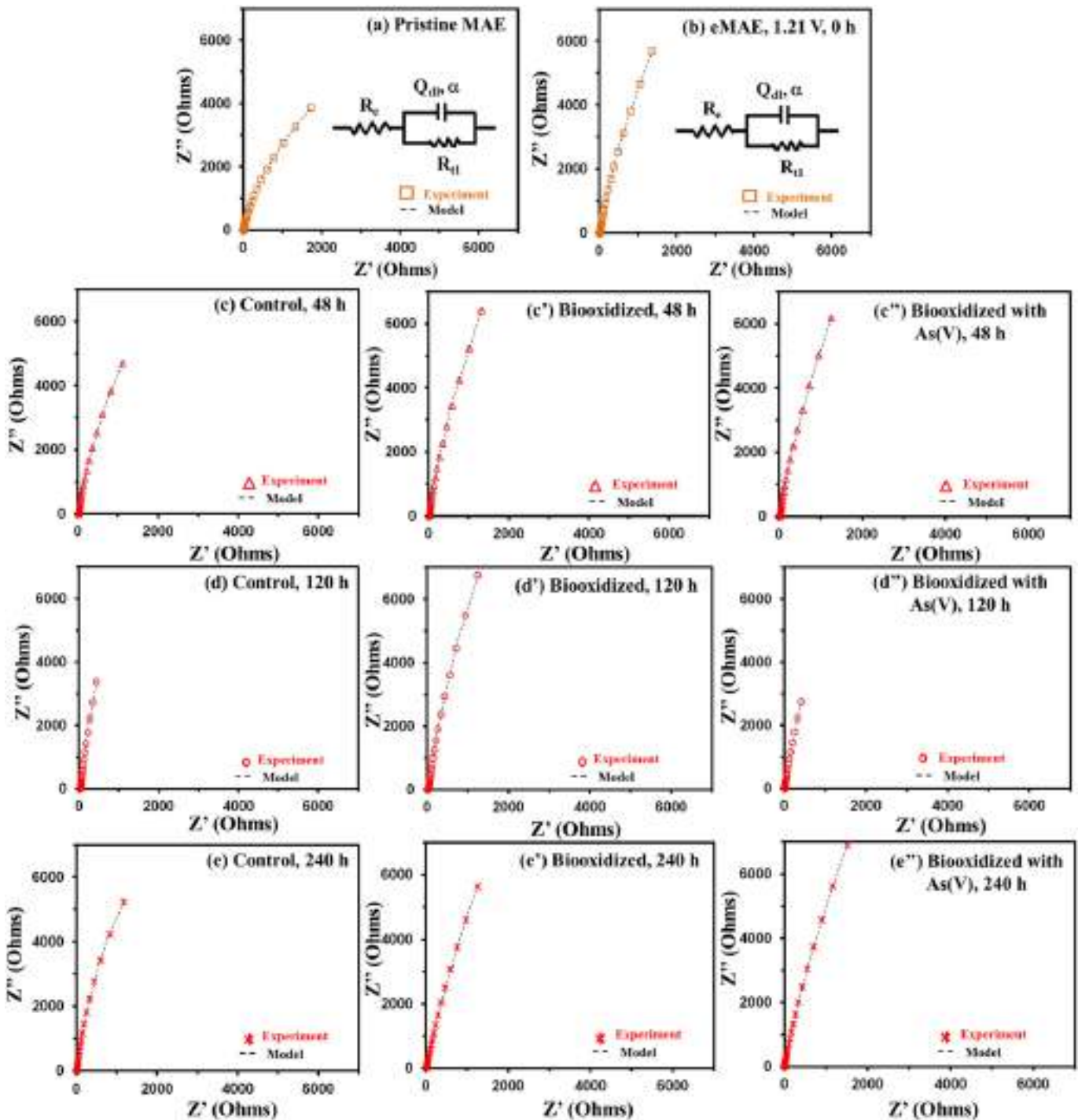


Fig. 7. Experimental (symbols) and fitted (discontinuous lines) EIS spectra (Nyquist plots) of arsenopyrite electrodes: (a) pristine MAE, (b) eMAE surface oxidized in the acidified ATCC-125 culture solution (at pH 2.0), (c, d, e) abiotic control eMAE surfaces after 48, 120 and 240 h of assay, respectively; (c', d', e') biooxidized eMAE surfaces after 48, 120 and 240 h of assay, respectively; (c'', d'', e'') biooxidized eMAE surfaces with As(V) after 48, 120 and 240 h of assay, respectively. Equivalent electric circuits used to fit the spectra are included.

4. Conclusions

The oxidation mechanism of arsenopyrite by *Acidithiobacillus thiooxidans* was comprehensively studied in the presence and absence of supplementary arsenic for 240 h. Raman, SEM-EDS, AFM, Cyclic voltammetry, EIS and SDS-PAGE 1D techniques were used for these purposes. Biofilm formation and its evolution was dominated by mainly micro-colonies, including most significant stage at 48 h, where cell adhesion forces and total protein synthesis were considerably high (i.e. 1.84 nN and 47.7 mg L⁻¹, respectively). Biooxidation resulted in the

generation of partial and/or total cells covered by significant accumulation of secondary compounds for longer times (i.e. 240 h), with the corresponding decrease of cell adhesion forces, but increasing protein synthesis (i.e. 0.44 nN and 60.1 mg L⁻¹, respectively). A more compact biofilm was developed in the presence of supplementary arsenic in the system, whereby toxic arsenic does not hinder biofilm formation, but modifies its evolution, involving in general lower adhesion forces (i.e. 0.44 nN, at 48 h) and protein synthesis (i.e. 22.3 mg L⁻¹, at 240 h). Electrochemical analyses provided strong evidence of a biooxidation process controlled by direct cell attachment, as indicated by the absence

Table 5
Electrochemical parameters obtained from the fitting of the equivalent electric circuit to the experimental EIS spectra collected on pristine MAE, eMAE, and all variants of eMAE surfaces as a function of the biooxidation time.

Electrochemical parameters	Mineral surfaces (eMAE's)																							
	Biooxidized								Biooxidized with As(V)								Abiotic control							
	1 h	12 h	24 h	48 h	72 h	120 h	240 h		1 h	12 h	24 h	48 h	72 h	120 h	240 h		1 h	12 h	24 h	48 h	72 h	120 h	240 h	
R_e (ohm)	30.88	16.7	21.84	16.49	15.1	34.18	16.8	9.46	7.46	11	13.68	5.66	12.49	6.94	30.77	16.67	21.77	16.49	14.97	34.20	16.79			
R_{r1} (ohm), $\times 10^4$	3.48	10.99	4.04	6.13	11.77	8.68	7.97	6.27	8.15	10.53	6.02	4.65	6.41	7.49	2.58	3.11	2.05	3.88	4.19	10.33	3.58			
Q_{dl} (farad), $\times 10^{-3}$	2.23	1.92	2.01	1.96	2	1.9	2.08	1.97	1.86	1.81	2.03	2.04	2.02	1.74	2.57	2.78	2.89	2.64	2.78	2.58	2.55			
α_1	0.91	0.93	0.93	0.93	0.93	0.94	0.91	0.93	0.92	0.89	0.93	0.93	0.93	0.92	0.95	0.94	0.96	0.93	0.96	0.95	0.95			

R_e (pristine sample) = 16.61 Ω ; R_1 (pristine sample) = $6.42 \times 10^4 \Omega$; Q (pristine sample) = 2.10×10^{-3} farad; $\alpha_1 = 0.91$; R_e (eMAE sample) = 12.73 Ω ; R_{r1} (eMAE sample) = $2.02 \times 10^4 \Omega$; Q_{dl} (eMAE sample) = 2.58×10^{-3} farad; $\alpha_1 = 0.88$.

of significant diffusive contributions in the EIS spectra. Raman analyses suggested a continuous modification of surface to different reactive secondary phases (i.e. pyrite-like, S_n^{2-}/S^0 , orpiment-like), which are associated to direct cell attachment under adaptation of cells to toxic environment.

Acknowledgments

Financial support for this research work is greatly appreciated from CONACYT (grants 2012-183230 and 2013-205416). Hugo Ramírez-Aldaba and Omayra Paola Valles-Soto thank CONACYT for their academic scholarships (Grants 362184 and 292779, respectively). The authors thank Erasmo Mata (IG-UASLP) for the preparation and construction of massive arsenopyrite electrodes (MAE specimens), and to Dra. J. Viridiana García-Meza (UASLP) for valuable discussions.

References

- Almeida, C.M.V.B., Giannetti, B.F., 2003. Electrochemical study of arsenopyrite weathering. *Phys. Chem. Chem. Phys.* 5, 604–610. <http://dx.doi.org/10.1039/B210631K>.
- Benzaazoua, M., Marion, P., Robaut, F., Pinto, A., 2007. Gold-bearing arsenopyrite and pyrite in refractory ores: analytical refinements and new understanding of gold mineralogy. *Mineral. Mag.* 71, 123–142. <http://dx.doi.org/10.1180/minmag.2007.071.2.123>.
- Bevilaqua, D., Diéz-Perez, I., Fugivara, C.S., Sanz, F., Benedetti, A.V., García, O., 2004. Oxidative dissolution of chalcopyrite by *Acidithiobacillus ferrooxidans* analyzed by electrochemical impedance spectroscopy and atomic force microscopy. *Bioelectrochem.* 64, 79–84. <http://dx.doi.org/10.1016/j.bioelechem.2004.01.006>.
- Bevilaqua, D., Acciari, H.A., Arena, F.A., Benedetti, A.V., Fugivara, C.S., Tremiliosi-Filho, G., Júnior, O.G., 2009. Utilization of electrochemical impedance spectroscopy for monitoring bornite (Cu_5FeS_4) oxidation by *Acidithiobacillus ferrooxidans*. *Min. Eng.* 22, 254–262. <http://dx.doi.org/10.1016/j.biortech.2012.11.050>.
- Boukamp, B.A., 1989. *Equivalent Circuit: (equivcrt. pas): Software Manual*. Department of Chemical Technology, University of Twente.
- Bowen, T., Wang, F., Li, J., Sha, J., Lu, X., Han, X., 2013. Analysis of genes and proteins in *Acidithiobacillus ferrooxidans* during growth and attachment on pyrite under different conditions. *Geomicrobiol. J.* 30, 225–267. <http://dx.doi.org/10.1080/01490451.2012.668608>.
- Bradford, L., 1976. A rapid and sensitive method for the quantification of microgram quantities of protein utilizing the principle of protein dye binding. *Anal. Biochem.* 72, 248–252.
- Breed, A.W., Glatz, A., Hansford, G.S., Harrison, S.T.L., 1996. The effect of As (III) and As (V) on the batch bioleaching of a pyrite-arsenopyrite concentrate. *Min. Eng.* 9, 1235–1252. [http://dx.doi.org/10.1016/S0892-6875\(96\)00119-7](http://dx.doi.org/10.1016/S0892-6875(96)00119-7).
- Chandraprabha, M.N., Somasundaran, P., Natarajan, K.A., 2010. Modeling and analysis of nanoscale interaction forces between *Acidithiobacillus ferrooxidans* and AFM tip. *Colloids Surf. B* 75, 310–318. <http://dx.doi.org/10.1016/j.colsurfb.2009.09.002>.
- Chen, B.Y., Liu, H.L., Chen, Y.W., Cheng, Y.C., 2004. Dose-response assessment of metals toxicity upon indigenous *Thiobacillus thiooxidans* BC1. *Process Biochem.* 39, 735–745. [http://dx.doi.org/10.1016/S0032-9592\(03\)00180-8](http://dx.doi.org/10.1016/S0032-9592(03)00180-8).
- Collinet, M.N., Morin, D., 1990. Characterization of arsenopyrite oxidizing *Thiobacillus*. Tolerance to arsenite, arsenate, ferrous and ferric iron. *Antonie Van Leeuwenhoek* 57, 237–244. <http://dx.doi.org/10.1007/BF00400155>.
- Constantin, C.A., Chiriță, P., 2013. Oxidative dissolution of pyrite in acidic media. *J. Appl. Electrochem.* 43, 659–666. <http://dx.doi.org/10.1007/s10800-013-0557-y>.
- Dave, S.R., Gupta, K.H., Tipre, D.R., 2008. Characterization of arsenic resistant and arsenopyrite oxidizing *Acidithiobacillus ferrooxidans* from Hutti gold leachate and effluents. *Bioresour. Technol.* 99, 7514–7520. <http://dx.doi.org/10.1016/j.biortech.2008.02.019>.
- Devassia, P., Natarajan, K.A., 2010. Adhesion of *Acidithiobacillus ferrooxidans* to mineral surfaces. *Int. J. Miner. Process.* 94, 135–139. <http://dx.doi.org/10.1016/j.minpro.2010.02.003>.
- Dopson, M., Craig, B.A., Koppineedi, P.R., Bond, P.L., 2003. Growth in sulfidic mineral environments: metal-resistance mechanisms in acidophilic microorganisms. *Microbiol.* 149, 1959–1970. <http://dx.doi.org/10.1099/mic.0.26296-0>.
- Falco, L., Pogliani, C., Curutchet, G., Donati, E., 2003. A comparison of bioleaching of covellite using pure cultures of *Acidithiobacillus ferrooxidans* and *Acidithiobacillus thiooxidans* or a mixed culture of *Leptospirillum ferrooxidans* and *Acidithiobacillus thiooxidans*. *Hydrometallurgy* 71, 31–36. [http://dx.doi.org/10.1016/S0304-386X\(03\)00170-1](http://dx.doi.org/10.1016/S0304-386X(03)00170-1).
- Fantauzzi, M., Licheri, C., Atzei, D., Loi, G., Elsener, B., Rossi, G., Rossi, A., 2011. Arsenopyrite and pyrite bioleaching: evidence from XPS, XRD and ICP techniques. *Anal. Bioanal. Chem.* 401, 2237–2248. <http://dx.doi.org/10.1007/s00216-011-5300-0>.
- Florian, B., Noël, N., Sand, W., 2010. Visualization of initial attachment of bioleaching bacteria using combined atomic force and epifluorescence microscopy. *Min. Eng.* 23, 532–535. <http://dx.doi.org/10.1016/j.mineng.2010.02.002>.
- Florian, B., Noël, N., Thyssen, C., Felschau, I., Sand, W., 2011. Some quantitative data on bacterial attachment to pyrite. *Min. Eng.* 24, 1132–1138. <http://dx.doi.org/10.1016/j.mineng.2011.03.008>.
- Harneit, K., Göksel, A., Kock, D., Klock, J.H., Gehrke, T., Sand, W., 2006. Adhesion to metal sulfide surfaces by cells of *Acidithiobacillus ferrooxidans*, *Acidithiobacillus thiooxidans* and *Leptospirillum ferrooxidans*. *Hydrometallurgy* 83, 245–254. <http://dx.doi.org/10.1016/j.hydromet.2006.03.044>.
- Harrison, J.J., Turner, R.J., Ceri, H., 2005. Persister cells, the biofilm matrix and tolerance to metal cations in biofilm and planktonic *Pseudomonas aeruginosa*. *Environ. Microbiol.* 7, 981–994. <http://dx.doi.org/10.1111/j.1462-2920.2005.00777.x>.
- He, H., Xia, J.L., Hong, F.F., Tao, X.X., Leng, Y.W., Zhao, Y.D., 2012. Analysis of sulfur speciation on chalcopyrite surface bioleached with *Acidithiobacillus ferrooxidans*. *Min. Eng.* 27, 60–64. <http://dx.doi.org/10.1016/j.mineng.2011.12.012>.
- Hong, J., Silva, R.A., Park, J., Lee, E., Park, J., Kim, H., 2016. Adaptation of a mixed culture of acidophiles for a tank biooxidation of refractory gold concentrates containing a high concentration of arsenic. *J. Biosci. Bioeng.* 121, 536–542. <http://dx.doi.org/10.1016/j.jbiosc.2015.09.009>.
- Hope, G.A., Woods, R., Munce, C.G., 2001. Raman microprobe mineral identification. *Min. Eng.* 14, 1565–1577. [http://dx.doi.org/10.1016/S0892-6875\(01\)00175-3](http://dx.doi.org/10.1016/S0892-6875(01)00175-3).
- Jin, J., Shi, S., Liu, G., Zhang, Q., Cong, W., 2012. Arsenopyrite bioleaching by *Acidithiobacillus ferrooxidans* in a rotating-drum reactor. *Min. Eng.* 39, 19–22. <http://dx.doi.org/10.1016/j.mineng.2012.07.018>.
- Kendall, T.A., Lower, S.K., 2004. Forces between minerals and biological surfaces in aqueous solution. *Adv. Agron.* 82, 1–54. [http://dx.doi.org/10.1016/S0065-2113\(03\)82001-1](http://dx.doi.org/10.1016/S0065-2113(03)82001-1).
- Kim, H.A., Lee, K.Y., Lee, B.T., Kim, S., Kim, K.W., 2012. Comparative study of simultaneous removal of As, Cu, and Pb using different combinations of electrokinetics with bioleaching by *Acidithiobacillus ferrooxidans*. *Water Res.* 46, 5591–5599. <http://dx.doi.org/10.1016/j.watres.2012.07.044>.
- Ko, M.S., Park, H.S., Kim, K.W., Lee, J.U., 2013. The role of *Acidithiobacillus ferrooxidans* and *Acidithiobacillus thiooxidans* in arsenic bioleaching from soil. *Environ. Geochem. Health* 35, 727–733. <http://dx.doi.org/10.1007/s10653-013-9530-2>.
- Koehler, S., Farasin, J., Cleiss-Arnold, J., Arsène-Plöetz, F., 2015. Toxic metal resistance in biofilms: diversity of microbial responses and their evolution. *Res. Microbiol.* 166, 764–773. <http://dx.doi.org/10.1016/j.resmic.2015.03.008>.
- Laemmli, U.K., 1970. Cleavage of structural proteins during the assembly of the head of bacteriophage T4. *Nature* 227, 680–685.
- Lara, R.H., Valdez-Pérez, D., Rodríguez, A.G., Navarro-Contreras, H.R., Cruz, R., García-Meza, J.V., 2010. Interfacial insights of pyrite colonized by *Acidithiobacillus thiooxidans* cells under acidic conditions. *Hydrometallurgy* 103, 35–44. <http://dx.doi.org/10.1016/j.hydromet.2010.02.014>.
- Lara, R.H., García-Meza, J.V., González, I., Cruz, R., 2013. Influence of the surface speciation on biofilm attachment to chalcopyrite by *Acidithiobacillus thiooxidans*. *Appl. Microbiol. Biotechnol.* 97, 2711–2724. <http://dx.doi.org/10.1007/s00253-012-4099-8>.
- Leng, F., Li, K., Zhang, X., Li, Y., Zhu, Y., Lu, J., Li, H., 2009. Comparative study of inorganic arsenic resistance of several strains of *Acidithiobacillus thiooxidans* and *Acidithiobacillus ferrooxidans*. *Hydrometallurgy* 98, 235–240. <http://dx.doi.org/10.1016/j.hydromet.2009.05.004>.
- Lièvremon, D., Bertin, P.N., Lett, M.C., 2009. Arsenic in contaminated waters: biogeochemical cycle, microbial metabolism and biotreatment processes. *Biochimie* 91 (10), 1229–1237. <http://dx.doi.org/10.1016/j.biochi.2009.06.016>.
- Liu, H.L., Chen, B.Y., Lan, Y.W., Cheng, Y.C., 2003. SEM and AFM images of pyrite surfaces after bioleaching by the indigenous *Thiobacillus thiooxidans*. *Appl. Microbiol. Biotechnol.* 62, 414–420. <http://dx.doi.org/10.1007/s00253-003-1280-0>.

- Liu, Y., Dang, Z., Lu, G., Wu, P., Feng, C., Yi, X., 2011. Utilization of electrochemical impedance spectroscopy for monitoring pyrite oxidation in the presence and absence of *Acidithiobacillus ferrooxidans*. *Min. Eng.* 24, 833–838. <http://dx.doi.org/10.1016/j.mineng.2011.03.002>.
- Lu, P., Zhu, C., 2011. Arsenic Eh–pH diagrams at 25 °C and 1 bar. *Environ. Earth Sci.* 62, 1673–1683. <http://dx.doi.org/10.1007/s12665-010-0652-x>.
- Márquez, M.A., Ospina, J.D., Morales, A.L., 2012. New insights about the bacterial oxidation of arsenopyrite: a mineralogical scope. *Min. Eng.* 39, 248–254. <http://dx.doi.org/10.1016/j.mineng.2012.06.012>.
- McGuire, M.M., Edwards, K.J., Banfield, J.F., Hamers, R.J., 2001. Kinetics, surface chemistry, and structural evolution of microbially mediated sulfide mineral dissolution. *Geochim. Cosmochim. Acta* 65, 1243–1258. [http://dx.doi.org/10.1016/S0016-7037\(00\)00601-3](http://dx.doi.org/10.1016/S0016-7037(00)00601-3).
- Mycroft, J.R., Bancroft, G.M., McIntyre, N.S., Lorimer, J.W., Hill, I.R., 1990. Detection of sulphur and polysulphides on electrochemically oxidized pyrite surfaces by X-ray photoelectron spectroscopy and Raman spectroscopy. *J. Electroanal. Chem. Interfacial Electrochem.* 292, 139–152. [http://dx.doi.org/10.1016/0022-0728\(90\)87332-E](http://dx.doi.org/10.1016/0022-0728(90)87332-E).
- Ngoma, I.E., Ojumu, T.V., Harrison, S.T., 2015. Investigating the effect of acid stress on selected mesophilic micro-organisms implicated in bioleaching. *Min. Eng.* 75, 6–13. <http://dx.doi.org/10.1016/j.mineng.2015.02.007>.
- Nguyen, V.K., Lee, M.H., Park, H.J., Lee, J.U., 2015. Bioleaching of arsenic and heavy metals from mine tailings by pure and mixed cultures of *Acidithiobacillus* spp. *J. Ind. Eng. Chem.* 21, 451–458. <http://dx.doi.org/10.1016/j.jiec.2014.03.004>.
- Nöel, N., Florian, B., Sand, W., 2010. AFM & EFM study on attachment of acidophilic leaching organisms. *Hydrometallurgy* 104, 370–375. <http://dx.doi.org/10.1016/j.hydromet.2010.02.021>.
- Pinet, N., Tremblay, A., 2009. Structural analysis of the Velardeña mining district, Mexico: a faulted Au–Ag-rich hydrothermal system. *Can. J. Earth Sci.* 46, 123–138. <http://dx.doi.org/10.1139/E09-007>.
- Ram, R.J., VerBerkmoes, N.C., Thelen, M.P., Tyson, G.W., Baker, B.J., Blake, R.C., Banfield, J.F., 2005. Community proteomics of a natural microbial biofilm. *Science* 308, 1915–1920. <http://dx.doi.org/10.1126/science.1109070>.
- Rawlings, D.E., 2008. High level arsenic resistance in bacteria present in biooxidation tanks used to treat gold-bearing arsenopyrite concentrates: a review. *T. Nonferr. Metal Soc.* 18, 1311–1318. [http://dx.doi.org/10.1016/S1003-6326\(09\)60003-0](http://dx.doi.org/10.1016/S1003-6326(09)60003-0).
- Razo, I., Carrizales, L., Castro, J., Díaz-Barriga, F., Monroy, M., 2004. Arsenic and heavy metal pollution of soil, water and sediments in a semi-arid climate mining area in Mexico. *Water Air Soil Pollut.* 152, 29–152. <http://dx.doi.org/10.1023/B:WATE.0000015350.14520.c1>.
- Rodriguez, Y., Ballester, A., Blazquez, M.L., Gonzalez, F., Munoz, J.A., 2003. New information on the chalcopryrite bioleaching mechanism at low and high temperature. *Hydrometallurgy* 71 (1), 47–56. [http://dx.doi.org/10.1016/S0304-386X\(03\)00173-7](http://dx.doi.org/10.1016/S0304-386X(03)00173-7).
- Rohwerder, T., Sand, W., 2007. Mechanisms and biochemical fundamentals of bacterial metal sulfide oxidation. In *Microbial processing of metal sulfides*. Springer, Netherlands, pp. 35–58.
- Rohwerder, T., Gehrke, T., Kinzler, K., Sand, W., 2003. Bioleaching review part a. *Appl. Microbiol. Biotechnol.* 63, 239–248. <http://dx.doi.org/10.1007/s00253-003-1448-7>.
- Sampson, M.I., Phillips, C.V., Blake, R.C., 2000. Influence of the attachment of acidophilic bacteria during the oxidation of mineral sulfides. *Min. Eng.* 13, 373–389. [http://dx.doi.org/10.1016/S0892-6875\(00\)00020-0](http://dx.doi.org/10.1016/S0892-6875(00)00020-0).
- Sasaki, K., Tsunekawa, M., Ohtsuka, T., Konno, H., 1998. The role of sulfur-oxidizing bacteria *Thiobacillus thiooxidans* in pyrite weathering. *Colloids Surf. A* 133, 269–278. [http://dx.doi.org/10.1016/S0927-7757\(97\)00200-8](http://dx.doi.org/10.1016/S0927-7757(97)00200-8).
- Sasaki, K., Nakamura, Y., Hirajima, T., Tuovinen, O.H., 2009. Raman characterization of secondary minerals formed during chalcopryrite leaching with *Acidithiobacillus ferrooxidans*. *Hydrometallurgy* 95, 153–158. <http://dx.doi.org/10.1016/j.hydromet.2008.05.009>.
- Sharma, P.K., Das, A., Rao, K.H., Forssberg, K.S.E., 2003. Surface characterization of *Acidithiobacillus ferrooxidans* cells grown under different conditions. *Hydrometallurgy* 71, 285–292. [http://dx.doi.org/10.1016/S0304-386X\(03\)00167-1](http://dx.doi.org/10.1016/S0304-386X(03)00167-1).
- Tu, B., Li, J., Guo, Y., Guo, X., Lu, X., Han, X., 2014. Compensation phenomena found in *Acidithiobacillus ferrooxidans* after starvation stress. *J. Basic Microbiol.* 54, 598–606. <http://dx.doi.org/10.1002/jobm.201200637>.
- Tuovinen, O.H., Bhatti, T.M., Bigham, J.M., Hallberg, K.B., Garcia, O., Lindström, E.B., 1994. Oxidative dissolution of arsenopyrite by mesophilic and moderately thermophilic acidophiles. *Appl. Environ. Microbiol.* 60, 3268–3274. <http://dx.doi.org/10.0099-2241/94/S04.00+0>.
- Vu, B., Chen, M., Crawford, R.J., Ivanova, E.P., 2009. Bacterial extracellular polysaccharides involved in biofilm formation. *Molecules* 14, 2535–2554. <http://dx.doi.org/10.3390/molecules14072535>.
- Wang, S., Zhao, X., 2009. On the potential of biological treatment for arsenic contaminated soils and groundwater. *J. Environ. Manag.* 90, 2367–2376. <http://dx.doi.org/10.1016/j.jenvman.2009.02.001>.
- White, S.N., 2009. Laser Raman spectroscopy as a technique for identification of seafloor hydrothermal and cold seep minerals. *Chem. Geol.* 259, 240–252. <http://dx.doi.org/10.1016/j.chemgeo.2008.11.008>.
- Yoshida, T., Yamauchi, H., Sun, G.F., 2004. Chronic health effects in people exposed to arsenic via the drinking water: dose–response relationships in review. *Toxicol. Appl. Pharmacol.* 198, 243–252. <http://dx.doi.org/10.1016/j.taap.2003.10.022>.
- Zeng, W., Tan, S., Chen, M., Qiu, G., 2011. Detection and analysis of attached microorganisms on the mineral surface during bioleaching of pure chalcopryrite with moderate thermophiles. *Hydrometallurgy* 106, 46–50. <http://dx.doi.org/10.1016/j.hydromet.2010.11.014>.
- Zhu, J., Li, Q., Jiao, W., Jiang, H., Sand, W., Xia, J., Chai, L., 2012. Adhesion forces between cells of *Acidithiobacillus ferrooxidans*, *Acidithiobacillus thiooxidans* or *Leptospirillum ferrooxidans* and chalcopryrite. *Colloids Surf. B* 94, 95–100. <http://dx.doi.org/10.1016/j.colsurfb.2012.01.022>.
- Zhu, J., Wang, Q., Zhou, S., Li, Q., Gan, M., Jiang, H., Qin, W., Liu, X., Hu, Y., Qiu, G., 2015. Insights into the relation between adhesion force and chalcopryrite-bioleaching by *Acidithiobacillus ferrooxidans*. *Colloids Surf. B* 126, 351–357. <http://dx.doi.org/10.1016/j.colsurfb.2014.11.036>.

Assessment of biofilm changes and concentration-depth profiles during arsenopyrite oxidation by *Acidithiobacillus thiooxidans*

Hugo Ramírez-Aldaba^{1,2} · Jorge Vazquez-Arenas³ · Fabiola S. Sosa-Rodríguez⁴ ·
Donato Valdez-Pérez⁵ · Estela Ruiz-Baca² · Jessica Viridiana García-Meza⁶ ·
Gabriel Trejo-Córdova⁷ · René H. Lara²

Received: 6 January 2017 / Accepted: 23 June 2017 / Published online: 12 July 2017
© Springer-Verlag GmbH Germany 2017

Abstract Biofilm formation and evolution are key factors to consider to better understand the kinetics of arsenopyrite biooxidation. Chemical and surface analyses were carried out using Raman spectroscopy, scanning electron microscopy (SEM), confocal laser scanning microscopy (CLSM), glow discharge spectroscopy (GDS), and protein analysis (i.e., quantification) in order to evaluate the formation of intermediate secondary compounds and any significant changes arising in the biofilm structure of *Acidithiobacillus thiooxidans* during a 120-h period of biooxidation. Results show that the biofilm first evolves from a low cell density structure (1 to 12 h) into a formation of microcolonies (24 to 120 h) and then finally becomes enclosed by a secondary compound matrix that includes pyrite (FeS₂)-like, S_n²⁻/S⁰, and As₂S₃ compounds, as shown by Raman and SEM-EDS. GDS analyses (concentration-depth profiles, i.e., 12 h) indicate significant

differences for depth speciation between abiotic control and biooxidized surfaces, thus providing a quantitative assessment of surface-bulk changes across samples (i.e. reactivity and /or structure-activity relationship). Respectively, quantitative protein analyses and CLSM analyses suggest variations in the type of extracellular protein expressed and changes in the biofilm structure from hydrophilic (i.e., exopolysaccharides) to hydrophobic (i.e., lipids) due to arsenopyrite and cell interactions during the 120-h period of biooxidation. We suggest feasible environmental and industrial implications for arsenopyrite biooxidation based on the findings of this study.

Keywords Arsenopyrite biooxidation · *Acidithiobacillus thiooxidans* · Biofilm changes · Glow discharge spectroscopy · Surface analysis

Responsible editor: Robert Duran

Electronic supplementary material The online version of this article (doi:10.1007/s11356-017-9619-8) contains supplementary material, which is available to authorized users.

✉ René H. Lara
lcrh75@ujed.mx; lcrh75@hotmail.com

¹ Programa de Doctorado Interinstitucional en Ciencias Agropecuarias y Forestales, Universidad Juárez del Estado de Durango, Río Papaloapan y Blvd. Durango S/N, Col. Valle del Sur, 34120 Durango, DGO, Mexico

² Facultad de Ciencias Químicas, Universidad Juárez del Estado de Durango (UJED), Av. Veterinaria S/N, Circuito Universitario, Col. Valle del Sur, 34120 Durango, DGO, Mexico

³ Centro Mexicano para la Producción más Limpia, Instituto Politécnico Nacional, Avenida Acueducto s/n, Col. La Laguna Ticomán, 07340 Ciudad de México, Mexico

⁴ Universidad Autónoma Metropolitana-Azcapotzalco, Av. San Pablo 180, Azcapotzalco, 02200 Ciudad de México, Mexico

⁵ Instituto Politécnico Nacional, UPALM, Edif. Z-4 3er Piso, 07738 Ciudad de México, Mexico

⁶ Geomicrobiología, Facultad de Ingeniería, UASLP, Av. Sierra Leona 550, Lomas 2da, 78210 San Luis Potosí, SLP, Mexico

⁷ Centro de Investigación y Desarrollo Tecnológico en Electroquímica (CIDETEQ), Parque Tecnológico Querétaro-Sanfandila, 76703 Pedro Escobedo, QRO, Mexico

Introduction

Arsenopyrite (FeAsS) is the main As-bearing sulfide mineral (SM) in the lithosphere. Understanding the structure-activity relationship of FeAsS is important in order to help mitigate environmental problems (i.e., bioremediation) and to improve industrial bioleaching processes which use iron-oxidizing microorganisms (IOMs, *Leptospirillum ferrooxidans*) and/or sulfur-oxidizing microorganisms (SOMs, *Acidithiobacillus thiooxidans*) (Rohwerder and Sand 2007; Wang and Zhao 2009; Ko et al. 2013). Previous studies on arsenopyrite bioleaching have focused mainly on analyzing the interface arising between mineral and the microorganism *Acidithiobacillus ferrooxidans* since this IOM/SOM demonstrates enhanced capability to use the $\text{Fe}^{2+}/\text{Fe}^{3+}$ cycle and to directly oxidize sulfur compounds (i.e., S^- , S^{2-} , S_n^{2-} , S^0) (Rohwerder et al. 2003). The interaction between arsenopyrite and *A. thiooxidans* (SOM), however, remains poorly understood, and relevant aspects regarding biofilm formation and evolution, as well as the effect of toxins in the environment (i.e., arsenic) on biooxidation processes have been overlooked. Better understanding of such information is important because environmental toxins may strongly affect biofilm properties and, consequently, bioleaching rates and mechanisms (Devasia and Natarajan 2010). Establishing a correlation between the aforementioned parameters and/or monitoring changes in biofilm structure and composition would contribute to fundamental knowledge useful in order to progressively regulate the contributions of *A. thiooxidans* (i.e., isolation of metabolic capacity to attack S_n^{2-} and S^0 compounds) in the presence and absence of mixed cultures (Dopson and Lindström 2004; Rohwerder and Sand 2007) and to control arsenopyrite reactivity for a determined application. Likewise, knowledge generated by such an analysis would be favorable in designing efficient bioleaching systems (i.e., environmental and/or industrial) and in preventing environmental risks in areas where arsenopyrite biooxidation promotes dissemination of toxic arsenic into the environment (Lu and Wang 2012). Exploring the linkage this liberation has on the incidence of numerous forms of cancer (i.e., skin, lung, bladder) could also aid in improving human health (Yoshida et al. 2004).

Preliminary insights have suggested that biofilm structure changes significantly during the oxidation of arsenopyrite by *A. thiooxidans* and that biooxidation processes depend on direct cell attachment to arsenopyrite under the presence and absence of supplementary toxic arsenic (Ramírez-Aldaba et al. 2016). A comprehensive examination of the transient structures and composition of biofilms during arsenopyrite biooxidation, as well as an assessment of surface-mineral depth profiles, has, however, not been conducted. The present study uses Raman spectroscopy, glow discharge spectroscopy (GDS), SEM-EDS, confocal laser scanning microscopy

(CLSM), and protein analyses (i.e., quantification) to thoroughly investigate the aforementioned. It is expected that results from this study will allow better understanding of the factors that influence biofilm formation and evolution. Such knowledge could enhance arsenopyrite bioleaching and biooxidation processes and be useful under various applications (i.e., industrial, bioremediation).

Experimental section

Arsenopyrite preparation

Arsenopyrite samples were obtained from an auriferous mining area in Velardeña, Durango, located in Mexico's northwestern region (Pinet and Tremblay 2009). Selected samples were digested with acid ($\text{HCl} + \text{HNO}_3$, 3:1 v/v), and the resultant solutions were analyzed by microwave plasma-atomic emission spectrometry (AES-MP, Agilent 4100 spectrometer) to evaluate mineral composition and impurity content. SEM-EDS analyses (ZEISS-DSM950 coupled to EDX system) and X-ray diffraction patterns (Rigaku DMAX 2200) were used to examine impurities contained in pristine samples and to corroborate arsenopyrite identity, respectively. Coupons of arsenopyrite were employed for the construction of massive arsenopyrite electrodes (MAEs, exposed surface area is 1 cm^2), which were polished to obtain a mirror-like surface prior to each experiment. These MAE specimens were oxidized in an ATCC-125 (American Type Culture Collection) solution (acidified with H_2SO_4 at pH 2.0) by the application of an anodic pulse (E_a) at 1.21 V vs. SHE during 1 h using a Biologic SP-150 potentiostat/galvanostat. This E_a was selected according to previous electrochemical analyses (i.e., cyclic voltammetry) conducted for pristine samples in the same culture media (data not shown). Potentiostatic oxidation was carried out in a Pyrex™ glass three-electrode cell, with MAE and a graphite rod (Alfa Aesar, 99.9995% purity) as working and counter electrodes, respectively. A saturated sulfate electrode (0.615 V vs. SHE) was used as reference. This procedure and the usage of MAE specimens (instead of particles of arsenopyrite samples) allowed for rapid, controlled, significant, and quasi-homogeneous generation of secondary compounds (i.e., S_n^{2-} and S^0 , surface coating) on the electrochemically modified MAE surface (defined as eMAE in the remainder of the text) and facilitated the development of a biofilm which generated surface products at adequate levels for further spectroscopic, microscopic, and biochemical characterizations. S_n^{2-} and S^0 compounds act as electron donors (energy source) for *A. thiooxidans* during altered arsenopyrite biooxidation (Rohwerder et al. 2003) and stimulate the metabolic capability of *A. thiooxidans* to colonize the S_n^{2-} and S^0 substrate on the eMAE surface (Devasia and Natarajan 2010; Jin et al. 2012).

Biofilm formation and biooxidation assays

The strain of *A. thiooxidans* used in this study was ATCC no. 19377, aerobically cultivated at 28–30 °C in a 50-mL medium of acidified ATCC-125 (pH 2.0). The per liter composition of the acidified ATCC-125 solution medium was 10 g S⁰, 3.0 g KH₂PO₄, 0.4 g (NH₄)₂SO₄, 0.5 g MgSO₄·7H₂O, 0.25 g CaCl₂·2H₂O, and 0.01 g FeSO₄·7H₂O (JT Baker). The medium was distributed into 250-mL Erlenmeyer flasks and sterilized using an autoclave at 121 °C for 15 min. S⁰ and the eMAE were separately placed into glass petri dishes and statically sterilized under UV irradiation for 2 h. *A. thiooxidans* cells were grown until the exponential growth phase was attained with an average biomass concentration of ~10⁸ cells mL⁻¹. Cell counting was carried out using the UV-vis technique (Hach 5500 spectrophotometer) which relates biomass content to absorbance measurements. A Newsbauer camera was also used to confirm cell counts. Ten milliliters of the prepared culture was used as inoculum in the biotic experiments (biooxidation assays) for each time analyzed. Sterilized eMAE was then placed in 50 mL of ATCC-125 culture medium containing approximately 10⁷ cells mL⁻¹ at pH 2.0 (batch system). Abiotic control assays were also prepared in order to establish a fair comparison between chemical and biological oxidations. Resulting eMAE surfaces after biooxidation are referred to as “biooxidized eMAE surfaces,” whereas those after abiotic assays are referred to as “abiotic control eMAE surfaces.” Samples from abiotic controls and biooxidized eMAE surfaces were collected at 1, 12, 24, 48, 72, and 120 h, dried with a direct flow of chromatographic grade N₂, and prepared under inert conditions for further surface analyses. Duplicate measures for control and biooxidation assays were performed for every time increment.

Surface analysis

Surface characterizations for all types of MAE surfaces were performed using SEM-EDS, Raman spectroscopy, CLSM, and GDS techniques. Raman spectra were recorded with a Horiba XploRA™ PLUS spectrometer coupled with a SWIFT™ v2 confocal imaging module which used a solid-state laser beam ($\lambda = 532$ nm). For calibration purposes in Raman spectroscopy, a Si wafer disc (521 cm⁻¹) was used. The vibrational range was from 100 to 750 cm⁻¹ as the S_n²⁻ and S⁰ and main arsenic-bearing compounds show their main active modes within this interval (Mycroft et al. 1990; Márquez et al. 2012). At least 10 Raman spectra were collected for each sample. SEM analyses were performed using a ZEISS-DSM950 microscope coupled to EDX system. Biooxidized eMAE surfaces containing biofilms were fixed by immersion in a 3% (m/m) glutaraldehyde (grade I, Sigma-Aldrich) phosphate buffer (pH 7.2) at 4 °C for 24 h. They were then

rinsed with a phosphate buffer (pH 7.2). Biofilms were dehydrated by rinsing successively with various strengths of ethanol (ultrapure, Sigma-Aldrich) from 10 to 100% in concentration (v/v). Excess ethanol was then carefully removed from the samples, and they were then instantly frozen with liquid nitrogen and dried by lyophilization (Labconco FreeZone Freeze Dry System) at 0.13 mbar and -41 °C for 2 h. Samples were then placed into sealed glass vials and coated with a thin Au film. GDS analyses were performed using a glow discharge spectrometer Horiba Scientific GD profiler 2 using a current of 50 mA and 1000 W (140 °C) under vacuum conditions (~10⁻⁵ Torr). The spectrometer had a focal length of 1000 nm and was configured with 40 simultaneous detectors for the different atomic emission lines. The analytical area was 4 mm in diameter. Seven hundred volts and 20 mA were chosen for the excitation and sputtering processes, respectively. Note that the use of this technique to investigate biooxidized SM surfaces (i.e., surface-bulk changes) is unprecedented to our current state of knowledge. Therefore, it could provide a new perspective to account for the role of mineral properties on SM reactivity and biofilm performance, by indicating specific modifications on elemental composition (i.e., Fe, S, Mn, Mo, and C) in surface-depth profiles. CLSM experiments were carried out to estimate epifluorescence signals as an indirect approach to register changes in extracellular polymeric substance (EPS) secretion (i.e., biofilm progress) using a ZIESS LSM 710 microscope (Jena, Germany) and ZEN 2010 B SP1 software (Zhang and Fang 2001; Lei et al. 2009). Biofilms were fixed with a formaldehyde 1% (m/m) phosphate buffer (pH 7.2) at 4 °C for 2 h, to stain hydrophilic domains (i.e., exopolysaccharides) under dark conditions with lectin *Canavalia ensiformis* (Con-A, tetramethylrhodamine conjugated), using an excitation signal at 488 nm and an emission maxima signal at 575 nm. The molecular probe Nile Red (NR; Sigma) was used to stain hydrophobic domains (i.e., lipids) with an excitation signal of 515–560 nm and an emission maximum signal of 650 nm (González et al. 2012). Band pass filters were utilized for emissions at 575 and 650 nm. All data were corrected for background signals as much as possible. The biofilms were then scanned at a depth of 0.2 μm. The difference between the maxima of emitted signals and the corresponding filtering of such signals (I3 and N2.1 filters) allowed us to discriminate between exopolysaccharides (stained with Con-A) and hydrophobic domains of EPS (stained with NR). CLSM analysis for planktonic cells was also carried out in order to compare planktonic cells with biofilms. To do this, an aliquot of the cultivated strain was mounted directly on the eMAE surface (i.e., 0 h of biooxidation) under the same experimental conditions as described above.

Protein extraction and quantification

Four sterilized eMAEs (1 cm² of area) were placed into 50 mL of ATCC-125 culture medium containing $\sim 10^7$ cells mL⁻¹ at pH 2.0 (batch system) for each time frame analyzed. The biofilms were scraped from each biooxidized eMAE surface and put in Eppendorf™ vials. The cells were washed with buffer A (50 mM Tris-HCl pH = 7.5 and 1 mM PMFS) and centrifuged at 7000 g for 15 min (4 °C). The resulting pellets were resuspended using 300 μ L of sterile water. For extraction of the EPS, the pellets were treated with 300 μ L of buffer B (0.5% SDS, 10 mM DTT, 50 mM Tris-HCl pH = 7.5, 10 mM EDTA, and 1 mM PMFS) for 5 min (37 °C) using a gentle stirring technique in order to avoid cell breakage. The extract containing EPS was centrifuged at 13,000 \times g for 10 min (4 °C), and proteins were precipitated with 70% ethanol (v/v) for 3 h at -20 °C. The extract with the EPS-associated protein fraction was used for quantitative analyses (Table 2). Normalization of data was performed as follows (González et al. 2012; García-Meza et al. 2013): the protein concentration per eMAE-surficial area (1 cm²) was determined by the Bradford method (Bradford 1976) by comparing the measured absorption values (UV-vis 50 Bio-spectrophotometer) with those of a calibration range of albumin as standard of known concentrations (between 1 and 30 mg mL⁻¹). The present protocol allows for extraction of the EPS-associated protein (i.e., avoiding heating of the system to decrease cell lysis), thus permitting a quantitative assessment of the extracted proteins for each time point analyzed (Comte et al. 2006; Flemming and Wingender 2001; Jia et al. 2010; More et al. 2014).

Results and discussion

Mineralogical characterization of pristine arsenopyrite

Chemical analyses of the pristine arsenopyrite samples showed the following chemical composition: 96.56 (± 0.2) wt% FeAsS, 1.42 (± 0.3) wt% PbS, 0.88 (± 0.1) wt% ZnS, and 1.16 (± 0.3) wt% SiO₂. These impurities were identified as crystal inclusions using SEM-EDS (ESM, Fig. S1). The pure arsenopyrite sample corresponds to the XRD pattern JCPDS card no. 14-218; whence trace amounts of Mn and Mo, among others, were also detected by microwave plasma-atomic emission spectrometry.

Surface analysis for control and biooxidized samples

Raman study

Figure 1 (a) shows the Raman spectrum of the pristine MAE surface which exhibits some typical broad peaks at ~ 220 and

~ 277 cm⁻¹ (McGuire et al. 2001; Márquez et al. 2012). A summary of the characteristic transitions found in the present analysis encompass with pyrite (FeS₂), arsenopyrite (FeAsS), polysulfides (S_n²⁻), elemental sulfur (S⁰), and realgar (As₂S₂) structures is provided in the electronic supplementary material (ESM, Table S1). Raman spectra of As₂S₃, S⁰, and pristine pyrite are also shown to allow for comparisons with secondary compounds found in the present study (Fig. S1). Figure 1 (b) shows the Raman spectrum of potentiostatically oxidized MAE specimen (eMAE) in the ATCC-125 medium and mainly indicates the formation of S⁰ and S_n²⁻ phases (i.e., Fe_{1-x}As_{1-y}S_{1-z} at 127, 208, and 437–480 cm⁻¹, Table S1) and pyrite-like compounds (334 and 373 cm⁻¹, Table S1). The eMAE surface was considered the initial stage ($t = 0$ h) for abiotic and biooxidation assays. It was found that the secondary compounds were essentially the same (i.e., pyrite-like compounds, 341 and 373 cm⁻¹) for abiotic control eMAE surfaces in all assayed times; an example of these results is given in Fig. 1 (c) for 1 h of assay. These findings demonstrate that arsenopyrite underwent a slow chemical oxidation in the ATCC-125 medium and that the accumulation of refractory pyrite-like compounds was enhanced during this period (Ramírez-Aldaba et al. 2016). Figure 1 (d'-1 to d'-6) shows the Raman spectra for biooxidized eMAE surfaces at different exposure times. The formation of S_n²⁻ (458–465 cm⁻¹) and pyrite-like compounds (328 and 363–365 cm⁻¹) was evident until 24 h of the assay (Fig. 1 (d'-1 to d'-3), Table S1). A stronger biooxidation of arsenopyrite was then observed between 48 and 72 h of the assay, as indicated by the formation of a mixture of S⁰ (135, 206, and 465 cm⁻¹) and S_n²⁻ compounds (458 cm⁻¹) (Fig. 1 (d'-4 and d'-5); Table S1). A remarkable change in surface processes controlling biooxidation was observed after 120 h of the assay, after which two oxidized areas for the same eMAE sample including different secondary compounds were identified: S_n²⁻ (i.e., Fe_{1-x}As_{1-y}S, 465 cm⁻¹, Fig. 1 (d'-6), spectrum ii) and orpiment-like compounds (247, 320, and 360 cm⁻¹, Fig. 1 (d'-6), spectrum i; Table S1 and Fig. S1c). In the Raman analysis, peak shifts are expected due to mass changes in the structures of surface compounds (i.e., pyrite-like phase, S_n²⁻/S⁰), thus modifying their vibrational frequencies. These findings indicate a noteworthy interaction between *A. thiooxidans* and arsenopyrite, whence secondary compounds are formed as a result of direct cell attachment to induce progressive chemical surface transformations (Devasia and Natarajan 2010; Liu et al. 2011; Ramírez-Aldaba et al. 2016). The varied mixtures of S_n²⁻, S⁰, pyrite-like, and As₂S₃-like compounds (i.e., altered surface) in Fig. 1 were then associated to further differences in SM reactivity by modifying structure-activity relationships for arsenopyrite (see below, Fig. 2) under chemical (Mikhlin et al. 2006) and/or biological (Cruz et al. 2005) reactions. According to the literature (Liu et al. 2011), arsenopyrite oxidation by *A. ferrooxidans* results in the formation of realgar (As₂S₂)-like

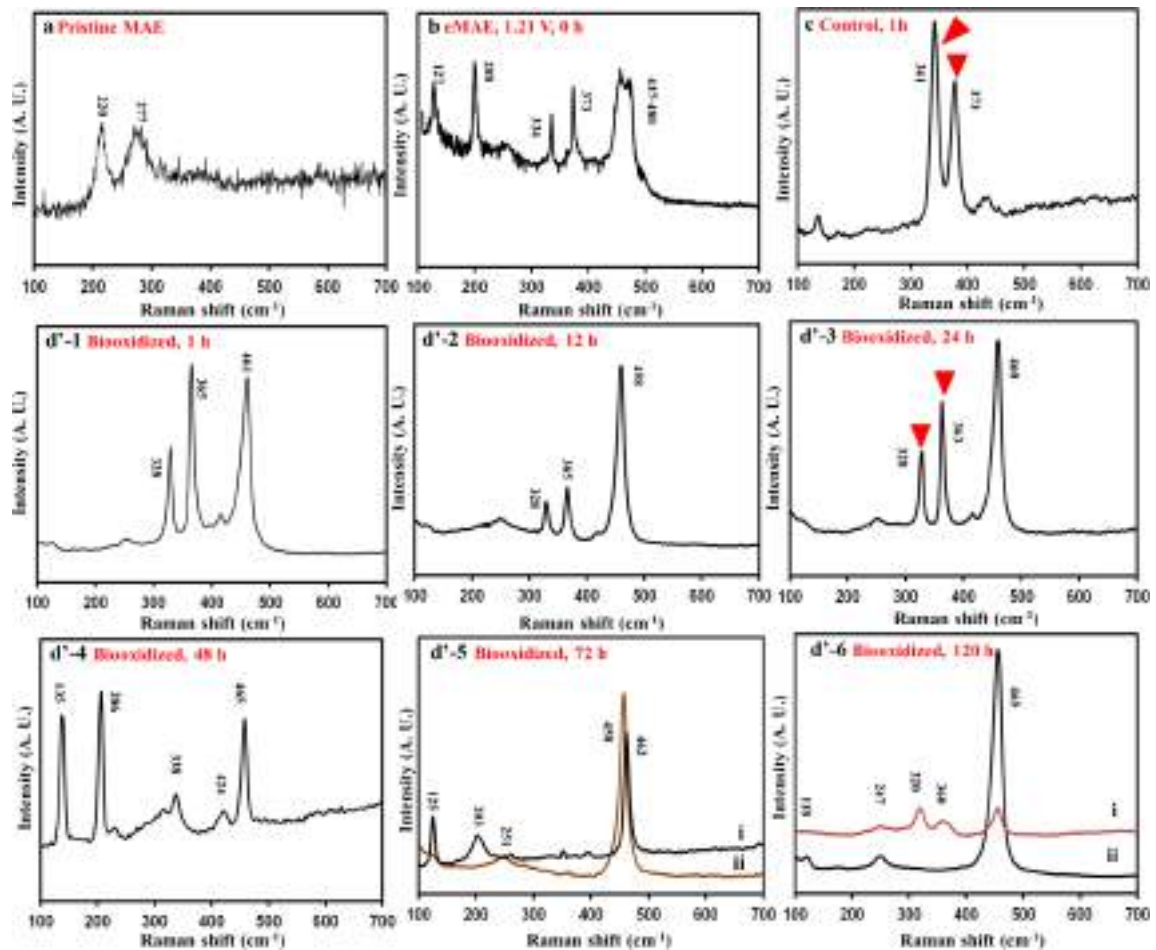


Fig. 1 Raman spectra on pristine MAE (a), eMAE surface (0 h) (b), abiotic control at 1 h (c), and biooxidized eMCE surfaces collected after different time intervals: 1 h (d'-1), 12 h (d'-2), 24 h (d'-3), 48 h (d'-4), 72 h (d'-5, spectra *i* and *ii*), and 120 h (d'-6, spectra *i* and *ii*). Abiotic control eMAE surfaces contained similar secondary compounds as indicated for

sample after 1 h of abiotic assay (c). The spectra *i* and *ii* in figures d'-5 and d'-6 indicate two different secondary phases identified for the same oxidized surface. Changes in specific Raman peak positions for pyrite-like phases are illustrated by red labels (inverted triangles) inside figures c and d'-3, for instance. Sample periods lasted for 60 s, $\lambda = 514$ nm, 25 A

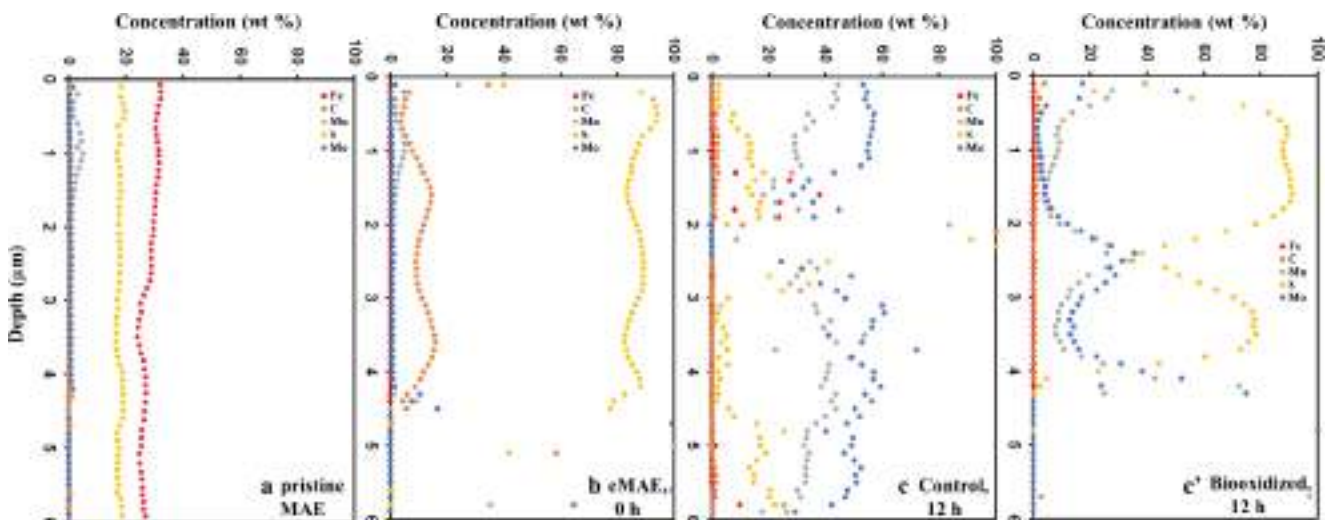


Fig. 2 Glow discharge spectroscopy spectra for pristine MAE (a), eMAE (without leaching) (b), abiotic control (c), and biooxidized eMAE (c') surfaces after 12 h of assay. Profiles for S, Fe, C, Mn, and Mo are illustrated in the figure

and oxide ferric compounds, in close agreement with our Raman study (Figs. 1 and S1; Table S1). Nonetheless, oxidation of arsenopyrite by *A. thiooxidans* involves intermediate stages to form pyrite-like and mainly S_n^{2-} and S^0 compounds (Fig. 1, Table S1). These results confirm differences in the chemical pathways for arsenopyrite oxidation by IOM and SOM cells (i.e., *A. thiooxidans*) which can be attributed to specific differences between cells and SM interactions (i.e., mineral-charged interface) (Devasia and Natarajan 2010; Crundwell 2015). Although not analyzed in the present manuscript, it is clear from the literature that this interaction involves a physicochemical process, since cell attachment to minerals entails a series of chemical reactions (Fowle and Fein 1999; Liermann et al. 2000a; Bennett et al. 2001; Devasia and Natarajan 2010). Bacteria have a competitive advantage over planktonic or groundwater-entrained cells through preferential acquisition of nutrients from the mineral surface (i.e., S_n^{2-}/S^0), protection from predation via biofilm formation, and communalism among various microbial species (Barker and Banfield 1996; Rogers et al. 1998; Ehrlich 2002; Devasia and Natarajan 2010). Bacteria can therefore promote or inhibit the rate of secondary mineral phase formation, weathering reactions through the generation of pH gradients at the interface, and complexation via exudates (Welch et al. 1999; Barker et al. 1998; Liermann et al. 2000b).

Glow discharge spectroscopy analysis

Figure 2 shows the GDS analysis for pristine (Fig. 2 (a)), eMAE (Fig. 2 (b)), control abiotic eMAE (Fig. 2 (c)), and biooxidized eMAE surfaces (Fig. 2 (d)) after 12 h. This time was selected based on the premise that biofilm organization changed from low cell density to microcolony structure around this time (Fig. 3 (d2 and d3)), representing an inflection point for further evaluation of the changes in surface-bulk relationships. The GDS spectrum of pristine MAE exhibited similar weight percentage profiles for Fe and S (Fig. 2 (a)) from the surface to the mineral bulk (i.e., 6 μm), which suggests that the MAE surface has not yet been transformed and mainly encompass their stoichiometries with the formation of an FeAsS structure, in agreement with Raman (Fig. 1 (a)) and SEM-EDS (Fig. S2). A higher amount (around 90%) of S was obtained for the eMAE surface from 0 to ~ 4.5 μm in depth (Fig. 2 (b)), indicating the S^- (i.e., pristine S in FeAsS lattice, Mikhlin et al. 2006) electrochemical oxidation to higher oxidation states (i.e., S_n^{2-} and S^0), as detected in previous experiments of Raman spectroscopy (Fig. 1 (b)) and SEM-EDS (Fig. 3 (b)). Particularly, the S profile described in Fig. 2 (b) indicates that the oxidation of sulfur species occurred from the inner crystal structure of MAE deeper than 4.5 μm (i.e., depletion of S species), presumably, following an atomic transport via point defects (i.e., vacancies, interstitials) which generates the growth of a film-containing oxidation products (i.e., S_n^{2-} and S^0) (Mikhlin

et al. 2006). Figure 2 (c) suggests that chemical weathering of arsenopyrite allows for the significant solid-state diffusion of trace impurities (i.e., Mn, Mo, 1–3 μm), which was significantly highlighted during the biooxidation process of arsenopyrite (Fig. 2 (c'), 1–2 μm). The significant presence of carbon on the eMAE surface was associated with the adsorption of CO_2 onto the mineral surfaces (Serre et al. 2007). Additionally, S compounds decreased during the initial biooxidation process (i.e., 0–1 μm), followed by the cyclic formation and depletion of these species indicating a sustained production of S_n^{2-} and S^0 compounds during the biooxidation process (i.e., 1–5 μm). These findings are in agreement with previous results (Fig. 1), whence variations in secondary compounds (i.e., pyrite-like, S_n^{2-} , S^0 , and As_2S_3 -like) were directly linked to dynamic surface-bulk changes (i.e., S phases, structure-activity relationship) in the GDS results (Fig. 2 (c')), which can be linked to mineral reactivity. In addition, these results provide a guideline to better assess the interactions of *A. thiooxidans* cells during the evolution of complex phenomena and processes during arsenopyrite biooxidation (i.e., surface-bulk changes) occurring in mixed bioleaching systems (i.e., *A. thiooxidans* and *A. ferrooxidans*) to better assess SM reactivity (i.e., specific structure-activity relationship) (Devasia and Natarajan 2010; Bobadilla-Fazzini et al. 2011).

Biofilm structure and composition

Figure 3 shows SEM images for pristine MAE (Fig. 3 (a)), eMAE (Figs. 3b), and biooxidized eMAE samples for all times assayed (Fig. 3 (d1 to 3d6)). The control samples exhibited a similar topography and morphology, as well as the same secondary products (i.e., pyrite-like compounds) in all times sampled, in agreement with Fig. 1 only displays analysis for samples collected at 12 h of chemical weathering. The identification of secondary compounds was achieved on the EDS basis (for instance, ESM, Fig. S5). Figure 4 exhibits the CLSM images for the biooxidized eMAE samples for all times assayed, depicting epifluorescence for exopolysaccharides in green and lipids in red (ESM, Fig. S4). The corresponding merge illustrating the relative predominance of these compounds is depicted in Fig. 4b–g for a complete microscopic description. This figure includes analysis of planktonic cells compared with cells forming biofilms. SEM-EDS analyses confirmed the findings of the Raman study (Fig. 1). Noteworthy are the chemical oxidation of S_n^{2-} and S^0 for the abiotic control eMAE surfaces, the further accumulation of refractory pyrite-like compounds at all time intervals (Fig. 3 (c)), and the formation of S_n^{2-} , S^0 , pyrite-like, and As_2S_3 compounds on biooxidized eMAE surfaces due to *A. thiooxidans* (Figs. 1 and 3 (d1 to d6), Table S1). Accordingly, scattered attached cells as low-density biofilm (i.e., incipient biofilm) on eMAE and secondary products (i.e., S_n^{2-} and S^0) were identified in the first hour of biooxidation (Figs. 3 (d1) and 4b), while

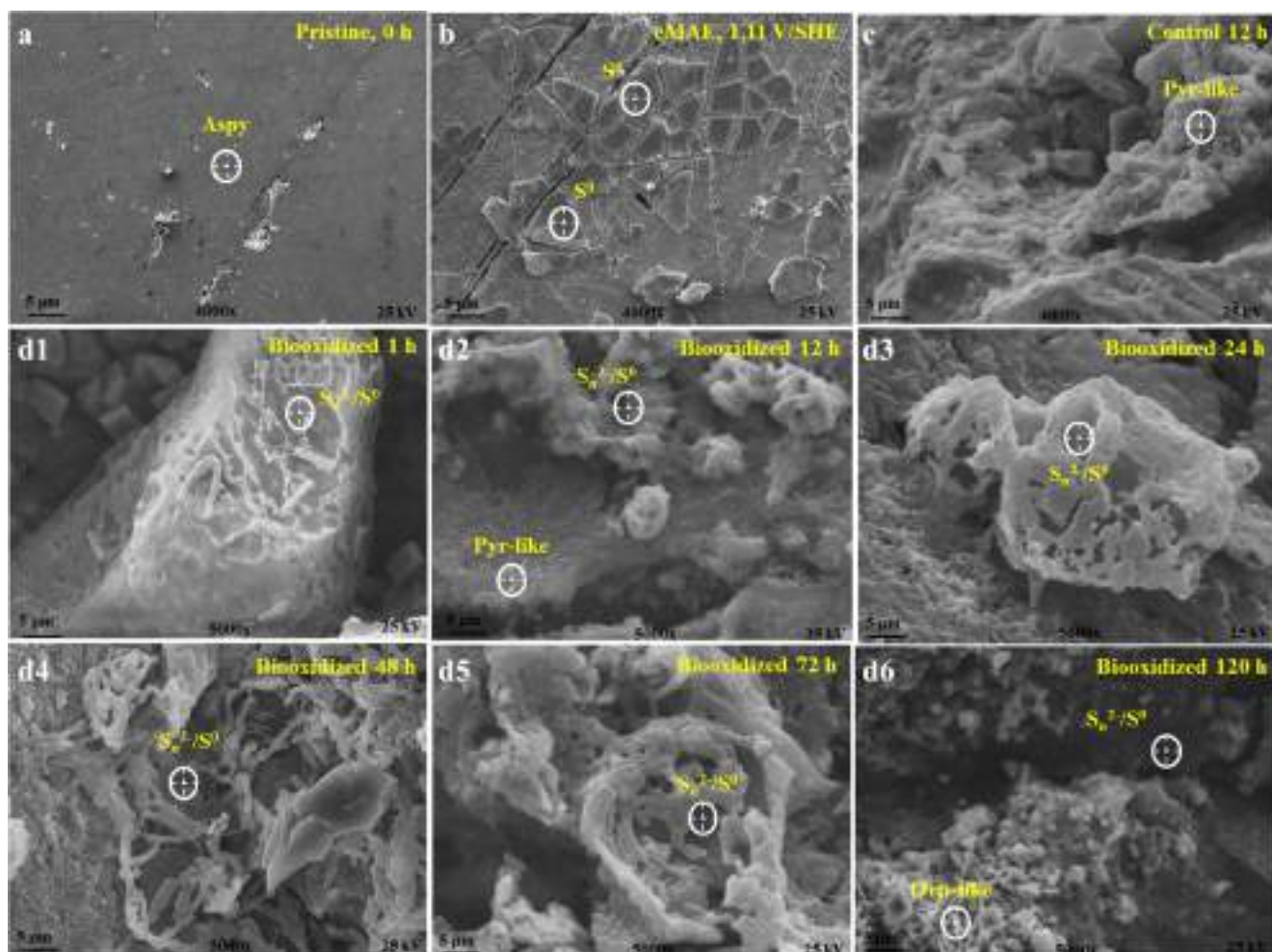


Fig. 3 Typical SEM images of the pristine MAE surface (a), eMAE surface (without leaching) (b), abiotic control eMAE surfaces after 12 h of assay (c), and biooxidized eMAE surfaces after 1, 12, 24, 48, 72,

and 120 h of assay (d1, d2, d3, d4, d5, d6 respectively). *Aspy* FeAsS, *Pyrite-like* pyrite-like, *As₂S₃-like* orpiment-like, *S_n²⁻* polysulfide structures, *S⁰* elementary sulfur (according to EDS analyses, *n* = 10)

formed thin biofilms (i.e., low cell density) with hydrophilic exopolysaccharides after 12 h (Figs. 3 (d2) and 4c). Afterwards, the cell density increased after 24 h (Figs. 3 (d3) and 4d), but decreased remarkably at 120 h (Figs. 3 (d6) and 4g), when the biooxidized eMAE became hydrophobic mainly due to the presence of secondary *S_n²⁻*, *S⁰*, and *As₂S₃*-like compounds (Figs. 1 and 2). The mineral surface turned out to be more hydrophobic during the biooxidation assays (Table 1, Fig. 4b–g, i.e. yellow to red, ESM, Fig. S4), describing an increase of both hydrophobic exopolymers in EPS (i.e., lipoproteins) and residues, as well as the aforementioned hydrophobic pyrite-like, *As₂S₃*, *S_n²⁻*, and *S⁰* compounds. These findings suggest that biofilm structure evolves to a more stable configuration in order to interact with secondary compounds as suggested in Fig. 3 (d6) (i.e., 120 h). As indicated by previous results (Fig. 4), biofilm structure is heightened by the synthesis of lipoproteins and fatty acids which induces cohesiveness for the maintenance of biofilm integrity by *A. thiooxidans* (Bobadilla-Fazzini et al. 2011). The setting of

biofilm stability through the production of lipoproteins and fatty acids is similar to other non-leaching bacterial biofilms as well (Flemming et al. 2000; Lawrence et al. 2003). Additionally, the main EPS of *A. ferrooxidans* biofilms was hydrophilic polysaccharides (i.e., glucose, rhamnose, and mannose) and hydrophobic lipids or saturated fatty acids and lipopolysaccharides (Gehrke et al. 1998). A similar study conducted by Vu et al. (2009) reported that when *A. ferrooxidans* cells grew and developed attachments on *S⁰* and pyrite surfaces, more lipids were produced when compared with planktonic cells. All these statements agree with the presence of extracellular polysaccharides and hydrophobic domains during arsenopyrite oxidation by *A. thiooxidans* (Table 1, Figs. 3 and 4), indicating that interactions between leaching bacteria (i.e., *A. ferrooxidans*, *A. thiooxidans*) and *S_n²⁻* and *S⁰* (hydrophobic) compounds are hydrophobic once a stable biofilm occurs (Harneit et al. 2006, Harneit and Sand 2007). In addition, the amount of extracellular proteins increases during the assayed times (Table 2). Proteins may be hydrophilic (i.e.,

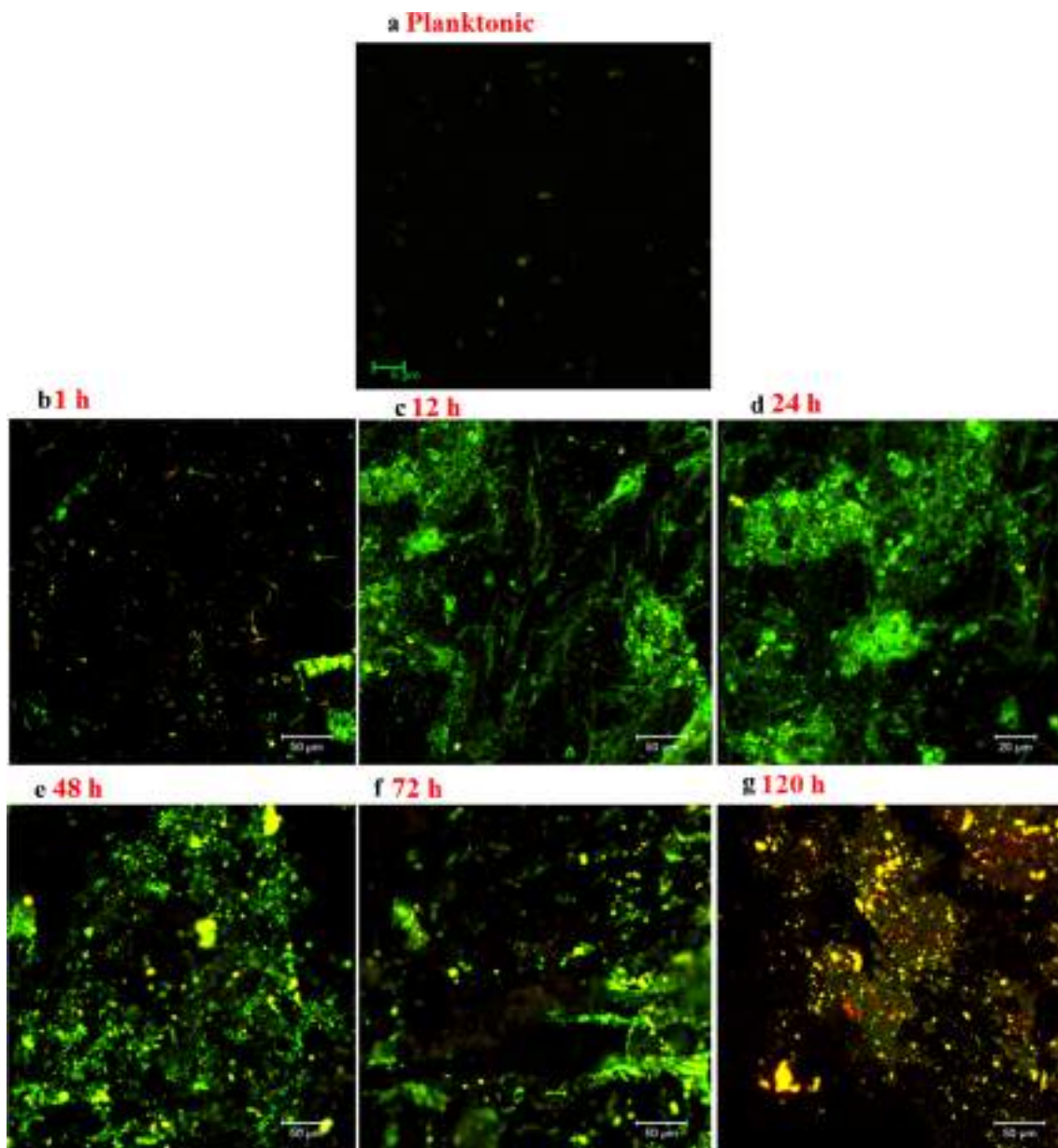


Fig. 4 CLSM images of *A. thiooxidans* for planktonic cells (a) and biofilms formed after the biooxidation of eMAE surfaces at different time intervals. In this figure, a merge between epifluorescence of hydrophilic domains as exopolysaccharides and hydrophobic domains as lipids is depicted from yellow to red, for 1 h (b), 12 h (c), (d) 24 h,

(e) 48 h, (f) 72 h and (g) 120 h of biooxidation. The total scanning area was $300 \times 300 \mu\text{m}$. The size bar scale is $50 \mu\text{m}$. Original epifluorescence from extracellular exopolysaccharides is green and red for lipids (ESM, Fig. S4)

glycoproteins) and hydrophobic (as lipoproteins). Some of them could be involved in cell attachment process at early assayed times (Arredondo et al. 1994; Flemming et al. 2000; Bobadilla-Fazzini et al. 2011; Flemming 2016), while some others involved in the stability of the biofilm after 24 h (Bobadilla-Fazzini et al. 2011), as suggested in Fig. 4 and Tables 1 and 2. Thus, the *A. thiooxidans* and arsenopyrite interaction was essentially hydrophilic due to small amount of proteins and a major amount of exopolysaccharides in EPS since the early stages of cell attachment (i.e., Fig. 4b, c; Tables 1 and 2). Note that *A. thiooxidans* modified the surface charge and the

hydropathy of the biooxidized eMAE surface (Holmes and Crundwell 2013) and consequently the overall microorganism-mineral interactions (Echeverría-Vega and Demergasso 2015), enhancing the biooxidation process of the arsenopyrite (Figs. 1, 2, 3, and 4). The nature and quantity of EPS in biofilms varied due to the charges on the mineral interface, as observed by Donlan (2002). These findings encompass with GDS analyses where S phases were depleted at 12 h of biooxidation (Figs. 1 and 2, i.e., 0–6 μm), illustrating specific mineralogical differences for the biofilm/arsenopyrite system and accounting for arsenopyrite reactivity (i.e., oxidation

Table 1 Epifluorescence values (arbitrary units (AU)) of biooxidized eMAE surfaces containing extracellular polysaccharides and lipids of *A. thiooxidans*-forming biofilms obtained using CLSM at different time intervals (data, $n = 30 \pm$ standard deviation). This Table shows data from planktonic cells for comparison purposes

Biooxidation time (h)	Exopolysaccharides (AU)	Lipids (AU)
0 (Planktonic)	45 ± 3.89	23 ± 3.48
1	62 ± 6.38	39 ± 4.27
12	125 ± 10.57	51 ± 6.35
24	143 ± 9.21	62 ± 6.38
48	120 ± 7.43	95 ± 7.58
72	111 ± 11.23	126 ± 3.07
120	103 ± 4.78	157 ± 9.78

capacity) (Fig. 2). Thus, *A. thiooxidans* biooxidizes and transforms the arsenopyrite surface regardless of the presence of abundant secondary compounds formed under different conditions (Sasaki et al. 1998, 2009) (i.e., Figs. 1, 2, and 3 (d6)). In the absence of *A. thiooxidans*, large amounts of secondary compounds (i.e., $K \cdot Fe_3(SO_4)_2(OH)_6$ and S^0) were produced during the bioleaching of arsenopyrite (Sasaki et al. 1998). Biofilms may be embedded in the secondary compound matrix with the progressive starvation and senescence of IOM cells (i.e., *A. ferrooxidans*) in mixed cultures (Henao and Godoy 2010). Further exploration of the role of protein production for sulfur oxidation, cell attachment, stability of biofilm structure, and arsenic tolerance during arsenopyrite oxidation by *A. thiooxidans* (i.e., proteomics and bioinformatics), as well as changes in biofilm production in the presence of supplementary arsenic, will be undertaken in our next study. Such research could help to identify key parameters accounting for changes in biofilm structure and function during the arsenopyrite biooxidation process.

Drewniak and Sklodowska (2013) recommended focus on diversity of biomining microorganisms that interact with arsenic-bearing minerals and their secondary compounds (i.e., As_2S_3 , As_2S_2) in order to understand (and improve) the broad range of biomining applications (i.e., bioleaching, bioremediation), as well as better understand the biological release of toxic arsenic into the environment. Our findings suggest that in the presence of *A. thiooxidans*, arsenopyrite

Table 2 Extracellular proteins ($\mu g \text{ cm}^{-2}$) of biofilms during biooxidation of eMAE surfaces (1 cm^2) by *A. thiooxidans* after the different assayed times

Biooxidation time (h)	Extracellular proteins ($\mu g \text{ cm}^{-2}$)
1	2.8
12	2.7
24	3.6
48	5.2
72	6.2
120	6.2

Extracellular proteins on planktonic cells were 1.9 mg L^{-1} as reference

significantly modifies surface structure-activity relationships (Fig. 2) as a direct result of chemical speciation (i.e., S^0 , S_n^{2-} , FeS_2 -like, As_2S_3 -like) (Fig. 1). Secondary compounds may then be prone to further (bio)oxidation which can contribute to the release of toxic forms of arsenic and acid into environment (i.e., soil, mining waste). These fundamentals are relevant since transient biofilm properties were disclosed for each particular time point during evolution of *A. thiooxidans* biofilms. This represents an advance in the understanding of specific bioleaching microorganisms and arsenopyrite interactions, which could, in turn, determine potential factors to enhance or diminish biooxidation activity of the *A. thiooxidans* and arsenopyrite system for a determined application (i.e., bioleaching, bioremediation).

Conclusions

The present study comprehensively examined the evolution of biofilm structure during arsenopyrite oxidation by the sulfur oxidizer *A. thiooxidans* at different time intervals (120 h), using Raman spectroscopy, SEM-EDS, CLSM, GDS, and protein analyses. Biofilm growth involved three main stages describing cells and arsenopyrite interactions: (1) an initial (1 to 12 h) interaction of few cells with surface compounds (i.e., S_n^{2-} and S^0) (incipient biofilm), (2) development of biofilm (i.e., microcolony) of hydrophobic characters (i.e., extracellular lipids) between 24 and 72 h, and (3) the evolution of biofilms into a more thicker hydrophobic structure, directly interacting with the secondary compounds (i.e., S_n^{2-} , S^0 , As_2S_3) on the arsenopyrite surface after 120 h. These stages were in agreement with quantitative assessments of extracellular proteins indicating variations in secreted proteins (Table 2). It is important to highlight that during the colonization process, biooxidation changed the surface-bulk arsenopyrite structure within the first 1–6 μm of depth through cyclic formation/oxidation of secondary compounds (i.e., S_n^{2-} and S^0), particularly emphasizing the structure-activity relationship of the biofilm/arsenopyrite system at early stages of the process (i.e., low cell density structure, 12 h). These changes provided direct evidence to correlate chemical surface speciation variations with SM reactivity, and therefore the potential dissolution (mobilization) of toxic arsenic to the environment.

Acknowledgments The financial support provided by CONACYT for this research is greatly appreciated (Grants 2012-183230 and 2013-205416). Hugo Ramírez-Aldaba also extends his gratitude to CONACYT for awarding him with his Doctoral scholarship (Grant 362184). Hugo Ramírez-Aldaba thanks FCQ-UJED and UAM-Iztapala for providing access to infrastructure and expertise for successful development of PhD research. The authors would like to thank Erasmo Mata-Martínez (IG-UASLP) for the preparation and construction of the massive arsenopyrite electrodes and Dr. Ángel G. Rodríguez-Vázquez (CIACYT, UASLP) for providing access to the equipment used in the Raman

analyses. We greatly appreciate the help from Bsc. Karla B. Rodríguez-Rojas (FCQ-UJED) for her assistance during protein extraction.

References

- Adav SS, Lee DJ, Ta JH (2008) Extracellular polymeric substances and structural stability of aerobic granule. *Water Res* 42:1644–1650. doi:10.1016/j.watres.2007.10.013
- Arredondo R, García A, Jeréz CA (1994) Partial removal of lipopolysaccharide from *Thiobacillus ferrooxidans* affects its adhesion to solids. *Appl Environ Microbiol* 60:2846–2851 <http://aem.asm.org/content/60/8/2846.short>
- Barker WW, Banfield JF (1996) Biologically versus inorganically mediated weathering reactions: relationships between minerals and extracellular microbial polymers in lithobiotic communities. *Chem Geol* 132:55–69
- Barker WW, Welch SA, Chu S, Banfield JF (1998) Experimental observations of the effects of bacteria on aluminosilicate weathering. *Am Mineral* 83:1551–1563
- Bennett PC, Rogers JR, Hiebert FK, Choi WJ (2001) Silicates, silicate weathering, and microbial ecology. *Geomicrobiol J* 18:3–19
- Bradford L (1976) A rapid and sensitive method for the quantification of microgram quantities of protein utilizing the principle of protein-dye binding. *Anal Biochem* 72:248–252. doi:10.1016/0003-2697(76)90527-3
- Clark RJ, Mirabaud S (2006) Identification of the pigments on a sixteenth century Persian book of poetry by Raman microscopy. *J Raman Spectrosc* 37:235–239. doi:10.1002/jrs.1473View
- Comte S, Guibaud G, Baudu M (2006) Relations between extraction protocols for activated sludge extracellular polymeric substances (EPS) and complexation properties. Part I Comparison of the efficiency of eight EPS extraction methods. *Enzyme Microb Technol* 38:237–245
- Crundwell FK (2015) The semiconductor mechanism of dissolution and the pseudo-passivation of chalcopyrite. *Can Metall Q* 54:279–288. doi:10.1179/1879139515Y.0000000007
- Cruz R, Lázaro I, González I, Monroy M (2005) Acid dissolution influences bacterial attachment and oxidation of arsenopyrite. *Miner Engineer* 18:1024–1031. doi:10.1016/j.mineng.2005.01.015
- Das T, Ayyappan S (1999) Factors affecting bioleaching kinetics of sulfide ores using acidophilic microorganisms. *Biometals* 12:1–10. doi:10.1023/A:1009228210654
- Devasia P, Natarajan KA, Sathyanarayana DN, Rao RG (1997) Surface chemistry of *Thiobacillus ferrooxidans* relevant to adhesion on mineral surfaces. *Appl Environ Microbiol* 59:4051–4055 <http://aem.asm.org/content/59/12/4051.short>
- Devasia P, Natarajan KA (2010) Adhesion of *Acidithiobacillus ferrooxidans* to mineral surfaces. *Int J Miner Process* 94:135–139. doi:10.1016/j.minpro.2010.02.003
- Donlan MR (2002) Biofilms: microbial life on surfaces. *Emerg Infect Dis* 8:881–890 https://wwwnc.cdc.gov/eid/article/8/9/02-0063_article
- Dopson M, Lindström E (2004) Analysis of community composition during moderately thermophilic bioleaching of pyrite, arsenical pyrite, and chalcopyrite. *Microb Ecol* 48. doi:10.1007/s00248-003-2028-1
- Drewniak L, Sklodowska A (2013) Arsenic-transforming microbes and their role in biomining processes. *Environ Sci Pollut Res* 20(11):7728–7739. doi:10.1007/s11356-012-1449-0
- Echeverría-Vega A, Demergasso C (2015) Copper resistance, motility and the mineral dissolution behavior were assessed as novel factors involved in bacterial adhesion in bioleaching. *Hydrometallurgy* 157:107–115. doi:10.1016/j.hydromet.2015.07.018
- Ehrlich HL (2002) *Geomicrobiology*. New York: Marcel Dekker. In: Madigan MT, Martinko JM, Parker J (eds) *Brock Biology of Microorganisms*. Prentice-Hall, Englewood Cliffs
- Fantauzzi M, Licheri C, Atzei D, Loi G, Elsener B, Rossi G, Rossi A (2011) Arsenopyrite and pyrite bioleaching: evidence from XPS, XRD and ICP techniques. *Anal Bioanal Chem* 401:2237–2248. doi:10.1007/s00216-011-5300-0
- Bobadilla Fazzini RA, Levican G, Parada P (2011) *Acidithiobacillus thiooxidans* secretome containing a newly described lipoprotein Licanantase enhances chalcopyrite bioleaching rate. *Appl Microbiol Biotechnol* 89:771–780. doi:10.1007/s00253-010-3063-8
- Flemming HC (2016) EPS—Then and Now. *Microorganisms* 4(4):41. doi:10.3390/microorganisms4040041
- Flemming HC, Wingender J, Mayer C, Korstgens V, Borchard W (2000) Cohesiveness in biofilm matrix polymers. In: Allison DG, Gilbert P, Lappin-Scott HM, Wilson M (eds) *Symposia-society for general microbiology*. Cambridge University Press, Cambridge, pp 87–106
- Flemming HC, Wingender J (2001) Relevance of microbial extracellular polymeric substances (EPS)-part I: structural and ecological aspects. *Water Sci Technol* 43(6):1–8
- Fowle DA, Fein JF (1999) Competitive adsorption of metal cations onto two gram positive bacteria: testing the chemical equilibrium model. *Geochim Cosmochim Acta* 63:3059–3067
- Frost RL, Martens WN, Kloprogge JT (2002) Raman spectroscopic study of cinnabar (HgS), realgar (As₄S₄), and orpiment (As₂S₃) at 298 and 77K. *Neues Jahrbuch für Mineralogie-Monatshefte* 10:469–480. doi:10.1127/0028-3649/2002/2002-0469
- García-Meza JV, Fernández JJ, Lara RH, González I (2013) Changes in biofilm structure during the colonization of chalcopyrite by *Acidithiobacillus thiooxidans*. *Appl Microbiol Biotechnol* 97:6065–6075. doi:10.1007/s00253-012-4420-6
- Gehrke T, Telegdi J, Thierry D, Sand W (1998) Importance of extracellular polymeric substances from *Thiobacillus ferrooxidans* for bioleaching. *Appl Environ Microbiol* 64:2743–2747 <http://aem.asm.org/content/64/7/2743.short>
- González DM, Lara RH, Alvarado KN, Valdez-Pérez D, Navarro-Contreras HR, Cruz R, García-Meza JV (2012) Evolution of biofilms during the colonization process of pyrite by *Acidithiobacillus thiooxidans*. *Appl Microbiol Biotechnol* 93:763–775. doi:10.1007/s00253-011-3465-2
- Heno DMO, Godoy MAM (2010) Jarosite pseudomorph formation from arsenopyrite oxidation using *Acidithiobacillus ferrooxidans*. *Hydrometallurgy* 104:162–168. doi:10.1016/j.hydromet.2010.05.012
- Harneit K, Göksel A, Kock D, Klock JH, Gehrke T, Sand W (2006) Adhesion to metal sulfide surfaces by cells of *Acidithiobacillus ferrooxidans*, *Acidithiobacillus thiooxidans* and *Leptospirillum ferrooxidans*. *Hydrometallurgy* 83:245–254. doi:10.1016/j.hydromet.2006.03.044
- Harneit K, Sand W (2007) Influence of growth substrate and attachment substratum on EPS and biofilm formation by *Acidithiobacillus ferrooxidans* A2. *Adv Mater Res* 20:385–385 <http://www.scientific.net/AMR.20-21.385>
- Hope GA, Woods R, Munce CG (2001) Raman microprobe mineral identification. *Miner Engineer* 14:1565–1577. doi:10.1016/S0892-6875(01)00175-3
- Holmes PR, Crundwell FJ (2013) Polysulfides do not cause passivation: results from the dissolution of pyrite and implications for other sulfide minerals. *Hydrometallurgy* 139:101–110. doi:10.1016/j.hydromet.2013.07.006
- Jia P, Zheng S, Long J, Zheng W, Zhao Z (2010) dmGWAS: dense module searching for genomewide association studies in protein-protein interaction networks. *Bioinformatics* 27(1):95–102. doi:10.1093/bioinformatics/btq615
- Jiao Y, Cody GD, Harding AK, Wilmes P, Schrenk M, Wheeler KE (2010) Characterization of extracellular polymeric substances from

- acidophilic microbial biofilms. *Appl Environ Microbiol* 76:2916–2922
- Jin J, Shi S, Liu G, Zhan Q, Cong W (2012) Arsenopyrite bioleaching by *Acidithiobacillus ferrooxidans* in a rotating-drum reactor. *Miner Engineer* 39:19–22. doi:10.1016/j.mineng.2012.07.018
- Ko MS, Park HS, Kim KW, Lee JU (2013) The role of *Acidithiobacillus ferrooxidans* and *Acidithiobacillus thiooxidans* in arsenic bioleaching from soil. *Environ Geochem Health* 35:727–733. doi:10.1007/s10653-013-9530-2
- Laemmli UK (1970) Cleavage of structural proteins during the assembly of the head of bacteriophage T4. *Nature* 227:680–685. doi:10.1038/227680a0
- Lara RH, García-Meza JV, Cruz R, Valdez-Pérez D, González I (2012) Influence of the sulfur species reactivity on biofilm conformation during pyrite colonization by *Acidithiobacillus thiooxidans*. *Appl Microbiol Biotechnol* 95:799–809. doi:10.1007/s00253-011-3715-3
- Lawrence JR, Swerhone GDW, Leppard GG, Araki T, Zhang X, West MM, Hitchcock AP (2003) Scanning transmission X-ray, laser scanning, and transmission electron microscopy mapping of the exopolymeric matrix of microbial biofilms. *Appl Environ Microbiol* 69:5543–5554. <http://aem.asm.org/content/69/9/5543.short>
- Lei J, Huaiyang Z, Xiaotong P, Zhonghao D (2009) The use of microscopy techniques to analyze microbial biofilm of the bio-oxidized chalcopyrite surface. *Miner Engineer* 22:37–42. doi:10.1016/j.mineng.2008.03.012
- Liermann LJ, Barnes AS, Kalinowski BE, Zhou X, Brantley SL (2000a) Microenvironments of pH in biofilms grown on dissolving silicate surfaces. *Chem Geol* 171:1–16
- Liermann LJ, Kalinowski BE, Brantley SL, Ferry JG (2000b) Role of bacterial siderophores in dissolution of hornblende. *Geochim Cosmochim Acta* 64:587–602
- Liu Y, Dang Z, Lu G, Wu P, Feng C, Yi X (2011) Utilization of electrochemical impedance spectroscopy for monitoring pyrite oxidation in the presence and absence of *Acidithiobacillus ferrooxidans*. *Miner Engineer* 24:833–838. doi:10.1016/j.mineng.2011.03.002
- Lu X, Wang H (2012) Microbial oxidation of sulfide tailings and the environmental consequences. *Elements* 8:119–124. doi:10.2113/gselements.8.2.119
- Manchur MA, Kikumoto M, Kanao T, Takada J, Kamimura K (2011) Characterization of an OmpA-like outer membrane protein of the acidophilic iron-oxidizing bacterium, *Acidithiobacillus ferrooxidans*. *Extremophiles* 15:403–410. doi:10.1007/s00792-011-0371-6
- Márquez MA, Ospina JD, Morales AL (2012) New insights about the bacterial oxidation of arsenopyrite: a mineralogical scope. *Miner Engineer* 39:248–254. doi:10.1016/j.mineng.2012.06.012
- McGuire MM, Edwards KJ, Banfield JF, Hamers RJ (2001) Kinetics, surface chemistry, and structural evolution of microbially mediated sulfide mineral dissolution. *Geochim Cosmochim Acta* 65:1243–1258. doi:10.1016/S0016-7037(00)00601-3
- Mikhlin YL, Romanchenko AS, Asanov IP (2006) Oxidation of arsenopyrite and deposition of gold on the oxidized surfaces: a scanning probe microscopy, tunneling spectroscopy and XPS study. *Geochim Cosmochim Acta* 70:4874–4888. doi:10.1016/j.gca.2006.07.021
- More TT, Yadav JS, Yan S, Tyagi RD, Surampalli RY (2014) Extracellular polymeric substances of bacteria and their potential environmental applications. *J Environ Manage* 144:1–25
- Mycroft JR, Bancroft GM, McIntyre NS, Lorimer JW, Hill IR (1990) Detection of sulphur and polysulphides on electrochemically oxidized pyrite surfaces by X-ray photoelectron spectroscopy and Raman spectroscopy. *J Electroanal Chem Interf Electrochem* 292:139–152. doi:10.1016/0022-0728(90)87332-E
- Núñez-Beltrán A, López-Romero E, Cuéllar-Cruz M (2017) Identification of proteins involved in the adhesion of *Candida* species to different medical devices. *Microb Pathog* 107:293–303. doi:10.1016/j.micpath.2017.04.009
- Pinet N, Tremblay A (2009) Structural analysis of the Velardeña mining district, Mexico: a faulted Au-Ag-rich hydrothermal system. *Can J Earth Sci* 46:123–138. doi:10.1139/E09-007
- Ramírez-Aldaba H, Valles OP, Vazquez-Arenas J, Rojas-Contreras JA, Valdez-Pérez D, Ruiz-Baca E, Meraz M, Lara RH (2016) Chemical and surface analysis during evolution of arsenopyrite oxidation by *Acidithiobacillus thiooxidans* in the presence and absence of supplementary arsenic. *Sci Total Environ* 566:1106–1119. doi:10.1016/j.scitotenv.2016.05.143
- Rawlings DE, Johnson DB (2007) The microbiology of biomining: development and optimization of mineral-oxidizing microbial consortia. *Microbiology* 153:315–324. doi:10.1099/mic.0.2006/001206-0
- Rohwerder T, Gehrke T, Kinzler K, Sand W (2003) Bioleaching review part A. *Appl Microbiol Biotechnol* 63:239–248. doi:10.1007/s00253-003-1448-7
- Rohwerder T, Sand W (2007) Mechanisms and biochemical fundamentals of bacterial metal sulfide oxidation. In *Microbial processing of metal sulfides* (pp. 35–58). Springer Netherlands. http://link.springer.com/chapter/10.1007%2F1-4020-5589-7_2
- Rogers JR, Bennett PC, Choi WJ (1998) Feldspars as a source of nutrients for microorganisms. *Am Mineral* 83:1532–1540
- Sasaki K, Tsunekawa M, Ohtsuka T, Konno H (1998) The role of sulfur-oxidizing bacteria *Thiobacillus thiooxidans* in pyrite weathering. *Colloids Surf A* 133:269–278. doi:10.1016/S0927-7757(97)00200-8
- Sasaki K, Nakamura Y, Hirajima T, Tuovinen OH (2009) Raman characterization of secondary minerals formed during chalcopyrite leaching with *Acidithiobacillus ferrooxidans*. *Hydrometallurgy* 95:153–158. doi:10.1016/j.hydromet.2008.05.009
- Serre C, Bourrelly S, Vimont A, Ramsahye NA, Maurin G, Llewellyn PL, Férey G (2007) An explanation for the very large breathing effect of a metal-organic framework during CO₂ adsorption. *Adv Mater* 19:2246–2251. doi:10.1002/adma.200602645
- Trentelman K, Stodulski L, Pavlosky M (1996) Characterization of pararealgar and other light-induced transformation products from realgar by Raman microspectroscopy. *Anal Chem* 68:1755–1761. <http://pubs.acs.org/doi/abs/10.1021/ac951097o>
- Vera M, Krok B, Bellenberg S, Sand W, Poetsch A (2013) Shotgun proteomics study of early biofilm formation process of *Acidithiobacillus ferrooxidans* ATCC 23270 on pyrite. *Proteomics* 13:1133–1144. doi:10.1002/pmic.201200386
- Vu B, Chen M, Crawford RJ, Ivanova EP (2009) Bacterial extracellular polysaccharides involved in biofilm formation. *Molecules* 14:2535–2554. doi:10.3390/molecules14072535
- Yoshida T, Yamauchi H, Sun GF (2004) Chronic health effects in people exposed to arsenic via the drinking water: dose-response relationships in review. *Toxicol Appl Pharmacol* 198:243–252. doi:10.1016/j.taap.2003.10.022
- Wang S, Zhao X (2009) On the potential of biological treatment for arsenic contaminated soils and groundwater. *J Environ Manage* 90:2367–2376. doi:10.1016/j.jenvman.2009.02.001
- Ward AT (1968) Raman spectroscopy of sulfur, sulfur-selenium, and sulfur-arsenic mixtures. *J Phys Chem* 72:4133–4139. doi:10.1021/j100858a031
- Welch SA, Barker WW, Banfield JF (1999) Microbial extracellular polysaccharides and plagioclase dissolution. *Geochim Cosmochim Acta* 63:1405–1419
- White SN (2009) Laser Raman spectroscopy as a technique for identification of seafloor hydrothermal and cold seep minerals. *Chem Geol* 259:240–252. doi:10.1016/j.chemgeo.2008.11.008
- Zhang T, Fang HHP (2001) Quantification of extracellular polymeric substances in biofilms by confocal laser scanning microscopy. *Biotechnol Lett* 23:405–409. doi:10.1023/A:1005620730265



Changes in biooxidation mechanism and transient biofilm characteristics by As(V) during arsenopyrite colonization with *Acidithiobacillus thiooxidans*

Hugo Ramírez-Aldaba^{1,7} · Jorge Vázquez-Arenas² · Fabiola S. Sosa-Rodríguez³ · Donato Valdez-Pérez⁴ · Estela Ruiz-Baca¹ · Gabriel Trejo-Córdoba⁵ · Miguel A. Escobedo-Bretado¹ · Luis Lartundo-Rojas⁶ · Patricia Ponce-Peña¹ · René H. Lara¹

Received: 30 January 2018 / Accepted: 23 May 2018
© Society for Industrial Microbiology and Biotechnology 2018

Abstract

Chemical and surface analyses are carried out using Raman spectroscopy, X-ray photoelectron spectroscopy (XPS), scanning electron microscopy (SEM–EDS), atomic force microscopy (AFM), confocal laser scanning microscopy (CLSM), glow discharge spectroscopy (GDS) and extracellular surface protein quantification to thoroughly investigate the effect of supplementary As(V) during biooxidation of arsenopyrite by *Acidithiobacillus thiooxidans*. It is revealed that arsenic can enhance bacterial reactions during bioleaching, which can strongly influence its mobility. Biofilms occur as compact-flattened microcolonies, being progressively covered by a significant amount of secondary compounds (S_n^{2-} , S^0 , pyrite-like). Biooxidation mechanism is modified in the presence of supplementary As(V), as indicated by spectroscopic and microscopic studies. GDS confirms significant variations between abiotic control and biooxidized arsenopyrite in terms of surface reactivity and amount of secondary compounds with and without As(V) (i.e. 6 μm depth). CLSM and protein analyses indicate a rapid modification in biofilm from hydrophilic to hydrophobic character (i.e. 1–12 h), in spite of the decrease in extracellular surface proteins in the presence of supplementary As(V) (i.e. stressed biofilms).

Keywords Arsenopyrite biooxidation · Stressed biofilms · *Acidithiobacillus thiooxidans* · Glow discharge spectroscopy · Supplementary As(V)

Electronic supplementary material The online version of this article (<https://doi.org/10.1007/s10295-018-2051-3>) contains supplementary material, which is available to authorized users.

✉ René H. Lara
lcrh75@ujed.mx; lcrh75@hotmail.com

- 1 Facultad de Ciencias Químicas, Departamento de Ciencia de Materiales, Laboratorio de Electroquímica y Análisis de Superficies, Universidad Juárez del Estado de Durango (UJED), Av. Veterinaria S/N, Circuito Universitario, Col. Valle del Sur, 34120 Durango, DGO, Mexico
- 2 Centro Mexicano para la Producción más Limpia, Instituto Politécnico Nacional, Avenida Acueducto S/N, Col. La Laguna Ticomán, 07340 Mexico City, Mexico
- 3 Crecimiento Económico y Medio Ambiente, Departamento de Economía, Universidad Autónoma

Introduction

Arsenic (As) dissemination is a serious environmental problem due to its toxic character by direct or indirect exposition to soil, air, and water [13]. This toxic element is released to the environment from natural and anthropogenic processes

Metropolitana-Azcapotzalco (UAM-A), Av. San Pablo 180, Azcapotzalco, 02200 Mexico City, Mexico

- 4 Instituto Politécnico Nacional (IPN), UPALM, Edif. Z-4 3er Piso, 07738 Mexico City, Mexico
- 5 Centro de Investigación y Desarrollo Tecnológico en Electroquímica (CIDETEQ), Parque Tecnológico Querétaro-Sanfandila, 76703 Pedro Escobedo, QRO, Mexico
- 6 Instituto Politécnico Nacional (IPN), CNMN, Av. Luis Enrique Erro S/N, Unidad Profesional Adolfo López Mateos, Zacatenco, 07738 Mexico City, Mexico
- 7 Facultad de Ciencias Forestales, UJED, Av. Río Papaloapan S/N, Col. Valle del Sur, 34120 Durango, DGO, Mexico

(i.e. water-bedrock weathering reactions, coal and steel production, mining activities) [1]. It is known that its occurrence, fate and mobilization can be affected by microbially mediated biogeochemical reactions (i.e. biooxidation, bioleaching), which considerably increase As dissemination [2]. Arsenopyrite (FeAsS) is the most important source of As in lithosphere, typically undergoing a significant biooxidation (and bioleaching) in soil and mining waste by *Acidithiobacillus ferrooxidans* and *A. thiooxidans* [3, 4]. To this concern, the study of arsenopyrite bioleaching has been mostly focused on understanding interactions with *A. ferrooxidans*, since this iron- and sulfur-oxidizing microorganism (IOM/SOM) presents an enhanced capacity to efficiently use the $\text{Fe}^{2+}/\text{Fe}^{3+}$ cycle, and to some extent, to oxidize sulfur compounds (i.e. S^- , S^{2-} , S^0) [5, 6]. In contrast, the analysis of sulfur-oxidizing microorganisms (SOM), such as *A. thiooxidans*, has been barely examined in spite of its great capacity to efficiently remove passive sulfur coating layers (i.e. S_n^{2-} , S^0) limiting the proficiency of *A. ferrooxidans* [5, 7, 8]. Thus, the study of the arsenopyrite biooxidation mechanism by single *A. thiooxidans* would certainly enable a better understanding of its contribution in mixed cultures [9, 10, 18].

To date, the interaction (i.e. biooxidation) arising between *A. thiooxidans* and arsenopyrite (i.e. at the interfacial level) remains poorly described, and particularly, when this interaction is affected by challenging environmental conditions (i.e. variations in pH, temperature, heavy metals). Our previous investigations have simulated this biooxidation process using electrochemical experiments, and performed a rapid evaluation of the transient biofilm characteristics without providing a detailed assessment of the effect of As on bacterial reactions [11, 12]. Particularly, additional evaluations concerning the role of As on biooxidation mechanism (*A. thiooxidans* and arsenopyrite), transient biofilm characteristics and chemical surface speciation are herein addressed, in order to understand biogeochemical cycles of As and the bacterial reactions affecting intrinsic arsenopyrite behavior. Likewise, bioleaching processes of arsenopyrite occur in the presence of important concentrations of As in the system, which are generated by the chemical and biological alteration of arsenopyrite (and As-rich mining waste) [3, 14, 31]. Additionally, leaching (and non-leaching) bacteria secrete extracellular polymeric substances (EPS), which are mainly composed of polysaccharides, proteins and lipids [15]. These substances possess a relevant role during cell attachment to sulfide minerals (SM), promoting biofilm stability [16, 17, 19], whence it is also a major concern to assess the biofilms characteristics in the presence of As(V) during arsenopyrite colonization with *A. thiooxidans*. In order to account for the effect of high As contains affecting the arsenopyrite and *A. thiooxidans* interactions, and the corresponding arsenopyrite structure–activity relationships, Raman, GDS,

XPS, SEM–EDS, AFM, CLSM and extracellular surface protein determinations are combined to describe the following aspects: (1) The effect of supplementary As(V) on the biooxidation pathways, (2) analysis of protein synthesis in biofilms under the effect of supplementary As(V), and (3) influence of challenging environmental conditions on transient biofilm properties. It is expected that these results contribute to gain a better understanding of bacterial reactions occurring during bioleaching of arsenopyrite in the presence of As in industrial and natural environments.

Materials and methods

Arsenopyrite samples

Massive arsenopyrite samples were obtained from auriferous mining area at Velardeña, Durango, Northwest of Mexico [21]. Purity of arsenopyrite samples, mineralogical identification, and the corresponding construction of massive arsenopyrite electrodes (MAE) were carried out as indicated in previous papers [11, 12]. Likewise, electrochemical oxidation of these MAE specimens allows a rapid and significant generation of secondary compounds (i.e. S_n^{2-} and S^0) (Electronic Supplementary Material, ESM, Fig. S1), which was induced as described in Refs. [11, 12] for use in abiotic and biotic experiments. Metabolic capacity of *A. thiooxidans* was then stimulated by presence of S_n^{2-} and S^0 compounds on the eMAE surfaces (i.e. energy source), allowing its colonization on the substrate [7, 15].

Biofilm formation and biooxidation assays

The strain used in this study was *A. thiooxidans* ATCC no. 19377, which was cultivated as indicated in Refs. [11, 12]. Thus, 10 mL of this culture was used as inoculum in biooxidation assays. Sterilized eMAE was placed in 50 mL ATCC-125 culture medium containing $\sim 10^7$ cells mL^{-1} at pH 2.0 (batch system) under sterile conditions. These experiments were conducted in the presence of supplementary As(V) (0.2 M $\text{NaH}_2\text{AsO}_4 \cdot \text{H}_2\text{O}$, JT Baker) [22, 23] aerobically incubated around 30 °C. Abiotic control assays were also carried out to establish a fair comparison between chemical and biological oxidation. The above supplementary As(V) concentration was chosen to induce biofilm stress. Although it is known that As (III) is more toxic than As (V) to biota, it is well known that bacteria *A. thiooxidans* have a complex system to eliminate As (V) via dissimilatory reduction of these species to As (III), utilizing complex *Ars-R*, *Ars-A*, *Ars-B* and *Ars-C* genes [14, 24, 25]. Negligible effects of As(V) are expected for planktonic cells at the beginning of biooxidation experiments, assuming that *A. thiooxidans* attaches fast enough to arsenopyrite as occurs for *A. ferrooxidans* in

similar systems [26]. The stability of As(V) compounds (i.e. H_2AsO_4^-) has been established according to observations published by Lu and Zhu [27]. Resulting eMAE surfaces after biooxidation process in the presence of supplementary As(V) are herein referred as ‘biooxidized eMAE surfaces with As(V)’, whereas those after produced abiotic oxidation with supplementary As(V) are referred as ‘abiotic control eMAE surfaces with As(V)’. Abiotic control and biooxidized eMAE surfaces with As(V) were collected at 1, 12, 24, 48, 72 and 120 h, dried with a direct flow of chromatographic grade N_2 , and prepared under inert conditions for surface analyses. All control and biooxidation assays were carried out at least by duplicate. Chemical and surface analyses obtained during biooxidation of arsenopyrite without the effect of supplementary As(V) can be consulted in our previous papers [11, 12].

Surface analysis

Sample preparation to conduct chemical and surface analyses (SEM–EDS, AFM, Raman, CLSM and GDS) for all type of MAE specimens has been described in our previous papers [11, 12]. Additionally, XPS analyses were carried out for a more detailed characterization of secondary sulfur compounds (i.e. S_n^{2-} and S^0) in MAE surfaces involving chemical bonding and composition. These studies were performed using a K-Alpha Thermo Scientific spectrometer with a monochromatized Al $\text{K}\alpha$ X-rays source (1486.6 eV), running at a power of 150 W. XPS narrow scans were collected at 60 eV pass energy. To detect and compensate the charge shift of the core level peaks, O1 s peak position at 531.0 eV was used as an internal standard. The base pressure in the analytical chamber was about 10^{-9} mbar. Spectra were collected at a normal take-off angle (90°) and the analysis area was $400 \times 400 \mu\text{m}^2$. All XPS spectra and obtained quantities correspond to an average of three measurements in different points of each sample. XPS S2p core level was then analyzed with Avantage v5.979 software from Thermo Scientific and fitted using a typical pseudo-Voigt function. A Shirley type background subtraction was used during fitting procedure. The pristine MAE sample was prepared in an argon atmosphere, whereas the rest of samples were prepared at room conditions.

Protein extraction

Protein analysis was performed in order to assess changes in biofilms and to connect these results with surface analysis and the effect of As(V). EPS-associated protein fraction (i.e. extracellular surface protein) was extracted from biofilms after biooxidation assays in the presence of supplementary As(V), according to experimental details provided in previous papers [11, 12]. To achieve this, four sterilized eMAE

surfaces ($\sim 1 \text{ cm}^2$ of area) were placed into 50 mL of ATCC-125 culture medium containing $\sim 10^7$ cells/mL and 0.2 M of $\text{NaH}_2\text{AsO}_4 \cdot \text{H}_2\text{O}$ (JT Baker) at pH 2.0 (batch system) for each evaluated time. Normalization of data was performed by relating the protein concentration per eMAE-surficial area (1 cm^2). The protein concentration was determined by the Bradford method [28] by comparing the measured absorption values (UV–Vis 50 Bio-spectrophotometer) with those of a calibration range of albumin as standard concentration ($1\text{--}30 \text{ mg mL}^{-1}$). This protocol enables the extraction of the EPS-associated protein fraction (i.e. avoiding heating of the system to decrease cell lysis), thus, allowing a quantitative assessment of the extracted proteins [29].

Results and discussion

Figure 1 shows Raman spectra for abiotic control eMAE surfaces with As(V) after 120 h (Fig. 1a) and biooxidized eMAE surfaces with As(V) collected after 1, 12, 24, 48, 72 and 120 h of assay (Fig. 1b1–b6, respectively). In order to compare the biological oxidation in the presence and absence of supplementary As(V), all results for the studied system without the effect of As(V) (i.e. Raman, SEM, CLSM, proteins extraction) should be consulted in Ramirez-Aldaba et al. [11, 12]. Abiotic control eMAE surfaces with As(V) essentially show the same secondary compounds (i.e. pyrite-like phases, at 329 and 363 cm^{-1} , Fig. 1a), which is similar to that observed for abiotic control samples in the absence of As(V) [12]. This finding suggests minor or negligible precipitation of As-bearing secondary compounds during chemical weathering due to the absence of bacteria (i.e. contamination), including biooxidation experiments. Raman spectra for biooxidized eMAE surfaces with As(V) indicated the presence of well-defined S^0 at 1 h ($134, 201, 455 \text{ cm}^{-1}$, Fig. 1b1), and S_n^{2-} at 12 h (473 cm^{-1} , Fig. 1b2, Table S1 in [12]). Additionally, a mixture of pyrite-like and $\text{S}^0/\text{S}_n^{2-}$ phases was identified at 24 h ($353, 393 \text{ cm}^{-1}$; $125, 204, 462 \text{ cm}^{-1}$ spectrum *i*; 462 cm^{-1} spectrum *ii*, Fig. 1b3), and S_n^{2-} compounds after 48 h (467 cm^{-1} , Fig. 1b4). Finally, S^0 was identified at 72 h ($125, 204, 461 \text{ cm}^{-1}$, Fig. 1b5) and a mixture of pyrite-like and S_n^{2-} after 120 h ($355, 366; 473 \text{ cm}^{-1}$, Fig. 1b6, Table S1 in [12]). A general comparison between Raman spectra obtained for biooxidized eMAE surfaces [12] and biooxidized eMAE surfaces with As(V) (Fig. 1b1) revealed a delay in early stages of biooxidation process in the presence of supplementary As(V), since well-defined S^0 was observed in both systems, indicating minor *A. thiooxidans* and arsenopyrite interaction (i.e. 1 h). This inhibition in the biooxidation process represents sluggishness in the colonization mechanisms in which *A. thiooxidans* adjust to face this microenvironment (i.e. As) [18, 30, 31]. These findings also indicate that *A. thiooxidans* sustain biooxidation activity after incipient stage (i.e. stressed biofilms, 12 to

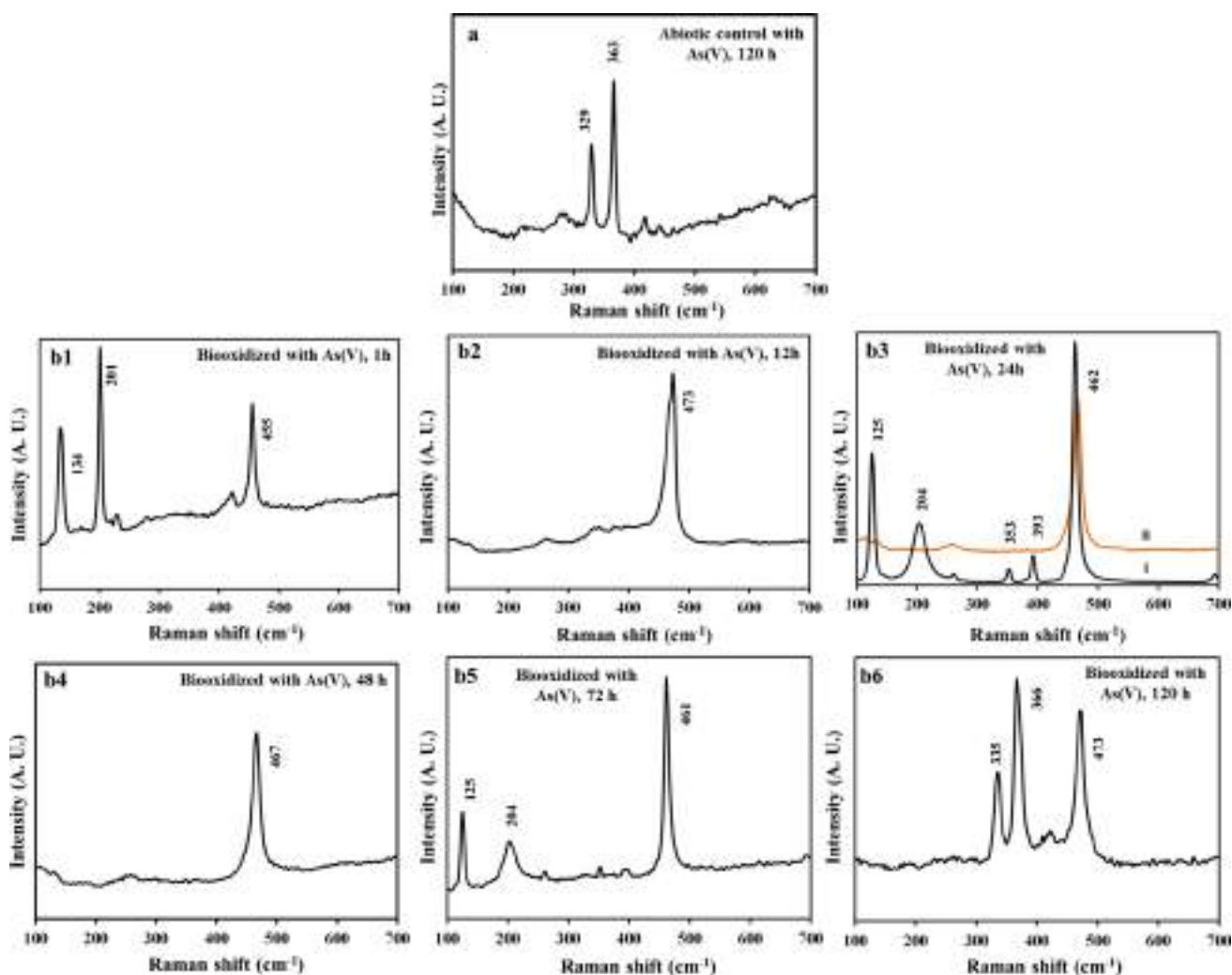


Fig. 1 Raman spectra obtained from abiotic control with As(V) at 120 h (**a**), and biooxidized eMAE samples with As(V) for 1 (**b1**), 12 (**b2**), 24 (**b3**, spectra i, ii), 48 (**b4**), 72 (**b5**) and 120 h (**b6**). Abiotic

control eMAE surfaces contained similar secondary compounds for all analyzed times. 60 s of collection time. $\lambda = 514$ nm. 25 A

120 h), which involves a different biooxidation process (or mechanism) regarding previous observations (i.e. chemical surface speciation), and in agreement with literature [2, 23].

Figure 2 shows the corresponding fitting procedures of S2p spectra for typical pristine MAE surface (Fig. 2a), eMAE surface (without leaching) (Fig. 2b), and samples collected after 24 and 120 h in the presence (Fig. 2c', d', respectively) and absence (Fig. 2c'', d'', respectively) of supplementary As(V). Additionally, Figure S2 shows fitting procedures of S2p spectra for samples collected after 48 h in the presence and absence of supplementary As(V) and the corresponding control sample. A summary of S2p peak parameters and the corresponding binding energies to identify chemical bonding of sulfur species are listed in Tables S2 and S3, respectively. The S2p spectrum in the pristine MAE surface shows a major doublet, with a S2p_{3/2} component located at ~162.3 eV, commonly assigned to

(AsS)²⁻ species in mineral crystal lattices (Fig. 2a, Tables S2 and S3). A second minor doublet with a S2p_{3/2} component at ~161.3 eV reflects the presence of S₂²⁻ species. Finally, a third doublet with a S2p_{3/2} component arising at ~164.0 eV is attributed to S⁰/S_n²⁻ species due to uncontrolled oxidation (Table S2, [32–34]). The S2p spectrum of the eMAE specimen reveals the additional presence of sulfate (i.e. ~168.5 eV) and sulfite (i.e. SO_x²⁻)-like species (~166.3 eV) (Fig. 2b, Tables S2 and S3). This spectrum also shows the concomitant decrease of (AsS)²⁻ species (~162.3 eV) and the progressive enrichment of a mixture of S_n²⁻ and S⁰ compounds (~163.3 eV) (Fig. 2b, Tables S2 and S3). These findings confirm the presence of S⁰ and S_n²⁻ coating layers on the eMAE specimens, in agreement with Raman study (Table S2, [12]). The higher production of S₂²⁻ species (Fig. 2b) regarding the pristine MAE specimen (Fig. 2a) is presumably associated with the formation

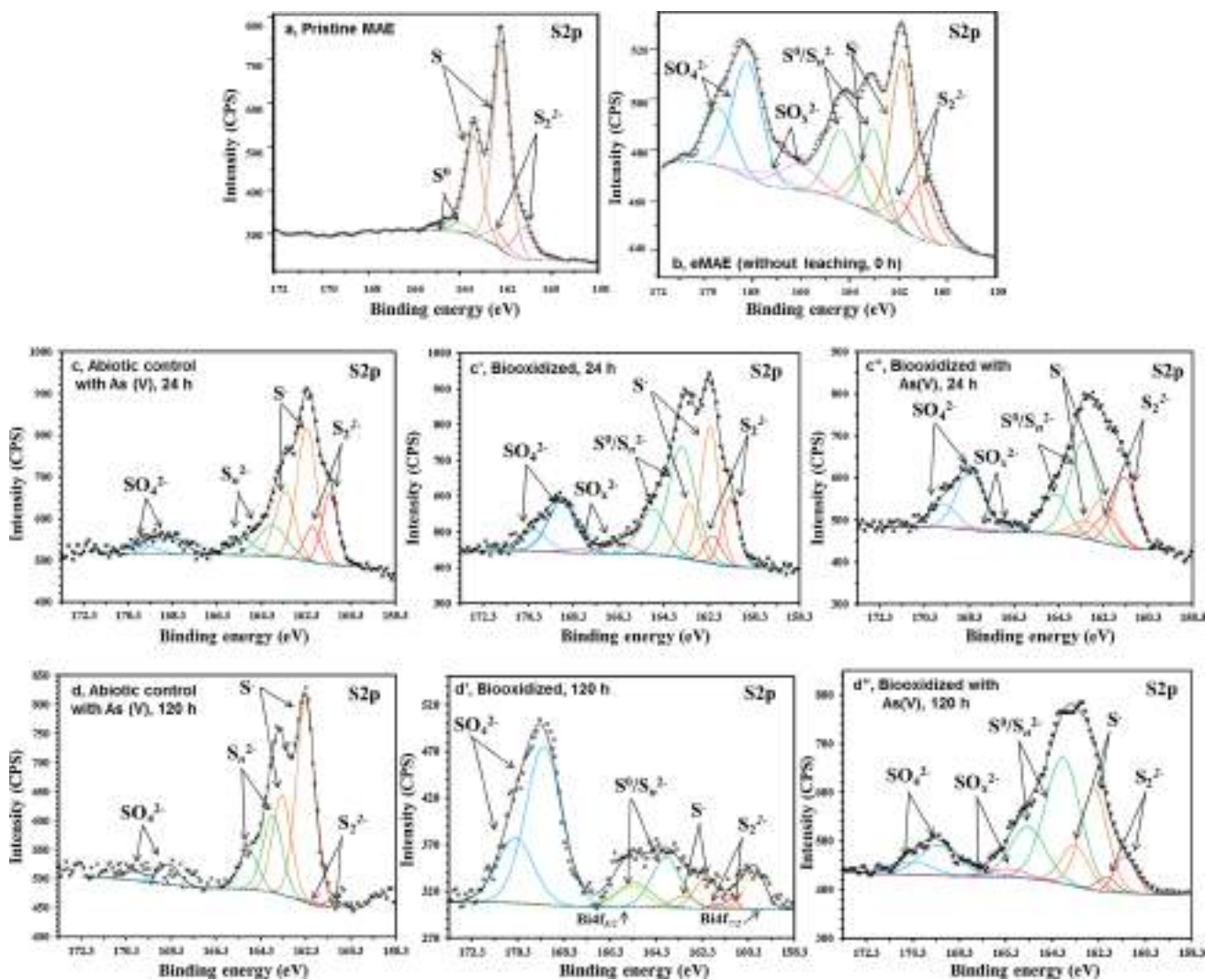


Fig. 2 XPS S2p spectra collected for pristine MAE (**a**), eMAE specimen (without leaching) (**b**), abiotic control surfaces (**c**, **d**), biooxidized eMAE surfaces (**c'**, **d'**) and biooxidized eMAE surfaces with As(V) (**c''**, **d''**) after 24 and 120 h of assay, respectively

of the pyrite-like compound (i.e. FeS_2 , S_2^{2-} , i.e. [34]); also in connection with Raman study (Fig. 1).

The fitting of the S2p spectra for abiotic control eMAE samples in general excludes the presence of the sulfite (SO_x^{2-})-like species and shows minor formation of sulfates (Figs. 2c, d, S2, for 24, 48 and 120 h, respectively; Tables S2 and S3). These findings suggest a trend for the progressive accumulation of refractory secondary compounds (i.e. S^0 , S_n^{2-} , pyrite-like); in agreement with Raman study (Fig. 1a). The fittings of the S2p spectra for biooxidized eMAE surfaces (i.e. without As(V)) (Figs. 2c', d', S2, for 24, 48 and 120 h, respectively) and biooxidized eMAE surfaces with As(V) (Figs. 2c'', d'', S2, for 24, 48 and 120 h, respectively) show clear differences regarding controls and between biooxidized eMAE surfaces without As(V). These spectra indicate variations in the composition and amount of secondary sulfur compounds. The presence of sulfates is the

highest one after 120 h of assay (Fig. 2d', Tables S2 and S3) if compared against other biooxidation times. Additionally, higher production of S^0 and S_n^{2-} is clearly identified when the presence of SO_x^{2-} -like species is negligible (Fig. 2c', d', S2, for 24, 48 and 120 h, respectively; Tables S2 and S3). These suggest that most important stage of biooxidation process occur after 120 h in the presence and absence of As(V), in spite of sluggishness observed in early biooxidation in the presence of As(V). The main differences identified in the S2p spectra of biooxidized eMAE surfaces with As(V) regarding biooxidized eMAE samples indicated enhanced cyclic variations for S_n^{2-} , S^0 and soluble sulfur species (Fig. 2, Tables S2 and S3), thus, revealing dynamic characteristics for transient bacteria and arsenopyrite interactions. Note that S2p spectrum after 120 h of assay requires an additional doublet, which is associated to Bi_xO_y -like phase involving the main signal of $\text{Bi}4f_{7/2}$ at ~ 159.9 eV (Fig. 2d',

Tables S2 and S3). This element emerges from mineral bulk impurities in arsenopyrite specimens collected from skarn or vein ore deposits [32].

The understanding of incipient structure–activity relationships (i.e. concentration vs depth profiles) was previously determined at 12 h of biooxidation in the absence of supplementary As(V) [12]. In order to investigate more profoundly the intrinsic arsenopyrite biogeochemical behavior (i.e. S) during bacterial reactions in the presence of As(V) and for a more extended time interval, eMAE samples were analyzed using GDS (i.e. 6 μm depth) after 24 and 120 h in the presence and the absence of supplementary As(V). Figure S3 also exhibits GDS analysis for biooxidized sample with As(V) after 12 h of assay for a fair comparison. Figure 3 exhibits spectra for this technique of abiotic control eMAE (Fig. 2a, b), biooxidized eMAE surfaces (Fig. 2a', b') and biooxidized eMAE surfaces with As(V) (Fig. 2a'', b'') after 24 and 120 h of assay, respectively. GDS spectra for pristine MAE, eMAE and controls and biooxidized samples without As(V) can be consulted in Ramírez-Aldaba et al. [12]. GDS spectra of pristine MAE and eMAE surfaces display a typical behavior for a FeAsS structure and a remarkable production of sulfur compounds around 90% wt ([12], from 0 to ~4.5 μm in depth), respectively, confirming the starting surface condition for abiotic control and biooxidation assays, in agreement with XPS (Fig. 2b). The presence of Mn and Mo (1–6 μm depth) is a natural content in arsenopyrite lattices (i.e. impurities), since these elements were not previously observed in Fig. 1. Additionally, the

presence of carbon in eMAE surface (Fig. 3) and abiotic controls (Figs. 3a, b) were associated to readily adsorption of CO_2 on mineral surface [33]. Accordingly, the increment of carbon between 1 and 6 μm depth was then associated to the rise of surface area (i.e. increment or higher accumulation of secondary compounds) due to chemical oxidation of arsenopyrite [11]. The presence of higher amounts of carbon in concentration vs. depth profiles for all type of biooxidized eMAE surfaces was mainly associated to occurrence of EPS composing biofilms, in agreement with Zhu et al. [34]. Note that concentration of sulfur compounds was similar between eMAE surface [12] and biooxidized eMAE surface with As(V) after 1 h (data not shown), hence, confirming the observations made above by Raman and XPS studies (i.e. sluggish incipient biooxidation).

Concentration vs. depth profiles obtained for abiotic control eMAE surfaces indicated the progressive accumulation of secondary sulfur compounds, which is more evident after 120 h of abiotic oxidation (Fig. 3b). In contrast, a significant cyclic production-depletion process of sulfur compounds was identified for biooxidized eMAE samples after 12 (Fig. S3) and 24 h (Fig. 3a') of assay, whereby sulfur compounds were virtually depleted after 120 h of biooxidation (Fig. 3b'). Remarkably, biooxidation process in the presence of supplementary As(V) indicated proficient bacterial capacity to sustain cyclic biooxidation, as indicated by testing after 24 and 120 h of assay (Figs. 3a'', b'', respectively). These findings and the intense changes in the concentration–depth profiles (i.e. sulfur compounds, 6 μm) identified for the rest of the

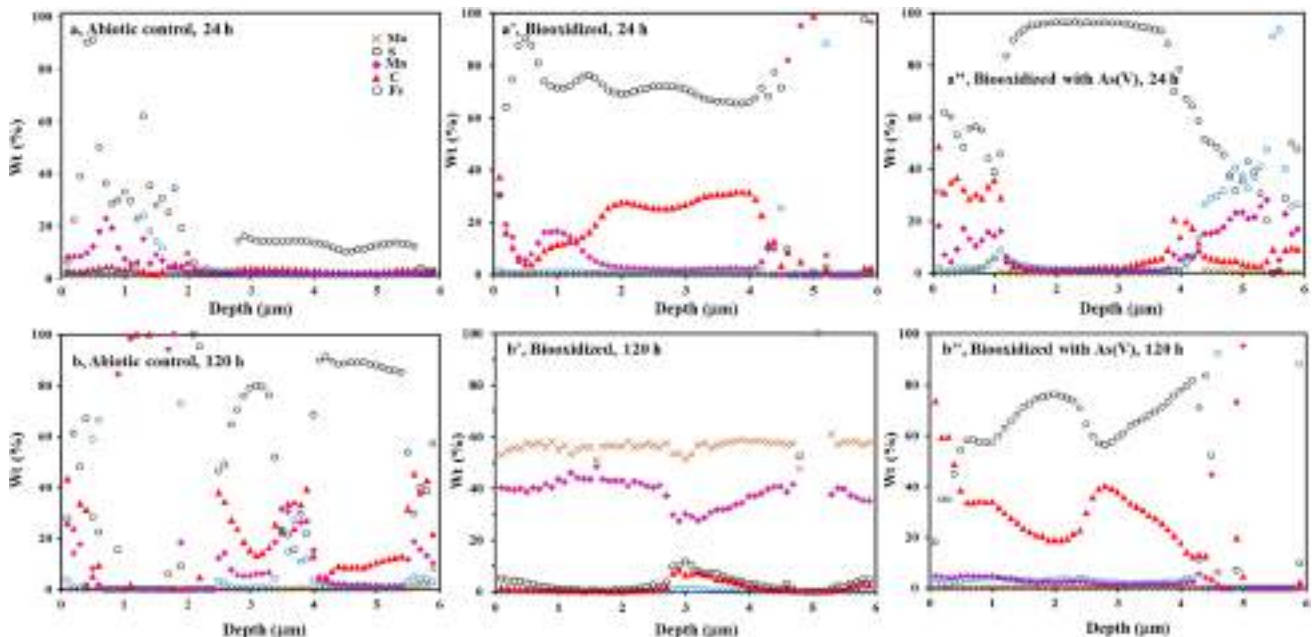


Fig. 3 Global Discharge Spectroscopy spectra for abiotic control eMAE surfaces (**a**, **b**), biooxidized eMAE surfaces (**a'**, **b'**) and biooxidized eMAE surfaces with As(V) (**a''**, **b''**) after 24 and 120 h of assay, respectively. Profiles for S, Fe, C, Mn and Mo are illustrated in the figure

biooxidized samples confirm that the bacterial mechanism has changed in the presence of supplementary As(V) (i.e. stressed biofilms). Some investigations have analyzed intrinsic arsenopyrite and pyrite biogeochemical behavior using quantitative X-ray photoelectron spectroscopy-based depth profiling (i.e. *A. ferrooxidans*) [34–36]. These reports indicated in general an enrichment of Fe, S and As compounds as a function of depth (i.e. 3.5 μm), which was directly associated with bacterial reactions mediating indirect *A. ferrooxidans* attachment. Figure 3 confirms a dynamic bacterial biooxidation behavior (i.e. cyclic production-depletion of secondary sulfur compounds, 1–6 μm depth) instead of a progressive accumulation of secondary compounds. However, this mechanism of biooxidation is sluggish in the initial stages, and even slower in the latest stages in the presence of supplementary As(V) (Fig. 3). These findings reveal a different bacterial interaction, which was associated with the type of *A. thiooxidans* attachment to arsenopyrite (i.e. direct) [11, 38], in comparison with typical *A. ferrooxidans* attachment (i.e. indirect) [6, 10, 37].

An assessment of the eMAE surface status was previously provided for 48 and 240 h of biooxidation in order to visualize biofilms evolution by AFM under the presence and absence of supplementary As(V) [11]. In the present study, this information is complemented with additional AFM observations in order to achieve a full and comprehensive description of surface processes under these conditions. Figure S4 shows typical images of abiotic control eMAE (Figs. S4a, S4b), and attached cells of *A. thiooxidans* on biooxidized eMAE (Figs. S4a', S4b') and biooxidized eMAE surfaces with As(V) (Figs. S4a'', S4b'') after 12 (i.e. incipient biofilms) and 72 h (i.e. well micro-colony structure development) of assay, respectively. The surface of the abiotic control eMAE samples shows bigger structures than those observed in the eMAE surface [11], after 12 and 72 h of chemical weathering (Fig. S4), respectively, which is consistent with progressive accumulation of refractory pyrite-like compounds (Fig. 1a). In the absence of supplementary As(V), biofilms undergo a transition from monolayer of attached cells with a typical size between 1 and 2 μm (Fig. S4a', i.e. 12 h), in agreement with observations made by Liu et al. [38], to micro-colonies (Fig. S4b', i.e. 72 h). Note that details associated with the underlying modified arsenopyrite surface and secondary compounds are distinguishable, thus, supporting direct cell attachment mediating arsenopyrite and *A. thiooxidans* interactions (Figs. S4a', S4b') [11]. Attached cells seem to be progressively embedded in the resulting secondary compounds (Fig. S4b'). A low cell density flattened-structure was distinguishable on the biooxidized eMAE surfaces with As(V) after 12 h (Fig. S4a''), while major formation of secondary compounds supports the idea that stressed biofilms induce dynamic biooxidation with the accelerated production of secondary compounds (i.e.

after 72 h, Fig. S4b''), in agreement with GDS observations (Fig. 3a'', b''). These findings provide a critical perspective on response of attached *A. thiooxidans* cells to altered arsenopyrite mainly in the presence of supplementary As(V), and offer an starting point for the understanding of SOM leaching cells behavior facing challenging environments (i.e. at the interfacial level).

Figure 4 shows SEM images complementary to previous assessments [11, 12] whereby the effect of supplementary As(V) on transient biofilm properties was further assessed. Therefore, Fig. 4 includes SEM–EDS analyses for abiotic control eMAE with As(V) after 120 h (for instance, Fig. 4a), and biooxidized eMAE samples with As(V) for all assayed times (Figs. 4b1–b5). The abiotic control samples in the presence of As(V) exhibited a similar topographic-morphologic behavior regarding abiotic control samples without supplementary As(V) [12], as well as the same secondary products in all sampled times (i.e. pyrite-like phase). This finding supports negligible precipitation of As-bearing compounds in abiotic control and all type of biooxidized surfaces induced by medium conditions (i.e. contamination), as previously discussed in the Raman study (Fig. 1a). The identification of secondary compounds was carried out by the energy-dispersive X-ray spectroscopy (data not shown). Figure 4 indicated the presence of spread attached cells in incipient stages (Fig. 4b1, b2), and also confirmed the occurrence of compact-flattened micro-colonies with high production of bacterial EPS in the presence of supplementary As(V) for later stages of biooxidation, as indicated by AFM (Fig. S4). These findings involving spread and few attached cells (Fig. 4b1, b2) enable to explain sluggishness in incipient biooxidation stages in the presence of supplementary As(V), in agreement with previous results (Figs. 1, 2, 3, S4) [39]. However, subsequent biooxidation stages indicated important formation of bacterial EPS composing compact-flattened micro-colonies in the presence of supplementary As(V) (Fig. 4b3–b5), thus, confirming occurrence of stressed biofilms interacting with secondary compounds (i.e. S_n^{2-} , S^0 , pyrite-like) (Fig. 4b5). According to literature [19, 20, 40], the secretion of exopolysaccharides is a prerequisite of *A. ferrooxidans* cells for pyrite attachment, which could be a common requirement for all leaching bacteria when facing stressing conditions (i.e. As).

Figure 5 shows CLSM images for biooxidized eMAE samples with As(V) for all assayed times (Fig. 5a1–a6), complementary to AFM and SEM studies. In this figure, a merge between epifluorescence for exopolysaccharides (displayed originally in green) and lipids (displayed originally in red) was perceived. A compilation of epifluorescence data from cells forming biofilms in the presence of supplementary As(V) was depicted in Table S4. Likewise, CLSM images without the effect of supplementary As(V) can be consulted in [12], for comparison purposes. Figure 5

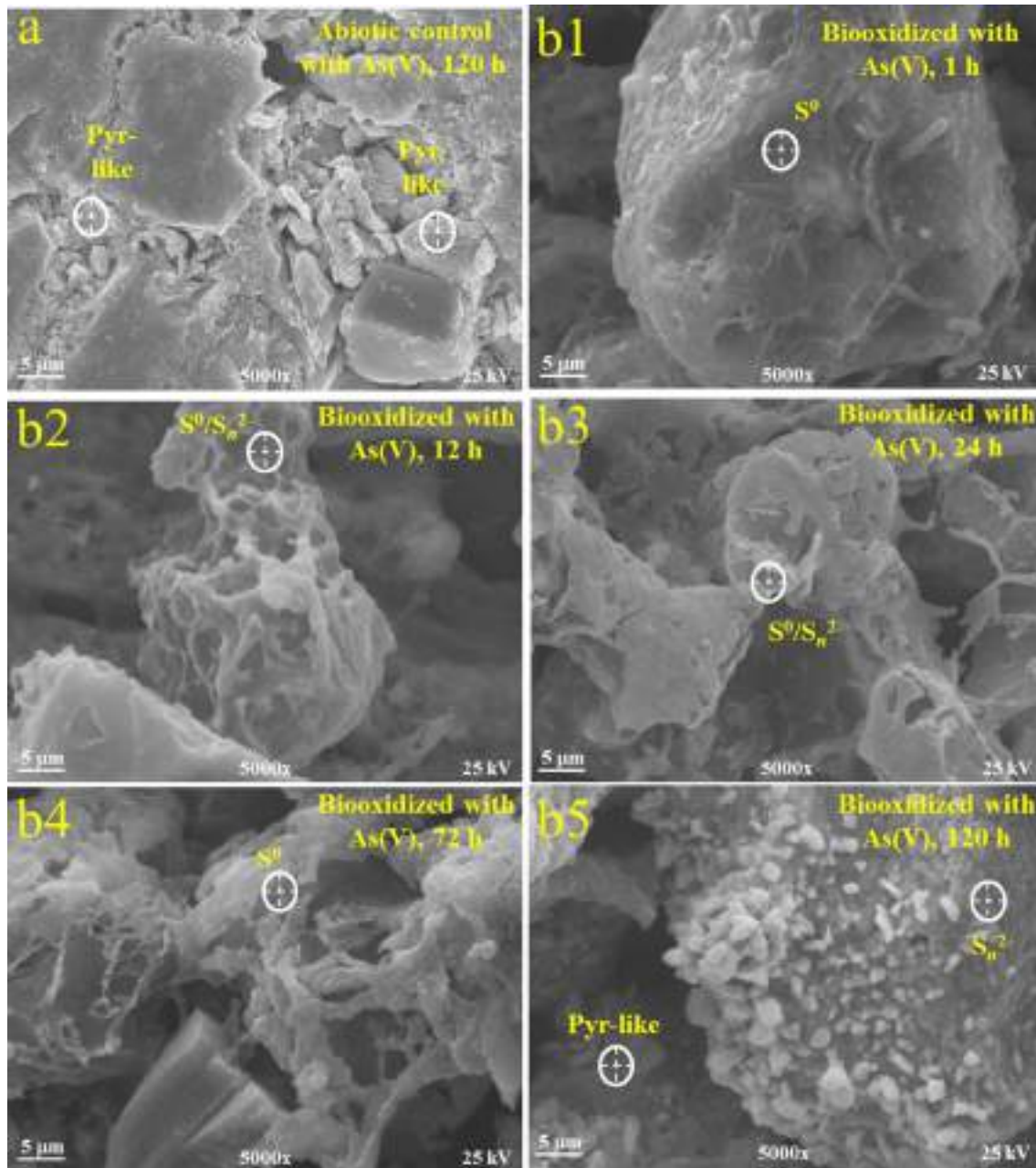


Fig. 4 Typical SEM images of the abiotic control eMAE surfaces with As(V) after 120 h of assay (**a**) and biooxidized eMAE surfaces with As(V) after 1 (**b1**), 12 (**b2**), 24 (**b3**), 48 (**b4**), 72 (**b4**), and 120 h

(**b5**) of assay. Aspy = FeAsS; Pyr-like = pyrite-like; S_n^{2-} = polysulfide structures; S^0 = elementary sulfur (according to EDS analyses, $n = 10$)

confirmed the formation and evolution of stressed biofilms due to significant presence of extracellular lipids and exopolysaccharides (i.e. α -mannose, α -glucose) in bacterial EPS [39]; in agreement with previous observations of SEM-EDS study (Fig. 4). Additionally, sluggish incipient biooxidation was correlated with low cell density structure, higher production of exopolysaccharides and minor presence of extracellular lipids (i.e. 1 h, Fig. 5a1, Table S4). The cell density structure of biofilms increased between 24

and 72 h (Figs. 4b4, b5, 5a3, a5, respectively), thus, involving a noteworthy and rapid increment of extracellular lipids (i.e. yellow to red) to configure compact-flattened microcolonies since 12–24 h of biooxidation (Figs. 4b2–b3, 5a2–a3, respectively, Table S4). These findings indicated the establishment of a more hydrophobic surface (i.e. stressed biofilms and S_n^{2-}/S^0 compounds) due to bacterial reactions, which occurs more rapid in the presence of supplementary As(V), in comparison with that depicted in Ramirez-Aldaba

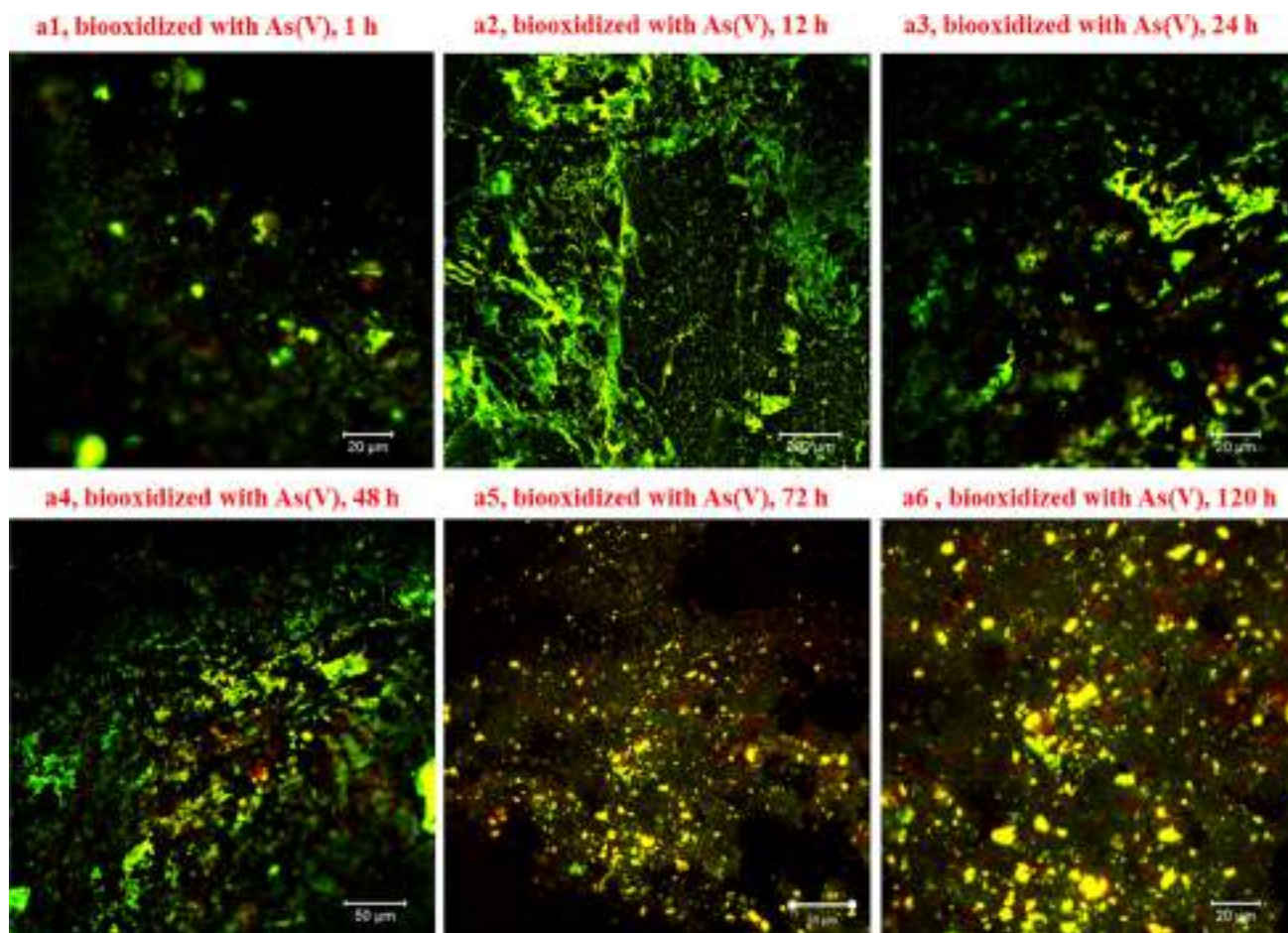


Fig. 5 CLSM images (merge) of *A. thiooxidans* for biofilms formed after the biooxidation of eMAE surfaces under the influence of supplementary As(V) after 1 h (**a1**), 12 h (**a2**), 24 h (**a3**), 48 h (**a4**), 72 h (**a5**) and 120 h (**a6**) of assay. Original epifluorescence of hydropho-

bic domains as exopolysaccharides is shown in green and the original contribution of hydrophobic domains is in red. Merge is appreciated as a transition from yellow to red. Scanning areas of $300 \times 300 \mu\text{m}$

et al. [12] (i.e. without As). Note that the increment of bacterial EPS is a typical response of microorganisms to face stressing environment and conditions (i.e. pH, As, heavy metals, temperature) [2, 39, 41], in agreement with Figs. 3, 4, 5; helping to determine structure and function of extracellular lipids in stressed biofilms (i.e. leaching cells).

The highest surface hydrophobicity was then identified after 120 h of assay in the presence of supplementary As(V) (Fig. 5a6). Altered arsenopyrite surface was mainly dominated by abundant hydrophobic secondary pyrite-like, S_n^{2-} and S^0 compounds (Figs. 1, 2, 3), as well as stressed biofilms with higher secretion of extracellular lipids (i.e. lipopolysaccharides) (Figs. 4, 5, S4, Table S4) [17]. The rapid establishment of hydrophobic biofilms after 12 h (Fig. 5a2, Table S4) relies on the configuration of a more stable biofilm and its progressive enclosure in secondary products (i.e. pyrite-like, S_n^{2-} , S^0) (Figs. S4b'', 4b5). According to literature, biofilm structures organize and evolve depending on substrate properties and their electrochemical

characteristics [40, 42, 43]. While bacterial reactions promote secretion of extracellular lipoproteins and fatty acids to sustain bioleaching activity [15, 44]; these characteristics (i.e. biofilm, surface-bulk structure) can be significantly modified by influence of toxic microenvironments (i.e. As (V)). Therefore, these data confirm a strong relationship between chemical surface speciation (i.e. 1–6 μm depth) and bacterial reactions to supplementary As(V).

Table 1 shows the quantification of extracellular surface proteins forming biofilms (i.e. EPS-associated protein fraction) for all times in the presence of supplementary As(V). Quantification of the corresponding extracellular surface proteins in the absence of supplementary As(V) is presented in Ramirez-Aldaba et al. [12], for comparison purposes. A general diminution of extracellular surface proteins was observed for all the experiments, which adequately agrees with observations for biofilm evolution (Figs. 4, 5, S4, Table 1). Not surprisingly, lower protein production was identified for stressed biofilms, regarding protein production

Table 1 Extracellular surface proteins of biofilms during biooxidation of eMAE surfaces with As(V) by *A. thiooxidans* at different times

Biooxidation time (hours)	Extracellular surface proteins under the presence of toxic As(V) $\mu\text{g cm}^{-2} \pm \text{SD}$
1	1.2 ± 0.1
12	1.8 ± 0.1
24	2.6 ± 0.05
48	4.1 ± 0.08
72	4.8 ± 0.1
120	4.3 ± 0.1

Extracellular surface proteins on planktonic cells in the presence of supplementary As(V) are 1.7 mg L^{-1} as reference

SD standard deviation

without the effect of supplementary As(V) [12]. These proteins ranged from 1.2 to $4.3 \mu\text{g cm}^2$, indicating a general decreasing range from 28 to 40% (i.e. damaged biofilm). The highest protein production was observed between 24 and 48 h, which corresponded to specific point where biofilm organization was changed from incipient structure to compact-flattened micro-colonies in the presence of supplementary As(V) (Figs. 4, 5, Table 1). This suggested an adaptation period of cells to As(V) during biooxidation (i.e. 1–12 h), followed by minor and sustained biooxidation capacity [14, 24, 25]. Additionally, Devasia and Natarajan [15] distinguished proteinaceous compounds on the surface of *A. ferrooxidans* cells attached to pyrite, whence they concluded that an induction of relatively hydrophobic proteins is required for cell attachment to S_n^{2-} and S^0 compounds [45], in agreement with our findings (Fig. 5, Tables S4 and 1). Hence, the reduction of extracellular surface proteins revealed stages of difference sensibility of *A. thiooxidans* biofilms responding to arsenopyrite interactions and supplementary As(V) adaptation. According with Figs. 1, 2, 3, 4, 5 (and Tables S4 and 1), after initial sluggishness (i.e. 1 h) bacterial activity was still active in the presence of supplementary As(V), as described by extracellular surface proteins behavior together with changes in chemical speciation (i.e. concentration vs. depth profiles). These facts agree with observations made for microorganisms previously adapted to As species (i.e. *A. ferrooxidans*, *Leptospirillum ferrooxidans*, *Acidithiobacillus caldus*) [23, 31, 41], whereby our results exhibit intermediate stages comprising biooxidation process in the presence of supplementary As(V). These results confirmed a change in a transient biooxidation mechanism, which relies on the status of the *A. thiooxidans* and arsenopyrite interactions (i.e. stressed biofilms) [46]. Further studies (i.e. proteomics and bioinformatics approach) will be devoted to analyze the influence of supplementary As(V) on bacterial responses facing

challenging environments, thus, increasing the knowledge of protein production in the presence of As(V) for leaching bacteria. Indeed, this research could assist the identification of sensitive parameters accounting for changes in biofilm structure and performance during arsenopyrite biooxidation. The transient molecular response of the biofilms can be significantly elucidated by testing other relevant environmental conditions, such as heavy metals, various forms of arsenic and the inclusion of different mineral compounds in the system [37, 41]. Indeed, this analysis could reveal new insights regarding bacterial reactions (i.e. sensitive factors) during arsenopyrite biooxidation by *A. thiooxidans* and/or mixed cultures (i.e. *A. thiooxidans* and *A. ferrooxidans*) [18, 42].

Conclusions

The present study provides a new perspective disclosing crucial stages of *A. thiooxidans* and arsenopyrite interactions affected by supplementary As(V) after 5 days. Particular emphasis is placed to illustrate arsenopyrite surface-bulk changes (i.e. concentration depth-profiles) resulting from stressed biofilm performance. Raman, XPS, SEM-EDS, CLSM, GDS and EPS-associated protein fraction were synergistically combined to determine the following findings in the presence of supplementary As(V), regarding previous observations [11, 12]: (1) Surface hydrophathy overcomes rapid change from hydrophilic (i.e. exopolysaccharides) to hydrophobic (i.e. extracellular lipids) character occurring at early biooxidation stages (i.e. 1–12 h). (2) Formation of more compact-flattened microcolonies with higher production of bacterial EPS after 24 h. (3) Progressive cells covered by abundant amount of secondary products after 120 h. (4) Sluggish initial biooxidation process (i.e. 1 h). (5) General diminution of extracellular surface proteins for stressed biofilms, in comparison with non-stressed biofilms. (6) Significant variations in arsenopyrite reactivity (i.e. concentration-depth profiles), and (7) Change in biooxidation mechanisms as a consequence of aforementioned bacterial reactions in the presence of supplementary As(V).

Acknowledgements Financial support for this research from CONACYT (Grants 2012-183230 and 2013-205416) is greatly appreciated. Hugo Ramírez-Aldaba thanks CONACYT for his Doctoral scholarship (Grant 362184). The authors thank Erasmo Mata-Martínez (IG-UASLP) for the preparation and construction of massive arsenopyrite electrodes, Ángel G. Rodríguez-Vázquez (CIACyT, UASLP) for access to Raman analyses, and Karla B. Rodríguez-Rojas (FCQ-UJED) for assistance during protein extractions.

References

1. Bhattacharya P, Welch AH, Stollenwerk KG, McLaughlin MJ, Bundschuh J, Panaullah G (2007) Arsenic in the environment:

- biology and chemistry. *Sci Total Environ* 379:109–120. <https://doi.org/10.1016/j.scitotenv.2007.02.037>
2. Kruger MC, Bertin PN, Heipieper HJ, Arsène-Ploetze F (2013) Bacterial metabolism of environmental arsenic—mechanisms and biotechnological applications. *Appl Microbiol Biotechnol* 97:3827–3841. <https://doi.org/10.1007/s00253-013-4838-5>
 3. Wang S, Zhao X (2009) On the potential of biological treatment for arsenic contaminated soils and groundwater. *J Environ Manag* 90:2367–2376. <https://doi.org/10.1016/j.jenvman.2009.02.001>
 4. Drewniak L, Sklodowska A (2013) Arsenic-transforming microbes and their role in biomining processes. *Environ Sci Pollut Res* 20:7728–7739. <https://doi.org/10.1007/s11356-012-1449-0>
 5. Rohwerder T, Gehrke T, Kinzler K, Sand W (2003) Bioleaching review part A. *Appl Microbiol Biotechnol* 63:239–248. <https://doi.org/10.1007/s00253-003-1448-7>
 6. Rohwerder T, Sand W (2007) Mechanisms and biochemical fundamentals of bacterial metal sulfide oxidation. In: *Microbial processing of metal sulfides*, pp 35–58. Springer, Berlin. https://doi.org/10.1007/1-4020-5589-7_2
 7. Sasaki K, Tsunekawa M, Ohtsuka T, Konno H (1998) The role of sulfur-oxidizing bacteria *Thiobacillus thiooxidans* in pyrite weathering. *Coll Surf A* 133:269–278. [https://doi.org/10.1016/S0927-7757\(97\)00200-8](https://doi.org/10.1016/S0927-7757(97)00200-8)
 8. Zhang J, Zhang X, Ni Y, Yang X, Li H (2007) Bioleaching of arsenic from medicinal realgar by pure and mixed cultures. *Process Biochem* 42:1265–1271. <https://doi.org/10.1016/j.procbio.2007.05.021>
 9. Ko MS, Park HS, Kim KW, Lee JU (2013) The role of *Acidithiobacillus ferrooxidans* and *Acidithiobacillus thiooxidans* in arsenic bioleaching from soil. *Environ Geochem Health* 35:727–733. <https://doi.org/10.1007/s10653-013-9530-2>
 10. Liu H, Gu G, Xu Y (2011) Surface properties of pyrite in the course of bioleaching by pure culture of *Acidithiobacillus ferrooxidans* and a mixed culture of *Acidithiobacillus ferrooxidans* and *Acidithiobacillus thiooxidans*. *Hydrometallurgy* 108:143–148. <https://doi.org/10.1016/j.hydromet.2011.03.010>
 11. Ramírez-Aldaba H, Valles OP, Vazquez-Arenas J, Rojas-Contreras JA, Valdez-Perez D, Ruiz-Baca E, Meraz M, Lara RH (2016) Chemical and surface analysis during evolution of arsenopyrite oxidation by *Acidithiobacillus thiooxidans* in the presence and absence of supplementary arsenic. *Sci Total Environ* 566:1106–1119. <https://doi.org/10.1016/j.scitotenv.2016.05.143>
 12. Ramírez-Aldaba H, Vazquez-Arenas J, Sosa-Rodríguez FS, Valdez-Pérez D, Ruiz-Baca E, García-Meza JV, Trejo-Córdoba G, Lara RH (2017) Assessment of biofilm changes and concentration-depth profiles during arsenopyrite oxidation by *Acidithiobacillus thiooxidans*. *Environ Sci Pollut Res* 24:20082–20092. <https://doi.org/10.1007/s11356-017-9619-8>
 13. Mohammed-Abdul KS, Jayasinghe SS, Chandana EP, Jayasumana C, De Silva PMC (2015) Arsenic and human health effects: a review. *Environ Toxicol* 40:828–846. <https://doi.org/10.1016/j.etap.2015.09.016>
 14. Rawlings DE (2008) High level arsenic resistance in bacteria present in biooxidation tanks used to treat gold-bearing arsenopyrite concentrates: a review. *Trans Non Metals Soc China* 18:1311–1318. [https://doi.org/10.1016/S1003-6326\(09\)60003-0](https://doi.org/10.1016/S1003-6326(09)60003-0)
 15. Devasia P, Natarajan KA (2010) Adhesion of *Acidithiobacillus ferrooxidans* to mineral surfaces. *Int J Miner Process* 94:135–139. <https://doi.org/10.1016/j.minpro.2010.02.003>
 16. Yu ZJ, Yu RL, Liu AJ, Jing L, Zeng WM, Liu XD, Qiu GZ (2017) Effect of pH values on extracellular protein and polysaccharide secretions of *Acidithiobacillus ferrooxidans* during chalcopyrite bioleaching. *Trans Non Metals Soc China* 27:406–412. [https://doi.org/10.1016/S1003-6326\(17\)60046-3](https://doi.org/10.1016/S1003-6326(17)60046-3)
 17. Bobadilla-Fazzini RA, Levican G, Parada P (2011) *Acidithiobacillus thiooxidans* secretome containing a newly described lipoprotein Licanantase enhances chalcopyrite bioleaching rate. *Appl Microbiol Biotechnol* 89:771–780. <https://doi.org/10.1007/s00253-010-3063-8>
 18. Deng S, Gu G, Wu Z, Xu X (2017) Bioleaching of arsenopyrite by mixed cultures of iron-oxidizing and sulfur-oxidizing microorganisms. *Chemosphere* 185:403–411. <https://doi.org/10.1016/j.chemosphere.2017.07.037>
 19. Harneit K, Göksel A, Kock D, Klock JH, Gehrke T, Sand W (2006) Adhesion to metal sulfide surfaces by cells of *Acidithiobacillus ferrooxidans*, *Acidithiobacillus thiooxidans* and *Leptospirillum ferrooxidans*. *Hydrometallurgy* 83:245–254. <https://doi.org/10.1016/j.hydromet.2006.03.044>
 20. Harneit K, Sand W (2007) Influence of growth substrate and attachment substratum on EPS and biofilms formation by *Acidithiobacillus ferrooxidans* A2. *Adv Mat Res* 20:385. <https://doi.org/10.4028/www.scientific.net/AMR.20-21.385>
 21. Pinet N, Tremblay A (2009) Structural analysis of the Velardeña mining district, Mexico: a faulted Au-Ag-rich hydrothermal system. *Can J Earth Sci* 46:123–138. <https://doi.org/10.1139/E09-007>
 22. Collinet MN, Morin D (1990) Characterization of arsenopyrite oxidizing *Thiobacillus*. Tolerance to arsenite, arsenate, ferrous and ferric iron. *Antonie Van Leeuwenhoek* 57:237–244. <https://doi.org/10.1007/BF00400155>
 23. Leng F, Li K, Zhang X, Li Y, Zhu Y, Lu J, Li H (2009) Comparative study of inorganic arsenic resistance of several strains of *Acidithiobacillus thiooxidans* and *Acidithiobacillus ferrooxidans*. *Hydrometallurgy* 98:235–240. <https://doi.org/10.1016/j.hydromet.2009.05.004>
 24. Dopson M, Baker-Austin C, Koppineedi PR, Bond PL (2003) Growth in sulfidic mineral environments: metal resistance mechanisms in acidophilic micro-organisms. *Microbiology* 149:1959–1970. <https://doi.org/10.1099/mic.0.26296-0>
 25. Koechler S, Farasin J, Cleiss-Arnold J, Arsène-Ploetze F (2015) Toxic metal resistance in biofilms: diversity of microbial responses and their evolution. *Res Microbiol* 166:764–773. <https://doi.org/10.1016/j.resmic.2015.03.008>
 26. Noël N, Florian B, Sand W (2010) AFM and EFM study on attachment of acidophilic leaching organisms. *Hydrometallurgy* 104:370–375. <https://doi.org/10.1016/j.hydromet.2010.02.021>
 27. Lu P, Zhu C (2011) Arsenic Eh–pH diagrams at 25 C and 1 bar. *Environ Earth Sci* 62:1673–1683. <https://doi.org/10.1007/s12665-010-0652-x>
 28. Bradford L (1976) A rapid and sensitive method for the quantification of microgram quantities of protein utilizing the principle of protein dye binding. *Anal Biochem* 72:248–252. [https://doi.org/10.1016/0003-2697\(76\)90527-3](https://doi.org/10.1016/0003-2697(76)90527-3)
 29. Comte S, Guibaud G, Baudu M (2006) Relations between extraction protocols for activated sludge extracellular polymeric substances (EPS) and complexation properties. Part I. Comparison of the efficiency of eight EPS extraction methods. *Enzyme Microb Technol* 38:237–245. <https://doi.org/10.1016/j.enzmictec.2005.06.016>
 30. Elzaky M, Attia YA (1995) Effect of bacterial adaptation on kinetics and mechanisms of bioleaching ferrous sulfides. *Chem Eng J Biochem Eng J* 56:B115–B124. [https://doi.org/10.1016/0923-0467\(94\)06086-X](https://doi.org/10.1016/0923-0467(94)06086-X)
 31. Park J, Han Y, Lee E, Choi U, Yoo K, Song Y, Kim H (2014) Bioleaching of highly concentrated arsenic mine tailings by *Acidithiobacillus ferrooxidans*. *Sep Purif Technol* 133:291–296. <https://doi.org/10.1016/j.seppur.2014.06.054>
 32. Hu X, Cai Y, Zhang Y (2017) Hydrothermal alteration of arsenopyrite by acidic solutions. *Appl Geochem* 77:102–115. <https://doi.org/10.1016/j.apgeochem.2016.08.009>
 33. Mycroft JR, Bancroft GM, McIntyre NS, Lorimer JW, Hill IR (1990) Detection of sulphur and polysulphides on electrochemically oxidized pyrite surfaces by X-ray photoelectron spectroscopy

- and Raman spectroscopy. *J Electroanal Chem Interf Electrochem* 292:139–152. [https://doi.org/10.1016/0022-0728\(90\)87332-E](https://doi.org/10.1016/0022-0728(90)87332-E)
34. Nesbitt HW, Muir IJ (1998) Oxidation states and speciation of secondary products on pyrite and arsenopyrite reacted with mine waste waters and air. *Miner Petrol* 62:123–144. <https://doi.org/10.1007/BF01173766>
35. Jones RA, Koval SF, Nesbitt HW (2003) Surface alteration of arsenopyrite (FeAsS) by *Thiobacillus ferrooxidans*. *Geochim Cosmochim Acta* 67:955–965. [https://doi.org/10.1016/S0016-7037\(02\)00996-1](https://doi.org/10.1016/S0016-7037(02)00996-1)
36. Li J, Lu J, Lu X, Tu B, Ouyang B, Han X, Wang R (2015) Sulfur transformation in microbially mediated pyrite oxidation by *Acidithiobacillus ferrooxidans*: insights from X-ray photoelectron spectroscopy-based quantitative depth profiling. *Geomicrobiol J* 33:118–134. <https://doi.org/10.1080/01490451.2015.1041182>
37. Dave SR, Gupta KH (2007) Interactions of *Acidithiobacillus ferrooxidans* with heavy metals, various forms of arsenic and pyrite. *Adv Mater Res* 20:423–426. <https://doi.org/10.4028/www.scientific.net/AMR.20-21.423>
38. Liu HL, Chen BY, Lan YW, Cheng YC (2003) SEM and AFM images of pyrite surfaces after bioleaching by the indigenous *Thiobacillus thiooxidans*. *Appl Microbiol Biotechnol* 62:414–420. <https://doi.org/10.1007/s00253-003-1280-0>
39. Dheer R, Patterson J, Dudash M, Stachler EN, Bibby KJ, Stolz DB, Stolz JF (2015) Arsenic induces structural and compositional colonic microbiome change and promotes host nitrogen and amino acid metabolism. *Toxicol Appl Pharmacol* 289:397–408. <https://doi.org/10.1016/j.taap.2015.10.020>
40. Donlan MR (2002) Biofilms: microbial life on surfaces. *Emerg Infect Dis* 8:881–890. <https://doi.org/10.3201/eid0809.020063>
41. Zhang X, Feng YL, Li HR (2016) Enhancement of bio-oxidation of refractory arsenopyritic gold ore by adding pyrolusite in bioleaching system. *Trans Nonferrous Metals Soc China* 26:2479–2484. [https://doi.org/10.1016/S1003-6326\(16\)64339-X](https://doi.org/10.1016/S1003-6326(16)64339-X)
42. Crundwell FK (2015) The semiconductor mechanism of dissolution and the pseudo-passivation of chalcopyrite. *Can Metall Q* 54:279–288. <https://doi.org/10.1179/1879139515Y.0000000007>
43. Echeverría-Vega A, Dermargasso C (2015) Copper resistance, motility and the mineral dissolution behavior were assessed as novel factors involved in bacterial adhesion in bioleaching. *Hydrometallurgy* 157:107–115. <https://doi.org/10.1016/j.hydromet.2015.07.018>
44. Lawrence JR, Swerhone GDW, Leppard GG, Araki T, Zhang X, West MM, Hitchcock AP (2003) Scanning transmission X-ray, laser scanning, and transmission electron microscopy mapping of the exopolymeric matrix of microbial biofilms. *Appl Environ Microbiol* 69:5543–5554. <https://doi.org/10.1128/AEM.69.9.5543-5554.2003>
45. Arredondo R, García A, Jerez CA (1994) Partial removal of lipopolysaccharide from *Thiobacillus ferrooxidans* affects its adhesion to solids. *Appl Environ Microbiol* 60:2846–2851. <http://aem.asm.org/content/60/8/2846.short>
46. Kumar RN, Nagendran R (2007) Influence of initial pH on bioleaching of heavy metals from contaminated soil employing indigenous *Acidithiobacillus thiooxidans*. *Chemosphere* 66:1775–1781. <https://doi.org/10.1016/j.chemosphere.2006.07.091>



Revista Iberoamericana de Micología

www.elsevier.es/reviberoammicol



Original article

Identification of proteins in *Sporothrix schenckii sensu stricto* in response to oxidative stress induced by hydrogen peroxide

Estela Ruiz-Baca^{a,*}, Hilda Leyva-Sánchez^a, Bertha Calderón-Barraza^a, Ulises Esquivel-Naranjo^b, Everardo López-Romero^c, Angélica López-Rodríguez^a, Mayra Cuéllar-Cruz^{c,*}

^a Facultad de Ciencias Químicas, Universidad Juárez del Estado de Durango, Av. Veterinaria S/N, 34120 Durango, DGO, Mexico

^b Unidad de Microbiología Básica y Aplicada, Facultad de Ciencias Naturales, Universidad Autónoma de Querétaro, Anillo vial Fray Junípero Serra km 8 s/n, C.P. 76000, Santiago de Querétaro, QRO, Mexico

^c Departamento de Biología, División de Ciencias Naturales y Exactas, Campus Guanajuato, Universidad de Guanajuato, Campus Guanajuato, Noria Alta S/N, 36050 Guanajuato, GTO, Mexico

ARTICLE INFO

Article history:

Received 9 February 2018

Accepted 22 October 2018

Available online xxx

Keywords:

Sporothrix schenckii

H₂O₂

Oxidative stress

Reactive oxygen species

ABSTRACT

Background: Sporotrichosis is a fungal infection caused by the *Sporothrix schenckii* complex. In order to colonize the host, the pathogen must neutralize the reactive oxygen species produced by the phagocytic cells during the respiratory burst. Little is known about these mechanisms in *S. schenckii*.

Aims: To identify the proteins differentially expressed after the exposure of *S. schenckii sensu stricto* to different concentrations of H₂O₂.

Methods: Yeast cells of *S. schenckii sensu stricto* were exposed to increasing concentrations of H₂O₂. Proteins differentially expressed in response to oxidative stress were analyzed using two-dimensional polyacrylamide gel electrophoresis (2D-PAGE) and identified by MALDI-MS/MS. RT-PCR assays were performed to evaluate the transcription of genes of the identified proteins.

Results: Concentrations of H₂O₂ as high as 800 mM allowed cell growth, and 200 mM and 400 mM were selected for comparative analysis by 2D-PAGE. This analysis revealed at least five differentially expressed proteins, which were identified as heat shock 70 kDa protein (Hsp70), chaperonin GroEL, elongation factor 1-β (EF1-β), a hypothetical protein, and mitochondrial peroxiredoxin (Prx1). RT-PCR revealed that the transcription of the genes coding for some of these proteins are differentially regulated.

Conclusions: Based on these results, it is proposed that these proteins may be involved in the resistance of *S. schenckii* to oxidative stress, and play an important role in the fungus survival in the host.

© 2019 Asociación Española de Micología. Published by Elsevier España, S.L.U. All rights reserved.

Identificación de proteínas en *Sporothrix schenckii sensu stricto* en respuesta al estrés oxidativo inducido por peróxido de hidrógeno

RESUMEN

Antecedentes: La esporotricosis es una infección fúngica causada por el complejo *Sporothrix schenckii*. Para colonizar al huésped, los patógenos deben neutralizar las especies reactivas de oxígeno producidas por las células fagocíticas durante el estallido respiratorio. Poco se conoce sobre este mecanismo en *S. schenckii*.

Objetivos: Identificar proteínas diferencialmente expresadas durante la exposición de *S. schenckii sensu stricto* a diferentes concentraciones de H₂O₂.

Métodos: Levaduras de *S. schenckii sensu stricto* fueron expuestas a concentraciones crecientes de H₂O₂. Las proteínas diferencialmente expresadas en respuesta al estrés oxidativo fueron analizadas mediante electroforesis en geles de poliacrilamida en doble dimensión (2D-PAGE) e identificadas por MALDI-MS/MS. Se realizaron ensayos de RT-PCR para evaluar la transcripción de genes de las proteínas identificadas.

Palabras clave:

Sporothrix schenckii

H₂O₂

Estrés oxidativo

Especies reactivas del oxígeno

* Corresponding authors.

E-mail addresses: eruib@ujed.mx (E. Ruiz-Baca), mcuellar@ugto.mx (M. Cuéllar-Cruz).

<https://doi.org/10.1016/j.riam.2018.10.004>

1130-1406/© 2019 Asociación Española de Micología. Published by Elsevier España, S.L.U. All rights reserved.

Resultados: Concentraciones altas de H₂O₂ (800 mM) permitieron el crecimiento celular, y se seleccionaron las concentraciones de 200 y 400 mM para el análisis comparativo mediante 2D-PAGE. Este análisis reveló al menos cinco proteínas diferencialmente expresadas, identificadas como proteína de choque térmico de 70 kDa (Hsp70), chaperonina GroEL, factor de alargamiento 1-β (EF1-β), una proteína hipotética y peroxirredoxina mitocondrial (Prx1). La RT-PCR reveló que la transcripción de los genes que codifican para algunas de estas proteínas se regula diferencialmente.

Conclusiones: Con estos resultados pensamos que estas proteínas podrían estar involucradas en la resistencia de *S. schenckii sensu stricto* al estrés oxidativo y jugar un papel importante en la supervivencia del hongo en el huésped.

© 2019 Asociación Española de Micología. Publicado por Elsevier España, S.L.U. Todos los derechos reservados.

Sporotrichosis is a subcutaneous mycosis caused by the *Sporothrix schenckii* complex, a thermodimorphic fungus which is endemic in tropical and subtropical areas of Latin America. This disease has been reported as endemic because of the widespread use of immunosuppressive therapy, cancer, alcoholism and the incidence of acquired immunodeficiency syndrome (AIDS).¹⁷ Phenotypic and molecular studies have shown that *S. schenckii* is a complex of different cryptic species, some of which are considered of medical importance, such as *S. schenckii sensu stricto*, *Sporothrix brasiliensis*, *Sporothrix globosa*, *Sporothrix mexicana*, *Sporothrix luriei* and *Sporothrix pallida*.^{2,17-19}

As other pathogens, the first barrier that *Sporothrix* must overcome to colonize its host is the immune system itself. Upon interaction with pathogens, phagocytes produce reactive oxygen species (ROS) during the oxidative burst, which are essential components of the immune response against the invading microorganisms.^{4,27} ROS are mainly formed in the mitochondrial electron transport chain by the partial reduction of O₂, generating superoxide anions (O₂^{•-}), hydrogen peroxide (H₂O₂) and hydroxyl radicals (HO[•]). Pathogens have developed mechanisms involving enzymatic and non-enzymatic systems that enable them to detoxify ROS and evade phagocytic cells.²⁷ After the phagocytosis of *S. schenckii*, monocytes and macrophages are strongly induced to produce ROS.²⁵ It has been shown that in this organism, the superoxide radical has fungistatic and fungicidal activity, and its absence is associated with higher mortality in experimental mouse infections.¹⁴ Despite the relevance of this anti-oxidant activity, there are few studies dealing with the responses of *Sporothrix* to oxidative stress (OS).²² It is well documented that the response to OS (OSR) depends on the phase growth of the pathogen as it has been demonstrated that exponentially growing cells are more susceptible than those in the stationary phase of growth.^{6,8,21,31} A recent work in this laboratory has focused on the mechanisms used by *S. schenckii sensu stricto* to respond to OS in the stationary phase of growth. This phase is of special interest as cells remain in quiescent state and very much emulate their lifestyle in nature.^{21,32} Quiescent cells represent almost 60% of earth biomass and they can survive for long periods of time, sometimes years, in the absence of nutrients, a feat of astonishing resilience.¹¹ It has been reported that in pathogenic organisms such as some *Candida* species, the stationary phase favours colonization of the human host where they remain quiescent until optimal nutrient conditions exist to infect and invade it. *S. schenckii* exhibits a similar behaviour. While in some *Candida* species some proteins involved in the OSR have been identified,^{7,23} the same is not true for *S. schenckii* complex.

On this background, we considered it relevant to identify proteins potentially involved in the OSR following exposure of stationary phase yeast cells of *S. schenckii sensu stricto* to H₂O₂. We identified at least five proteins that were up- or down-regulated

after exposing the pathogen to increasing concentrations of H₂O₂. RT-PCR revealed that transcription of genes coding for some of these proteins are differentially regulated. We propose that these proteins are involved in the mechanisms of resistance against ROS and may contribute to the survival of the fungus in the host.

Material and methods

Strain and culture conditions

Throughout this study, the *S. schenckii* ATCC 58251 strain was used. To obtain the yeast morphotype cells in the stationary-phase, 500-ml Erlenmeyer flasks containing 200 ml of brain heart infusion medium (BHI, Difco) were inoculated with 5 × 10⁵ conidia·ml⁻¹ and incubated at 37 °C for 8 days on a rotary shaker at 120 rpm. Yeast cells were harvested by centrifugation at 7000 × g for 10 min and used for the assays described below.

Assays of H₂O₂ susceptibility

S. schenckii was grown for 8 days at 37 °C. To assay H₂O₂ susceptibility, yeast cells were diluted in fresh BHI medium to an OD_{600nm} of 0.5 in sterile deionized water. The cultures were divided in equal parts, exposed to different H₂O₂ concentrations (0 to 1000 mM) and shaken (120 rpm) at 37 °C. After 60 min, an aliquot was taken from the cultures treated with the oxidant, adjusted to an OD_{600nm} of 0.5 and used to prepare exponential dilutions in 96-well boxes. Each dilution was spotted onto YPG plates (0.3% yeast extract, 1% peptone, and 2% glucose) and incubated at 37 °C for 48 h. The experiments were carried out thrice. These protocols were adapted from previous studies with other organisms.^{6,7}

Extraction of proteins

Non-exposed and H₂O₂-exposed cell cultures were centrifuged at 13,000 × g at 4 °C for 15 min and the supernatant was carefully discarded. The cell pellet was washed thrice with washing buffer [200 mM Tris-HCl, pH 8.5, 1 mM phenylmethylsulfonyl fluoride (PMSF)] by centrifugation at 7000 × g at 4 °C for 10 min. Washed cells were resuspended in lysis buffer (200 mM Tris-HCl, pH 8.5, 1 mM PMSF, 200 mM NaCl, 0.5% SDS, 25 mM EDTA) and broken with glass beads (0.45–0.5 mm in diameter) by alternate periods of breaking (40 s) and cooling (60 s) until all cells were broken. The cell homogenate was centrifuged at 7000 × g at 4 °C for 10 min. The supernatant was carefully aspirated with a Pasteur pipette and the cell pellet was discarded. Proteins in the supernatant were precipitated with 70% (v/v) ethanol at –20 °C for 3 h and stored at –70 °C until further use. Protein concentration was determined by the DC method (Bio-Rad) using bovine serum albumin (BSA) as standard.

2D-PAGE and image analysis

2D-PAGE was performed using 7-cm strips with an immobilized 4–7 pH gradient (Bio-Rad) as described by Ruiz-Baca et al.²⁶ Briefly, samples containing 80 µg of total protein were cleaned using the cleaning kit from Bio-Rad (2D Clean-Up Kit) as described above and resuspended in 140 µl of rehydration buffer [7 M urea, 2 M thiourea, 4% CHAPS, 50 mM dithiothreitol (DTT), 0.2% ampholytes (Biolyte 3/10) and 0.001% bromophenol blue]. After rehydration for 16 h, the strips were subjected to isoelectric focusing with voltage gradients of 0 to 250 V for 15 min, 250 to 4000 V for 2 h, and 4000 V to completion at 8500 V/h. After isoelectric focusing, the strips were incubated sequentially for 15 min in equilibrium buffer I (0.375 mM Tris/HCl, pH 8.8, 6 M urea, 20% glycerol, 2% SDS and 0.5% DTT) and equilibrium buffer II (0.375 mM Tris/HCl, pH 8.8, 6 M urea, 20% glycerol, 2% SDS and 2% iodoacetamide) under constant stirring. For the second dimension, the strips were placed on top of a 10% SDS-PAGE gel and covered with a 0.5% agarose overlay. The proteins were separated at 95 V for 2 h in a Mini-Protean 3 system (Bio-Rad) and then stained with colloidal Coomassie blue. Images were captured with a ChemiDoc™ XRS+ System (Bio-Rad) and analyzed with a PDQuest™ 2-D (Bio-Rad) software. Comparisons of the gels were done using a synthetic image containing all the protein spots of analyzed gels. The intensity of the spots was normalized and validated in the master gel. A spot was considered relevant when there was a minimum of a two-fold difference in its intensity as compared with the corresponding spot obtained from the oxidant-untreated sample.

Protein identification

Spots of interest were manually excised from 2D electrophoresis gels. The gel pieces were destained and enzymatically digested according to the modified protocol of Shevchenko et al.³⁰ Resulting tryptic peptides were concentrated to an approximate volume of 10 µl. Nine µl of this sample were loaded onto a ChromXP Trap Column C18-CL precolumn (Eksigent, Redwood City CA); 350 µm × 0.5 mm, 120 Å pore size, 3 µm particle size and desalted with 0.1% trifluoroacetic acid (TFA) in H₂O at a flow rate of 5 µl/min during 10 min. Then, peptides were loaded and separated on a Waters BEH130 C18 column (Waters, Milford, MA); 100 µm × 100 mm, 130 Å pore size, 1.7 µm particle size, using a HPLC Ekspert nanoLC 425 (Eksigent, Redwood City CA) with 0.1% TFA in H₂O and 0.1% TFA in acetonitrile (ACN) as mobile phases A and B, respectively, under the following lineal gradient: 0–3 min 10% B (90% A), 60 min 60% B (40% A), 61–64 min 90% B (10% A), 65 to 90 min 10% B (90% A) at a flow rate of 250 nl/min. Eluted fractions were automatically mixed with a solution of 2 mg/ml of α-cyano-4-hydroxycinnamic acid (CHCA) in 0.1%TFA and 50% ACN as a matrix, spotted in a stainless steel plate of 384 spots using a MALDI

Ekspot (Eksigent, Redwood City CA) with a spotting velocity of 20 s per spot at a matrix flow rate of 1.6 µl/min. The spots generated were analyzed by a MALDI-TOF/TOF 4800 Plus mass spectrometer (ABSciex, Framingham MA). Each MS Spectrum was acquired by accumulating 1000 shots in a mass range of 850–4000 Da with a laser intensity of 3700. The 100 more intense ions with a minimum signal-noise of 20 were programmed to fragmenting. The MS/MS spectra were obtained by fragmentation of selected precursor ions using collision induced dissociation and acquired by 3000 shots with a laser intensity of 4400. Generated MS/MS spectra were compared using a Protein Pilot software v. 2.0.1 (ABSciex, Framingham, MA) against *S. schenckii* strain ATCC 58251 and 1099-18 database (downloaded from Uniprot; 8673 and 10292 protein sequences, respectively) using Paragon algorithm. The search parameters were carbamidomethylated cysteine, trypsin as a cut enzyme, all the biological modifications and amino acid substitution set by the algorithm, as well as phosphorylation emphasis and Gel-based ID as special factors. The detection threshold was considered in 1.3 to acquire 95% of confidence. The identified proteins were grouped by ProGroup algorithm in the software to minimize redundancy.

Reverse transcription-PCR (RT-PCR)

Total RNA from *Sporothrix* cells was isolated using the Trizol reagent (Invitrogen) according to the manufacturer's instructions, and DNase I (Invitrogen) was used to eliminate DNA contamination. Synthesis of cDNA and PCR were carried out as described elsewhere using the ImProm-II™ Reverse Transcription System (Promega). The expression levels of *prx1* and *hsp70* genes were normalized by β-tubulin gene (*tub*). The RT primers used for each gene are shown in Table 1. Synthesis of cDNA was carried out at 42 °C for *prx1*, *hsp70* and *tub* genes and PCR was performed at 58 °C for the three analyzed genes. PCR amplification of DNase-treated RNA was performed without the reverse-transcription procedure (No-RT). Lack of amplification of PCR products confirmed the complete elimination of DNA from RNA samples. The PCR products were visualized on agarose gel stained with ethidium bromide. The quantification of PCR products was carried out using an ImageJ1.51j8 software (Wayne Rasband, National Institutes of Health, USA).

Statistical analysis

The quantification of PCR products were analyzed by a single-factor ANOVA in a completely randomized design with three levels of peroxide concentration. Then, a Tukey post hoc multiple comparison of means with a 95% family-wise confidence level was performed. A *p* < 0.05 was considered statistically significant. These analyses were performed using R, a programming language for statistical computing.²⁴

Table 1
Proteins separated on 2D-PAGE gels and analyzed by MALDI-MS/MS.

Spot	Protein name	Mass (kDa)	pI	Peptide matching	Sequence coverage (%)	Expression	Function
1	Heat shock 70kDa protein	69	4.8	25	37.7	Upregulated/ Downregulated	Interaction with the host, Response to stress
2	Chaperonin GroEL	61	5.4	44	59.6	Upregulated/ Downregulated	Folding, assembly, and translocation of proteins
3	Hypothetical protein	88	5.9	4	2.4	Downregulated	Unknown
4	Elongation factor 1-β	26	4.3	6	30.6	Upregulated/ Downregulated	Protein biosynthesis
5	Mitochondrial peroxiredoxin-1	25	5.6	10	32.9	Upregulated	Response to stress

Mass spectra were analyzed with Protein Pilot software v. 2.0.1 (ABSciex, Framingham MA) against *S. schenckii*. Protein name: protein name as deduced by comparing peptide sequences via the software BLAST. Molecular weight (kDa): theoretical molecular mass predicted from the amino acid sequence of the identified protein. pI: theoretical isoelectric point predicted from the amino acid sequence of the identified protein. Sequence coverage: coverage of the amino acid sequence of the identified protein. Peptide matching: number of matched peptides based on MS/MS data searching, excluding the duplicate matches.

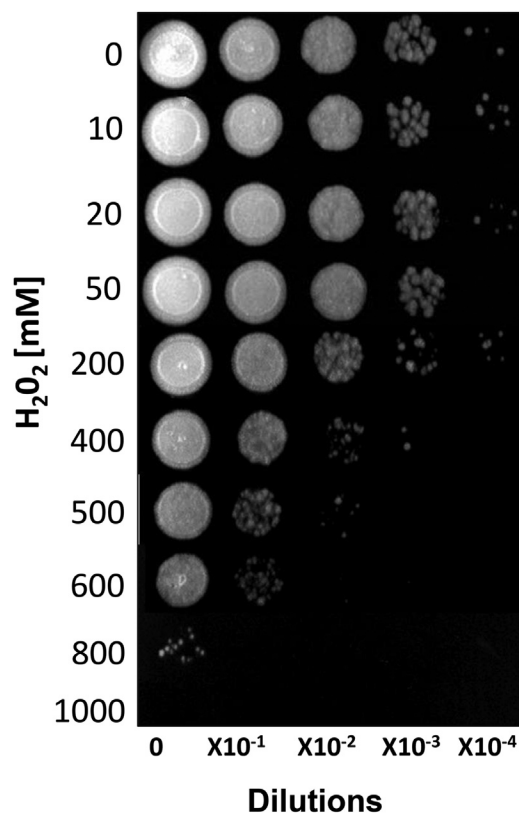


Fig. 1. Susceptibility of *S. schenckii sensu stricto* to H₂O₂. Cultures of stationary-phase yeast cells (OD_{600nm} 0.5) were incubated under constant stirring in the presence of the indicated concentrations of H₂O₂ at 37 °C. Samples of these suspensions were exponentially diluted in 96-well plates and each dilution was spotted onto YPG plates that were incubated at 37 °C. Growth was inspected after 48 h.

Results

Susceptibility to H₂O₂

To increase our knowledge of the resistance mechanisms of *S. schenckii sensu stricto*, we considered it relevant to identify some proteins presumptively involved in OSR. To this purpose, stationary-phase cultures of yeast cells of the fungus were exposed to increasing concentrations of H₂O₂ (Fig. 1). Fungal growth was not affected when cell dilutions were exposed to concentrations between 0 and 50 mM of H₂O₂. At 200 mM, inhibition was observed at a cell dilution of 1×10^{-2} . At 400 mM and at a dilution of 1×10^{-1} ,

fungal growth decreased and was fully inhibited at all higher cell dilutions with no significant differences at 500 mM. At 600 mM, growth decreased at dilution 0, with poor growth at 800 mM and full inhibition at 1000 mM.

Differential expression of proteins during OSR

Based on their effect on growth, concentrations of 0, 200 and 400 mM H₂O₂ were selected to carry out a comparative analysis of the total protein expression by *S. schenckii sensu stricto*. Analysis by 2D-PAGE at different concentrations of H₂O₂ showed the presence of at least five differentially expressed proteins (Fig. 2) which were identified as a heat shock 70 kDa protein (Hsp70), chaperonin GroEL, elongation factor 1-β (EF1-β), a hypothetical protein and mitochondrial peroxiredoxin (Prx1) (Table 1). Accordingly, an upregulated expression of Hsp70 and Prx1 was observed (Fig. 2; spots 1 and 5, respectively). Other proteins that were either up- or downregulated were chaperonin GroEL and EF-1β (Fig. 2; spots 2 and 4, respectively). Also, a downregulated expression of a hypothetical protein was observed in response to OS (Fig. 2; spot 3).

Analysis of transcriptional expression

To determine whether the regulation of identified proteins occurred at the transcriptional level, we evaluated the expression of genes encoding Prx1 and Hsp70. To this purpose, it was important to assess the quality of the RNA obtained from *S. schenckii sensu stricto* as it has been reported that ROS can damage nucleic acids.⁴ It was observed that the ribosomal RNA bands were well defined indicating that it was suitable for analysis (Fig. 3A). Following exposure to H₂O₂, significant differences were found in the expression of the *prx1* and *hsp70* genes at 200 and 400 mM H₂O₂ ($p < 0.05$) as compared with the control. On the other hand, *prx1* showed a significant increase at 400 mM H₂O₂ compared with 200 mM H₂O₂ ($p < 0.05$), while *hsp70* showed a significant decrease at 400 mM H₂O₂ compared with 200 mM ($p < 0.05$) (Fig. 3B and C).

Discussion

Identification of proteins potentially involved in the resistance of *S. schenckii sensu stricto* to oxidant agents is a useful approach to understand how the fungus can protect itself from OS. Here, stationary-phase yeast cells of the fungus were subjected to OS with different concentrations of H₂O₂. This oxidant started to affect the growth of *S. schenckii* at 200–400 mM, the inhibition increased at 600 mM and no cells remain viable at 1000 mM. In other pathogenic fungi such as *Paracoccidioides brasiliensis* and *Candida* species, the

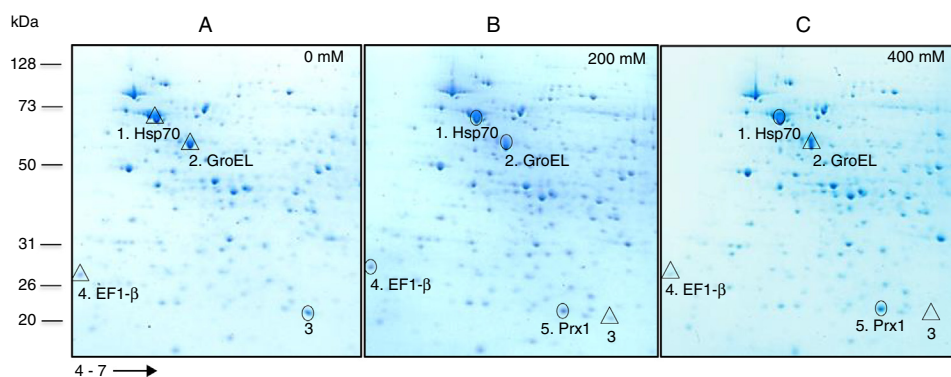


Fig. 2. Analysis of total protein extracts from yeast cells of *S. schenckii sensu stricto* by 2D-PAGE in a pH 4–7 gradient in gels stained with colloidal Coomassie Blue, after exposure to 0 (A), 200 (B) and 400 (C) mM H₂O₂. Spots marked with circles and triangles correspond to up- and down-regulated proteins, respectively, with respect to the reference condition. kDa, kilodalton.

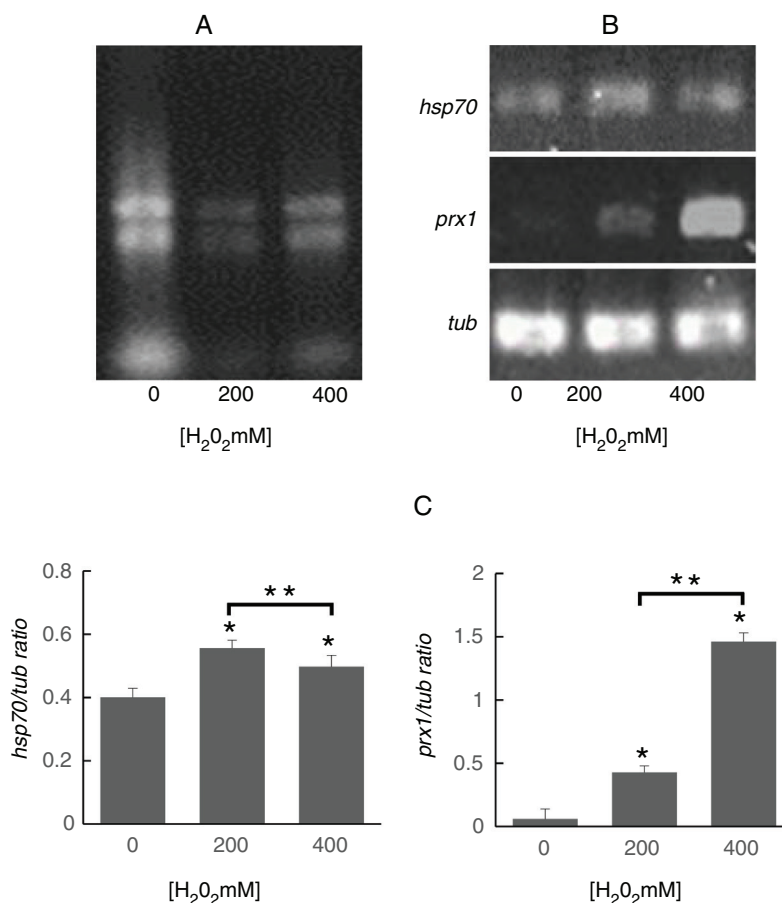


Fig. 3. Analysis of *prx1* and *hsp70* gene expression by RT-PCR. (A) Total RNA of *S. schenckii sensu stricto* exposed to the indicated concentrations of H₂O₂. (B) RT-PCR products from the analysis of *hsp70*, *prx1* and *tub* gene expression in *S. schenckii sensu stricto*. (C) Densitometry of the bands was measured using the ImageJ 1.51j8 software. The quantification of *prx1* and *hsp70* was performed. Data are presented as the mean \pm SD, $n = 3$. *Significant differences as compared to control ($p < 0.05$). **Significant differences between concentrations of H₂O₂ ($p < 0.05$).

response to oxidative stress in the growth phase was different.^{1,8,23} Yeast cells of *P. brasiliensis* in the stationary phase were more resistant to H₂O₂ than their counterparts in the exponential phase after exposure to 0–100 mM H₂O₂. The survival rates of cells from both phases exceeded 70% with all tested concentrations of H₂O₂.⁸ In contrast, species of the *Candida* genus in the stationary phase of growth reveals that *C. albicans* is more susceptible to H₂O₂ as its growth was completely inhibited at 300 mM. Other species such as *C. glabrata* and *C. parapsilosis* survived at 500 mM, while *C. krusei* did so at 1500 mM.²³ Resistance of *Candida* species to H₂O₂ has also been observed by other authors,¹ thus reinforcing the notion that pathogenic organisms have developed mechanisms to detoxify H₂O₂ that enable them to evade the immune system and colonize the host.

2D-PAGE of extracts from *S. schenckii sensu stricto* yeast cells exposed to two concentrations of H₂O₂ showed the presence of at least five differentially expressed proteins. These were identified as Hsp70, chaperonin GroEL, a hypothetical protein, EF-1 β and mitochondrial Prx1 (Fig. 2, spots 1–5, respectively. See also Table 1). Fungal Hsp70 has been implicated in various cellular functions, including OS, cell adhesion, macrophage activation, receptor expression and macromolecule internalization.^{15,28} Studies in species of *Candida*,⁷ *P. brasiliensis*⁹ and *Cryptococcus neoformans*²⁵ suggest an important role of Hsp70 in the interaction with host cells and in the response to OS. On the other hand, the chaperonin GroEL in bacteria is required for the proper folding of many proteins. Studies indicate that these chaperones are overexpressed under

conditions of cellular stress, including heat, so they are considered as heat shock proteins⁵. On its part, EF-1 β plays an important role in protein synthesis. Accordingly, McGoldrick et al.²⁰ reported 67 sequences of glutathione transferase-like proteins encoded in 21 fungal species, some related to EF-1 β , suggesting their involvement in the ROS. Also, the differentiated expression of EF-1 β was noted in *Candida* species exposed to H₂O₂ and menadione, reinforcing its role in the stress response, perhaps as a modulator of transcription of other proteins.²³

Another protein identified here was a mitochondrial Prx1. Fungal peroxiredoxins are ubiquitous enzymes that protect cells against OS.^{12,29} An *in silico* analysis by Ortega et al.²² demonstrated that both *S. brasiliensis* and *S. schenckii sensu stricto* have four putative peroxiredoxins in their genome, but to date it is unknown which of these genes are modulated by H₂O₂. In accordance with our results, a proteomic analysis in *Aspergillus fumigatus* revealed the differential expression of 28 proteins, including Prx1, which increased their concentration after 45 min of exposure to H₂O₂.¹⁶ In the same line, Kusch et al.¹⁵ exposed *C. albicans* to two oxidizing agents, H₂O₂ and diamide, and observed the differential expression of 52 proteins, including Ip2431p, which is homologous to Tsa1p in *S. cerevisiae* where it plays the role of a peroxiredoxin. Another study in *Candida* species exposed to H₂O₂ and menadione revealed the differential expression of 15 moonlight-like cell wall proteins including Tsa1p,²³ while in *S. cerevisiae* it was proposed that Prx1 acts as a redox signalling molecule that oxidizes Trx3. At high concentration oxidized Trx3 can produce apoptosis,

indicating that when Prx1 is unable to detoxify reactive mitochondrial oxygen species it induces apoptosis to remove the affected cells.¹³ Further studies by proteomics and bioinformatic approaches about the response to OS in exponentially and stationary-phase in *Sporothrix* will be necessary to get a deeper knowledge of the defense mechanisms of this pathogen as they occur in the phagocyte.

To determine whether the regulation of the identified proteins occurred at the transcriptional level, the expression of the genes encoding Hsp70 and Prx1 was evaluated. To this purpose, it was important to assess the quality of the RNA obtained from *S. schenckii sensu stricto* as it has been reported that ROS can damage nucleic acids⁴. The ribosomal RNA bands were well defined indicating that it was suitable for analysis (Fig. 3A). Following the exposure of *S. schenckii sensu stricto* to H₂O₂, significant differences were found ($p < 0.05$) in the expression levels of *prx1* and *hsp70* genes. Thus, while a significant increase in the expression of *prx1* and *hsp70* were observed at 200 and 400 mM H₂O₂ compared with the control, a significant decrease in *hsp70* occurred at 400 mM H₂O₂ compared with 200 mM H₂O₂ (Fig. 3B and C). These results are in agreement with those obtained from the proteomic analysis carried out after the exposure of *S. schenckii sensu stricto* yeast cells to ROS (Fig. 2), therefore indicating that changes observed for the proteins identified in this study are regulated at the transcriptional level.

Comparative studies of the virulence of *S. schenckii* complex demonstrated that *S. brasiliensis* was the most virulent followed by *S. schenckii sensu stricto*, *S. globosa*, *S. mexicana* y *S. pallida*.³ Fernandes et al.¹⁰ evaluated the secretion profiles of proteins from different isolates of *S. schenckii sensu stricto*, *S. brasiliensis* and *S. globosa*, and reported the expression of different proteins. They also observed that the humoral response of animals infected with these species was different. The most virulent isolates shared two common antigens of 60 kDa and 110 kDa, which are likely to be involved in virulence. In the same line, Ortega et al.²² observed that *S. brasiliensis* was more resistant to stress by peroxides as compared with *S. schenckii sensu stricto*, suggesting that the *S. schenckii* species exhibit different strategies for adaptation, depending on the route of infection, a phenomenon most likely related with virulence.

Conclusions

Based on the results presented in this study, we propose that the identified proteins are likely to be involved in the resistance of this fungus against OS, helping the pathogen to evade the host phagocytic cells, reach the blood stream and cause an invasive mycosis.

Conflict of interests

The authors declare that there were no conflicts of interest with any organization or entity with a financial interest, or financial conflict with the material discussed in this work.

Acknowledgments

The authors appreciate the technical assistance and facilities provided for the analysis of MALDI-MS/MS by M.C. Emmanuel Ríos Castro of the Unidad de Genómica, Proteómica y Metabólica (LaNSE; CINVESTAV-Unidad Ciudad de México, México). We are grateful to M.C. Omar Posada-Villarreal for his support in the statistical analysis. This work was supported by grant CB-2011 No.167737 from the Consejo Nacional de Ciencia y Tecnología (CONACyT, México) to ERB.

Appendix A. Supplementary data

Supplementary data associated with this article can be found, in the online version, at <https://doi.org/10.1016/j.riam.2018.10.004>.

References

1. Abegg MA, Alabarse PV, Casanova A, Hoscheid J, Salomon TB, Hackenhaar FS, et al. Response to oxidative stress in eight pathogenic yeast species of the genus *Candida*. *Mycopathologia*. 2010;170:11–20.
2. Alba-Fierro CA, Pérez-Torres A, Toriello C, Romo-Lozano Y, López-Romero E, Ruiz-Baca E. Molecular components of the *Sporothrix schenckii* complex that induce immune response. *Curr Microb*. 2016;73:292–300.
3. Arrillaga-Moncrieff I, Capilla J, Mayayo E, Marimon R, Mariné M, Gené J, et al. Different virulence levels of the species of *Sporothrix* in a murine model. *Clin Microbiol Infect*. 2009;15:651–5.
4. Brown A, Haynes K, Quinn J. Nitrosative and oxidative stress responses in fungal pathogenicity. *Curr Opin Microbiol*. 2009;12:384e39.
5. Chaston JJ, Smits C, Aragao D, Wong AS, Ahsan B, Sandin S, et al. Structural and functional insights into the evolution and stress adaptation of type II chaperonins. *Structure*. 2016;24:1–11.
6. Cuéllar-Cruz M, Briones-Martin-del-Campo M, Canas-Villamar I, Montalvo-Arredondo J, Riego-Ruiz L, Castaño I, et al. High resistance to oxidative stress in the fungal pathogen *Candida glabrata* is mediated by a single catalase, Cta1p, and is controlled by the transcription factors Yap1p, Skn7p, Msn2p, and Msn4p. *Eukaryot Cell*. 2008;7:814–25.
7. Cuéllar-Cruz M, Gutiérrez-Sánchez G, López-Romero E, Ruiz-Baca E, Villagómez-Castro JL, Rodríguez-Sifuentes JL. Identification of *Candida albicans* heat shock proteins and *Candida glabrata* and *Candida krusei* enolases involved in the response to oxidative stress. *Cent Eur J Biol*. 2013;8:337–45.
8. Dantas AS, Andrade RV, Carvalho MJ, Felipe MS, Campos EG. Oxidative stress response in *Paracoccidioides brasiliensis*: assessing catalase and cytochrome C peroxidase. *Mycol Res*. 2008;112:747–56.
9. De Arruda Grossklau D, Bailão AM, Vieira Rezende TC, Borges CL, de Oliveira MA, Parente JA, de Almeida Soares CM. Response to oxidative stress in *Paracoccidioides* yeast cells as determined by proteomic analysis. *Microbes Infect*. 2013;15:347–64.
10. Fernandes GF, dos Santos PO, Rodrigues AM, Sazaki AA, Burger E, de Camargo ZP. Characterization of virulence profile, protein secretion and immunogenicity of different *Sporothrix schenckii sensu stricto* isolates compared with *S. globosa* and *S. brasiliensis* species. *Virulence*. 2013;4:241–9.
11. Gray JV, Petsko GA, Johnston GC, Ringe D, Singer RA, Werner-Washburne M. Sleeping beauty: quiescence in *Saccharomyces cerevisiae*. *Microbiol Mol Biol Rev*. 2004;68:187–206.
12. Greetham D, Grant CM. Antioxidant activity of the yeast mitochondrial one-cys peroxiredoxin is dependent on thioredoxin reductase and glutathione *in vivo*. *Mol Cell Biol*. 2009;29:3229–40.
13. Greetham D, Kritsiligkou P, Watkins RH, Carter Z, Parkin J, Grant CM. Oxidation of the yeast mitochondrial thioredoxin promotes cell death. *Antioxid Redox Signal*. 2013;18:376–85.
14. Kajiwara H, Saito M, Ohga S, Uenotsuchi T, Yoshida S. Impaired host defense against *Sporothrix schenckii* in mice with chronic granulomatous disease. *Infect Immun*. 2004;72:5073–9.
15. Kusch H, Engelmann S, Albrecht D, Morschhäuser J, Hecker M. Proteomic analysis of the oxidative stress response in *Candida albicans*. *Proteomics*. 2007;7:686–97.
16. Lessing F, Kniemeyer O, Wozniok I, Loeffler J, Kurzai O, Haertl A, et al. The *Aspergillus fumigatus* transcriptional regulator AfYap1 represents the major regulator for defense against reactive oxygen intermediates but is dispensable for pathogenicity in an intranasal mouse infection model. *Eukaryot Cell*. 2007;6:2290–302.
17. López-Romero E, Reyes-Montes MR, Pérez-Torres A, Ruiz-Baca E, Villagómez-Castro JC, Mora-Montes HM, et al. *Sporothrix schenckii* complex and sporotrichosis, an emerging health problem. *Future Microbiol*. 2011;6:85–102.
18. Marimon R, Cano J, Gené J, Sutton D, Kawasaki M, Guarro J. *Sporothrix brasiliensis*, *S. globosa*, and *S. mexicana*. Three new *Sporothrix* species of clinical interest. *J Clin Microbiol*. 2007;45:3198–206.
19. Marimon R, Gené J, Cano J, Trilles L, Dos Santos Lazera M, Guarro J. Molecular phylogeny of *Sporothrix schenckii*. *J Clin Microbiol*. 2006;44:3251–6.
20. McGoldrick S, O'Sullivan SM, Sheehan D. Glutathione transferase-like proteins encoded in genomes of yeasts and fungi: insights into evolution of a multifunctional protein superfamily. *FEMS Microbiol Lett*. 2005;242:1–12.
21. Michán C, Pucio C. Growth phase-dependent variations in transcript profiles for thioredoxin- and glutathione-dependent redox systems followed by budding and hyphal *Candida albicans* cultures. *FEMS Yeast Res*. 2009;9:1078–90.
22. Ortega I, Soares-Felipe MS, Vasconcelos AT, Lopez-Bezerra LM, Da Silva Dantas A. Peroxide sensing and signaling in the *Sporothrix schenckii* complex: an *in silico* analysis to uncover putative mechanisms regulating the Hog1 and AP-1 like signaling pathways. *Med Mycol*. 2015;53:51–9.
23. Ramírez-Quijas MD, López-Romero E, Cuéllar-Cruz M. Proteomic analysis of cell wall in four pathogenic species of *Candida* exposed to oxidative stress. *Microb Pathog*. 2015;87:1–12.
24. R Core Team. R: A language and environment for statistical computing. Version 3.4.2 [software]. R Foundation for Statistical Computing, Vienna, Austria. 2017

- Sep 28. Available from: <https://cran.r-project.org/mirrors.html> Note: National Institutes of Health citation style; package "DescTools" was installed; URL from "citation()" command: <https://www.R-project.org/> [cited 15.09.18].
25. Romero-Martínez R, Wheeler M, Guerrero-Plata A, Rico G, Torres-Guerrero H. Biosynthesis and functions of melanin in *Sporothrix schenckii*. Infect Immun. 2000;68:3696–703.
 26. Ruiz-Baca E, Mora-Montes HM, López-Romero E, Toriello C, Mojica-Marín V, Urtiz-Estrada N. 2D-immunoblotting analysis of *Sporothrix schenckii* cell wall. Mem Inst Oswaldo Cruz. 2011;106:248–50.
 27. Seider K, Heyken A, Lüttich A, Miramón P, Hube B. Interaction of pathogenic yeasts with phagocytes: survival, persistence and escape. Curr Opin Microbiol. 2010;13:392–400.
 28. Silveira CP, Piffer AC, Kmetzsch L, Soares DA, Staats CC, Rodrigues ML, et al. The heat shock protein (Hsp) 70 of *Cryptococcus neoformans* is associated with the fungal cell surface and influences the interaction between yeast and host cells. Fungal Genet Biol. 2013;60:53–63.
 29. Srinivasa K, Kim NR, Kim J, Kim M, Bae JY, Jeong W, et al. Characterization of a putative thioredoxin peroxidase prx1 of *Candida albicans*. Mol Cells. 2012;33:301–7.
 30. Shevchenko A, Tomas H, Hawlis J, Olsen JV, Mann M. In-gel digestion for mass spectrometric characterization of proteins and proteomes. Nat Protoc. 2006;6:2856–60.
 31. Westwater C, Balish E, Schofield DA. *Candida albicans*-conditioned medium protects yeast cells from oxidative stress: a possible link between quorum sensing and oxidative stress resistance. Eukaryot Cell. 2005;4:1654–61.
 32. Zakrajšek T, Raspor P, Jamnik P. *Saccharomyces cerevisiae* in the stationary phase as a model organism-characterization at cellular and proteome level. J Proteomics. 2011;74:2837–45.